N 71-27015

NASA CONTRACTOR
REPORT

NASA CR-61353

SATURN V/SKYLAB MULTIPLE-PROTUBERANCE HEAT TRANSFER TEST DATA ANALYSIS

By W. L. Shaffer, C. P. Williamson,
and C. R. Mullen

The Boeing Company
Huntsville, Alabama

May 19, 1971

Prepared for

NASA-GEORGE C. MARSHALL SPACE FLIGHT CENTER
Marshall Space Flight Center, Alabama 35812

TECHNICAL REPORT STANDARD TITLE PAGE

1. REPORT NO.	2. GOVERNMENT ACCESSION NO.	3. RECIPIENT'S CATALOG NO.
NASA CR-61353		

4. TITLE AND SUBTITLE	5. REPORT DATE
SATURN V/SKYLAB MULTIPLE-PROTUBERANCE HEAT TRANSFER TEST DATA ANALYSIS	May 19, 1971
	6. PERFORMING ORGANIZATION CODE
7. AUTHOR(S)	8. PERFORMING ORGANIZATION REPORT #
W. L. Shaffer, C. P. Williamson, C. R. Mullen	
9. PERFORMING ORGANIZATION NAME AND ADDRESS	10. WORK UNIT NO.
The Boeing Company Huntsville, Alabama	11. CONTRACT OR GRANT NO. NAS8-5608
12. SPONSORING AGENCY NAME AND ADDRESS	13. TYPE OF REPORT & PERIOD COVERED
NASA Washington, DC 20546	CONTRACTOR REPORT
	14. SPONSORING AGENCY CODE

15. SUPPLEMENTARY NOTES

16. ABSTRACT

Multiple protuberance heat transfer data obtained from wind tunnel tests conducted at Langley Research Center are presented. The primary purpose of the test series was to determine the heat transfer to bodies submerged in the wake of, or having their surface impinged upon by the shock or shocks of one or more protuberances. Data were taken for Mach numbers of 2.49, 3.51 and 4.44 at a Reynolds number of 3×10^6/ft. Protuberance models consisted of (1) four models with a 15 or 30 degree forebody, constant cross-section center body and a 15-, 30-, or 90-degree afterbody, (2) a 14-degree ramp, and (3) four models of anti-flutter hat sections. The models were mounted on the tunnel sidewall test plate in singular and multiple configurations and heat transfer data recorded from thermocouples located on the test plate and models.

Additionally, test plate pressures were obtained in the vicinity of the hat section models. Some limited comparisons of theoretical heat transfer and the test data have been made.

17. KEY WORDS	18. DISTRIBUTION STATEMENT
Heat Transfer Multiple Protuberance Heat Transfer Wake Heating Shock Impingement Heating	Unclassified-Unlimited E. D. Geissler Director, Aero-Astrodynamics Laboratory

19. SECURITY CLASSIF. (of this report)	20. SECURITY CLASSIF. (of this page)	21. NO. OF PAGES	22. PRICE
UNCLASSIFIED	UNCLASSIFIED	153	$3.00

MSFC - Form 3292 (May 1969)

CONTENTS

ILLUSTRATIONS

ILLUSTRATIONS (Continued)

ILLUSTRATIONS (Continued)

ILLUSTRATIONS (Continued)

TABLES

REFERENCES

1. Boeing Document T5-6636, "Multiple-Protuberance Heat-Transfer Test Program - Data Report," December 7, 1970.

2. NASA TN D-5297, "Flow Field Measurements Downstream of Two Protuberances on a Flat Plate Submerged in a Turbulent Boundary Layer at Mach 2.49 and 4.44," July 1969.

3. Douglas Report SM-46735, "General Protuberance Heat-Transfer Test Final Report, Volume I, Langley Data Report," August 17, 1964.

4. Van Driest, E. R., "The Problem of Aerodynamic Heating," Aeronautical Engineering Review, October 1956.

5. Lee, Dorothy B., and Faget, Maxine A., "Charts Adapted from Van Driest's Turbulent Flat-Plate Theory for Determining Values of Turbulent Aerodynamic Friction and Heat-Transfer Coefficients," NACA TN 3811, October 1956.

6. Douglas Report SM-46735, "General Protuberance Heat-Transfer Test, Volume III, Data Evaluation Report," February 1967.

7. Couch, Lana Murphy; Stallings, Robert L., Jr.; and Collins, Ida K., "Heat Transfer Measurements on a Flat Plate with Attached Protuberances in a Turbulent Boundary Layer at Mach Numbers of 2.49, 3.51, and 4.44," NASA TN D-3736, December 1966.

8. Bogdonoff, S. M., "Some Experimental Studies of the Separation of Supersonic Turbulent Boundary Layers," Princeton University Report 336, June 1955.

9. Love, E. S., "Pressure Rise Associated with Shock-Induced Boundary-Layer Separation," NACA TN 3601, December 1955.

NOMENCLATURE

d	Protuberance height
H	Step height
h	Heat-transfer coefficient
$\bar{h}_c$	Average heat-transfer coefficient in gap
h_{c_L}	Heat-transfer coefficient at X = L
h_o	Heat-transfer coefficient, clean body
h_o'	Average clean-body heat-transfer coefficient at protuberance location
K	Thermal conductivity
L	Running length
M	Mach number
P_p	Plateau pressure
R_e	Reynolds number
X	Distance from plate leading edge
Y	Distance from plate centerline
Z	Vertical distance
δ	Boundary layer thickness

ACKNOWLEDGEMENTS

The analyses presented in this report were performed by W. L. Shaffer, C. P. Williamson and C. R. Mullen of the Aerophysics Group under the supervision of W. A. Smith. Questions concerning the material presented should be directed to C. R. Mullen, Mail Stop JC-35, 895-2980.

1.0 INTRODUCTION

This doucment contains an analysis of heat-transfer and pressure data (Reference 1) obtained during a multiple-protuberance heating test (Project 925) conducted at the Langley Research Center, July and August of 1970. The tests were conducted at Mach numbers of 2.49, 3.51 and 4.44 in the Unitary Plan Wind Tunnel with a nominal Reynolds number per foot of $3x10^6$.

The primary purpose of the test program was to investigate the effect of aerodynamic heating in the shock impingement and wake heating regions on and around multiple-protuberance configurations submerged in a turbulent boundary layer. The protuberance models were arranged to allow measurement of induced heating rates associated with single and multiple-protuberance disturbances.

Existing McDonnell-Douglas protuberance models (References 1 through 3) were refurbished and mounted to a new instrumented test plate in various configurations.

The data have been plotted to show the heating effects of multiple-protuberances and have been compared with analytical calculations and other data.

2.0 GENERAL TEST CONDITIONS AND ANALYSIS

The multiple-protuberance test incorporates the use of nine separate models (five instrumented) mounted in different combinations to an instrumented flat plate to form 19 different configurations. These configurations are shown in Figure 2-1 (configuration 1, the clean plate, is not shown).

All protuberance models and the test plate are shown schematically with dimensions in Figures 2-2, 2-3 and 2-4. The general protuberance shapes include a 15 or 30 degree forebody, constant cross-section centerbody, and a 15, 30 or 90 degree afterbody. Wind tunnel installation photographs of some configurations are shown in Figures 2-5 through 2-9. Additional details on the fabrication and instrumentation of the models and test plate are given in Reference 1.

The multiple protuberance configurations were tested at Mach numbers of 2.49, 3.51 and 4.44 at a nominal Reynolds number per foot of 3.0×10^6. The total temperature and pressure ranges were 610°R to 713°R and 2799 psf to 8686 psf respectively. The test schedule is presented in Table 2-I and contains tunnel total pressure, total temperature, Mach number, unit Reynolds number, and a description of the configuration for each test run. Pressure measurements were obtained for configuration 11, and heat-transfer measurements for all other configurations.

The models were mounted on the test plate which was a part of the tunnel wall during tests. The models were therefore immersed in the turbulent boundary layer of the tunnel wall. The boundary layer profiles were not measured during this test but have been measured in the past and are contained in Reference 2. These boundary layer profiles have been used in the analytical calculation (profiles do not agree with 1/7 power law distribution).

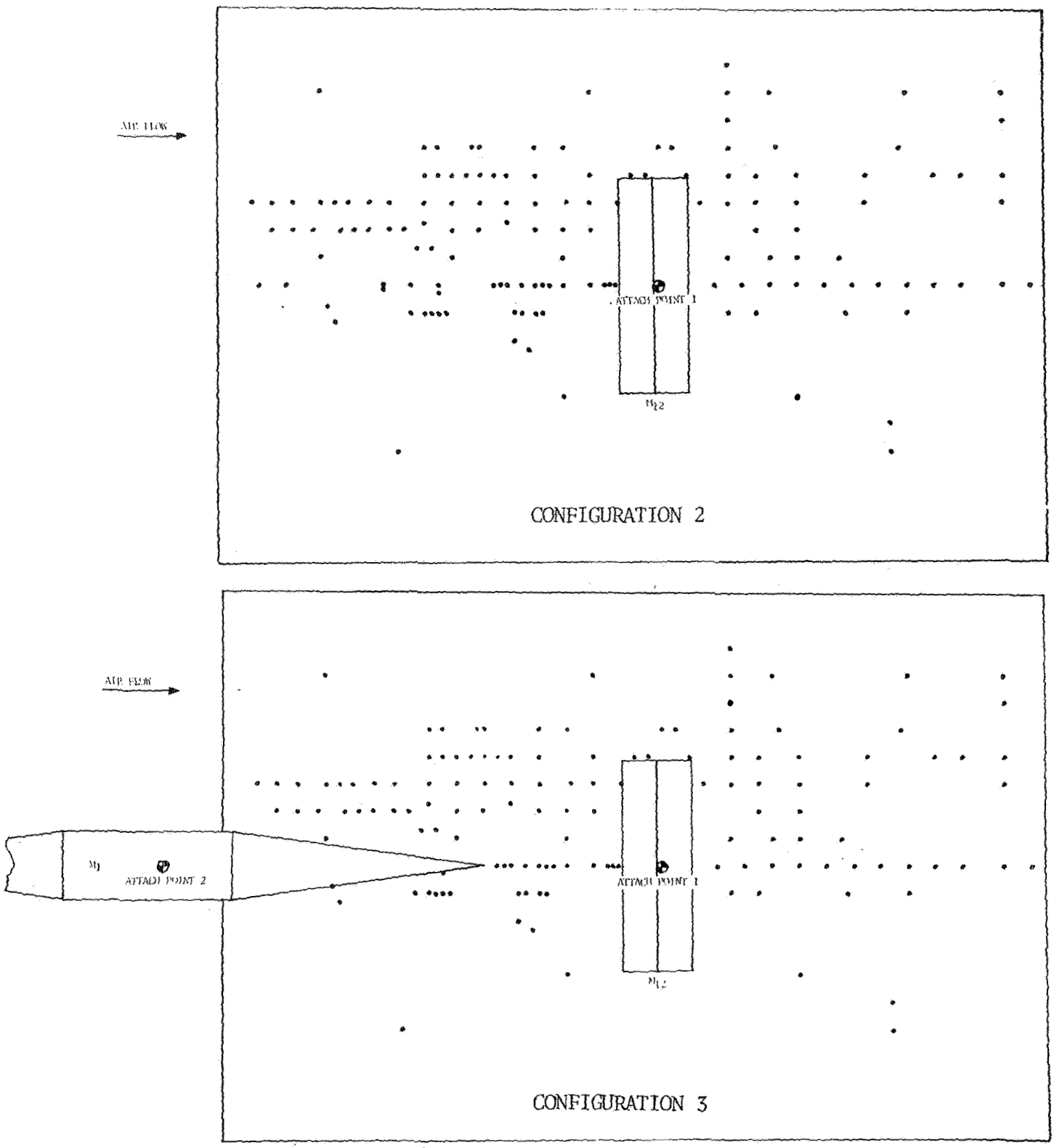

FIGURE 2-1. MULTIPLE-PROTUBERANCE TEST CONFIGURATIONS (Continued)

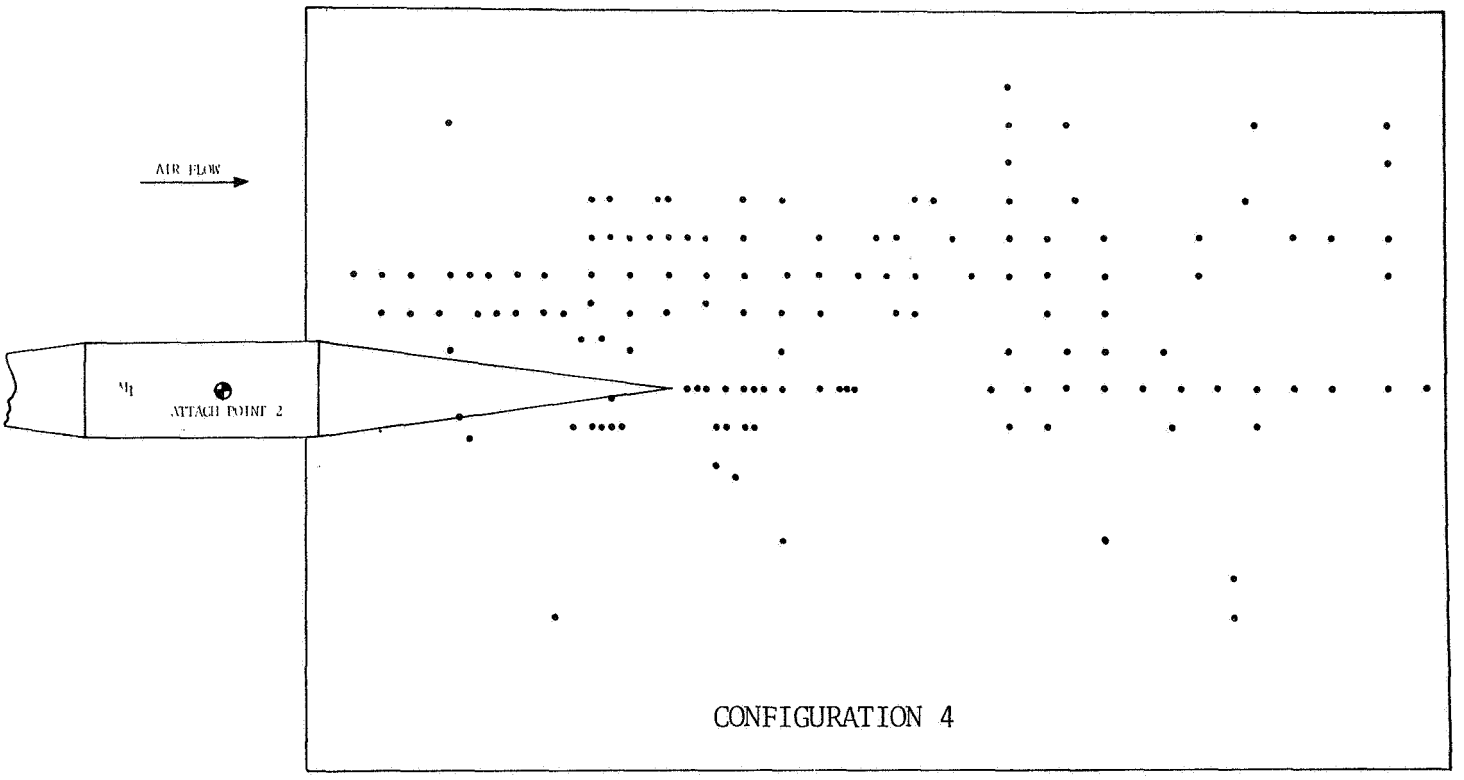

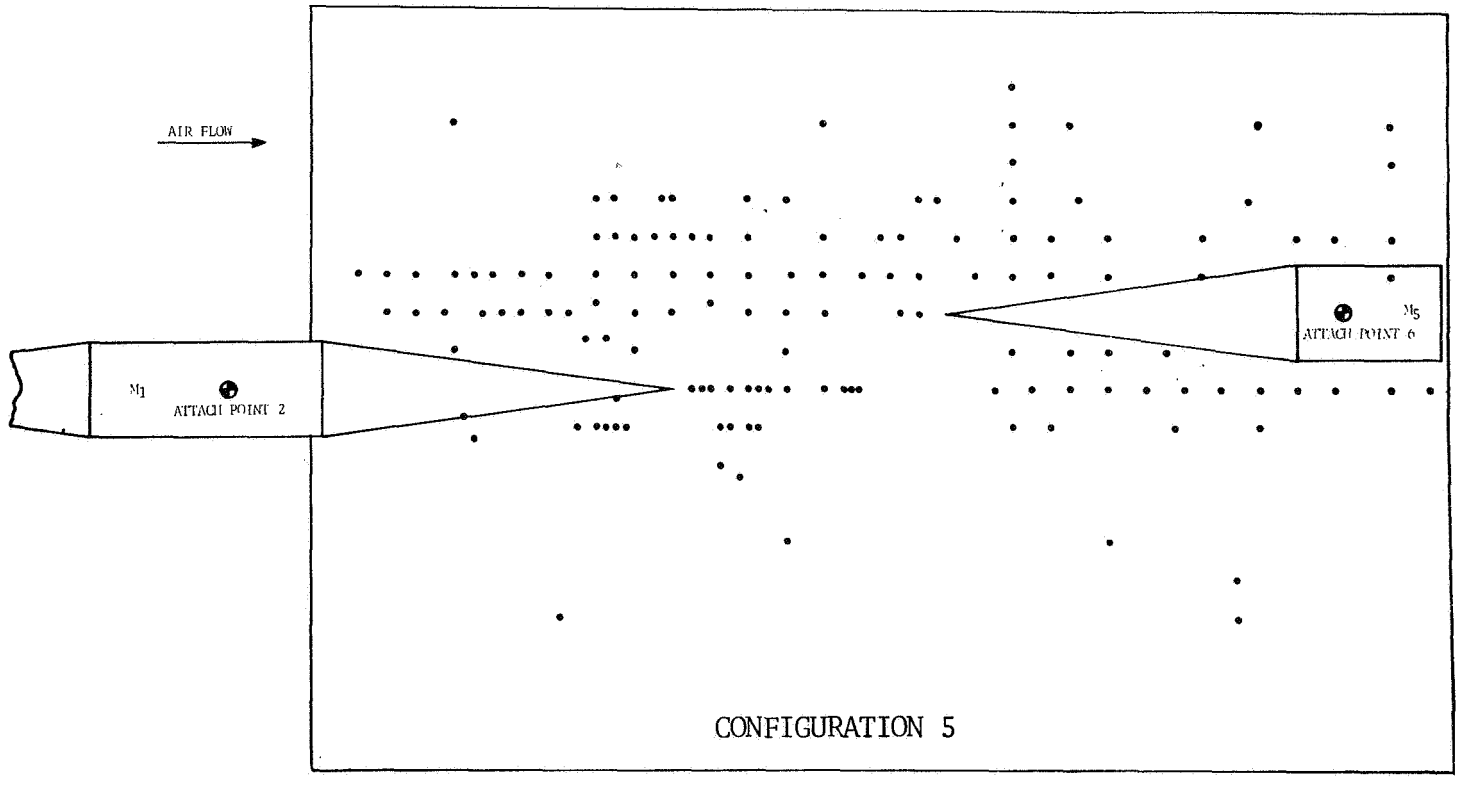

FIGURE 2-1. MULTIPLE-PROTUBERANCE TEST CONFIGURATIONS (Continued)

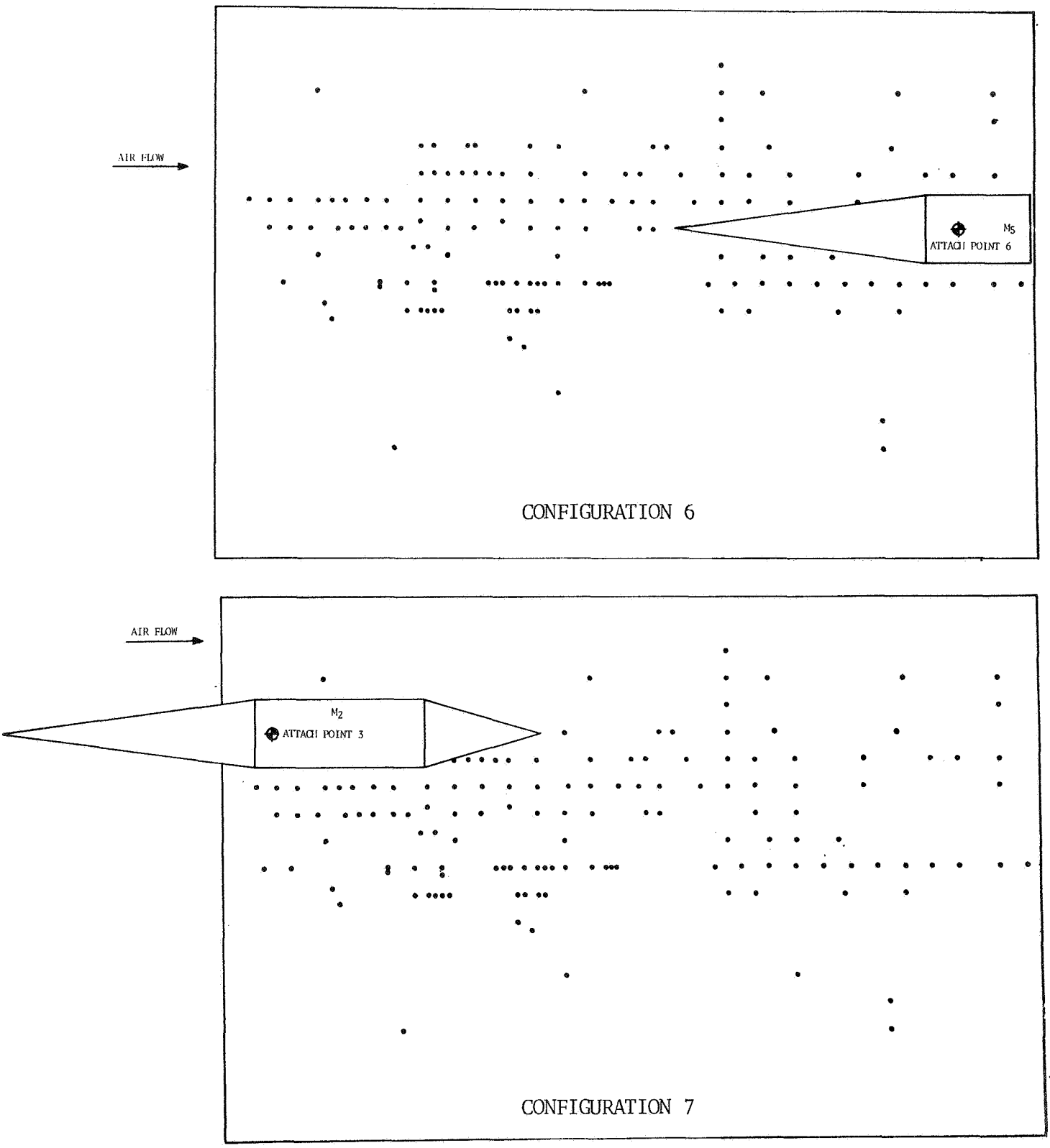

FIGURE 2-1. MULTIPLE-PROTUBERANCE TEST CONDIGURATIONS (Continued)

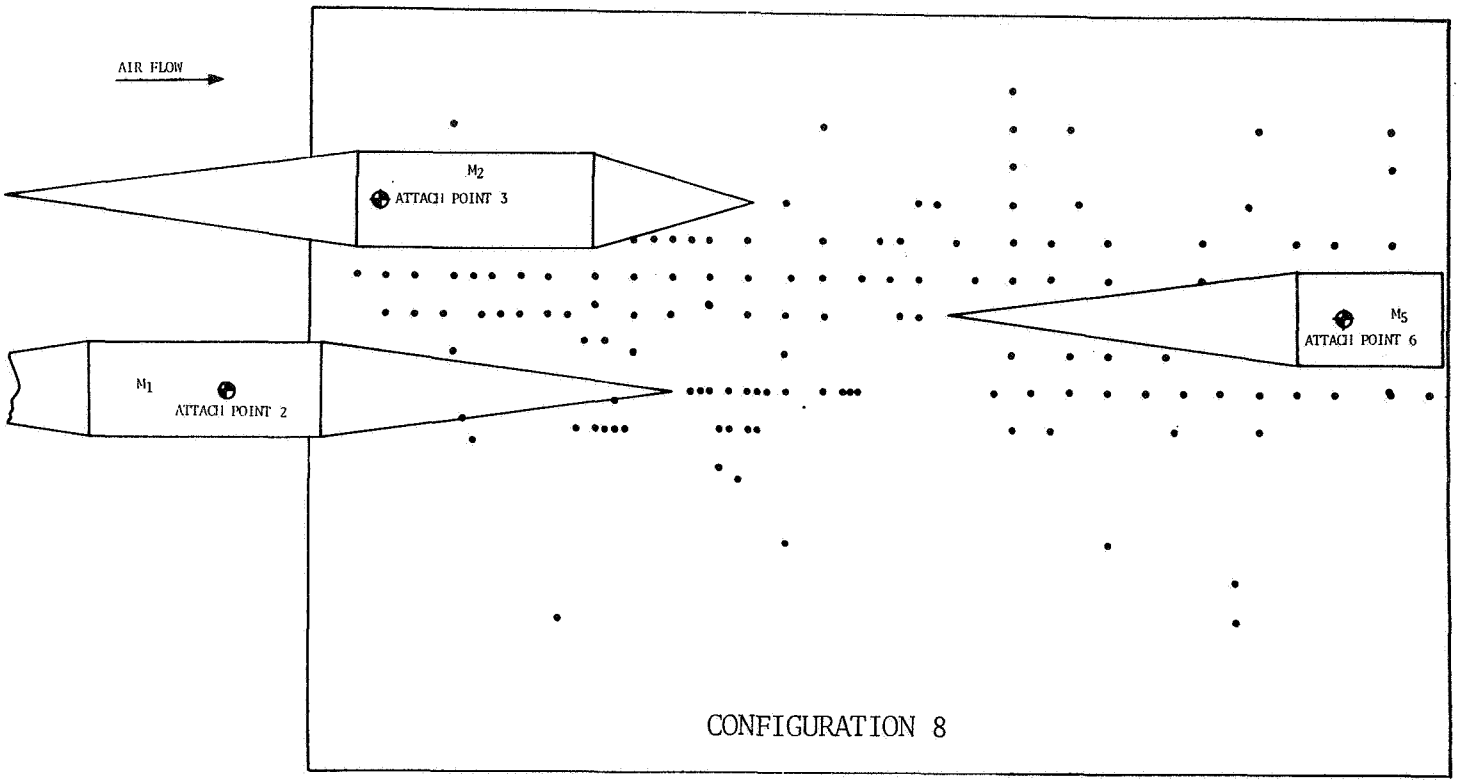

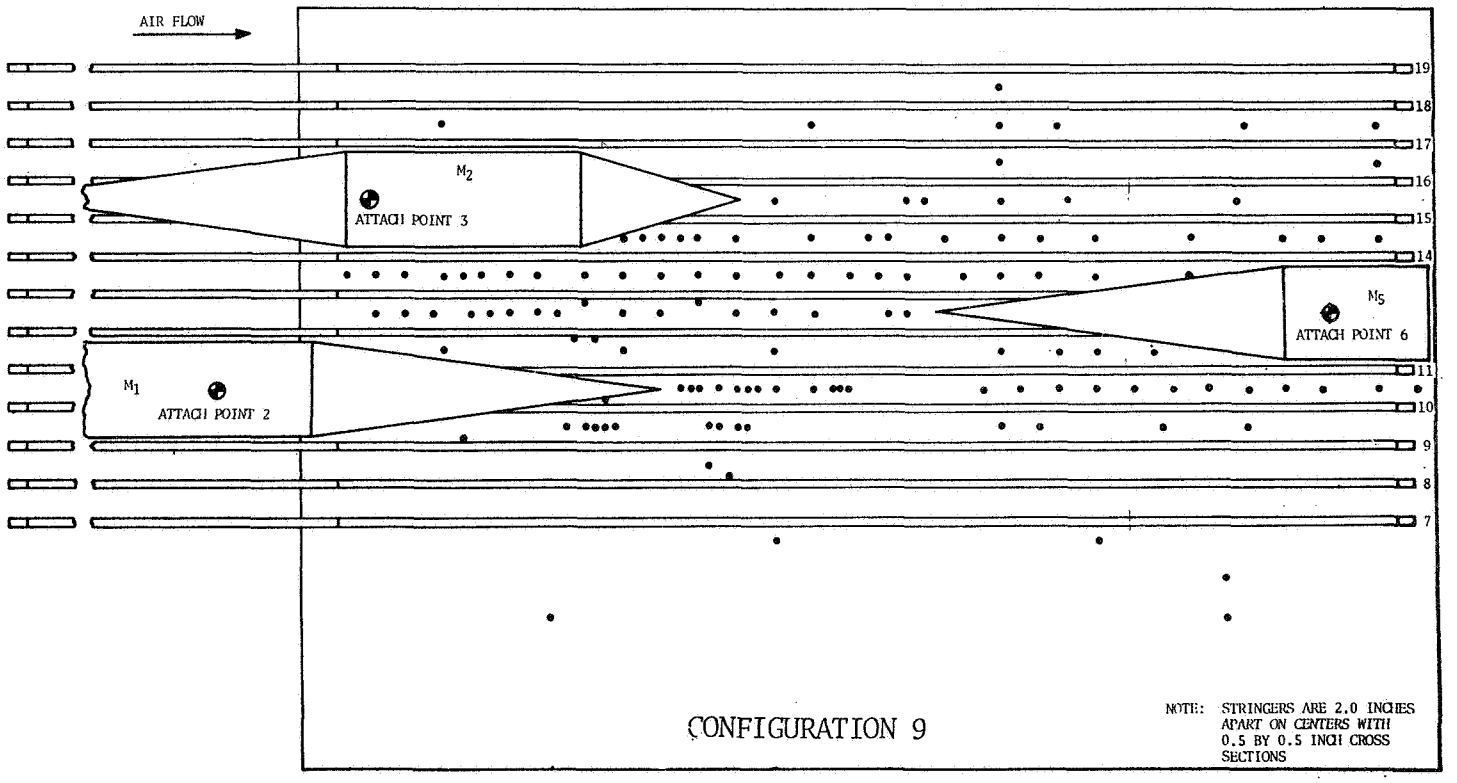

FIGURE 2-1. MULTIPLE-PROTUBERANCE TEST CONFIGURATIONS (Continued)

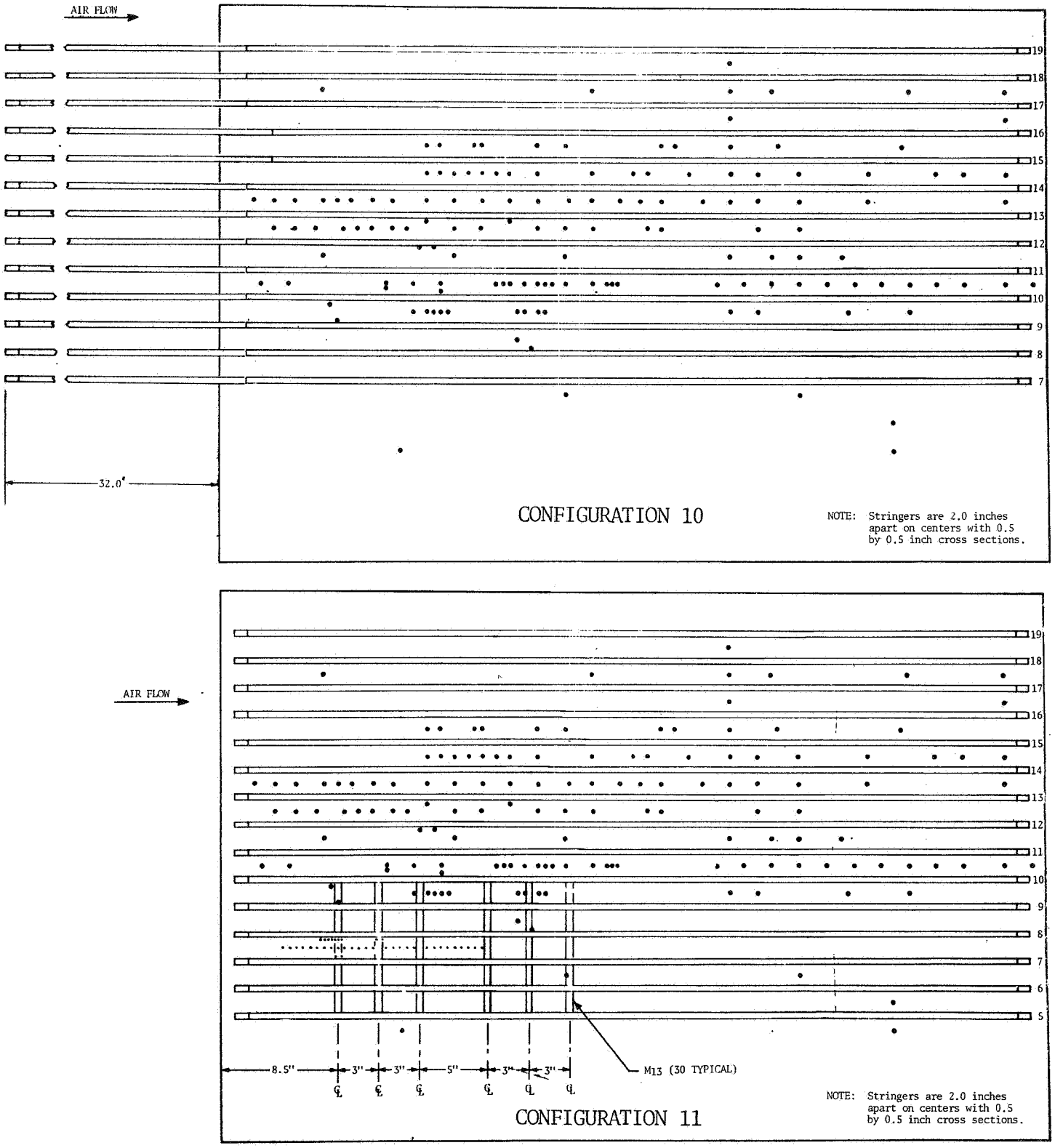

FIGURE 2-1. MULTIPLE-PROTUBERANCE TEST CONFIGURATIONS (Continued)

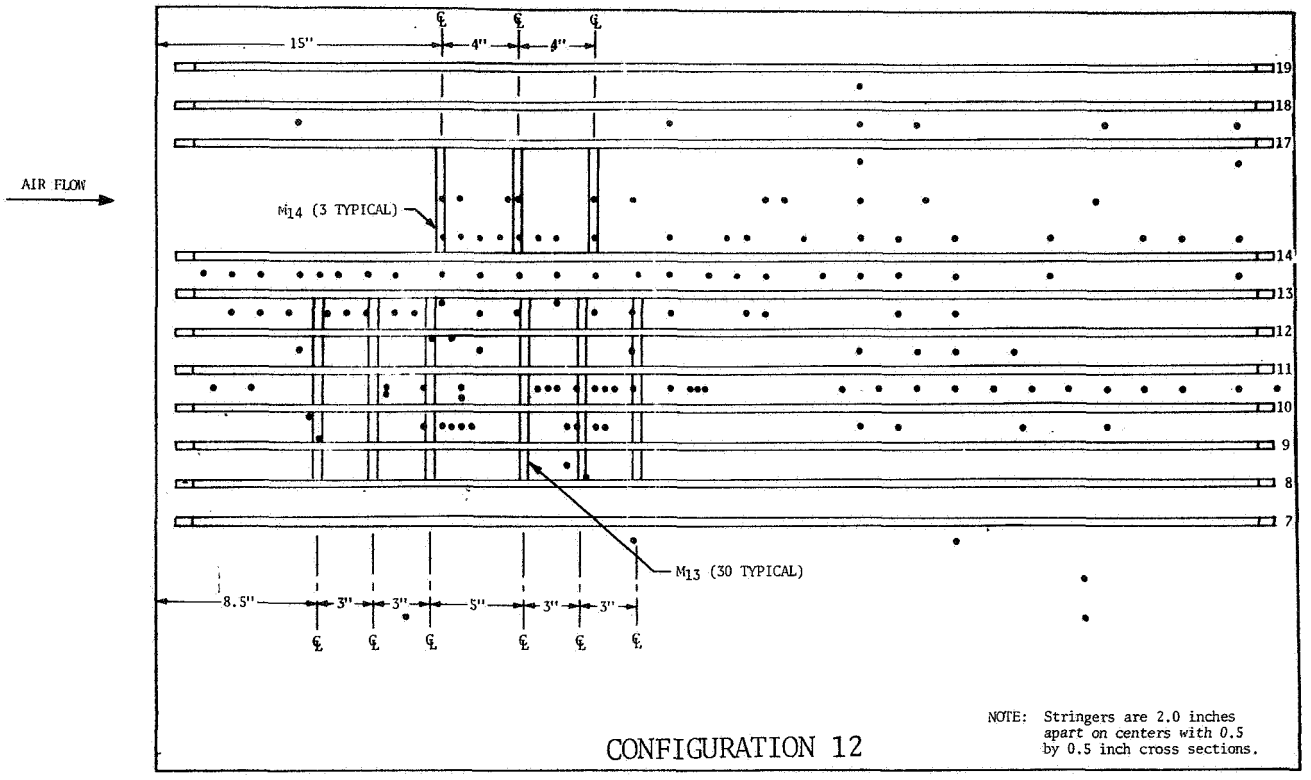

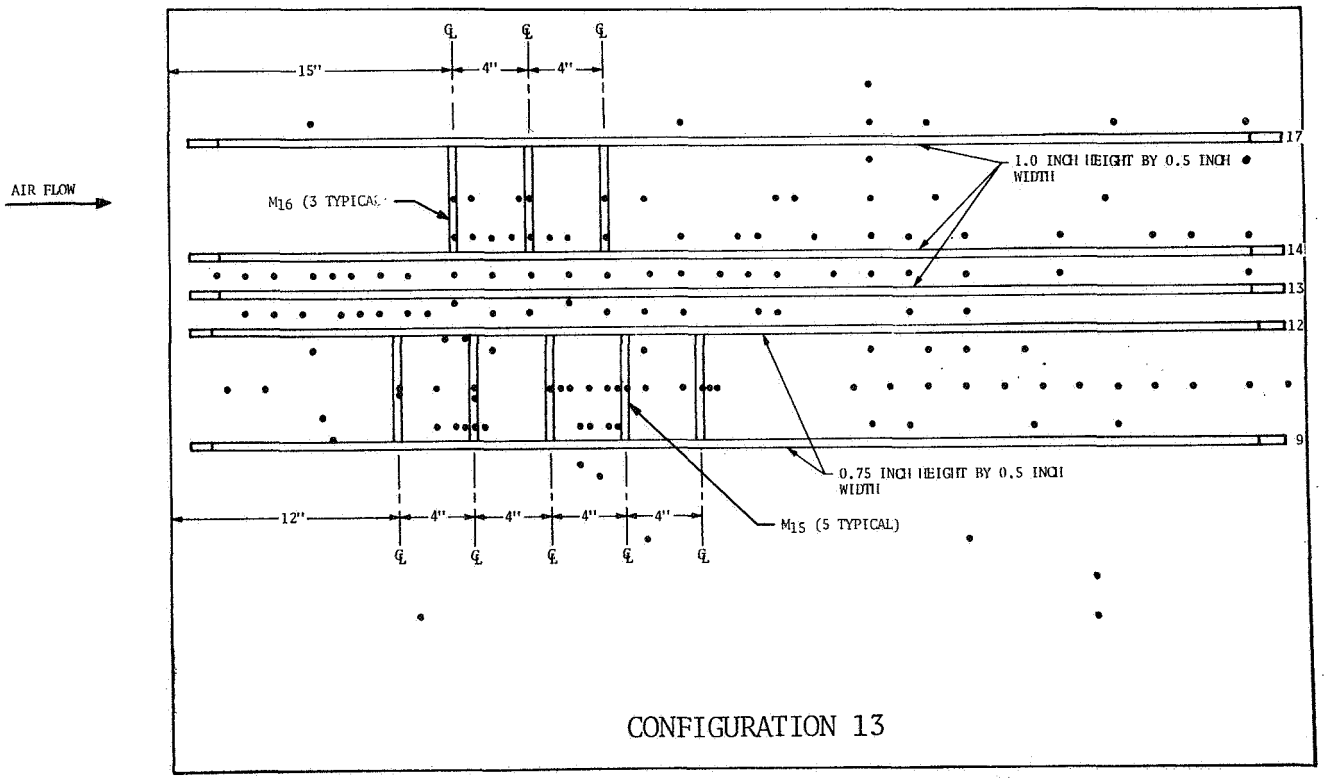

FIGURE 2-1. MULTIPLE-PROTUBERANCE TEST CONFIGURATIONS (Continued)

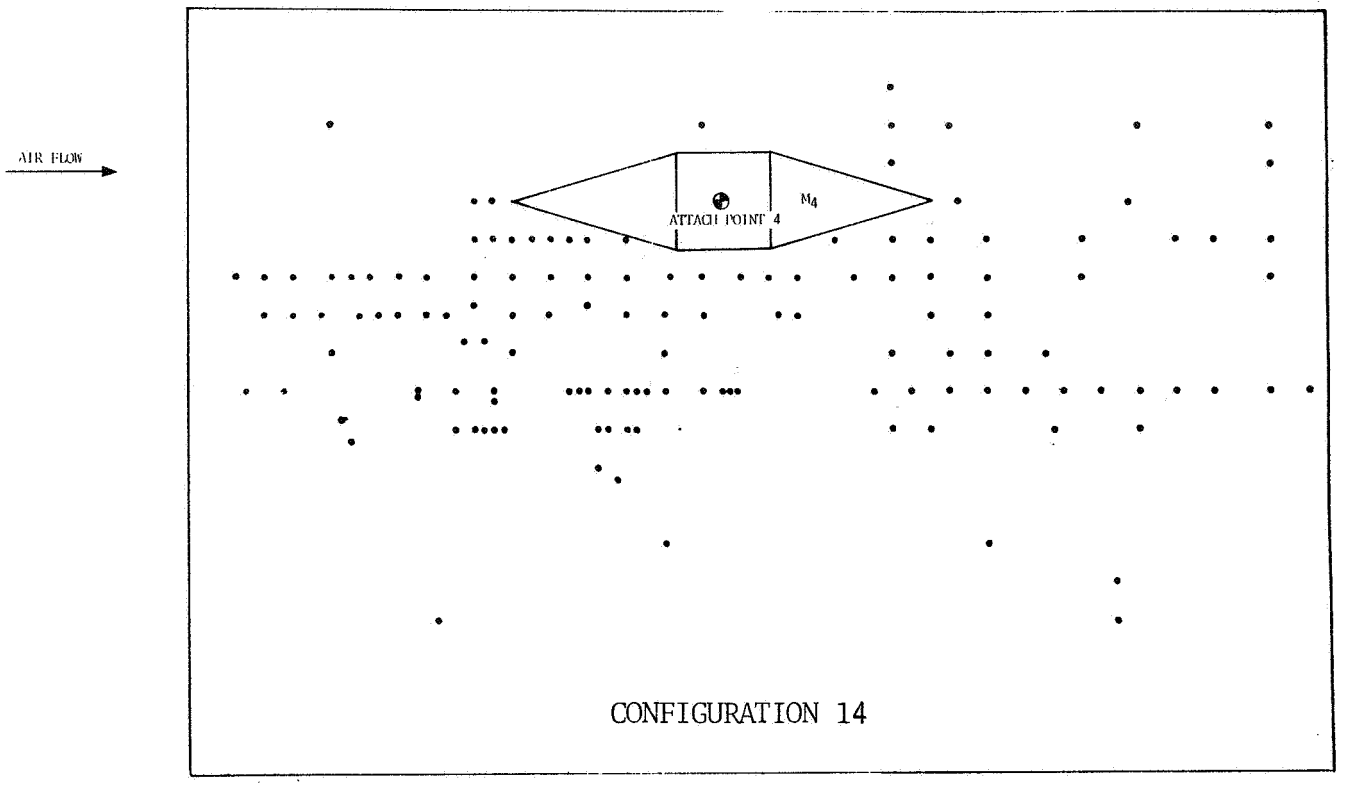

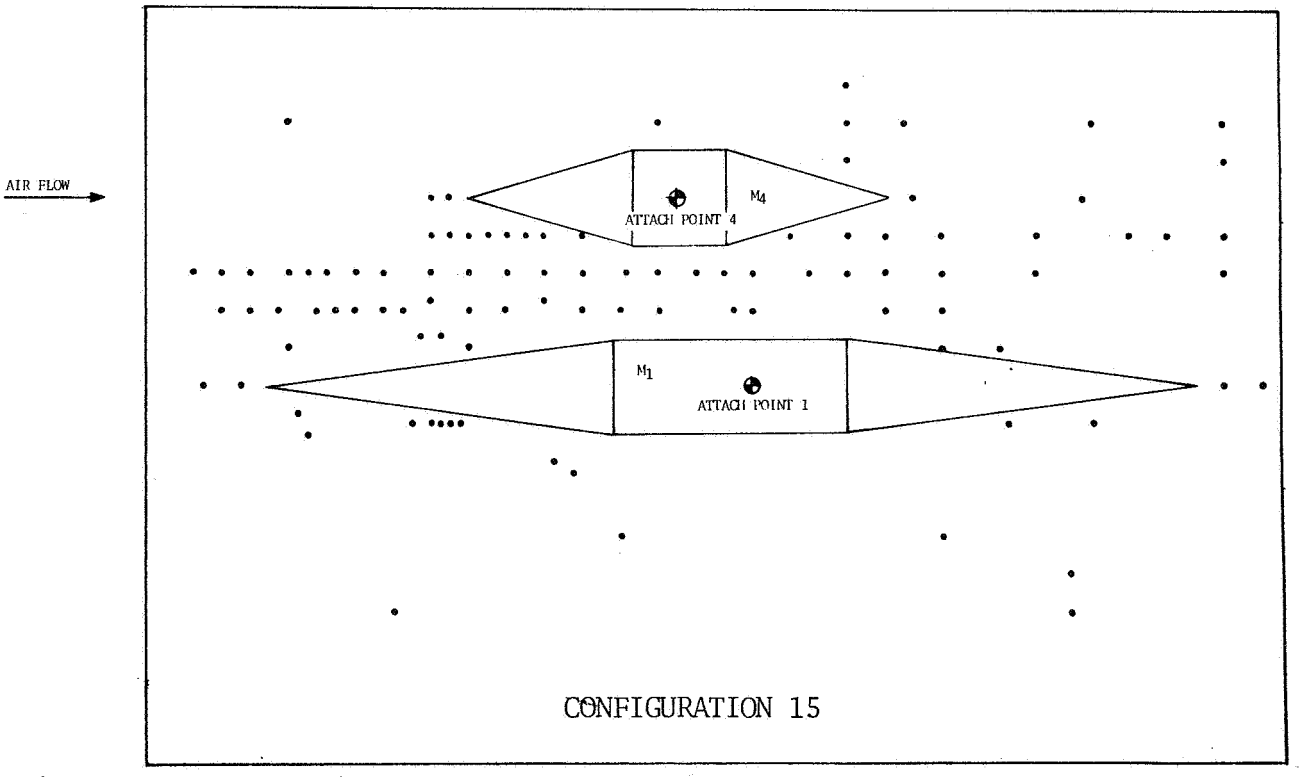

FIGURE 2-1. MULTIPLE-PROTUBERANCE TEST CONFIGURATIONS (Continued)

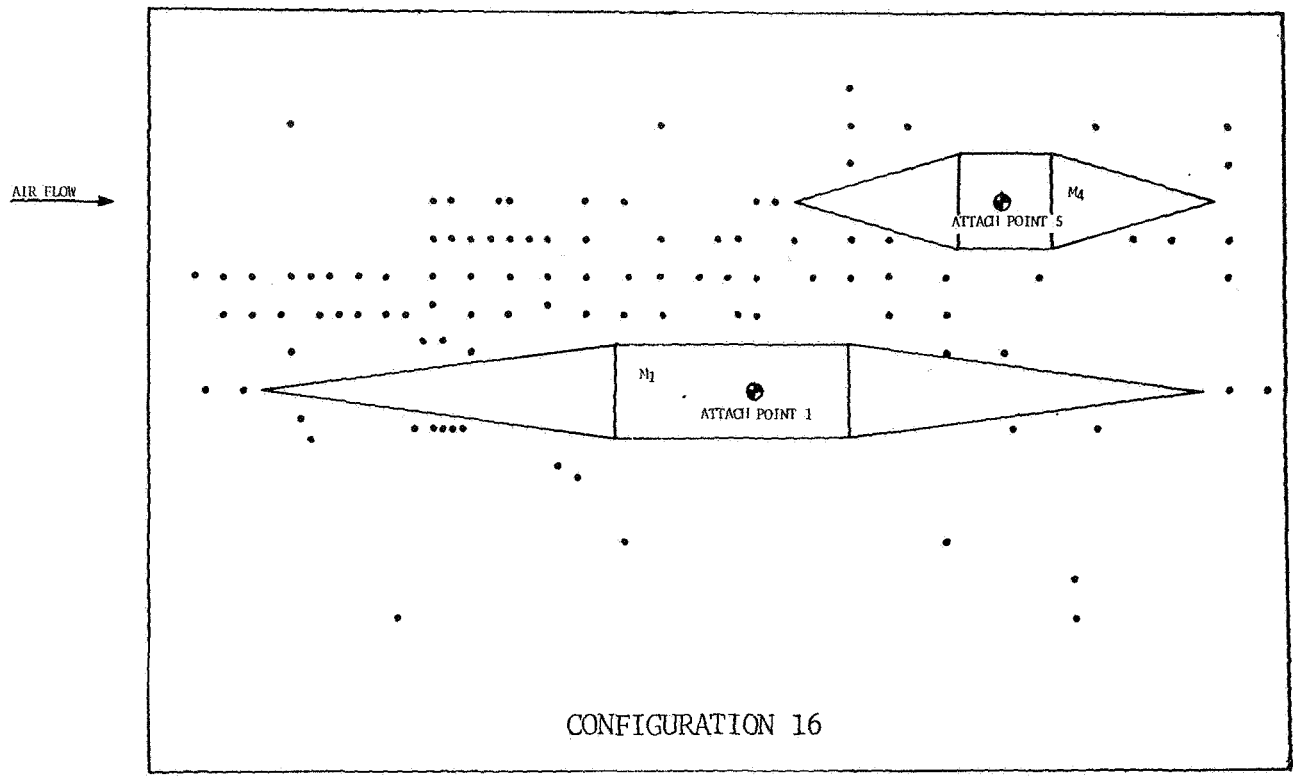

CONFIGURATION 16

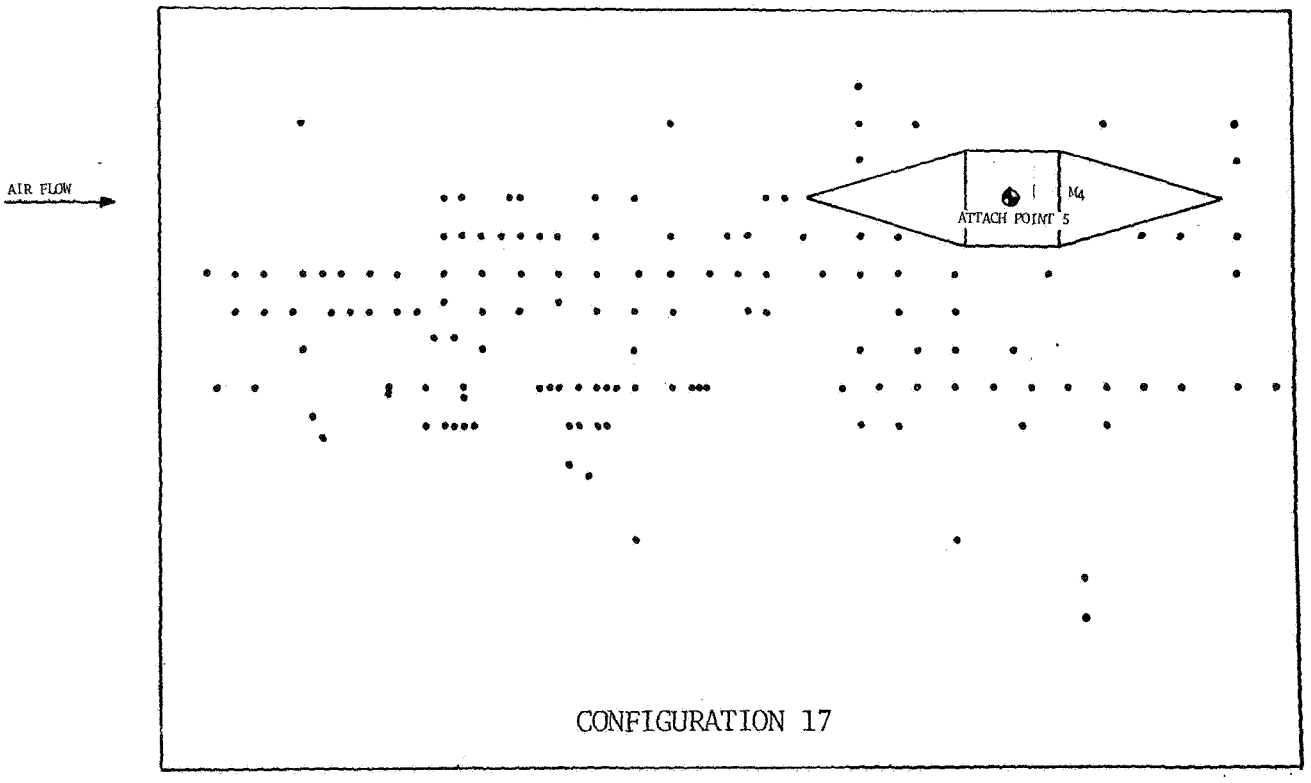

CONFIGURATION 17

FIGURE 2-1. MULTIPLE-PROTUBERANCE TEST CONFIGURATIONS (Continued)

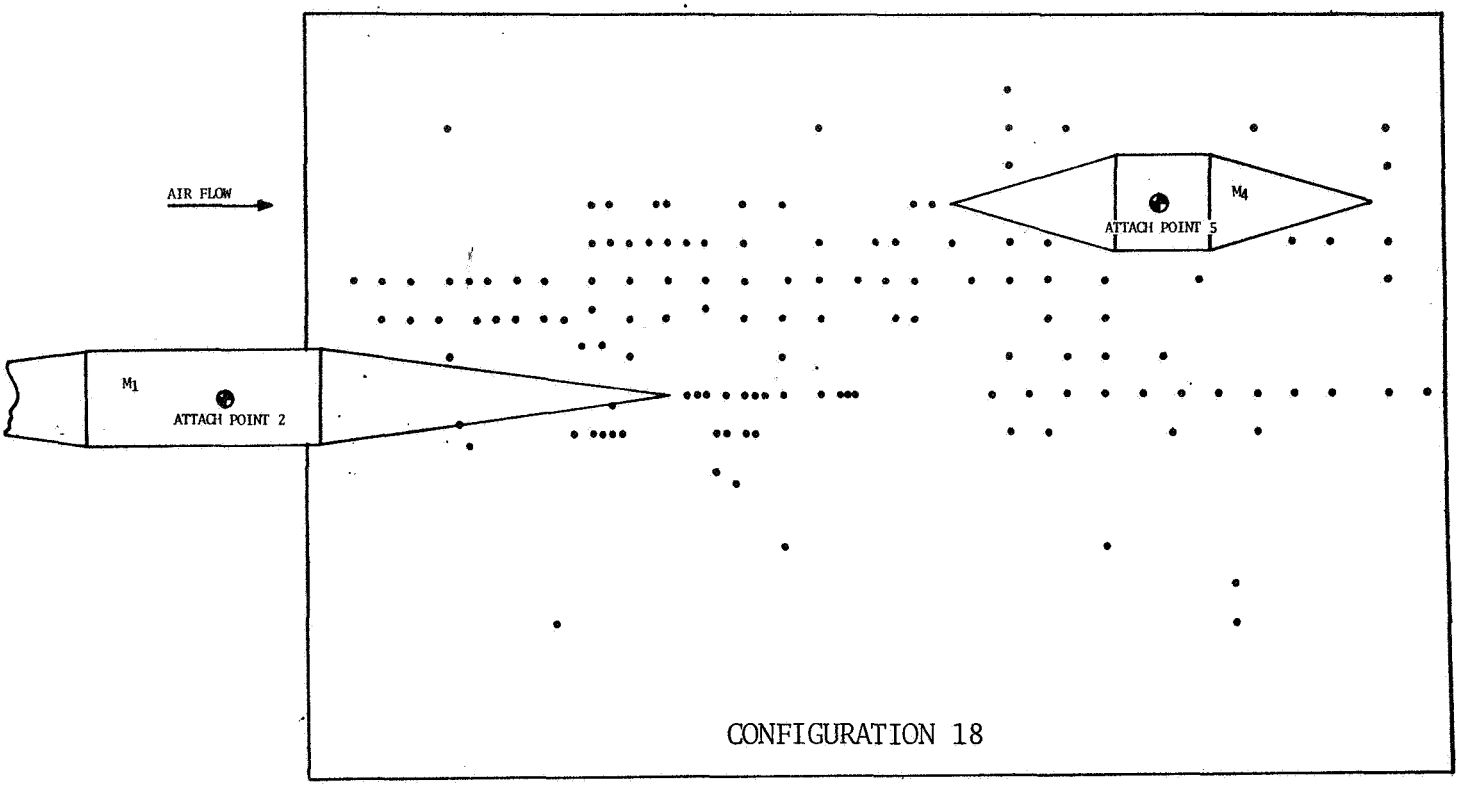

CONFIGURATION 18

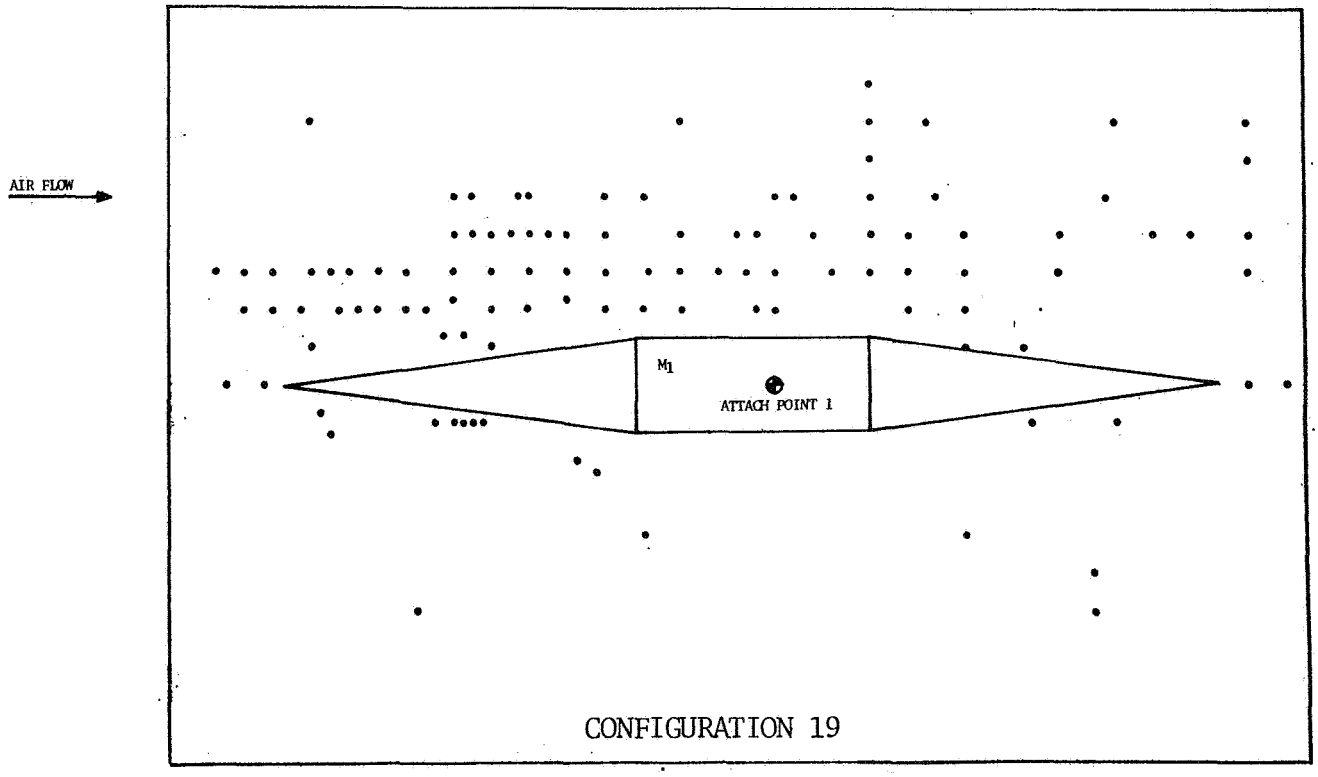

CONFIGURATION 19

FIGURE 2-1. MULTIPLE-PROTUBERANCE TEST CONFIGURATIONS (Concluded)

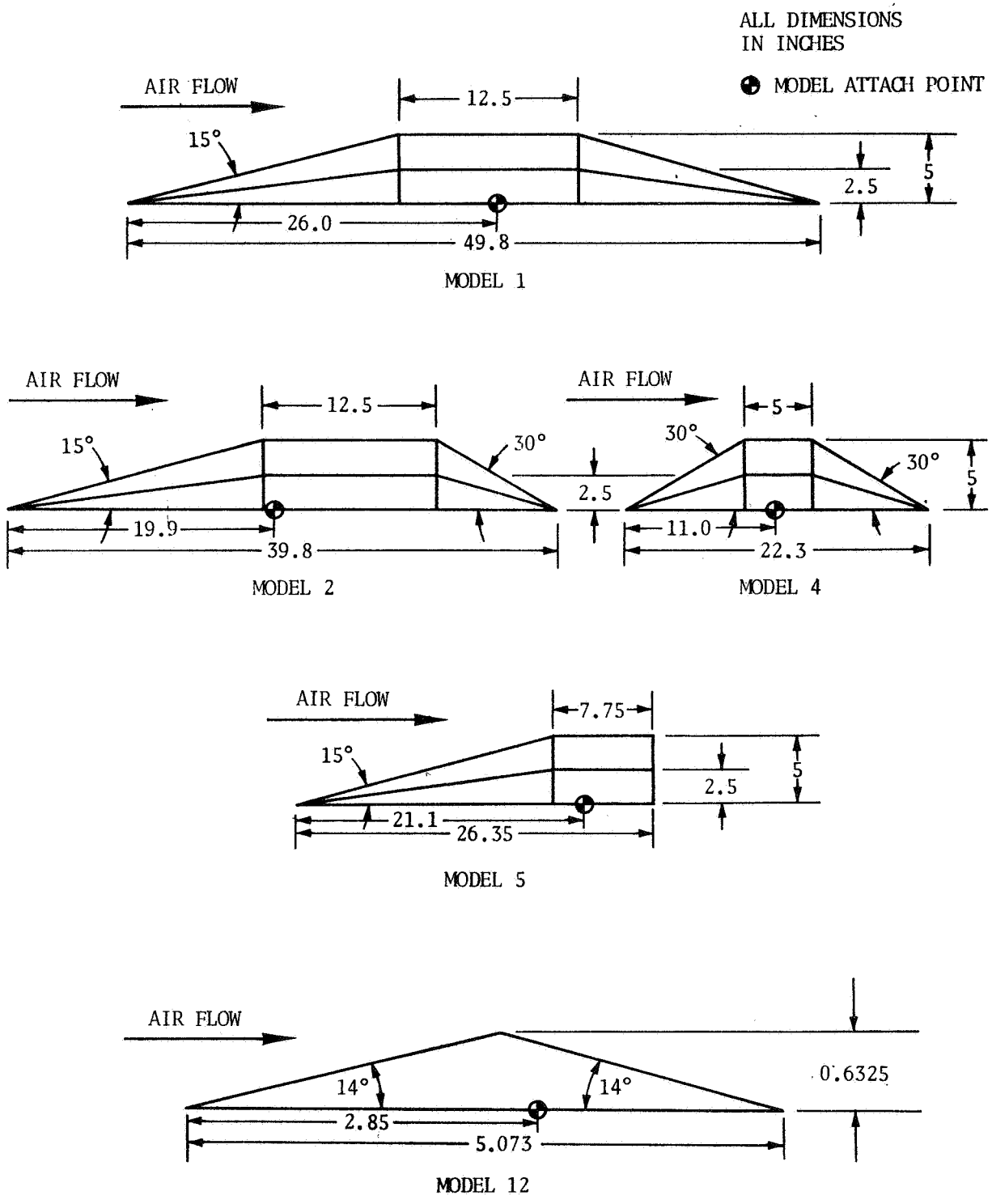

FIGURE 2-2. SCHEMATIC DRAWINGS OF GENERAL PROTUBERANCE MODELS

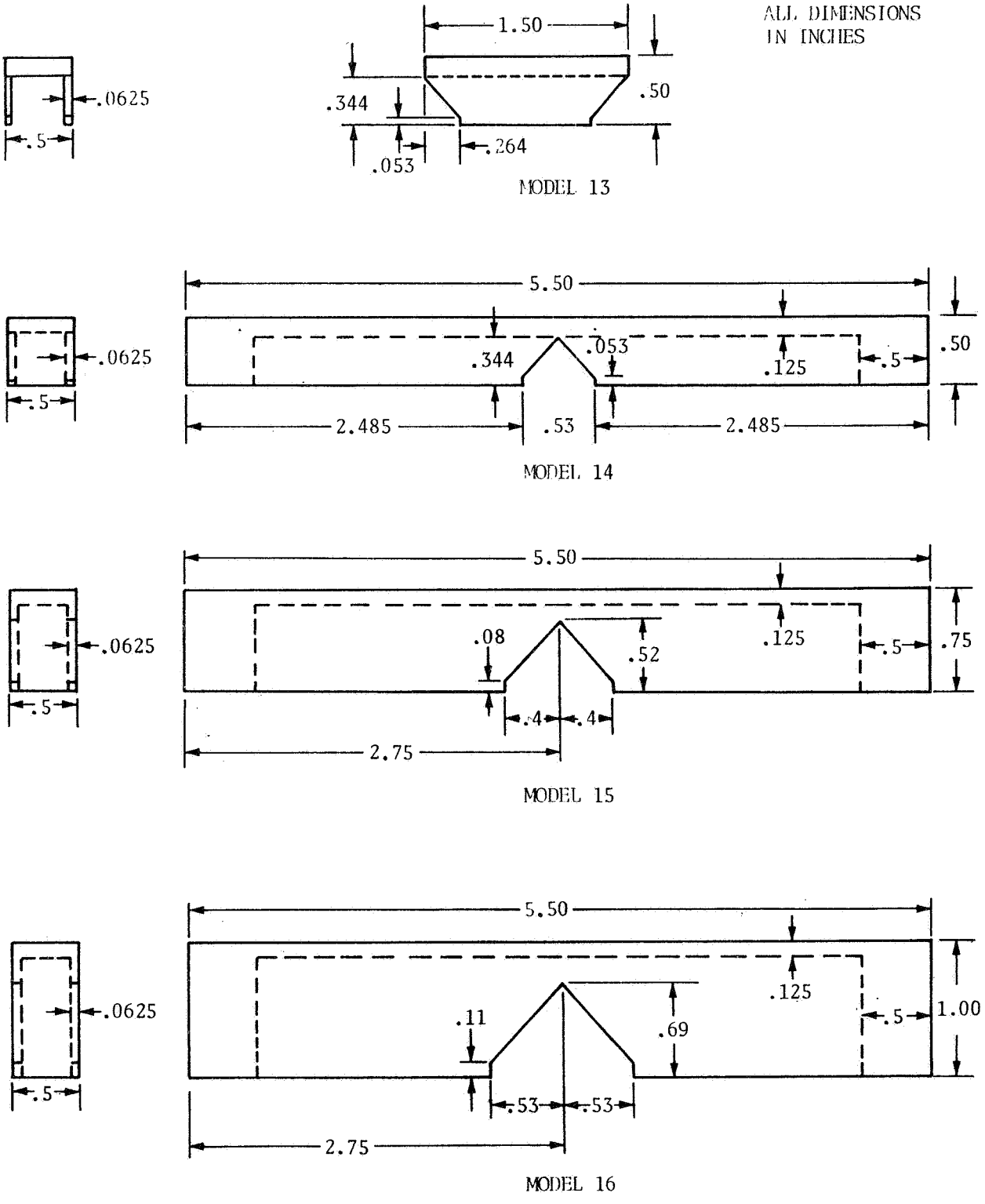

FIGURE 2-3. SCHEMATIC DRAWINGS OF HAT SECTION PROTUBERANCE MODELS

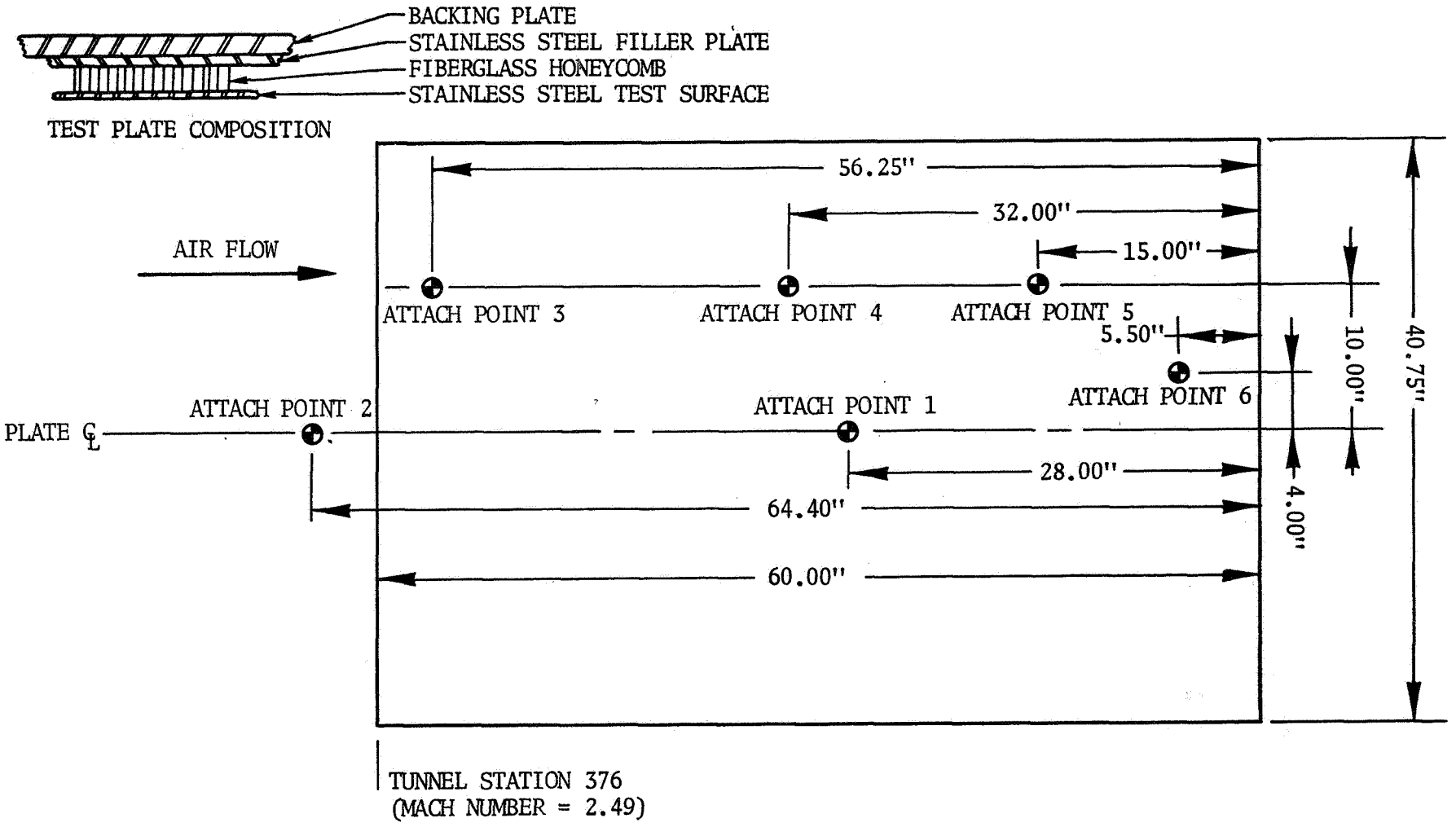

FIGURE 2-4. TEST PLATE, MODEL ATTACH POINT LOCATIONS AND NOMENCLATURE

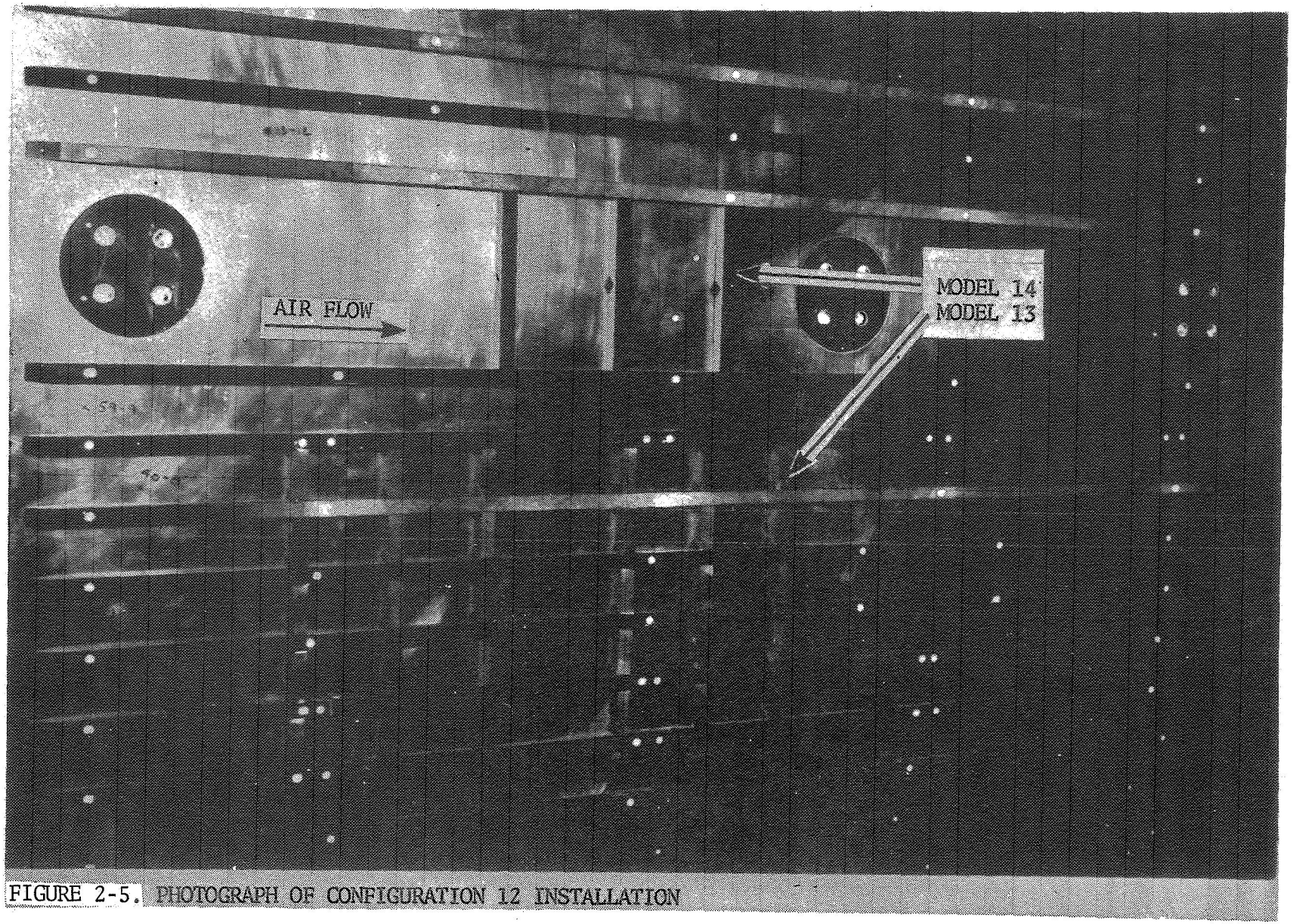

FIGURE 2-5. PHOTOGRAPH OF CONFIGURATION 12 INSTALLATION

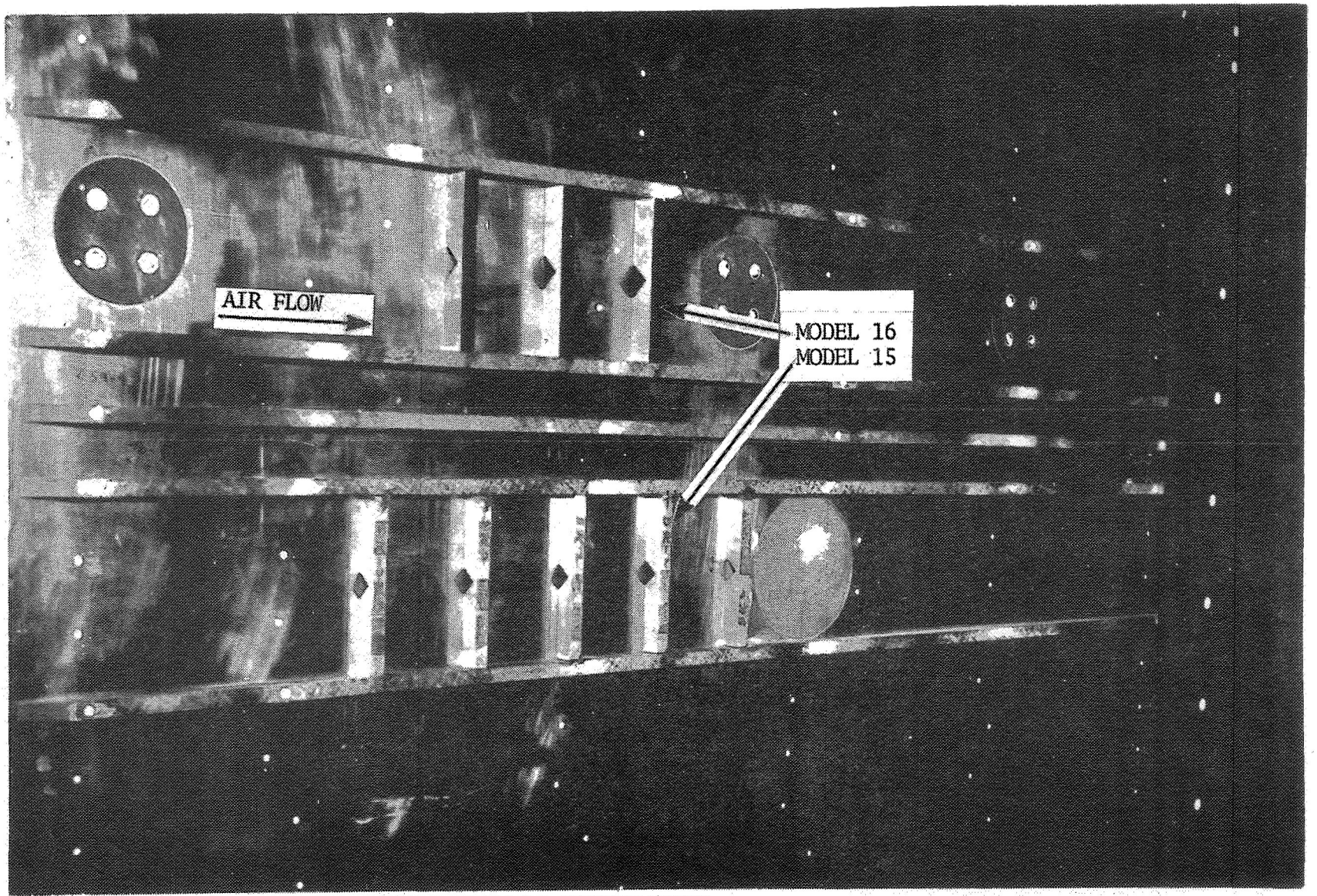

FIGURE 2-6. PHOTOGRAPH OF CONFIGURATION 13 INSTALLATION

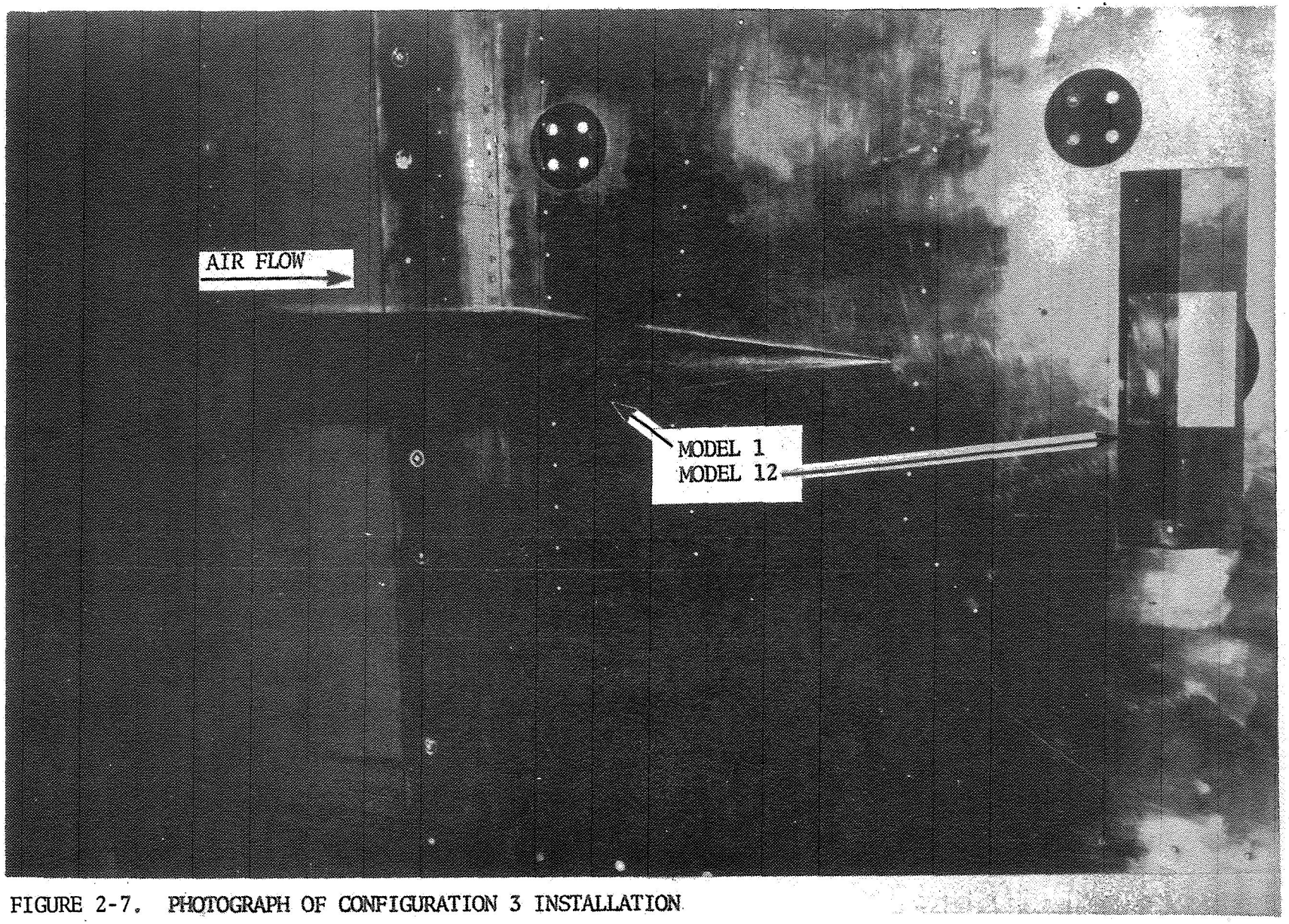

FIGURE 2-7. PHOTOGRAPH OF CONFIGURATION 3 INSTALLATION

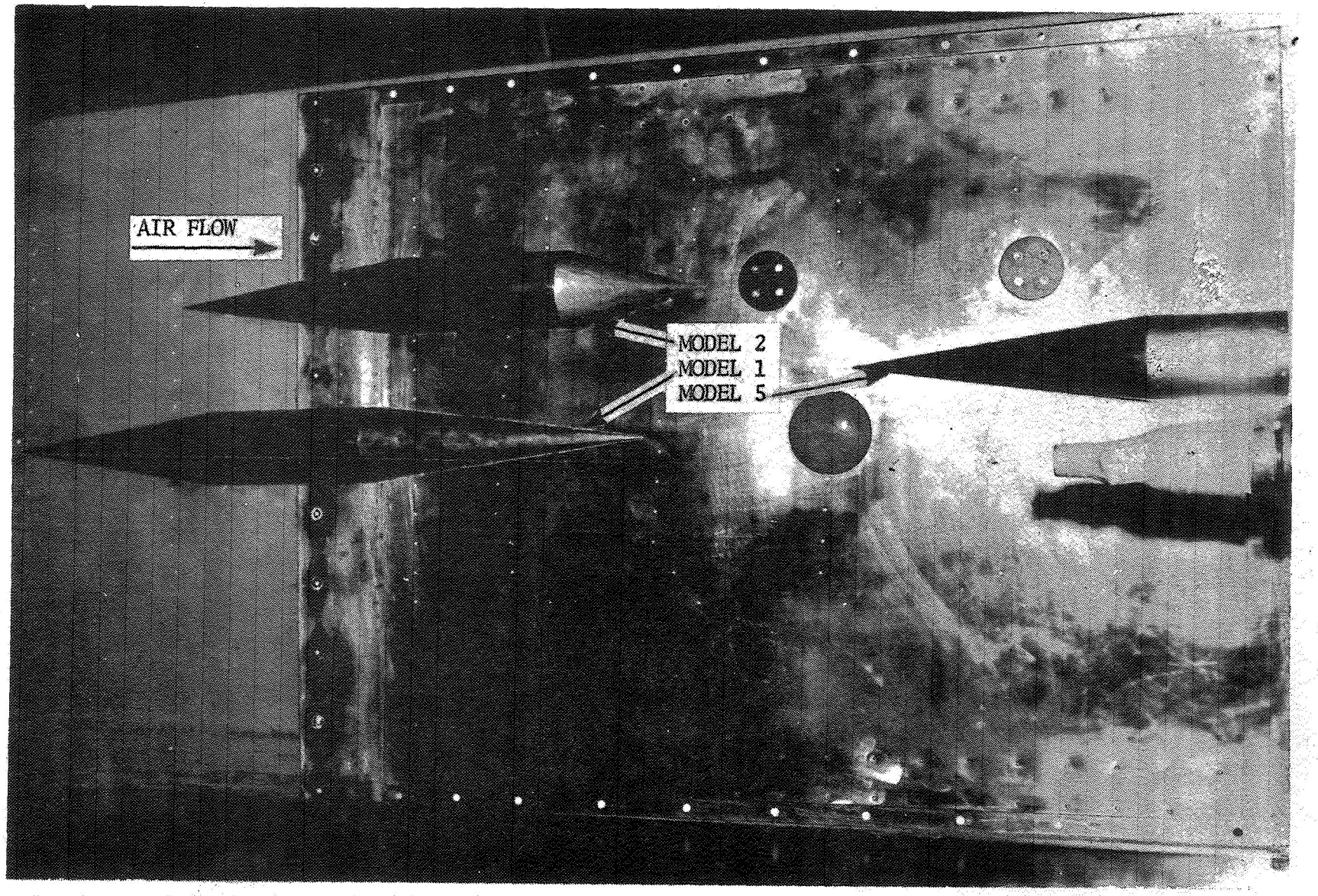

FIGURE 2-8. PHOTOGRAPH OF CONFIGURATION 8 INSTALLATION

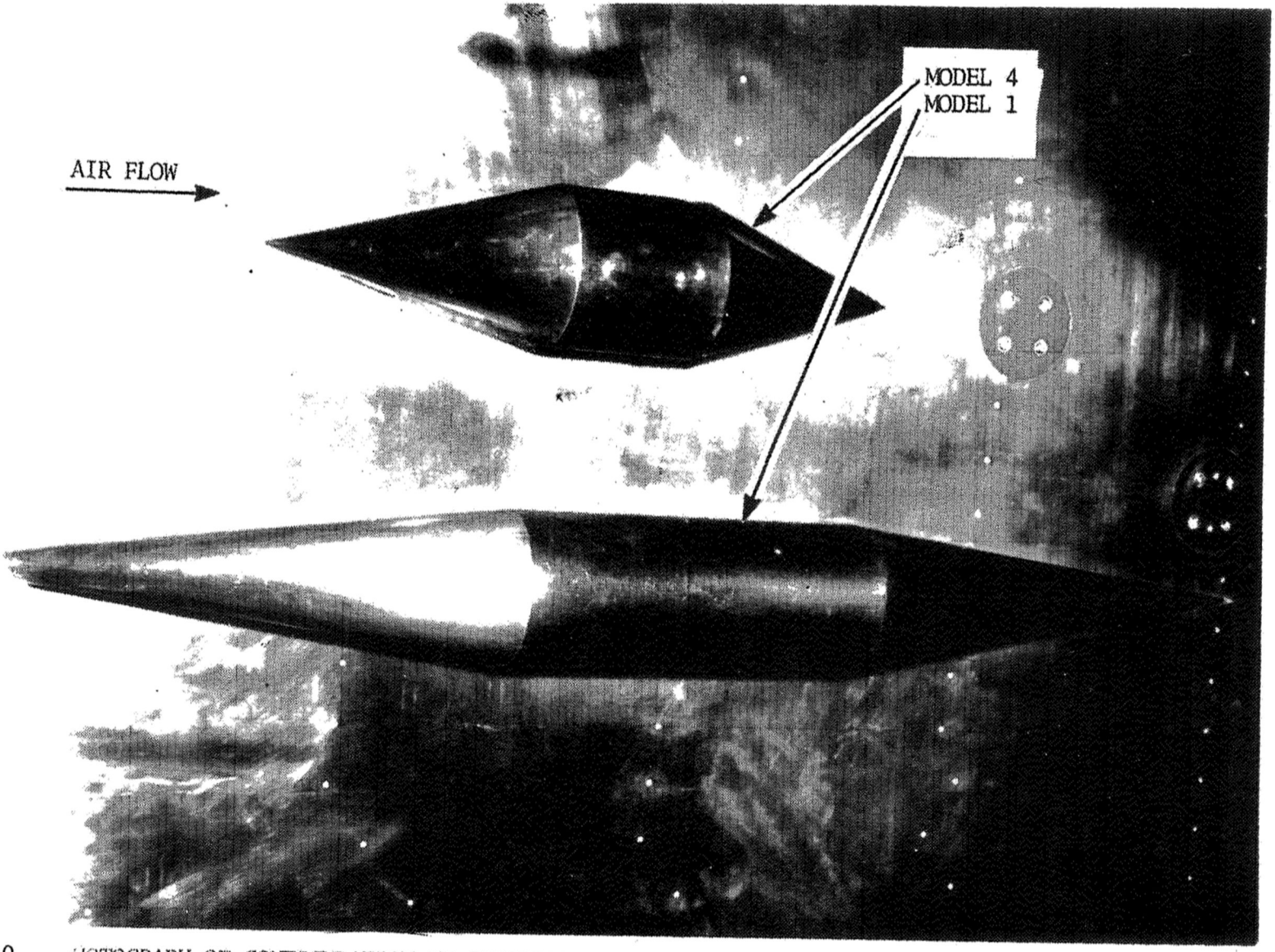

FIGURE 2-9. PHOTOGRAPH OF CONFIGURATION 15 INSTALLATION

TABLE 2-I. (Continued)

LANGLEY MULTIPLE-PROTUBERANCE TEST RUN SCHEDULE

RUN POINT	CONFIGURATION	MACH NO.	REYNOLDS NO./ FTx10^6	TOTAL TEMP. °R	TOTAL PRESS. PSF	PARAMETER INVESTIGATED
1-3	11	2.49	3.14	610	2799	M_{13} induced pressure field (pressure measurements during Run 1 only)
4		2.49	2.86		2550	
6		3.51	3.00		4241	
8		4.44	3.00	635	7267	
2-1	12	2.49	3.12	708	3237	M_{13} and M_{14} induced heating
2		3.51	3.00	706	5406	
3		4.44	3.25	678	8673	
3-2	12	2.49	3.07	709	3199	Configuration 12 repeated due to model difficulties during Run 2.
3		3.51	3.06	689	5318	
4		4.44	3.20	684	8670	
4-1	13	2.49	3.10	709	3211	M_{15} and M_{16} induced heating
2		3.51	3.00	707	5413	
3		4.44	3.16	689	8651	
5-1	14	3.51	3.05	697	5377	M_4 reference values
2		4.44	3.19	676	8511	
3		2.49	3.13	696	3171	
6-1	15	2.49	3.08	708	3187	M_4 shock impingement on M_1 forebody
2		3.51	3.01	702	5376	
3		4.44	3.07	687	8690	
7-6	19	2.49	3.06	712	3200	M_1 reference values
7		3.51	2.99	706	5385	
8		4.44	3.18	687	8680	
8-1	16	2.49	3.11	700	3176	M_4 shock impingement on M_1 afterbody
2		3.51	3.01	700	5330	
3		4.44	3.14	690	8654	

NOTES: M_1, M_2, M_4, M_5 and M_{12} are instrumented except for M_1 which is only instrumented on runs 6, 7 and 8. Stringer number 11 instrumented with thermocouples on runs 2 and 3. Stringer number 9 instrumented with pressure orifices on run 1.

TABLE 2-I. (Continued)

LANGLEY MULTIPLE-PROTUBERANCE TEST RUN SCHEDULE

RUN POINT	CONFIGURATION	MACH NO.	REYNOLDS NO./ FTx10^6	TOTAL TEMP. °R	TOTAL PRESS. PSF	PARAMETER INVESTIGATED
9-1	17	2.49	3.13	699	3189	M_4 reference values
2		3.51	2.99	706	5391	
3		4.44	3.18	686	8686	
10-1	1	2.49	3.04	713	3179	Clean plate reference values
2		3.51	2.96	710	5373	
3		4.44	3.20	684	8668	
11-1	9	2.49	3.09	710	3220	Effect of stringers on Configuration 8
2		3.51	2.98	711	5401	
3		4.44	3.17	689	8658	
12-1	8	2.49	3.07	714	3219	M_5 in M_1/M_2 combination wake
2		3.51	2.95	713	5390	
3		4.44	3.11	690	8591	
13-1	5	2.49	3.05	715	3207	M_5 in M_1 wake
2		3.51	2.98	711	5402	
3		4.44	3.19	683	8612	
14-1	6	2.49	3.04	718	3209	M_5 reference values
2		3.51	2.97	712	5392	
3		4.44	3.15	689	8630	
15-1	7	2.49	3.05	718	3219	M_2 reference values
2		3.51	2.95	711	5351	
3		4.44	3.14	685	8561	
16-1	4	2.49	3.05	715	3207	M_1 wake
2		3.51	2.97	711	5386	
3		4.44	3.11	693	8606	

NOTES: M_1, M_2, M_4, M_5 and M_{12} are instrumented except for M_1 which is only instrumented on runs 6, 7 and 8. Stringer number 11 instrumented with thermocouples on runs 2 and 3. Stringer number 9 instrumented with pressure orifices on run 1.

TABLE 2-I. (Concluded)

LANGLEY MULTIPLE-PROTUBERANCE TEST RUN SCHEDULE

RUN POINT	CONFIGURATION	MACH NO.	REYNOLDS NO./ FTx10^6	TOTAL TEMP. °R	TOTAL PRESS. PSF	PARAMETER INVESTIGATED
17-1	18	2.49	3.08	711	5207	M_4 in M_1 wake
2		3.51	2.99	707	5380	
3		4.44	3.15	689	8611	
18-1	3	2.49	3.06	714	3214	M_{12} in M_1 wake
2		3.51	2.97	709	5388	
3		4.44	3.23	680	8626	
19-1	2	2.49	3.05	717	3216	M_{12} reference values
2		3.51	2.95	713	5387	
3		4.44	3.16	686	8616	
20-1	10	2.49	3.08	712	3222	Plate with stringers reference values
2		3.51	2.95	712	5380	
3		4.44	3.14	691	8666	

NOTES: M_1, M_2, M_4, M_5 and M_{12} are instrumented except for M_1 which is only instrumented on runs 6, 7 and 8. Stringer number 11 instrumented with thermocouples on runs 2 and 3. Stringer number 9 instrumented with pressure orifices on run 1.

3.0 TEST PLATE ENVIRONMENT

Heating environments on the clean plate and stringer plate configurations and the protuberance effects on the test plate are discussed in the following paragraphs. A complete tabulation of test data is presented in Reference 1. Heat-transfer coefficient ratios for the test plate are presented in Appendix A for all test configurations and Mach numbers.

3.1 CLEAN PLATE AND PLATE WITH STRINGERS

Heat-transfer coefficients on the clean plate centerline are presented in Figure 3-1 as a function of distance from the plate leading edge. Corresponding measurements from a previous protuberance test (Reference 3) are included for comparison. The differences between present measurements and those presented in Reference 3 are attributable to data accuracy limits and variations in test surface flatness.

Theoretical flat plate heat-transfer coefficients were determined by the method of Van Driest for turbulent flow (References 4 and 5). The theoretical values are based on tunnel conditions, measured wall temperatures, a 5.0 inch boundary layer thickness, and Reynolds number per foot of 3.0×10^6. The Langley Unitary Plan Wind Tunnel test section boundary layer profiles used in the analysis were taken from Reference 2. Analytically determined heat-transfer coefficients are compared with the test results in Figure 3-2. The calculated coefficients exceed the test results at all Mach numbers. Heat loss through the support structure, which reduces the experimentally determined heat-transfer coefficient, was estimated to be about 10 percent. However, this accounts for only a portion of the difference between experimental data and analysis. Previous investigators (Reference 6) have reported similar non-correlation of analytical calculations and Langley protuberance test data. Reference 6 indicates that clean plate data correlation is improved by using a calculated recovery temperature (T_r) rather than the measured equilibrium temperature (T_e) in the data reduction equations. This procedure effectuates increases in the experimentally determined heat-transfer coefficients by a factor of approximately $(T_e - T_w)/(T_r - T_w)$. Application of this correction factor to the present clean plate data resulted in increases in the measured heat-transfer coefficient ranging from about 10 percent at Mach number 2.49 to about 25 percent at Mach number 4.44 as shown in Figure 3-2.

Heat-transfer coefficients obtained on the plate with longitudinal stringers (configuration 10) are presented in Figure 3-3 compared to clean plate data for each Mach number. The stringers reduce the clean plate coefficients about 10 percent at $M_\infty = 2.49$, 25 percent at $M_\infty = 3.51$, and 35 percent at $M_\infty = 4.44$. This reduced heating effect may be partially due to disturbances caused by the stringer leading edges.

3.2 PLATE ENVIRONMENT WITH ATTACHED SINGLE AND MULTIPLE-PROTUBERANCE MODELS

Heat-transfer coefficients measured on the test plate with protuberance models attached were reduced to ratio form (h/h_o) by division of the measured value by the clean plate heat-transfer coefficient obtained at the same measurement location. These ratios are shown in Figures A-1 through A-48 of the Appendix. Presentation of the data in ratio form reduced the effects of test plate fabrication imperfections and uncertainties in the thermal properties of the test plate material.

The test plate surface heat-transfer coefficient ratios presented in Appendix A indicate significant increases in the regions influenced by protuberance forebody compressions and protuberance wakes.

Two dimensional free stream oblique shock angles have been superimposed on selected figures in the Appendix for comparison with the heat-transfer coefficient ratios. It is evident after studying these figures, that the increases in heating begin a little ahead of the free stream shock location and extend down stream. The thick tunnel wall boundary layer causes the shock to affect the surface forward of the free-stream shock location.

The test plate heat-transfer coefficient ratios (h/h_o) as a function of distance (X) along the test plate at a constant distance (Y) from the plate centerline are presented in Figures 3-4 through 3-12 for various single and multiple-protuberance combinations at each test Mach number. These distributions are considered to be representative of the prominant heating effects measured on the test plate surface.

Figures 3-4 through 3-6 compare the heat-transfer coefficient ratios obtained on the plate centerline (Y = 0) for a double-wedge model (Model 12) mounted in the center of Model 1 wake to those obtained with Model 1 wake alone and Model 12 wake alone. The maximum h/h_o value for the Model 1 and Model 12 combination was greater at each Mach number than that for the Model 1 wake alone, and did not exceed a magnitude of 1.83. These increases occurred near the Model 12 base and did not persist over appreciable distances along the plate. At extreme downstream measurement locations the influence of Model 12 on the Model 1 wake was small. The double-wedge model generated less of a heating effect than Model 1 due to the double-wedge height of 0.6325 inches compared to Model 1 height of 5.0 inches. The h/h_o values in the Model 1 (15 degree afterbody) wake did not consistently increase with free-stream Mach number and exhibited a maximum value of 1.66 at $M_\infty = 2.49$. The heat-transfer coefficient ratio distributions obtained at the higher Mach numbers are, in general, more irregular (compare Figures 3-4 through 3-6) because of the decreased data accuracy at the higher Mach numbers.

3.2 (Continued)

Other configurations tested which consisted of a single protuberance model mounted in the proximity of the Model 1 wake did not generally increase the h/h_o magnitudes above those obtained in the Model 1 single wake.

Figures 3-7 through 3-9 compare the plate heat-transfer coefficient ratios obtained at locations 8.0 inches from the plate centerline (Y = 8.0) for Model 5 mounted in the aft double wake of Models 1 and 2 to those for Model 2 wake alone and Model 5 alone. Model 5 mounted in the double wake of Models 1 and 2 produced h/h_o magnitudes which exceeded those obtained at the same measurement locations in the Model 2 single wake or in the single Model 5 forebody compression region. However, this increase was not present at all locations upstream of Model 5. The maximum h/h_o values obtained in the double wake region near Model 5 were about equal to those obtained at locations further upstream in the Model 2 single wake (approximately 2.0).

The single wake of Model 2 (30 degree afterbody) induced maximum h/h_o values which did not consistently increase with free-stream Mach number, and did not exceed a magnitude of 2.08.

Figures 3-10 through 3-12 compare the plate heat-transfer coefficient ratios obtained for Model 4 mounted in the forebody compression region of Model 1 to those for Model 4 alone. The largest heating influence occurred near the forebody-centerbody junction of Model 4, and increased consistently with increasing free-stream Mach number to $h/h_o = 2.20$ at $M_\infty = 4.44$. The maximum heating rate obtained in the Model 4 (30 degree forebody) compression region was about equal for Model 4 single and Model 4 and Model 1 mounted in combination.

Heating environments were also obtained with Model 4 mounted in the afterbody expansion region of Model 1 (configuration 16). As seen in Appendix A, Figures A-37 through A-42, the heating effect of Model 4 forebody compression was decreased from that for Model 4 alone by the flow expansion around the Model 1 centerbody-afterbody junction.

The single Model 1 (15 degree forebody) compression effects are given in Appendix A, Figures A-46 through A-48 (configuration 19). The maximum h/h_o magnitude induced by the 15 degree forebody also occurred near the forebody-centerbody junction, but was lower than that for the 30 degree forebody of Model 4. The influence of Model 4 did not significantly increase the h/h_o magnitudes in the proximity of Model 1 forebody.

Theoretical values for the test plate heat-transfer coefficient ratios induced by the 15 and 30 degree forebody shocks were estimated using Van Driest's turbulent flat plate theory and flow properties behind the forebody shock. These estimates were divided by the theoretical clean plate values given in Figure 3-2. The calculated ratios are shown in Figure 3-13 as a function of free-stream Mach number for 15 and 30 degree forebodies. Included in Figure 3-13 are the single model ratios from measurements for Model 1, Model 5 and Model 4 (15, 15 and 30 degree forebodies, respectively). The experimental

3.2 (Continued)

values chosen for comparison are the peak ratios occurring along measurement locations 4.0 inches from the model centerline in the forebody compression region. The measured maximum ratios appear consistently lower than calculated values by 10 to 14 percent for the 15 degree forebody and 12 to 26 percent for the 30 degree forebody throughout the Mach number range. The calculation method thus yields valid effects of Mach number and forebody angle and heat-transfer coefficient ratio magnitudes which compare favorably but are consistently greater than measured maximum ratios. No analyses were made to evaluate protuberance wake flow fields and consequent heating effects.

The effect of stringers on plate heating distributions with attached protuberances was generally to lower the ratios induced on the clean plate (Figures A-22 through A-27). At measurement locations where the stringer plate heat-transfer coefficient ratio was larger than the corresponding clean-plate ratio, the conversion to heat-transfer coefficient magnitude yielded in most cases a lower heating rate in the presence of stringers.

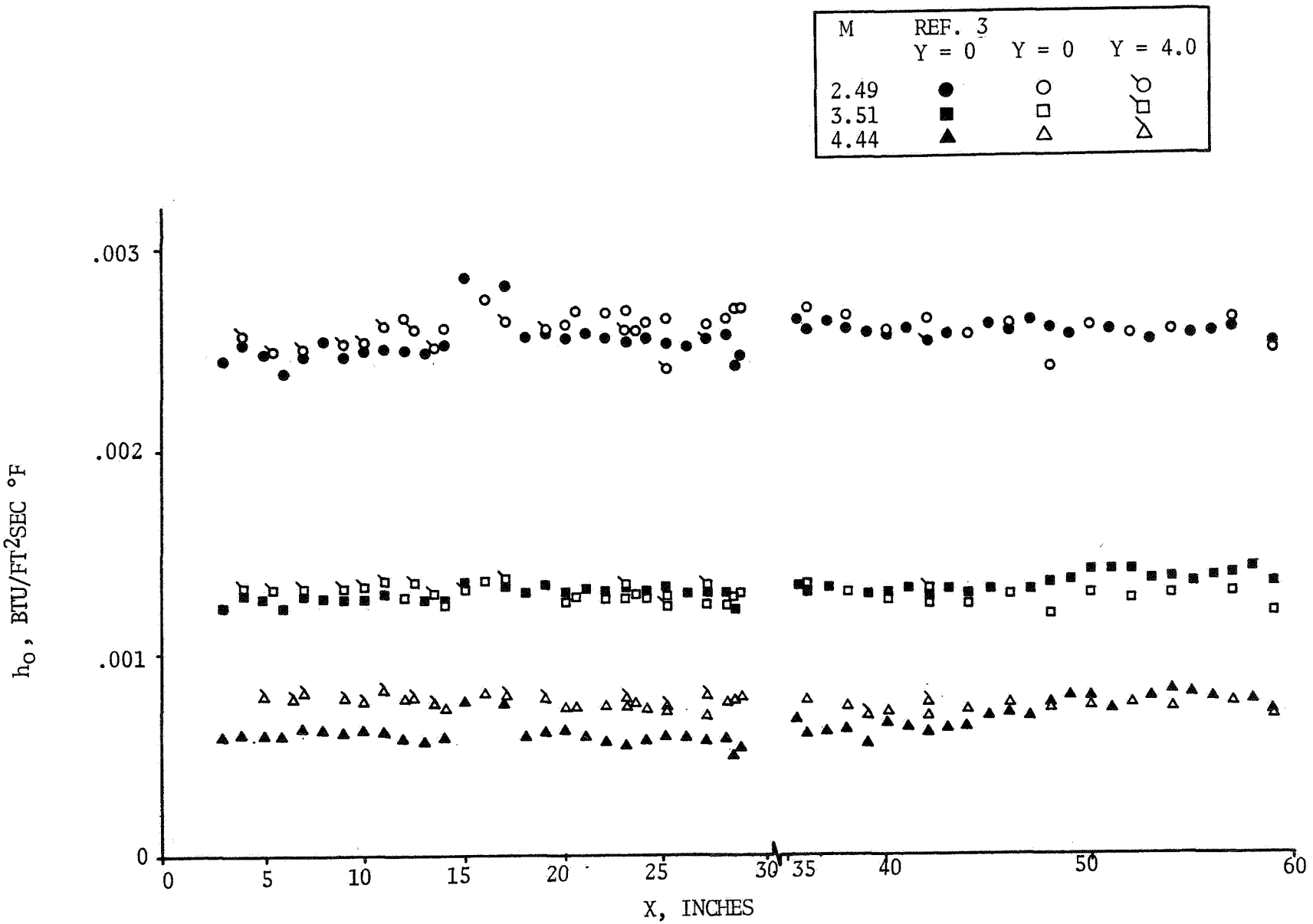

FIGURE 3-1. CLEAN PLATE HEAT-TRANSFER COEFFICIENT VARIATION WITH DISTANCE ALONG PLATE - CONFIGURATION 1

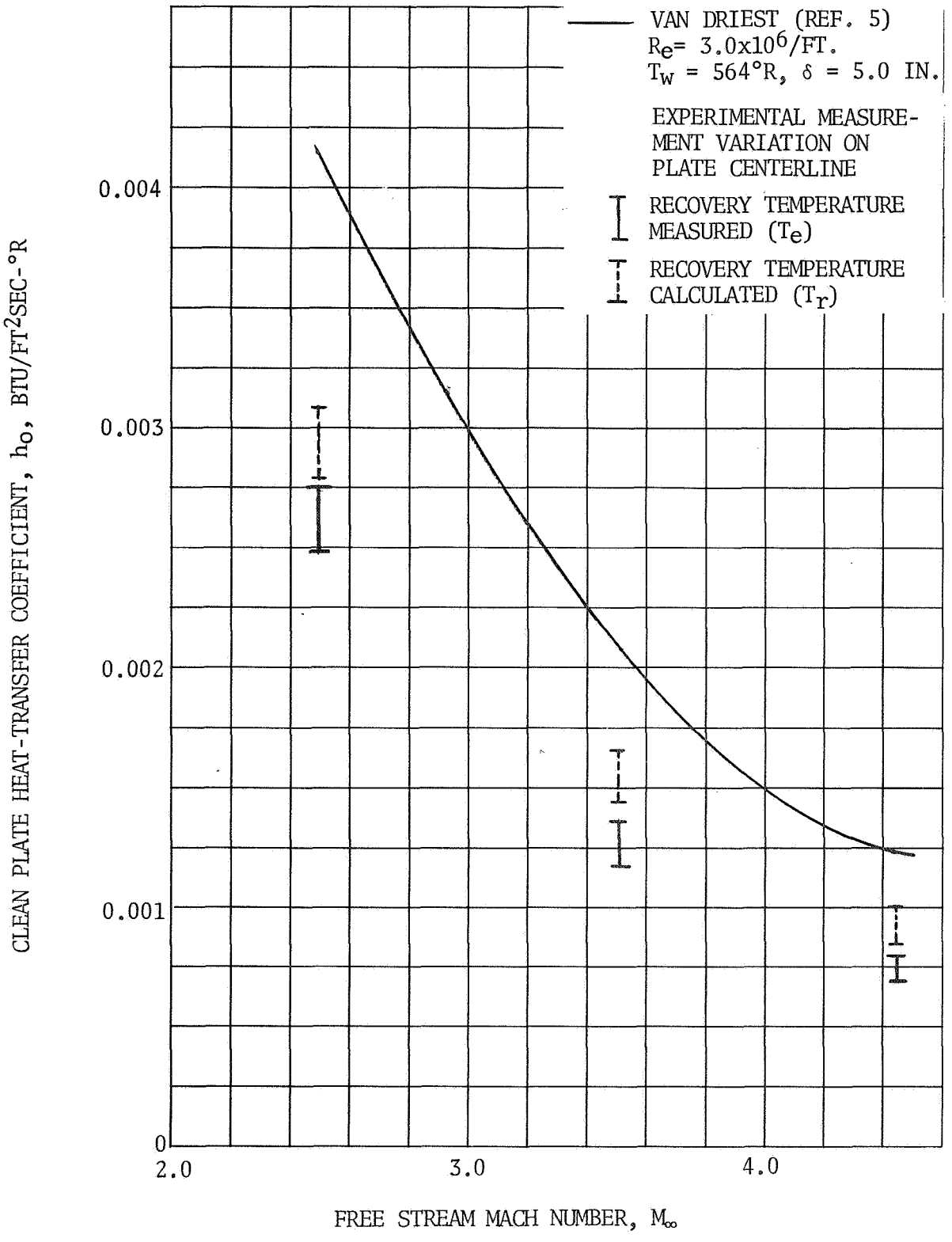

FIGURE 3-2. CLEAN PLATE HEAT-TRANSFER COEFFICIENT VARIATION WITH MACH NUMBER - CONFIGURATION 1

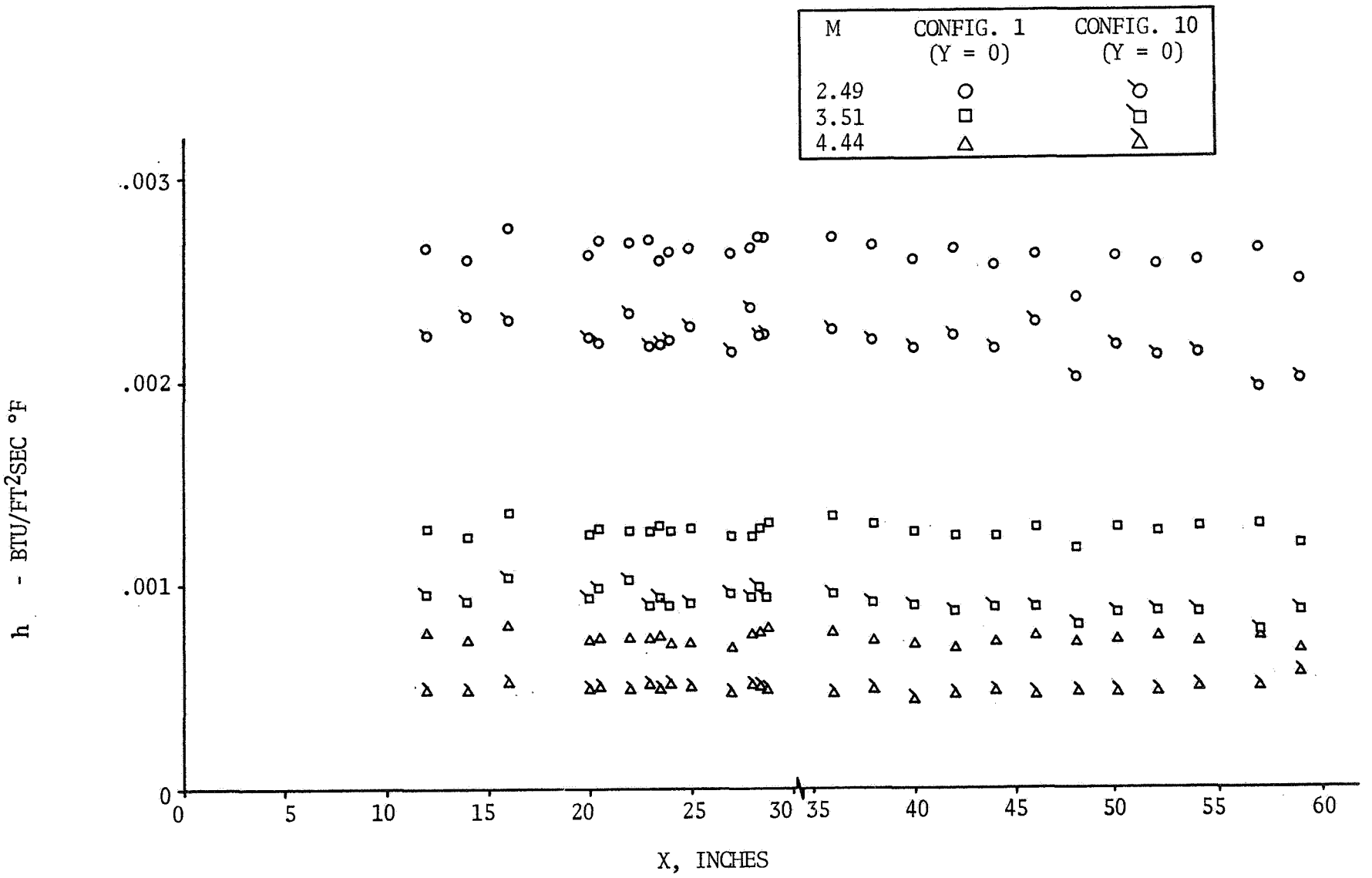

FIGURE 3-3. EFFECT OF STRINGERS ON PLATE HEAT-TRANSFER COEFFICIENT VARIATION WITH DISTANCE ALONG PLATE - CONFIGURATION 10

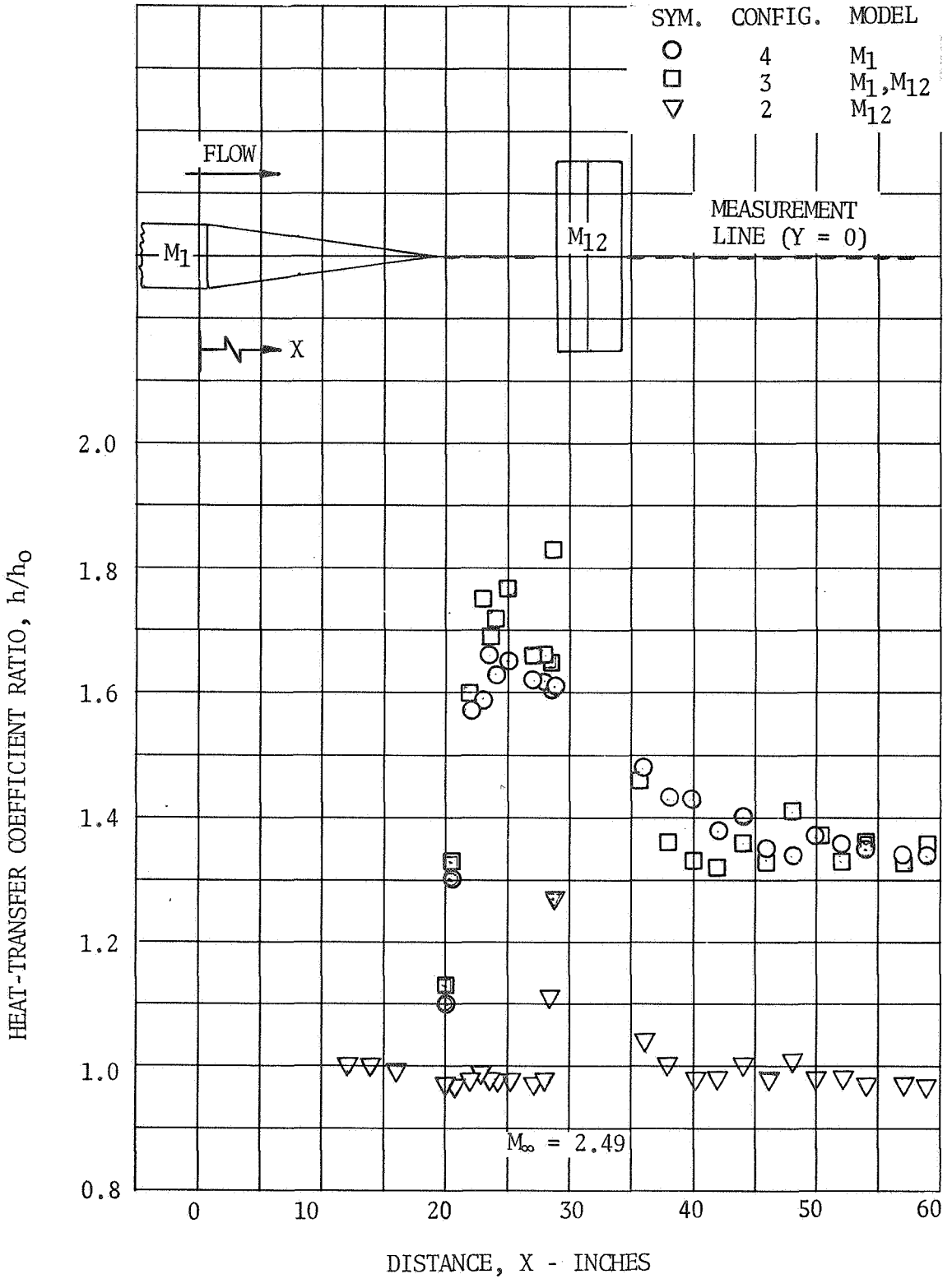

FIGURE 3-4. EFFECT OF DOUBLE WEDGE (MODEL 12) IN MODEL 1 WAKE ON PLATE HEAT-TRANSFER COEFFICIENT RATIO DISTRIBUTION AT MACH NUMBER 2.49 - CONFIGURATIONS 2, 3 AND 4

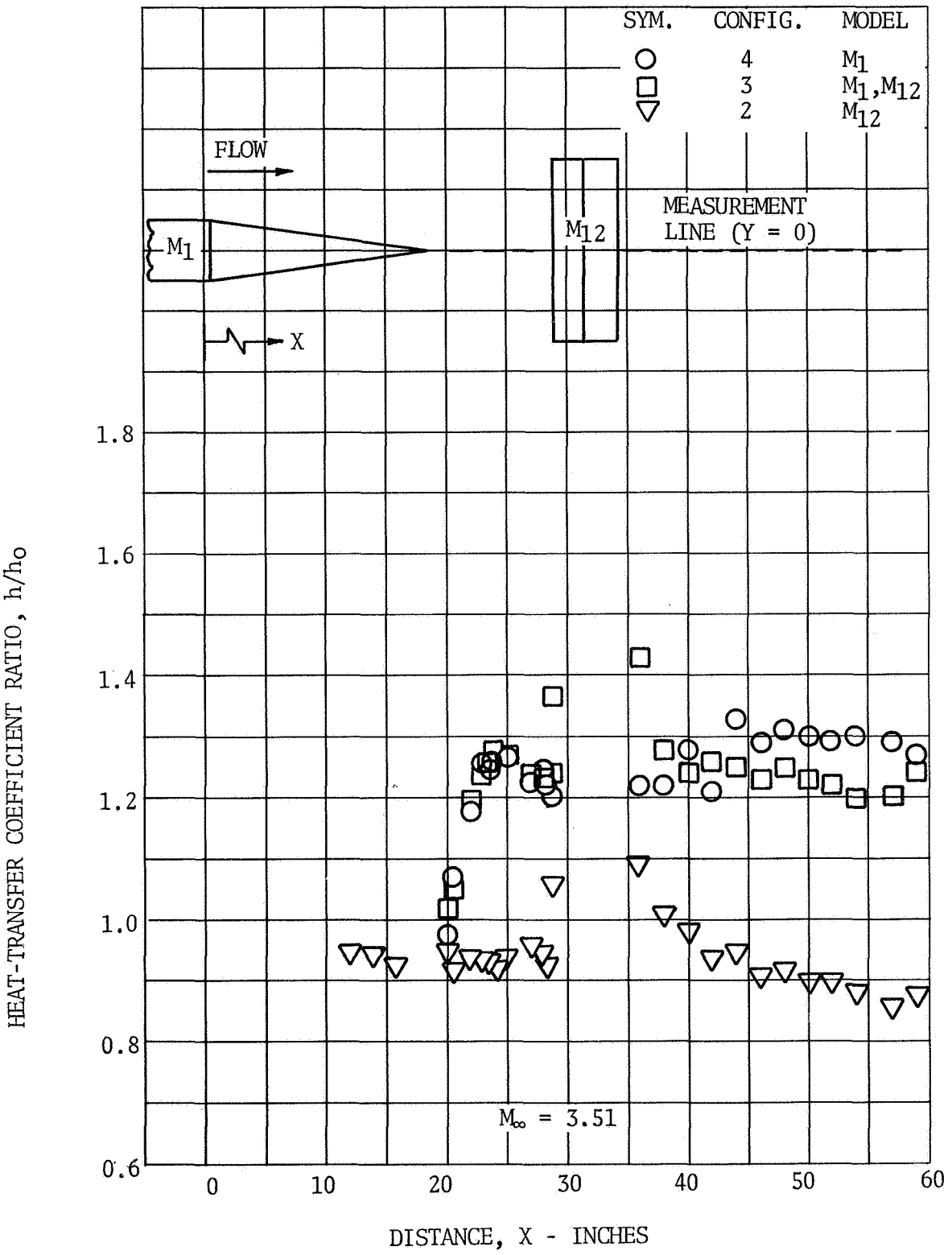

FIGURE 3-5. EFFECT OF DOUBLE WEDGE (MODEL 12) IN MODEL 1 WAKE ON PLATE HEAT-TRANSFER COEFFICIENT RATIO DISTRIBUTION AT MACH NUMBER 3.51 - CONFIGURATIONS 2, 3 AND 4

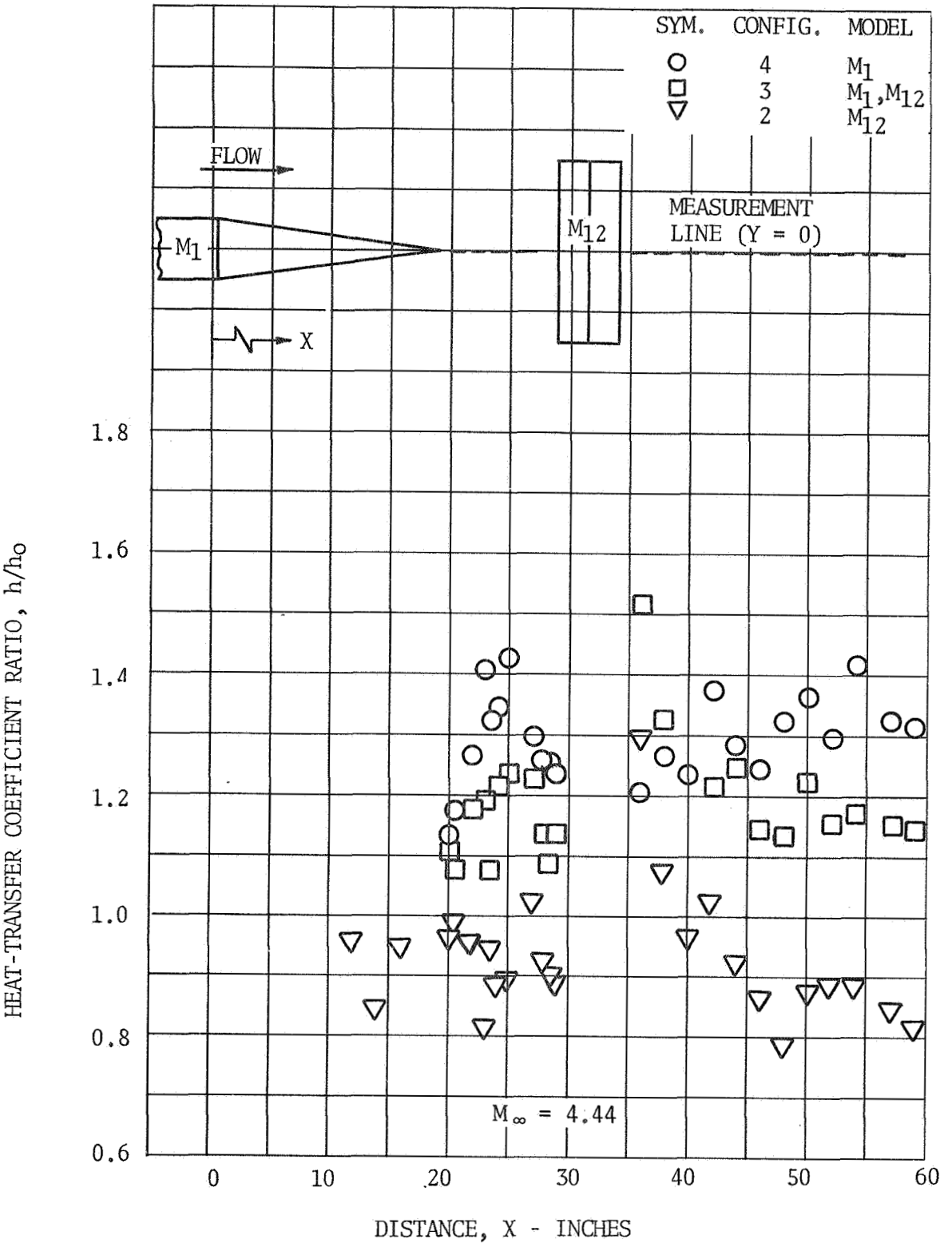

FIGURE 3-6. EFFECT OF DOUBLE WEDGE (MODEL 12) IN MODEL 1 WAKE ON PLATE HEAT-TRANSFER COEFFICIENT RATIO DISTRIBUTION AT MACH NUMBER 4.44 - CONFIGURATIONS 2, 3 AND 4

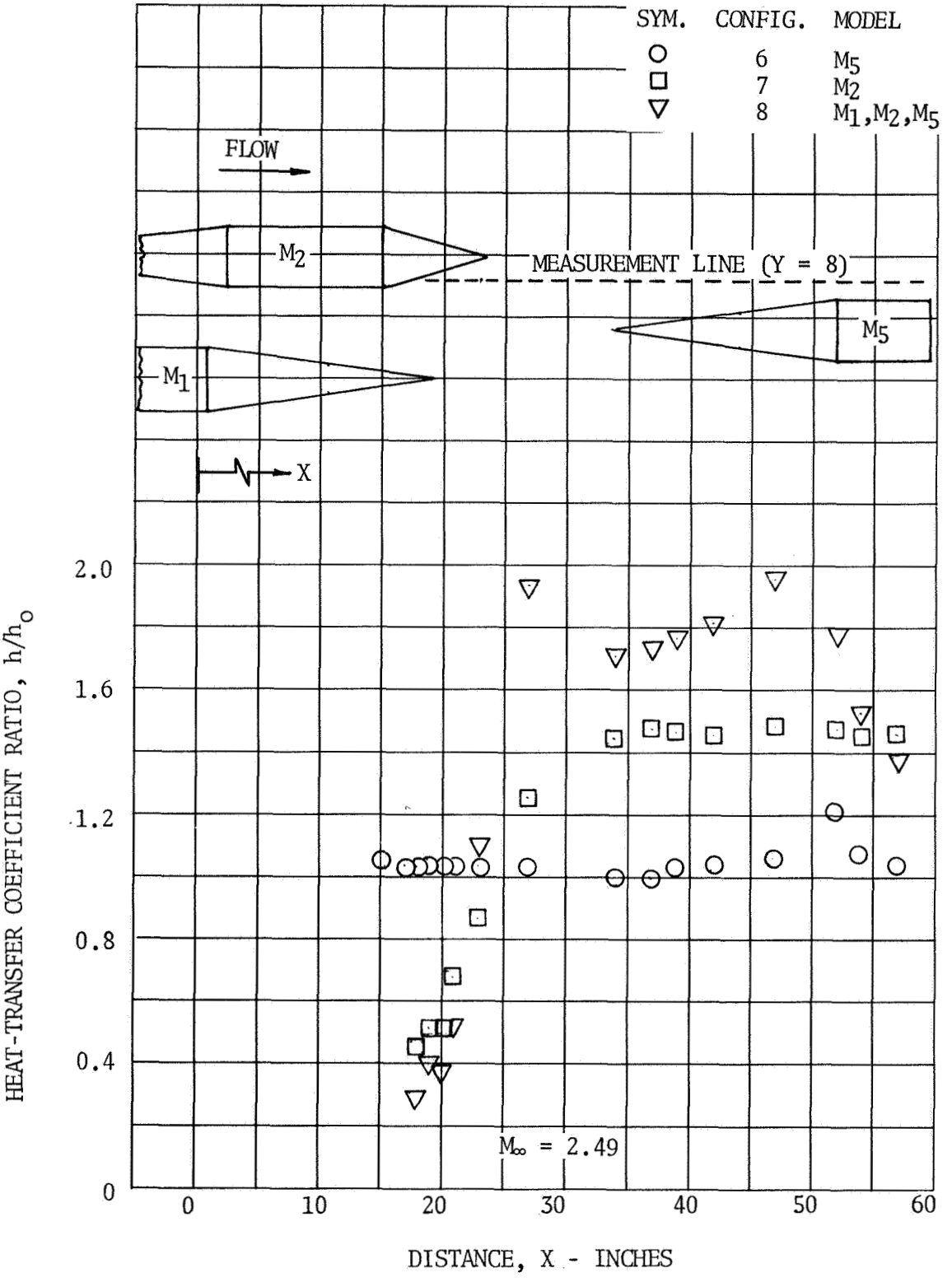

FIGURE 3-7. EFFECT OF MODEL 5 IN MODEL 1 AND 2 DOUBLE WAKE ON PLATE HEAT-TRANSFER COEFFICIENT RATIO DISTRIBUTION AT MACH NUMBER 2.49 - CONFIGURATIONS 6, 7 AND 8

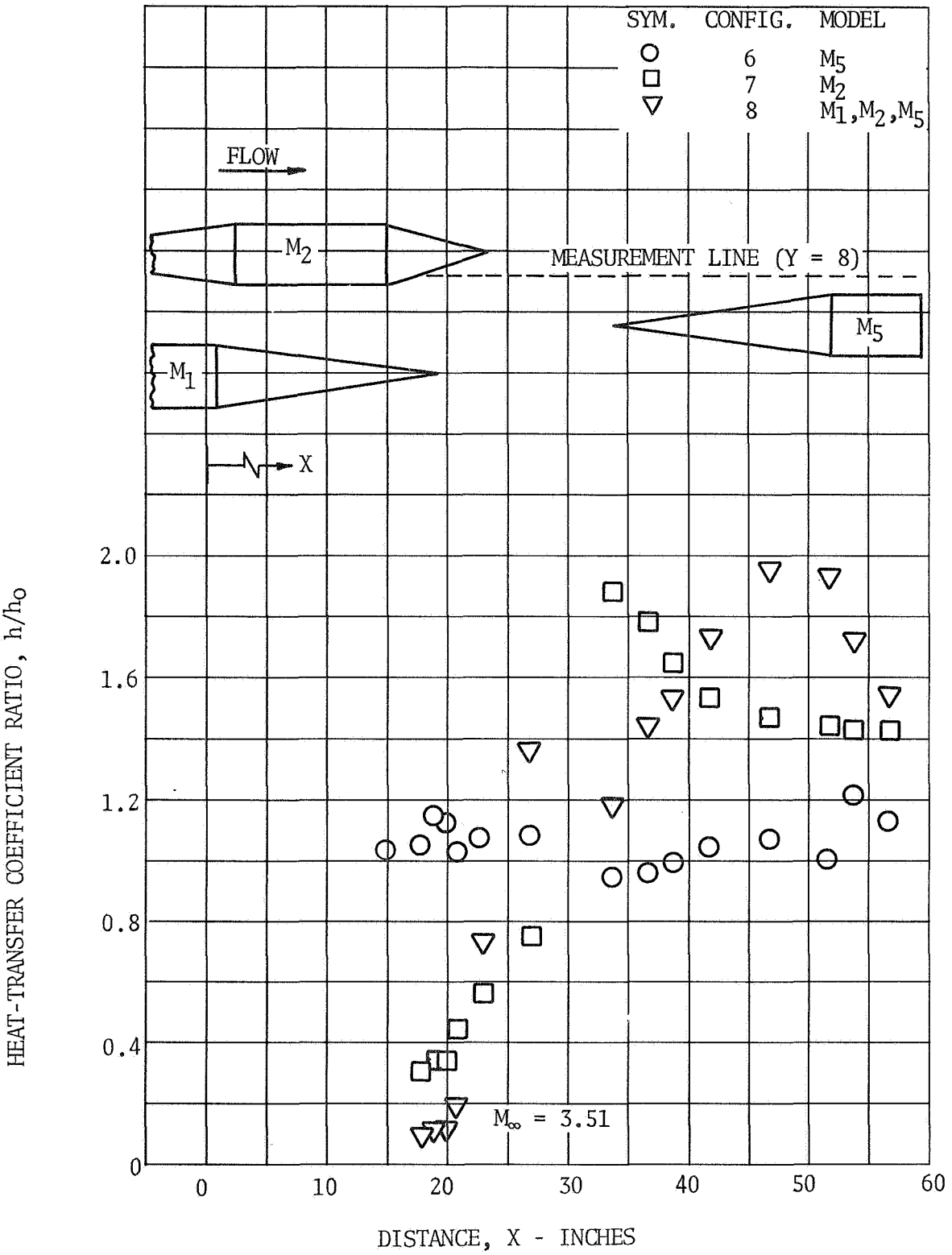

FIGURE 3-8. EFFECT OF MODEL 5 IN MODEL 1 AND 2 DOUBLE WAKE ON PLATE HEAT-TRANSFER COEFFICIENT RATIO DISTRIBUTION AT MACH NUMBER 3.51 - CONFIGURATIONS 6, 7 AND 8

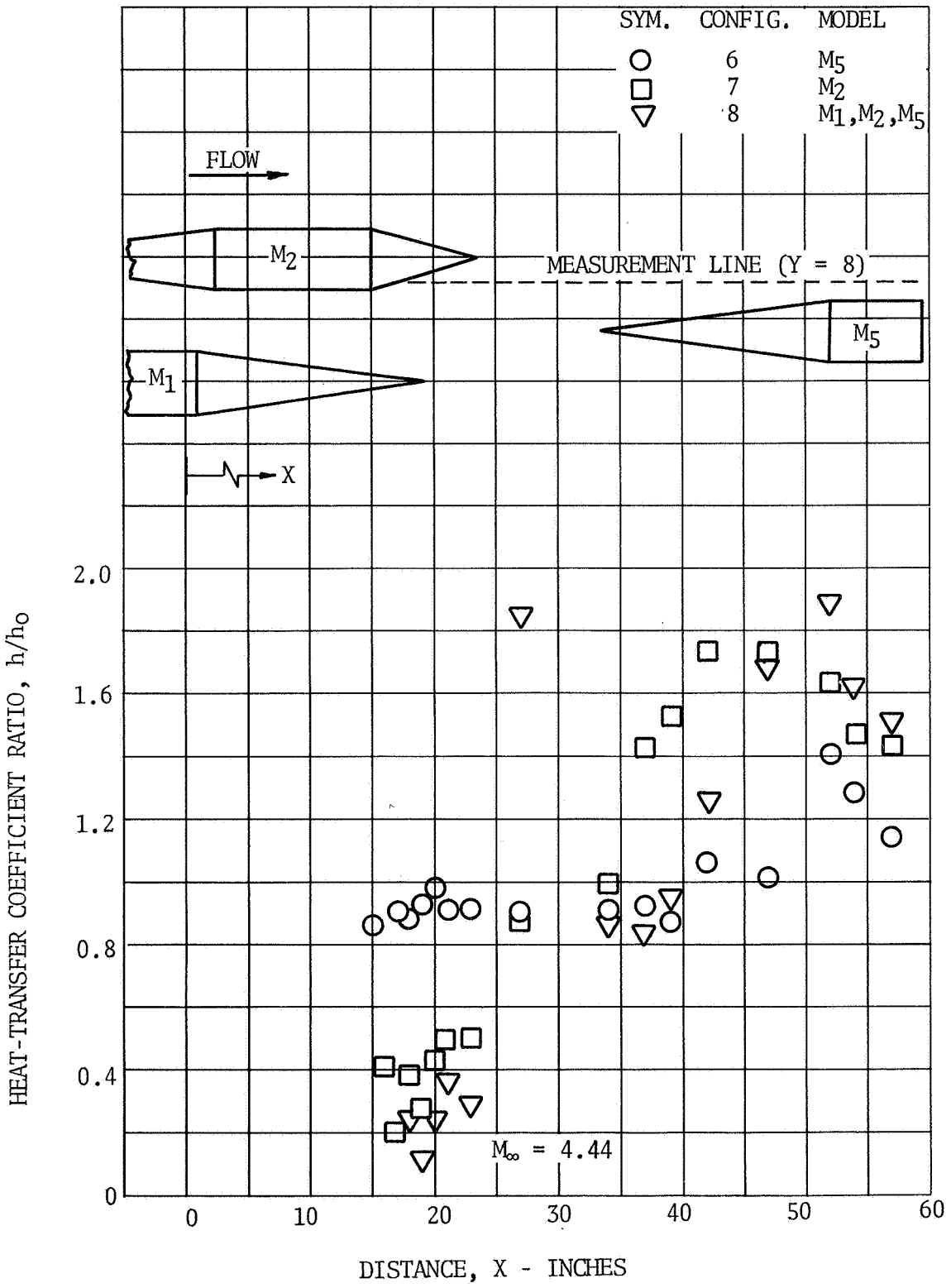

FIGURE 3-9. EFFECT OF MODEL 5 IN MODEL 1 AND 2 DOUBLE WAKE ON PLATE HEAT-TRANSFER COEFFICIENT RATIO DISTRIBUTION AT MACH NUMBER 4.44 - CONFIGURATIONS 6, 7 AND 8

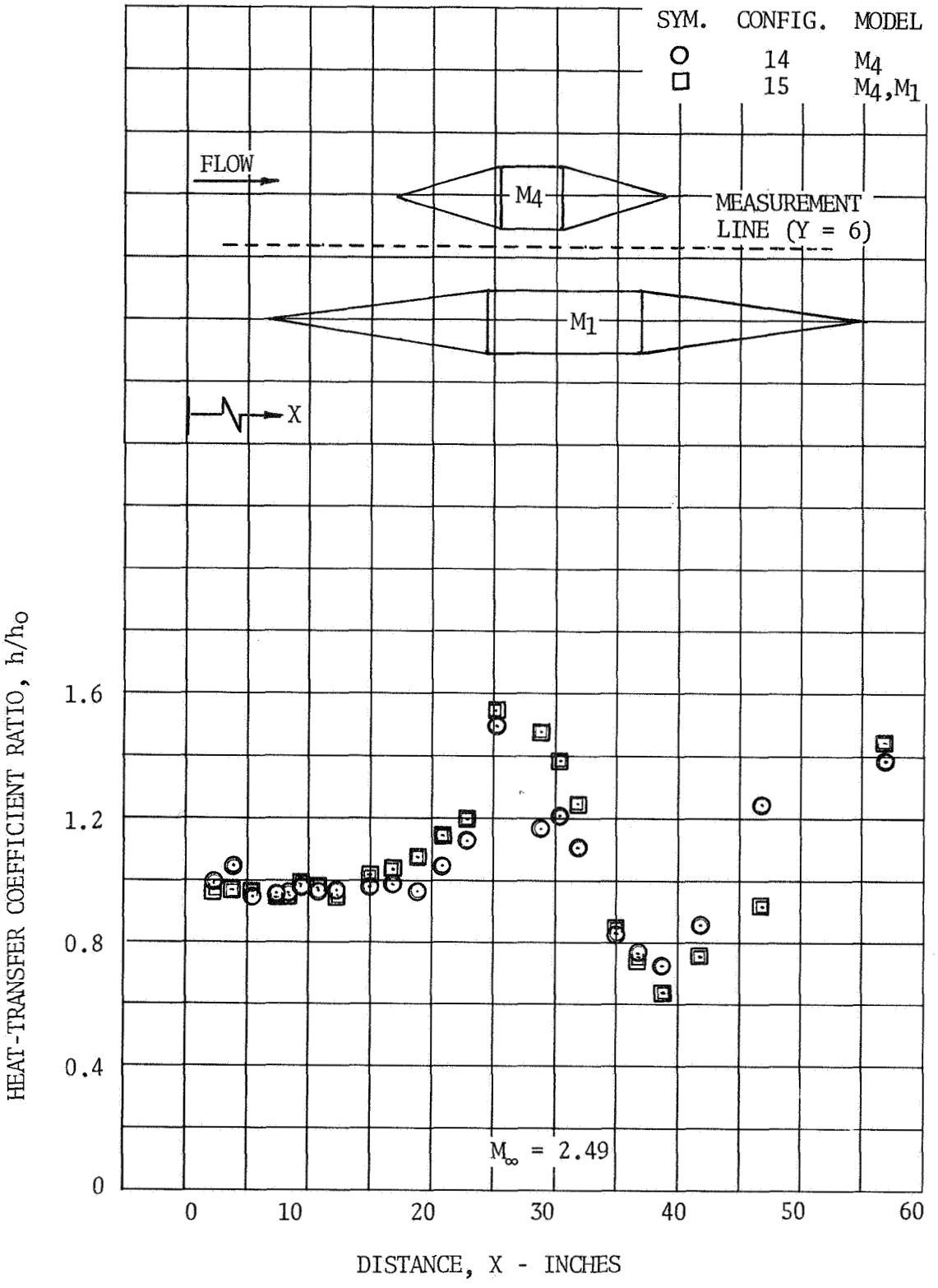

FIGURE 3-10. EFFECT OF MODEL 1 FOREBODY SHOCK COMPRESSION ON MODEL 4 INDUCED PLATE HEAT-TRANSFER COEFFICIENT RATIO DISTRIBUTION AT MACH NUMBER 2.49 - CONFIGURATIONS 14 AND 15

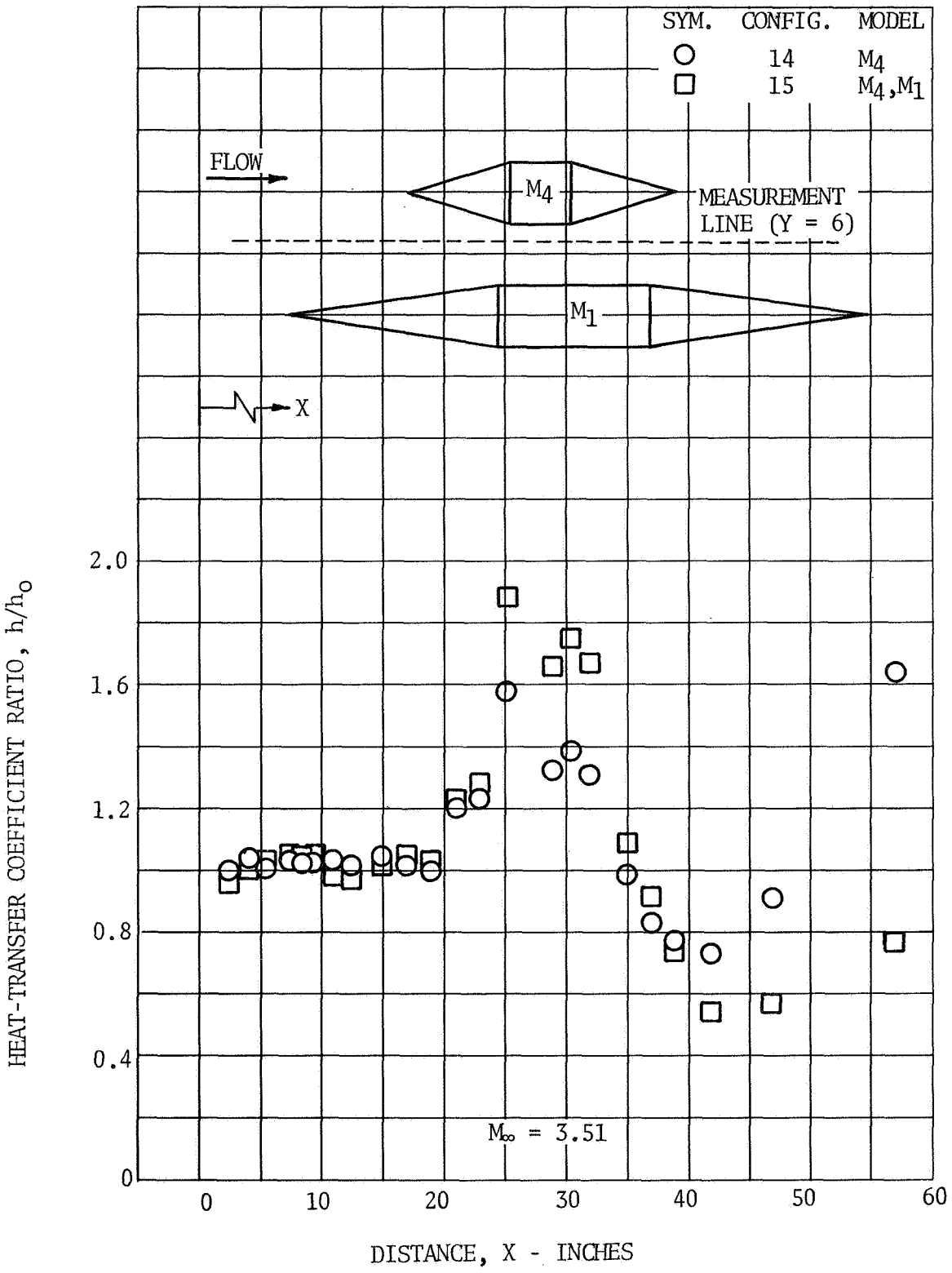

FIGURE 3-11. EFFECT OF MODEL 1 FOREBODY SHOCK COMPRESSION ON MODEL 4 INDUCED PLATE HEAT-TRANSFER COEFFICIENT RATIO DISTRIBUTION AT MACH NUMBER 3.51 - CONFIGURATIONS 14 AND 15

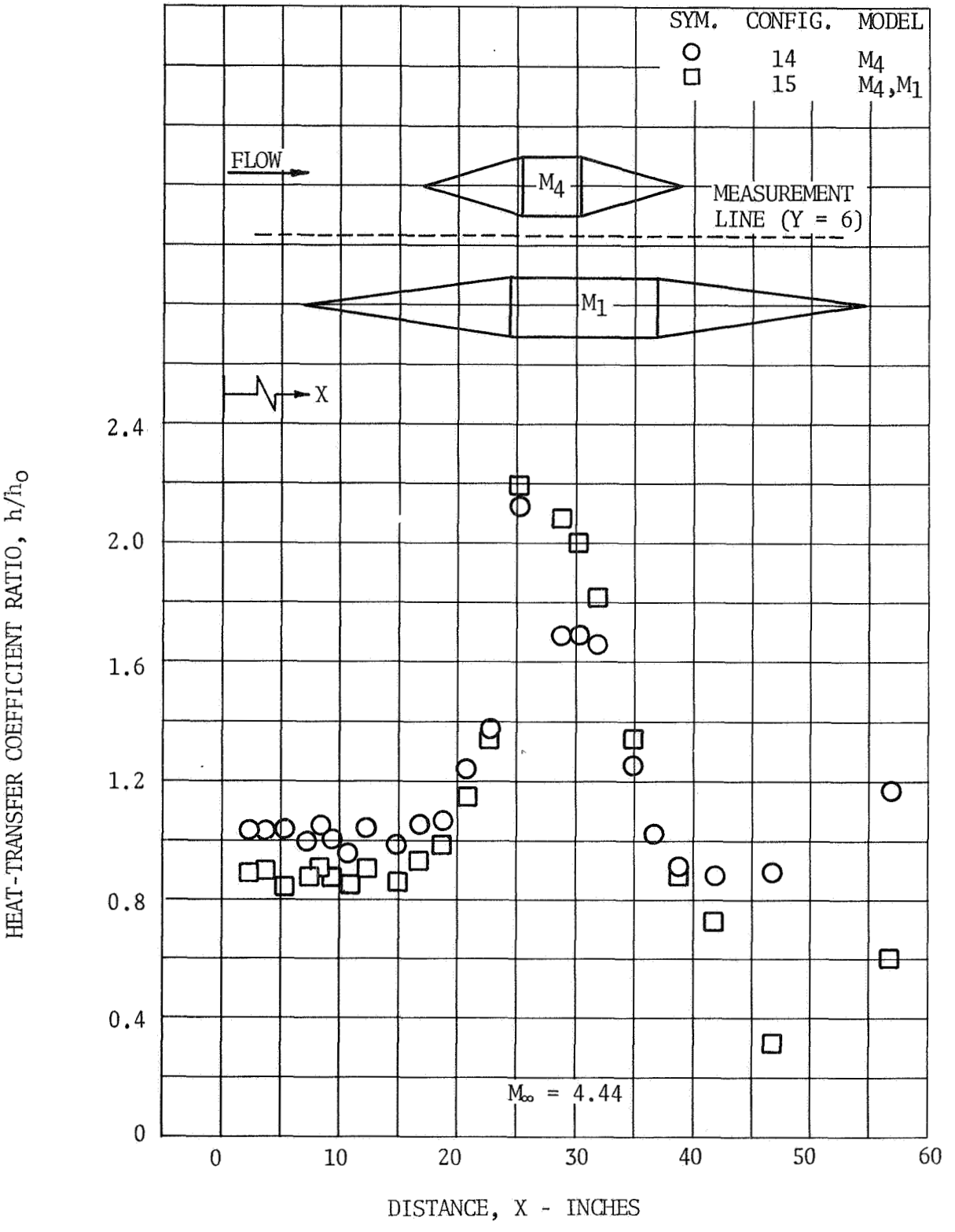

FIGURE 3-12. EFFECT OF MODEL 1 FOREBODY SHOCK COMPRESSION ON MODEL 4 INDUCED PLATE HEAT-TRANSFER COEFFICIENT RATIO DISTRIBUTION AT MACH NUMBER 4.44 - CONFIGURATIONS 14 AND 15

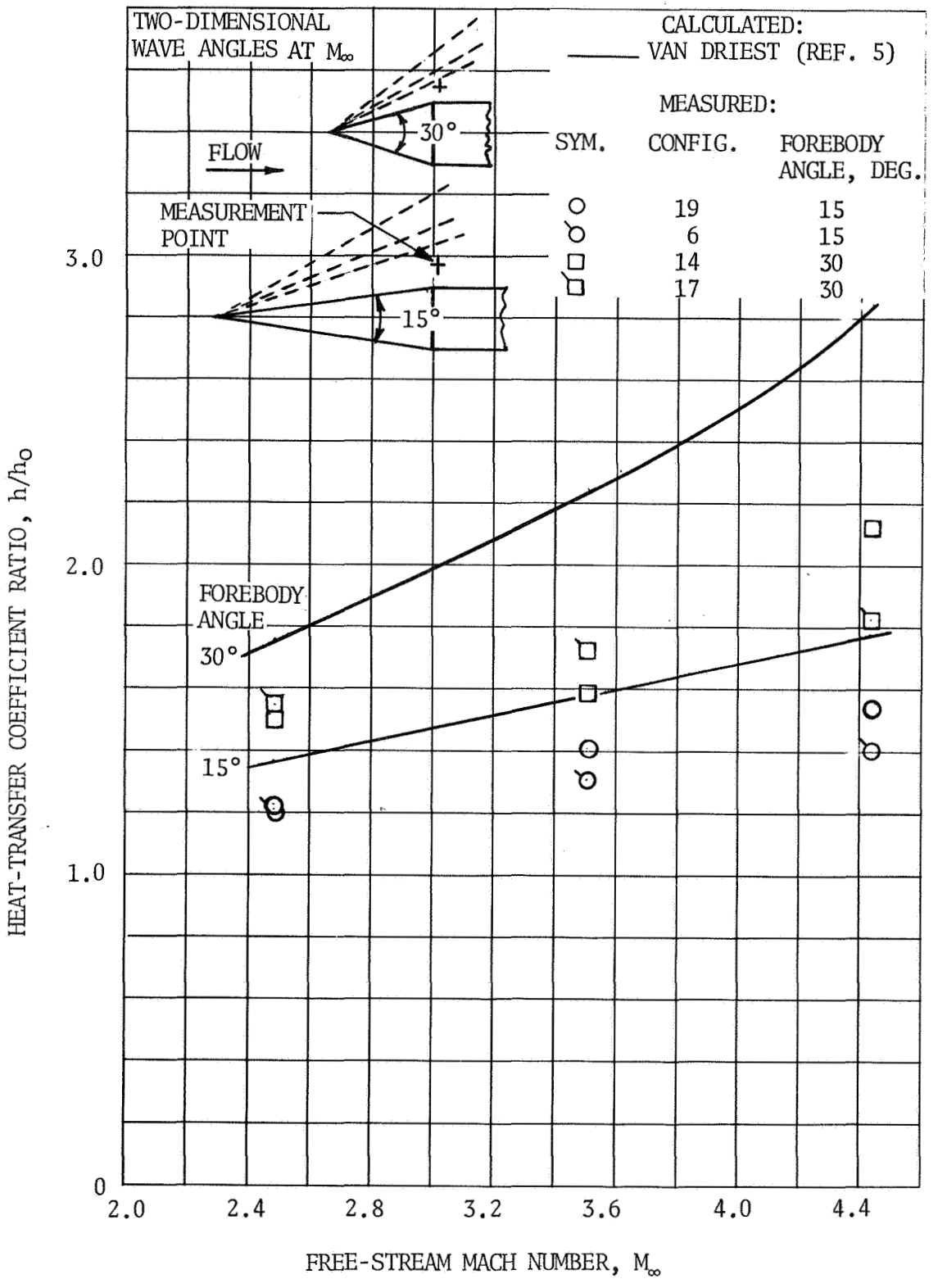

FIGURE 3-13. HEAT-TRANSFER COEFFICIENT RATIO INDUCED BY SINGLE PROTUBERANCE FOREBODY SHOCK COMPRESSION AS A FUNCTION OF MACH NUMBER

4.0 PROTUBERANCE MODEL ENVIRONMENT

Heating environments on the protuberance models tested are presented and discussed in the following paragraphs. These environments were measured on both single-protuberance and multiple-protuberance configurations. A complete tabulation of test data is presented in Reference 1. The heat-transfer coefficients on protuberance models were divided by an average of the clean plate values (h_o') obtained in and near the test plate surface area covered by the model base in order to obtain heat-transfer coefficient ratios. These ratios are presented in Appendix A of this report. Test configurations are shown in Figure 2-1.

Heat-transfer coefficient data measured along the centerline of Model 5 are presented in Figures 4-1, 4-2 and 4-3 for test configurations 6, 5 and 8, respectively. Test data for Model 5 alone (configuration 6) are presented in Figure 4-1 alone with analytically determined heat-transfer coefficients. It is evident in Figure 4-1 that the analytical calculations and test data correlate in both magnitude and trends. The increase in heating with distance along the conical forebody is caused by the variation in boundary layer properties. If the protuberance were in a free stream flow the heating would decrease with distance along forebody. Analytical values were determined by the method of Van Driest (References 4 and 5) with local flow properties determined as follows:

a) Forebody Surface

An attached conical shock wave based on the tunnel upstream flow parameters is developed on the protuberance model forebody. Local flow properties in the boundary layer ahead of the shock wave are determined from boundary layer distributions presented in Reference 2 at the height on the forebody for which heating is to be evaluated. These properties are modified by passing them through the conical shock and these properties are used in the heating calculation.

b) Centerbody, Forward End

Flow parameters at the edge of the boundary layer behind the shock wave are expanded around the cone/cylinder junction with the use of the Prandtly-Meyer relationships. Local flow conditions are then determined.

c) Centerbody, Aft End

Flow at the aft end of the centerbody is assumed to have returned to free stream conditions.

4.0 (Continued)

A plot of heat-transfer coefficient ratios (protuberance heat-transfer coefficients divided by clean plate value) versus Mach number is presented in Figure 4-4 for points on the forebody and top of Model 5. Data are presented for test configurations 5, 6 and 8. A comparison of data from the three configurations indicates a decrease in heating to the Model 5 forebody when the protuberance is placed in the wakes of Models 1 and 2.

Model 4 centerline heat-transfer coefficient values are presented in Figures 4-5 and 4-6 for configurations 14 and 15, respectively. In these configurations, Model 4 is located at attach point 4. A minor increase in heating on Model 4 centerline is noted from the interference effects of Model 1 (a cross plot of Figures 4-5 and 4-6 are shown in Figure 4-7).

Heat-transfer coefficient ratios are presented in Figure 4-8 for points along the side of Model 4. Data are presented in Figure 4-8 for configurations 14 and 15. The effect of the Model 1 wake region on Model 4 side areas adjacent to Model 1 is to increase the heating to Model 4 slightly.

Heat-transfer coefficient ratios are presented in Figure 4-9 for points along the side of Model 1. The effects of shock impingement from the Model 4 forebody shock wave on the side of Model 1 centerbody are evident.

In test configurations 16, 17 and 18, Model 4 was located at attach point 5 (17 inches aft of attach point 4). Heat-transfer coefficients along Model 4 centerline are presented in Figure 4-10 for configuration 17 (Model 4 alone) and in Figures 4-11 and 4-12 for configurations 16 and 18, respectively (Model 4 in Model 1 wakes).

Heat-transfer coefficient ratios for Model 4 alone and Model 4 in Model 1 wake regions are presented in Figure 4-13 as a function of Mach number. Generally lower values are observed on Model 4 in Model 1 wake regions. The shock strengths from Model 1 are less than from Model 4 and would therefore have less effect on Model 4 than Model 4 does on Model 1.

Heat-transfer coefficients along the centerline of Model 12 (double wedge) are presented in Figures 4-14 and 4-15 for configurations 2 and 3, respectively. Comparison of Figures 4-14 and 4-15 indicates that the effect of the aft wake of Model 1 (configuration 3) on Model 12 is to increase the heat-transfer coefficient values.

Two basic model forebody angles were tested. These were the 15-degree forebody (Models 1, 3 and 5) and the 30-degree forebody (Model 4). Data taken along the forebody centerline of Models 1, 3, 4 and 5 are plotted as a function of Z/δ in Figures 4-16, 4-17 and 4-18 for Mach numbers 2.49, 3.51 and 4.44, respectively. The test data indicate a reduction in forebody heating due to immersion in the boundary layer.

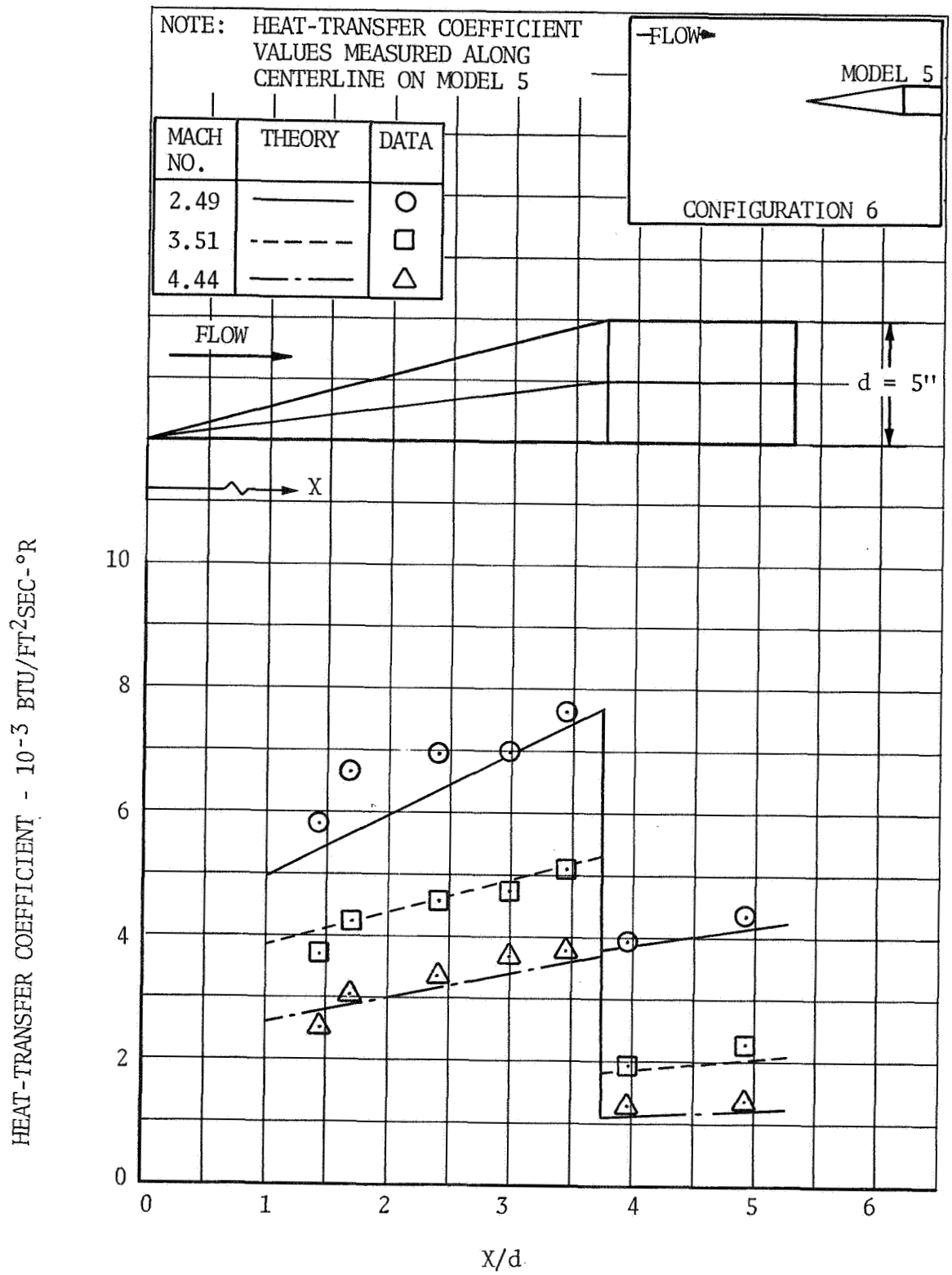

FIGURE 4-1. HEAT-TRANSFER COEFFICIENTS ON MODEL 5 CENTERLINE (CONFIGURATION 6)

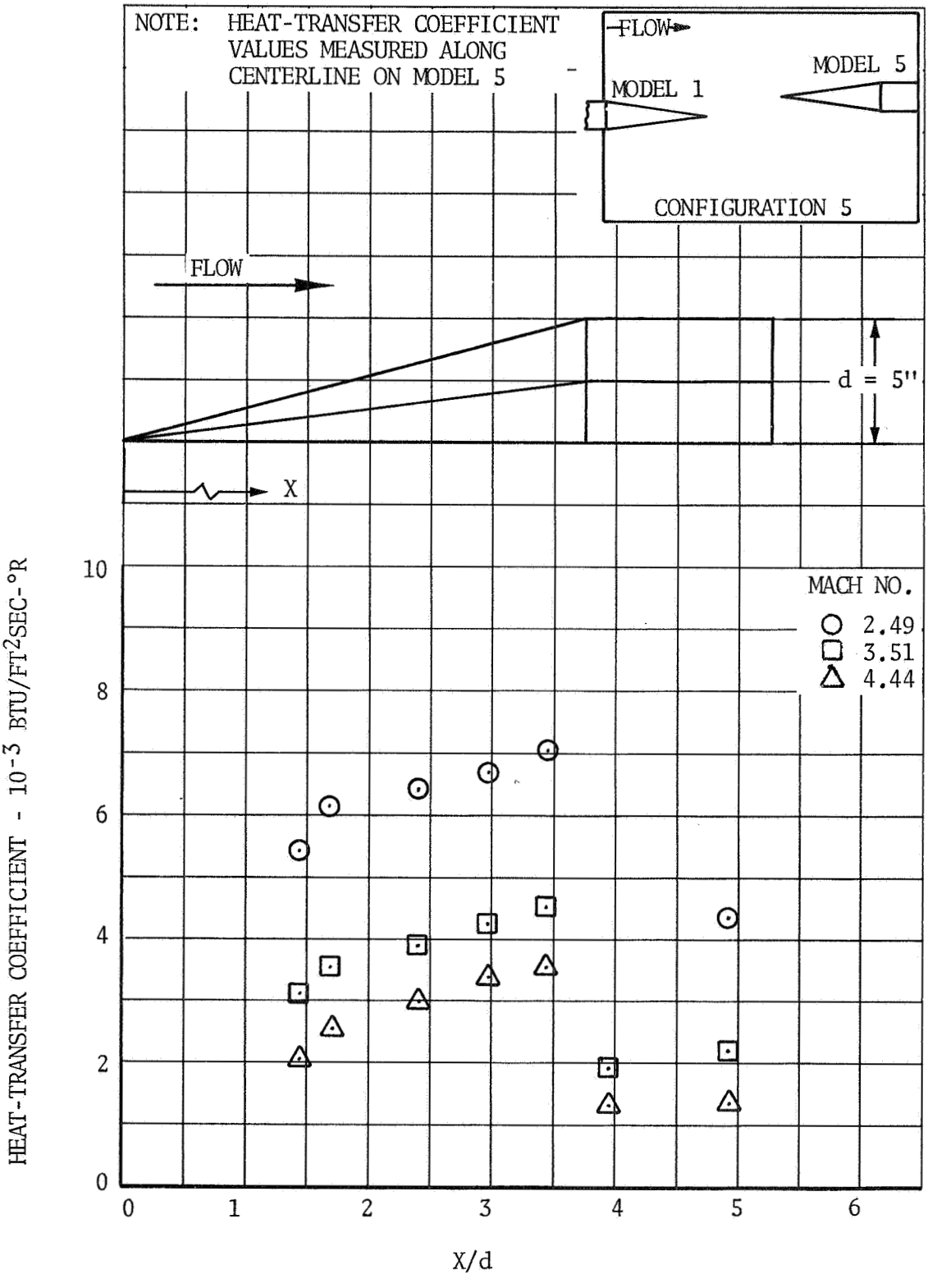

FIGURE 4-2. HEAT-TRANSFER COEFFICIENTS ON MODEL 5 CENTERLINE (CONFIGURATION 5)

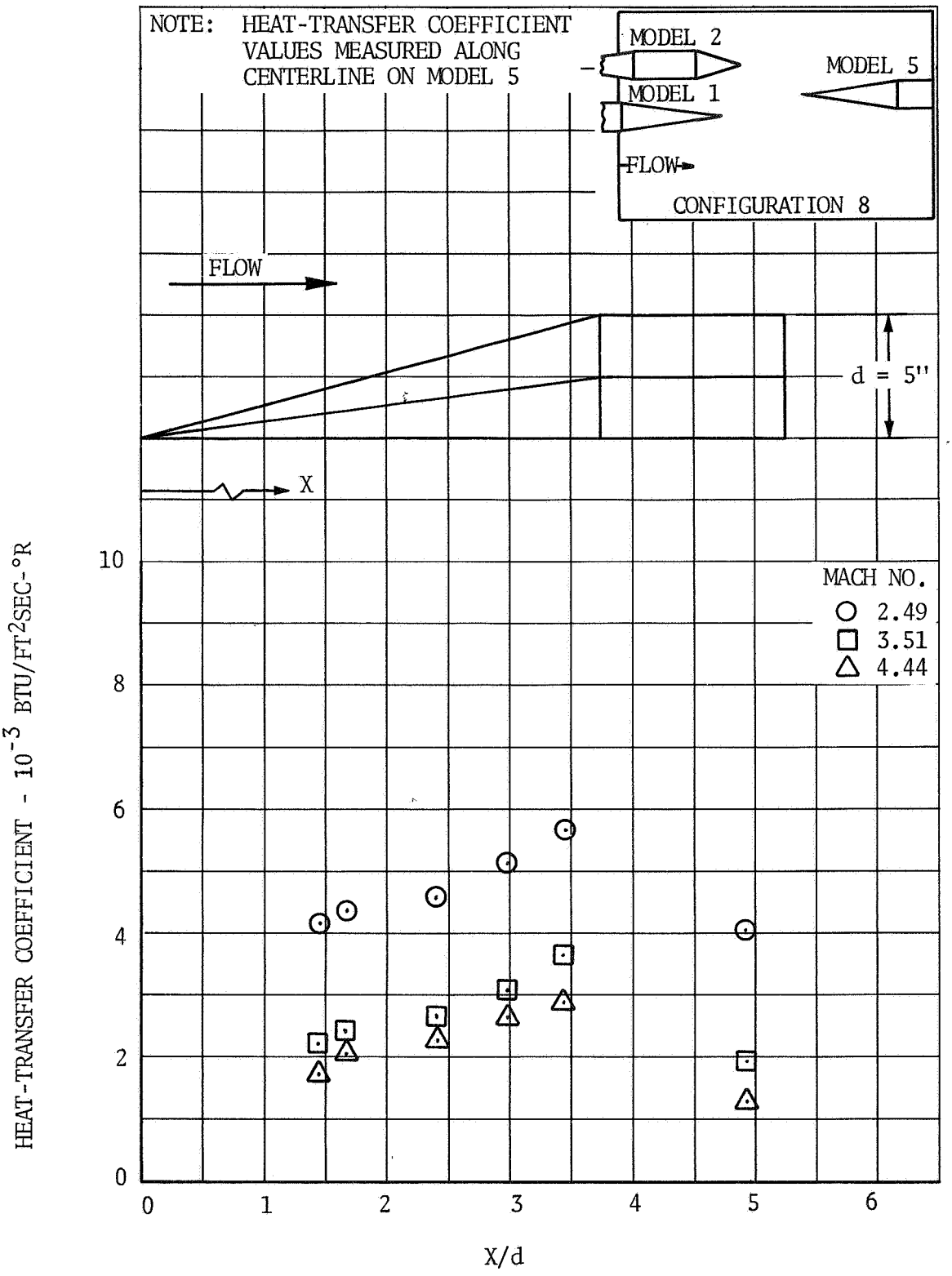

FIGURE 4-3. HEAT-TRANSFER COEFFICIENTS ON MODEL 5 CENTERLINE (CONFIGURATION 8)

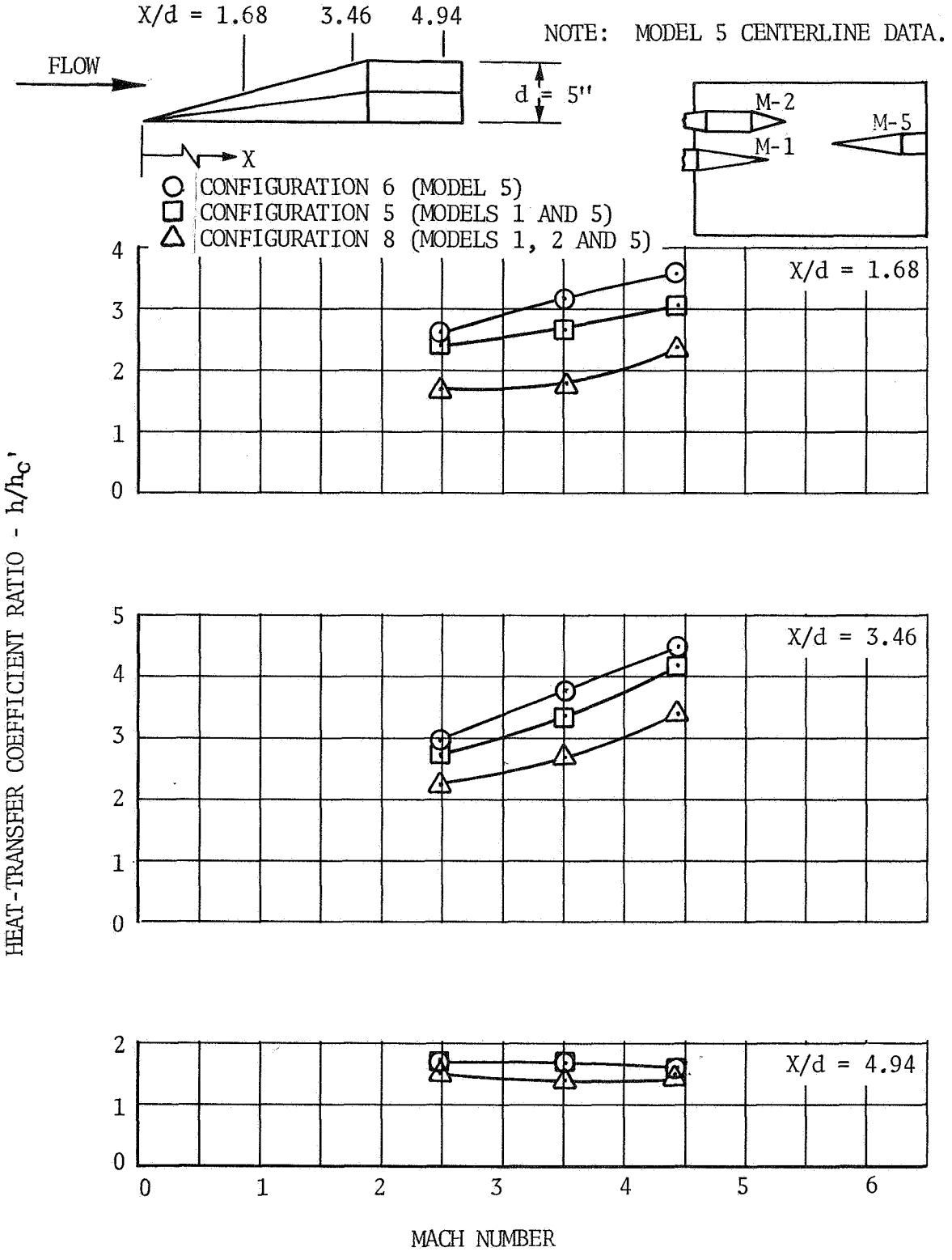

FIGURE 4-4. HEAT-TRANSFER COEFFICIENT RATIOS - MODEL 5 (CONFIGURATIONS 5, 6 AND 8)

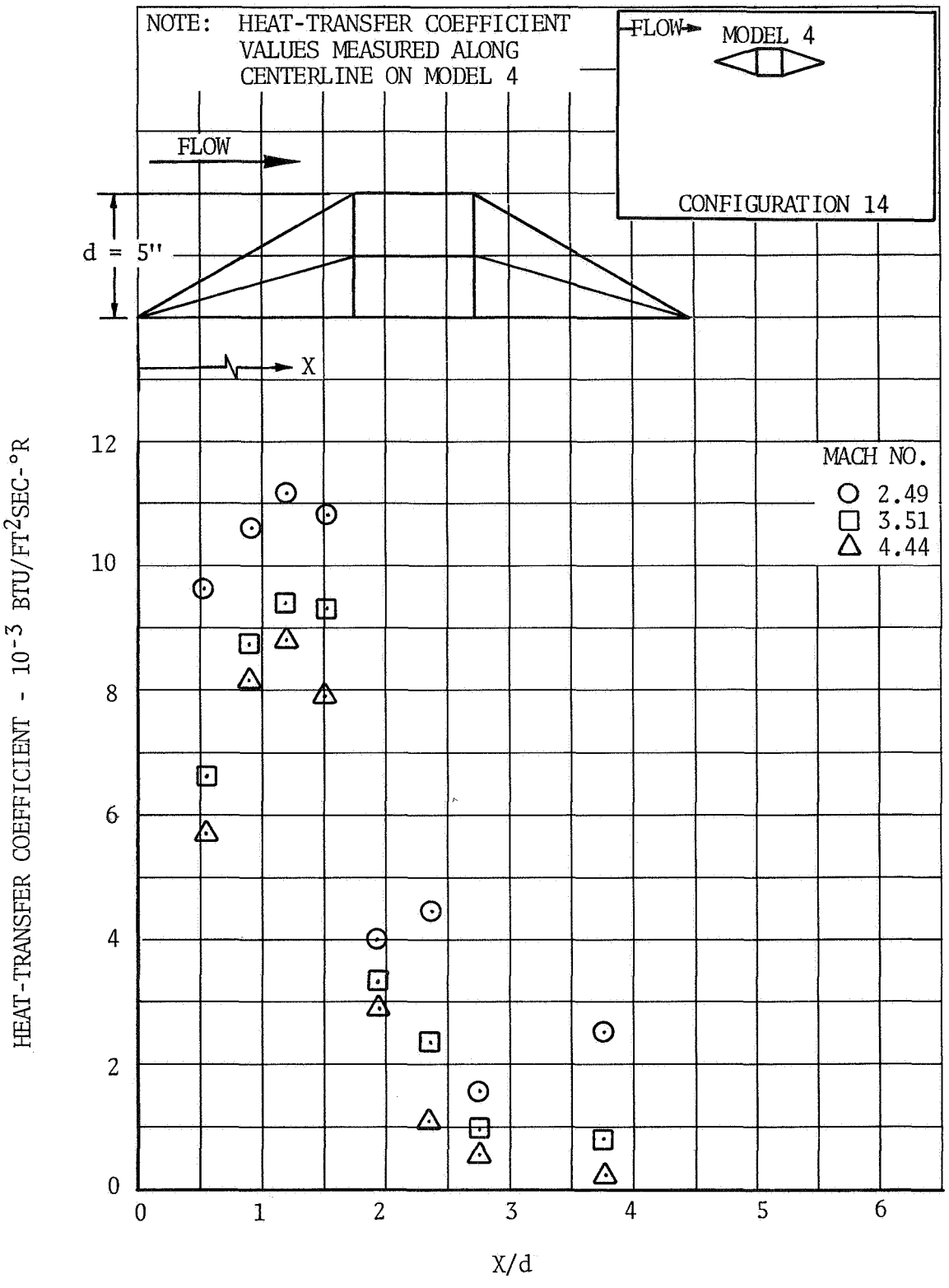

FIGURE 4-5. HEAT-TRANSFER COEFFICIENTS ON MODEL 4 CENTERLINE (CONFIGURATION 14)

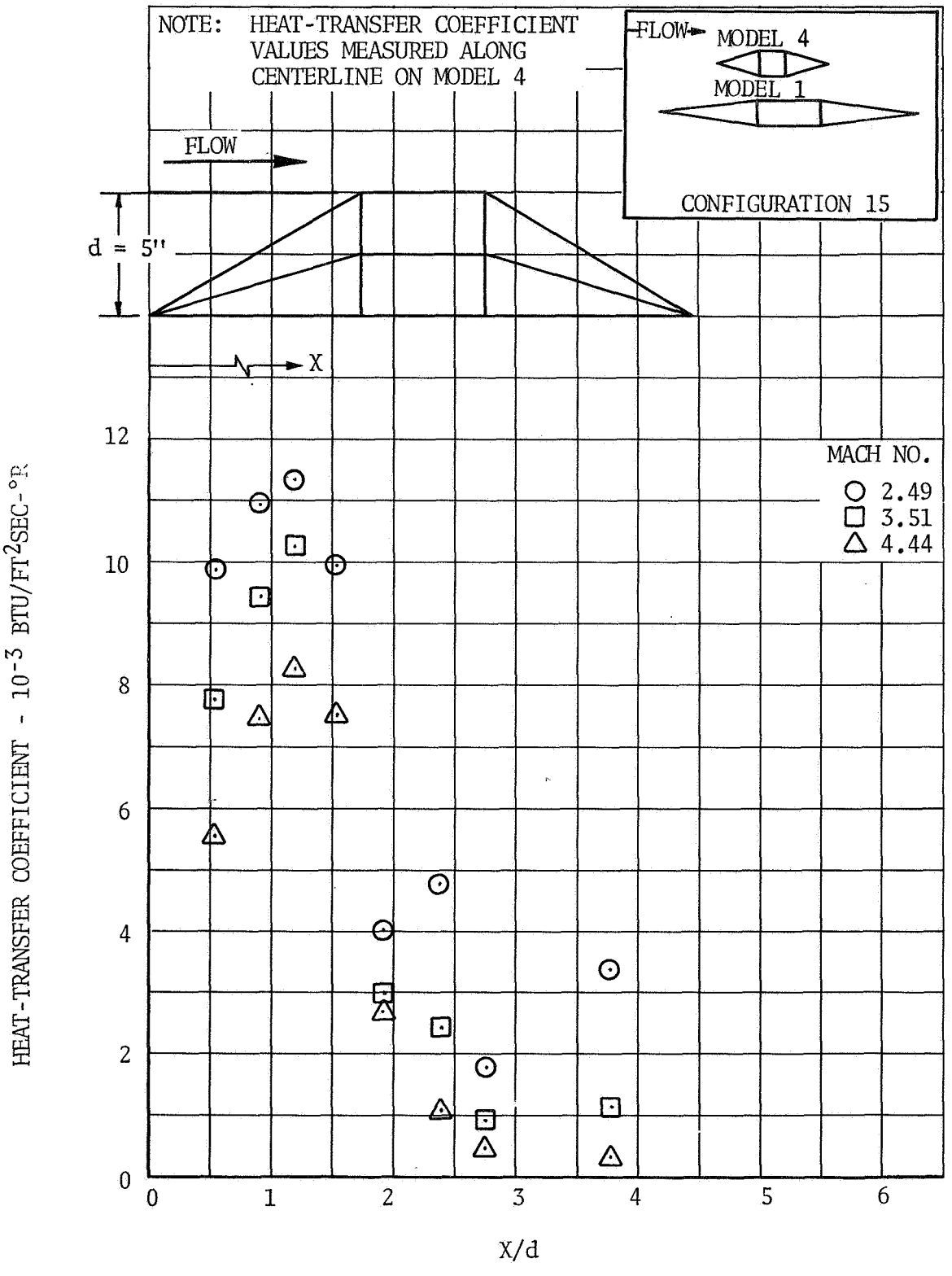

FIGURE 4-6. HEAT-TRANSFER COEFFICIENTS ON MODEL 4 CENTERLINE (CONFIGURATION 15)

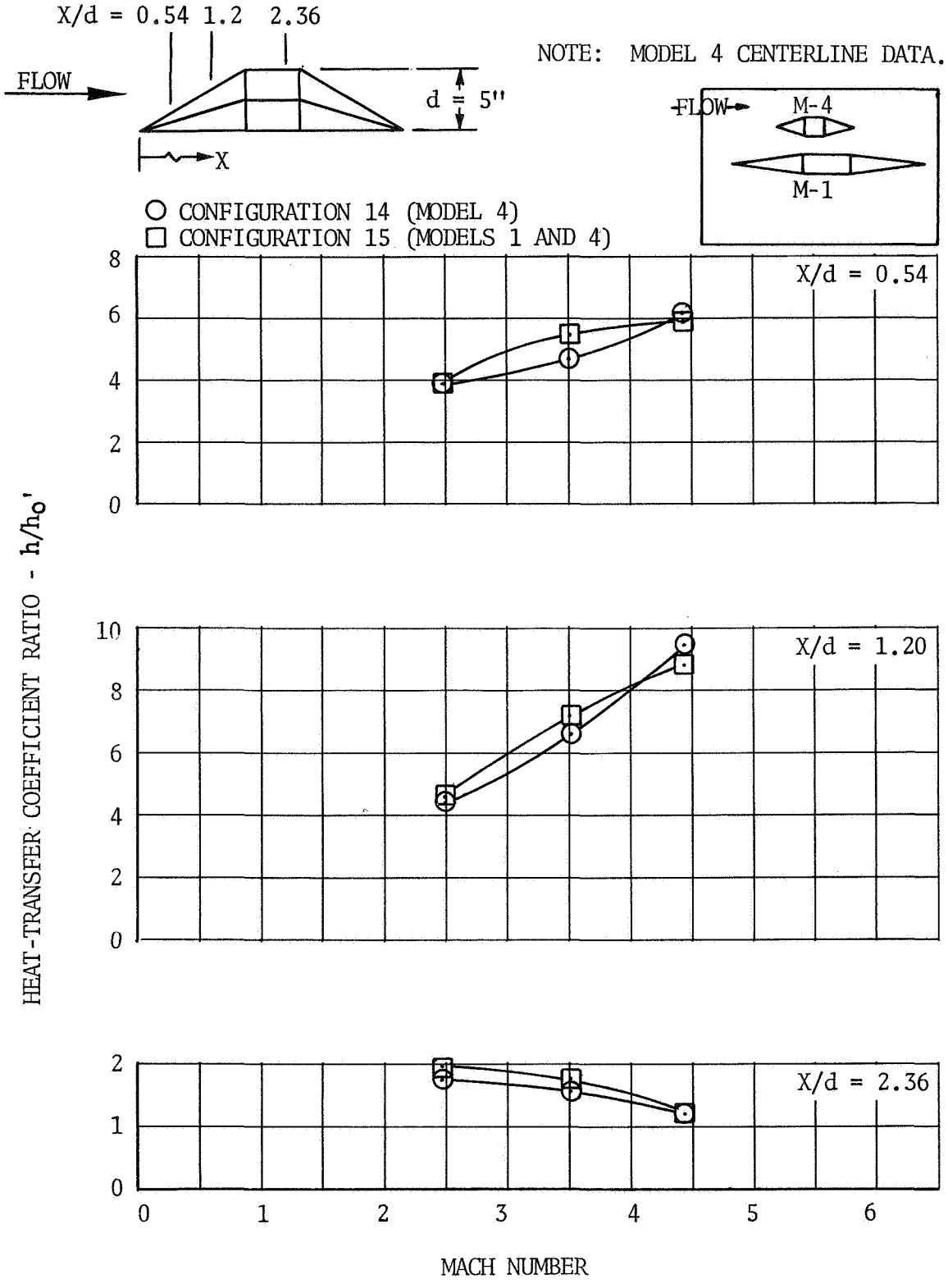

FIGURE 4-7. HEAT-TRANSFER COEFFICIENT RATIOS - MODEL 4 (CONFIGURATIONS 14 AND 15)

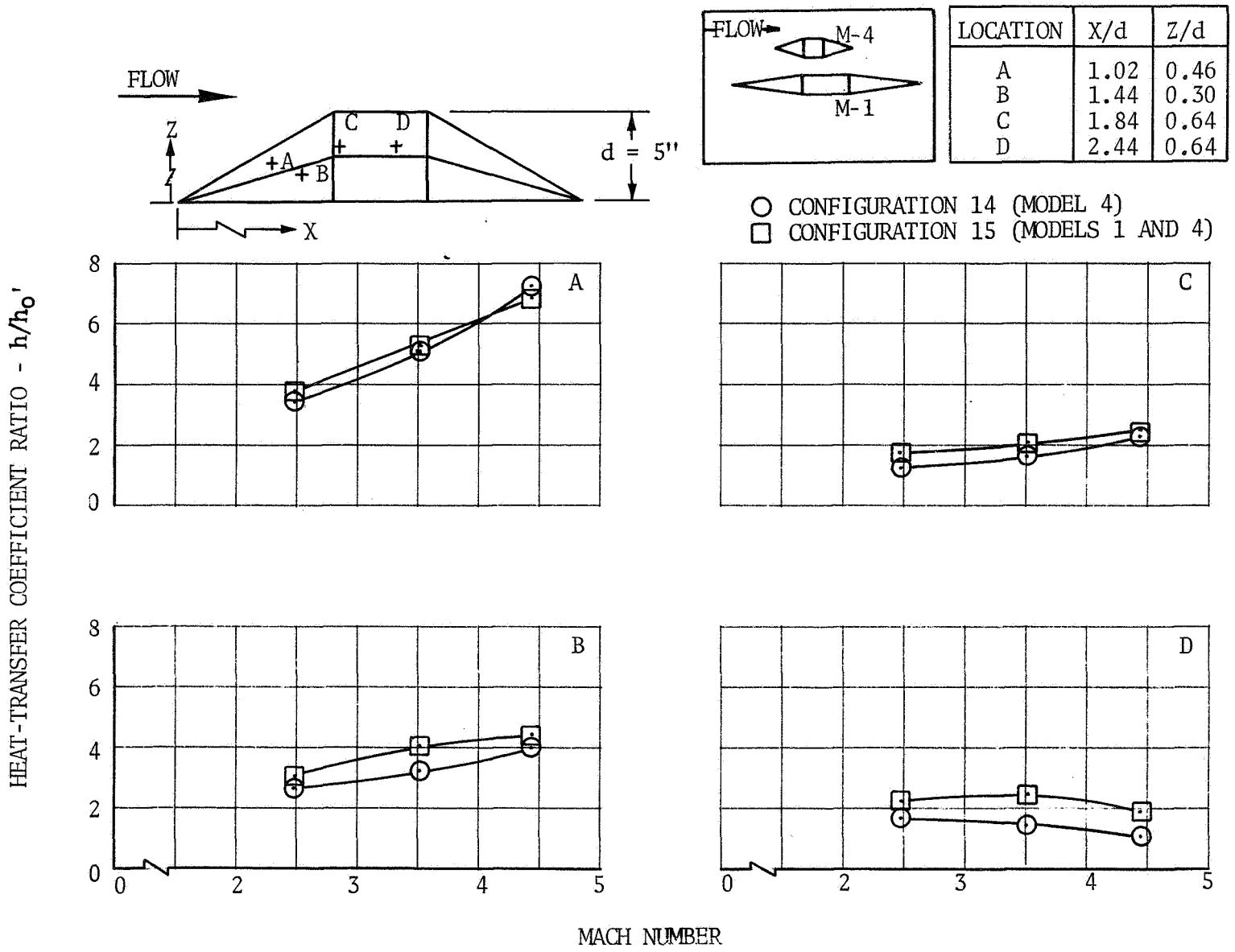

FIGURE 4-8. HEAT-TRANSFER COEFFICIENT RATIOS ON MODEL 4 SIDE (CONFIGURATIONS 14 AND 15)

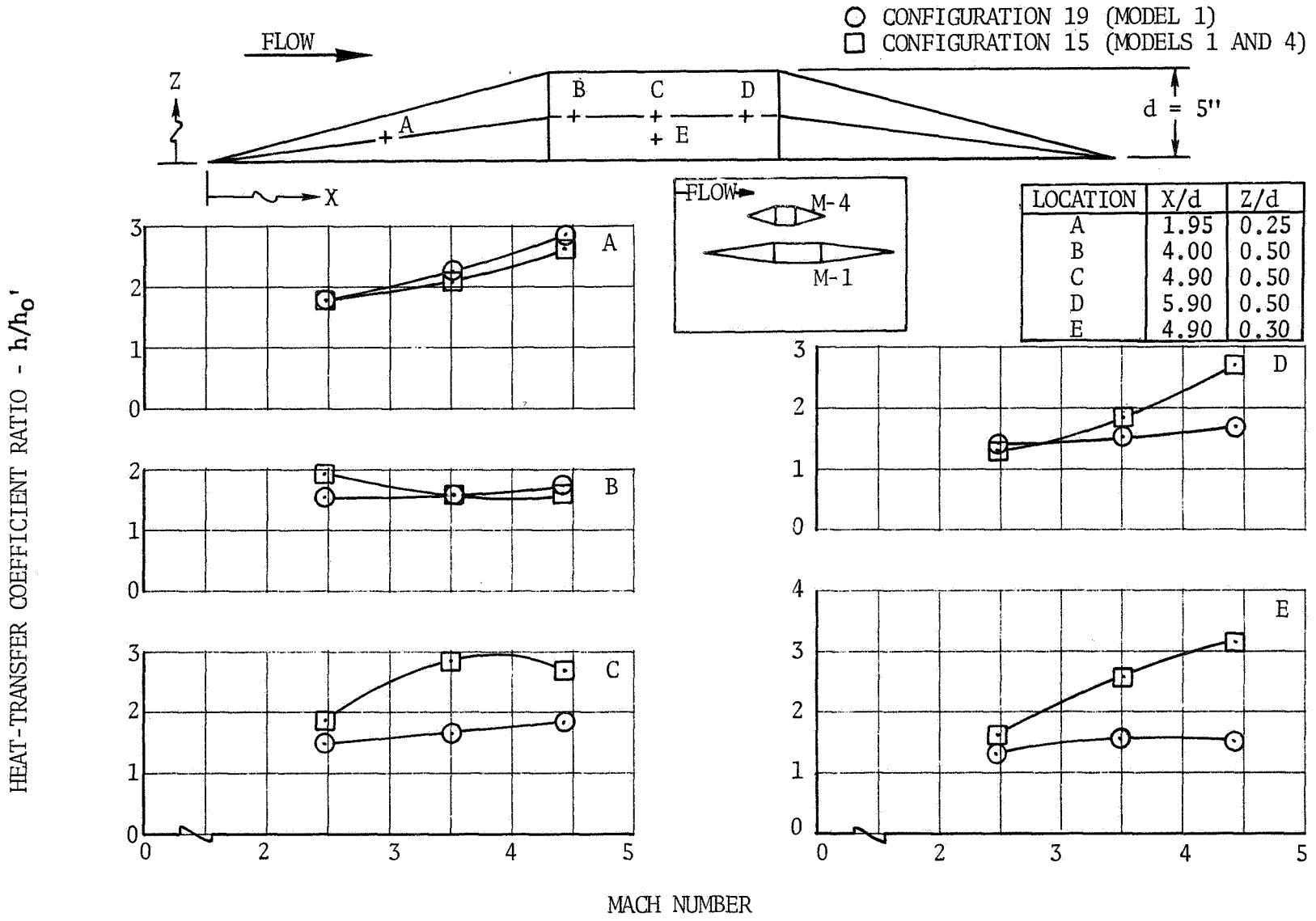

FIGURE 4-9. HEAT-TRANSFER COEFFICIENT RATIOS ON MODEL 1 SIDE (CONFIGURATIONS 15 AND 19)

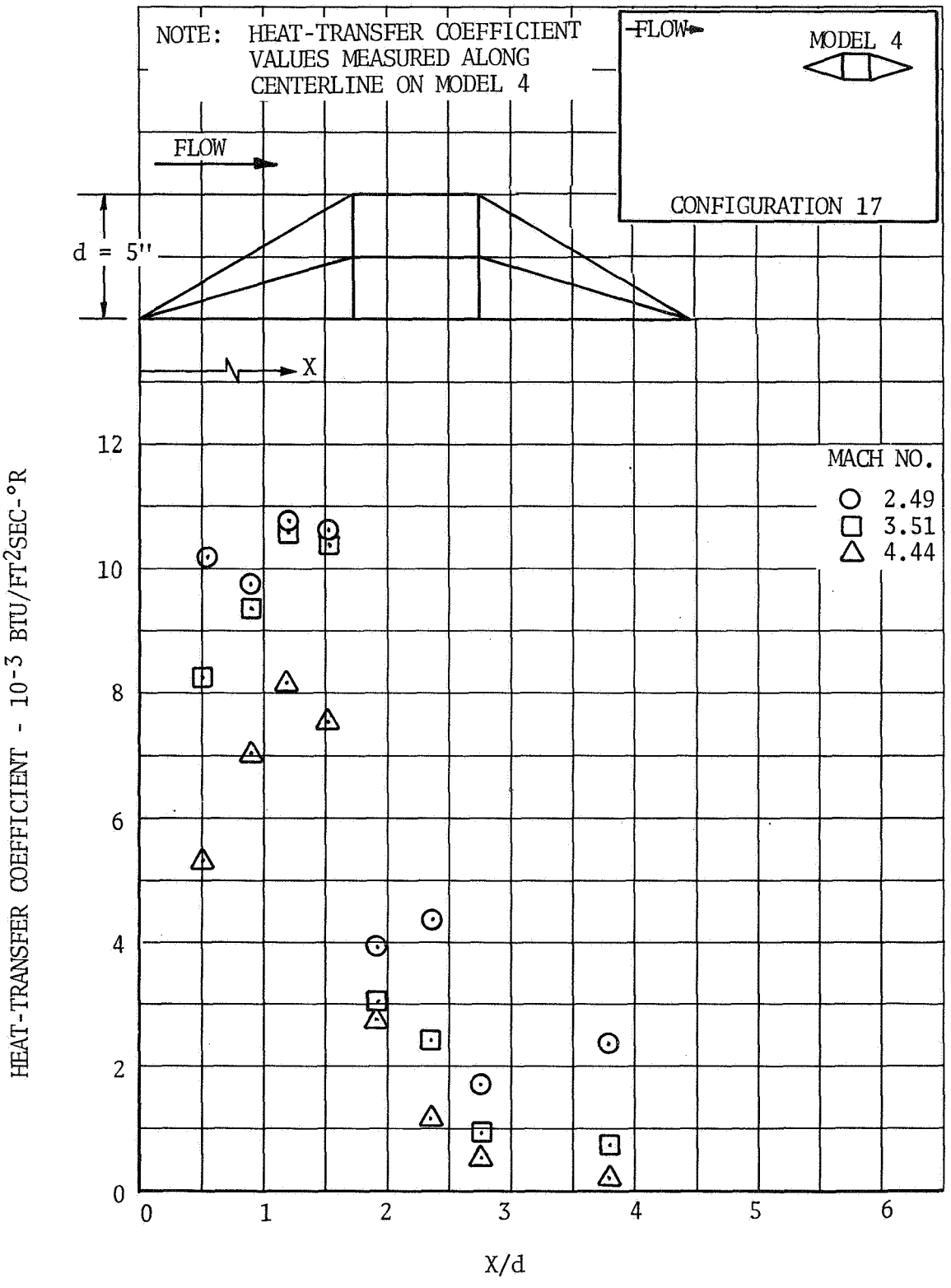

FIGURE 4-10. HEAT-TRANSFER COEFFICIENTS ON MODEL 4 CENTERLINE (CONFIGURATION 17)

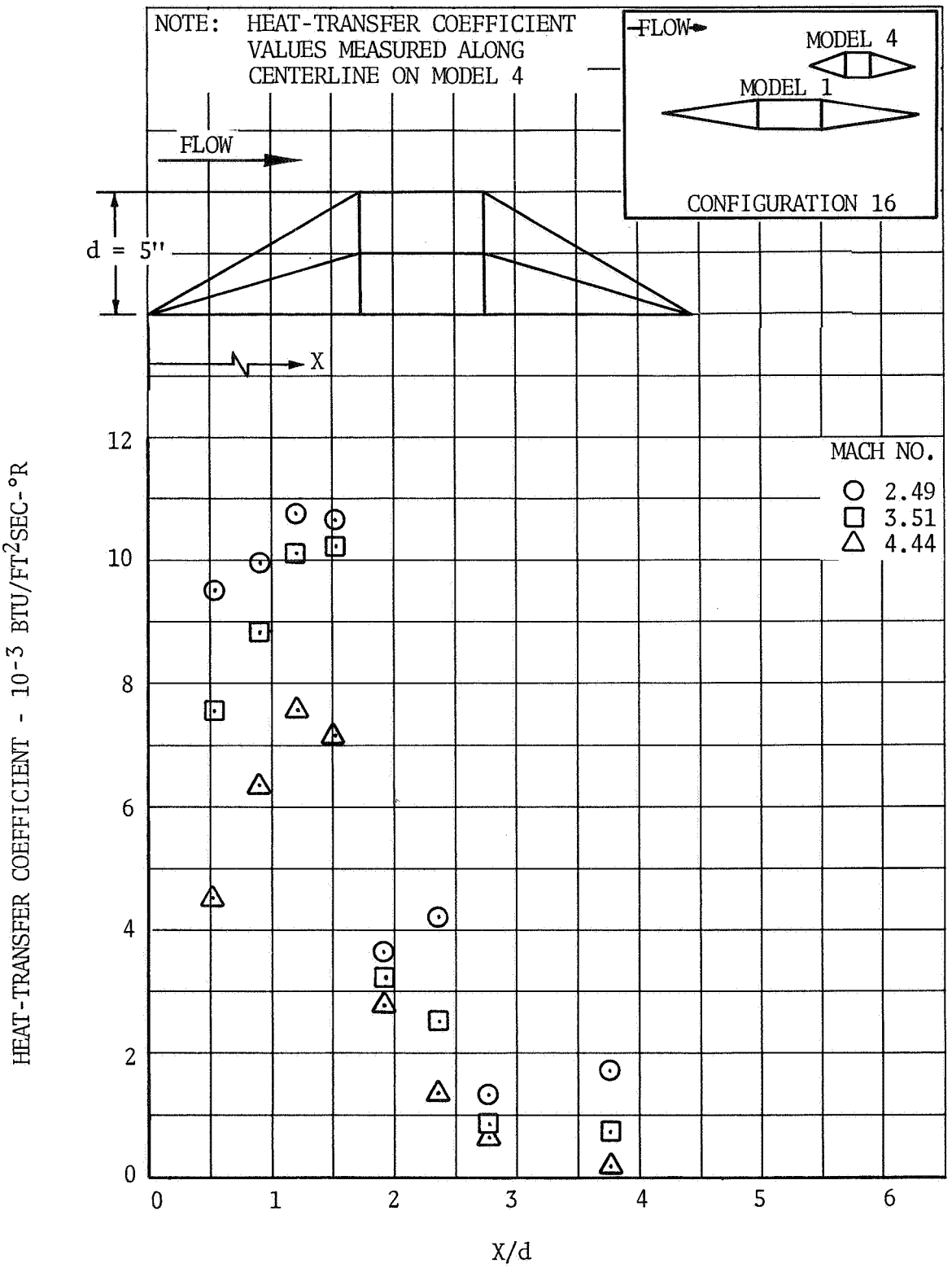

FIGURE 4-11. HEAT-TRANSFER COEFFICIENTS ON MODEL 4 CENTERLINE (CONFIGURATION 16)

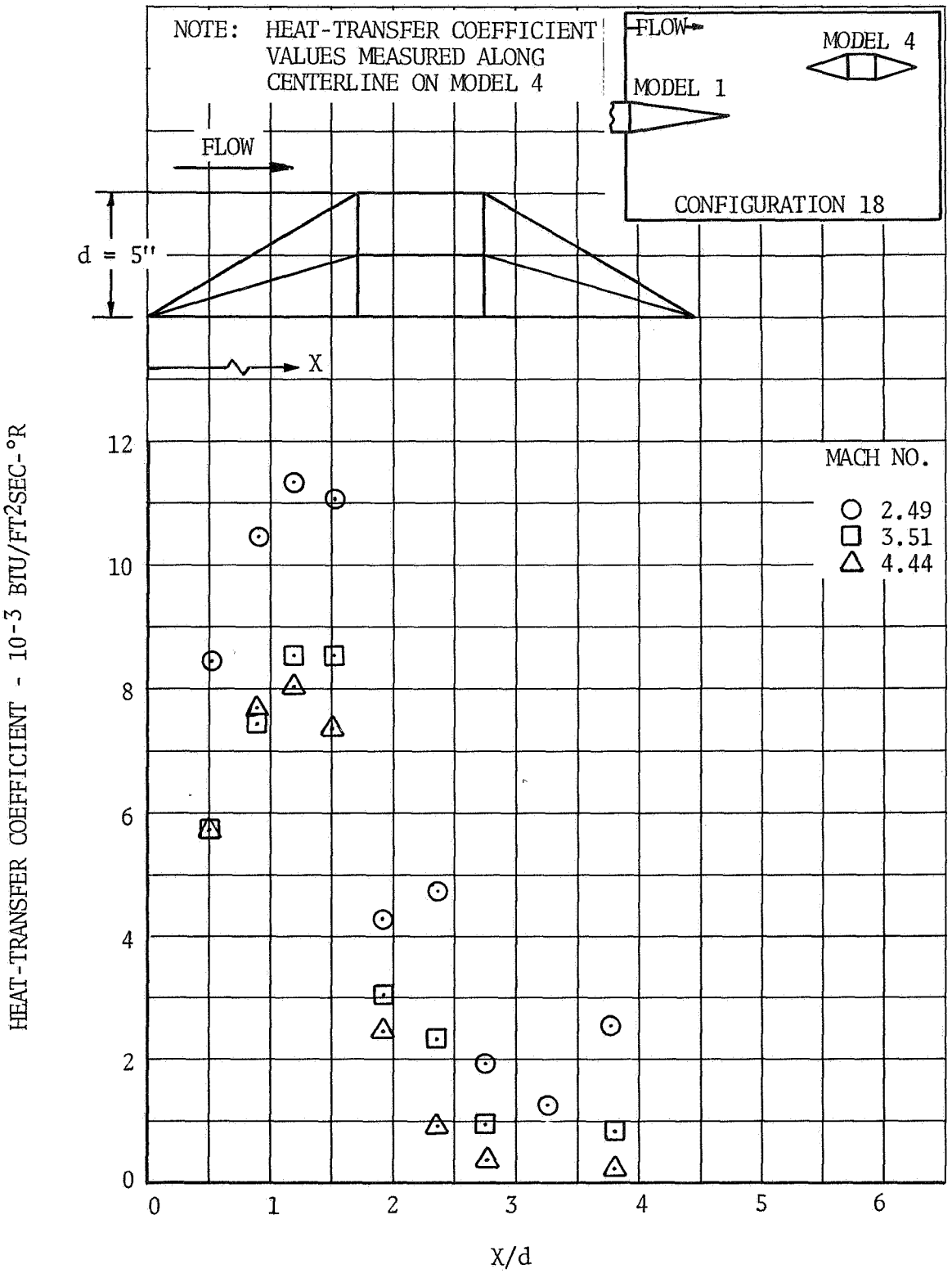

FIGURE 4-12. HEAT-TRANSFER COEFFICIENTS ON MODEL 4 CENTERLINE (CONFIGURATION 18)

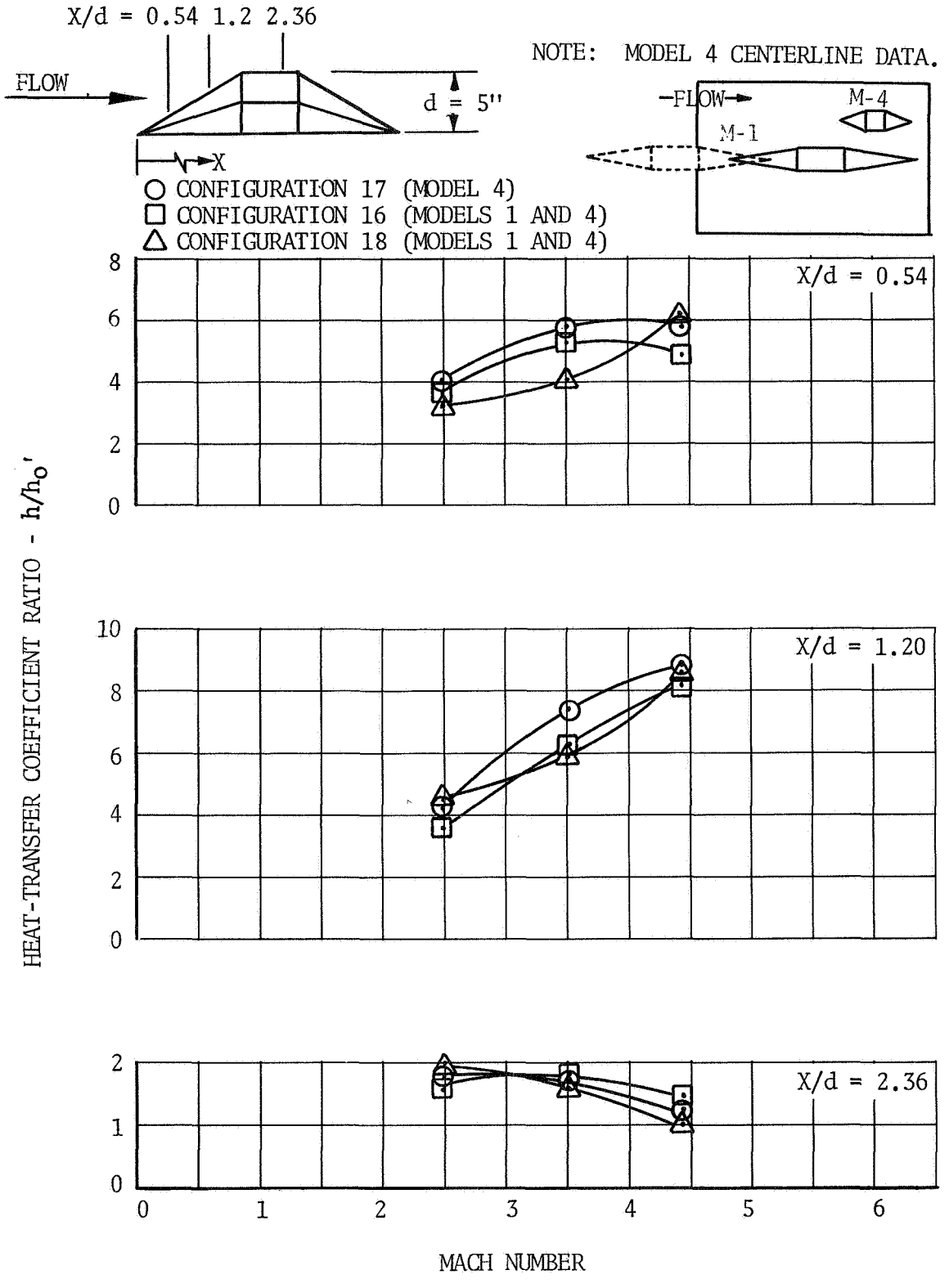

FIGURE 4-13. HEAT-TRANSFER COEFFICIENT RATIOS - MODEL 4 (CONFIGURATIONS 16, 17 AND 18)

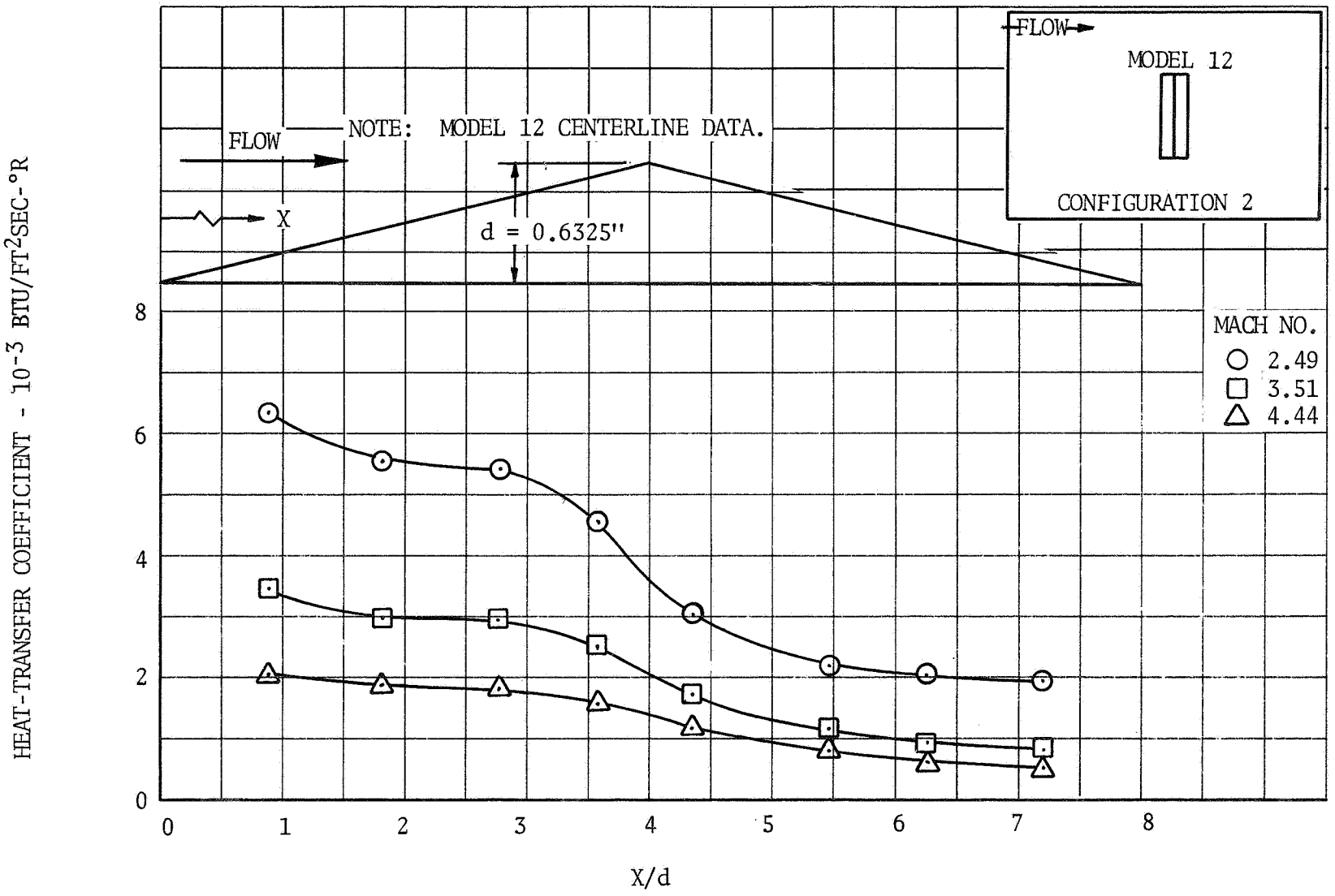

FIGURE 4-14. HEAT-TRANSFER COEFFICIENTS ON MODEL 12 CENTERLINE (CONFIGURATION 2)

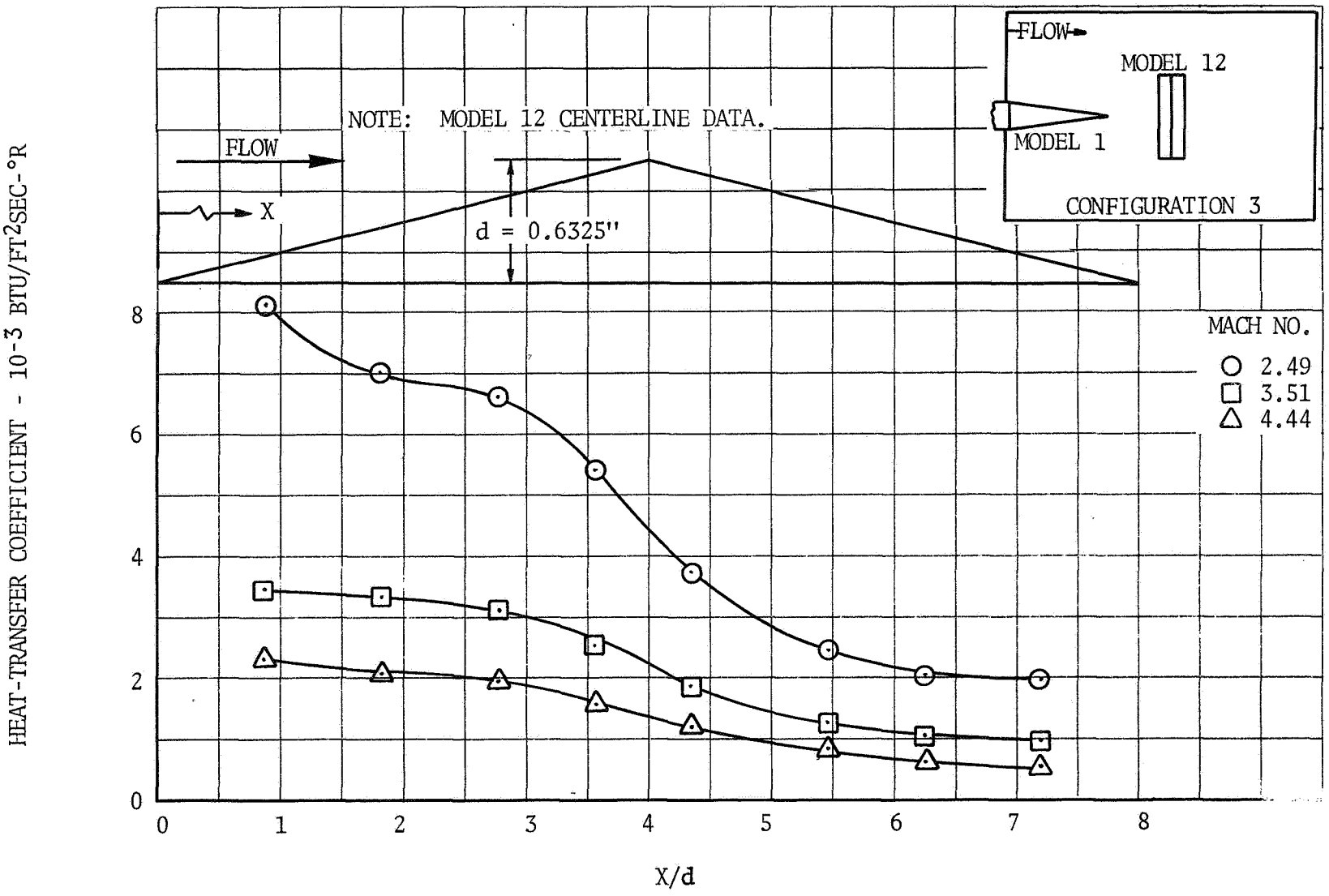

FIGURE 4-15. HEAT-TRANSFER COEFFICIENTS ON MODEL 12 CENTERLINE (CONFIGURATION 3)

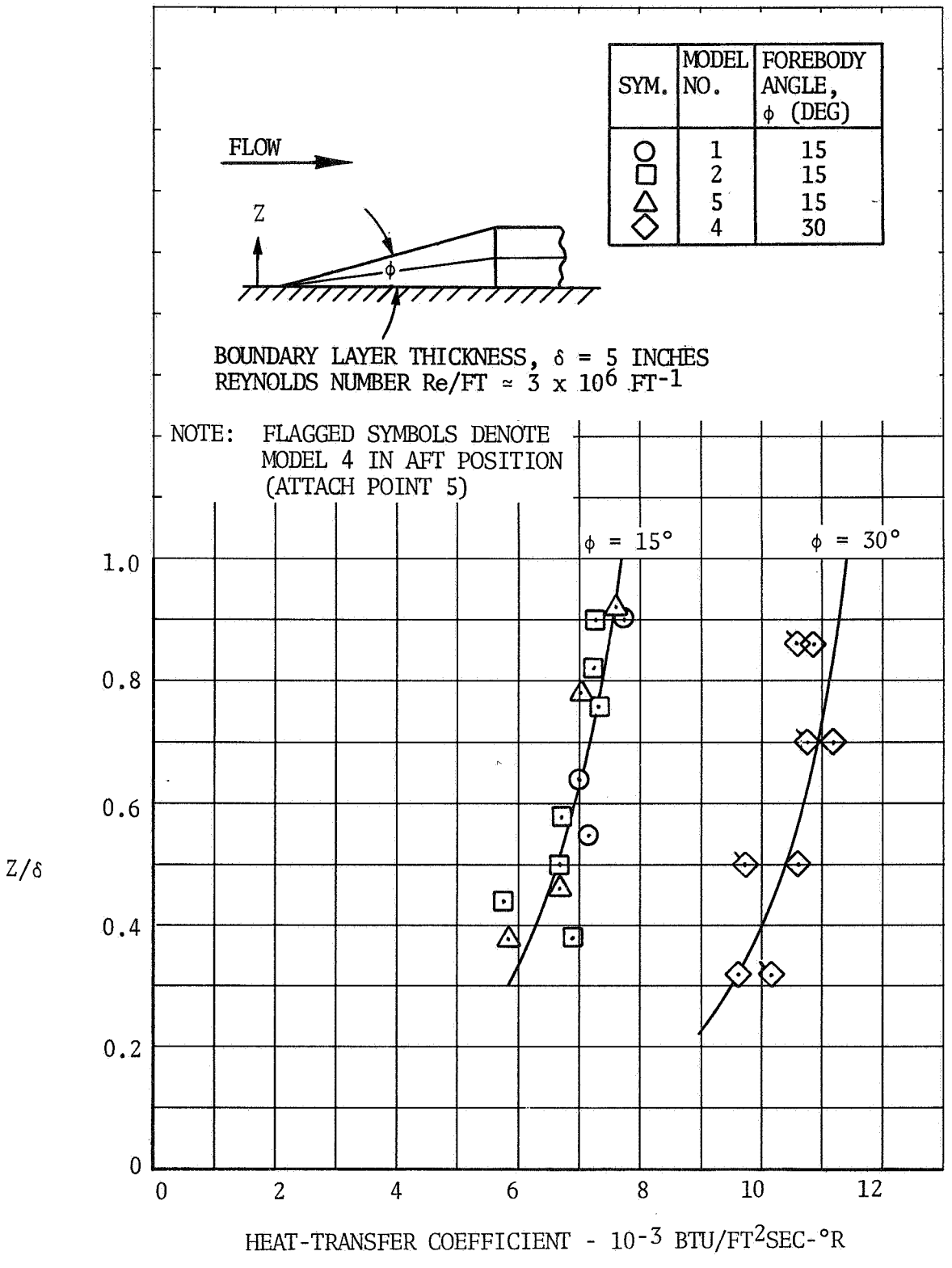

FIGURE 4-16. HEAT-TRANSFER COEFFICIENTS ON MODEL FOREBODIES - MODELS 1, 2, 4 AND 5 (M = 2.49)

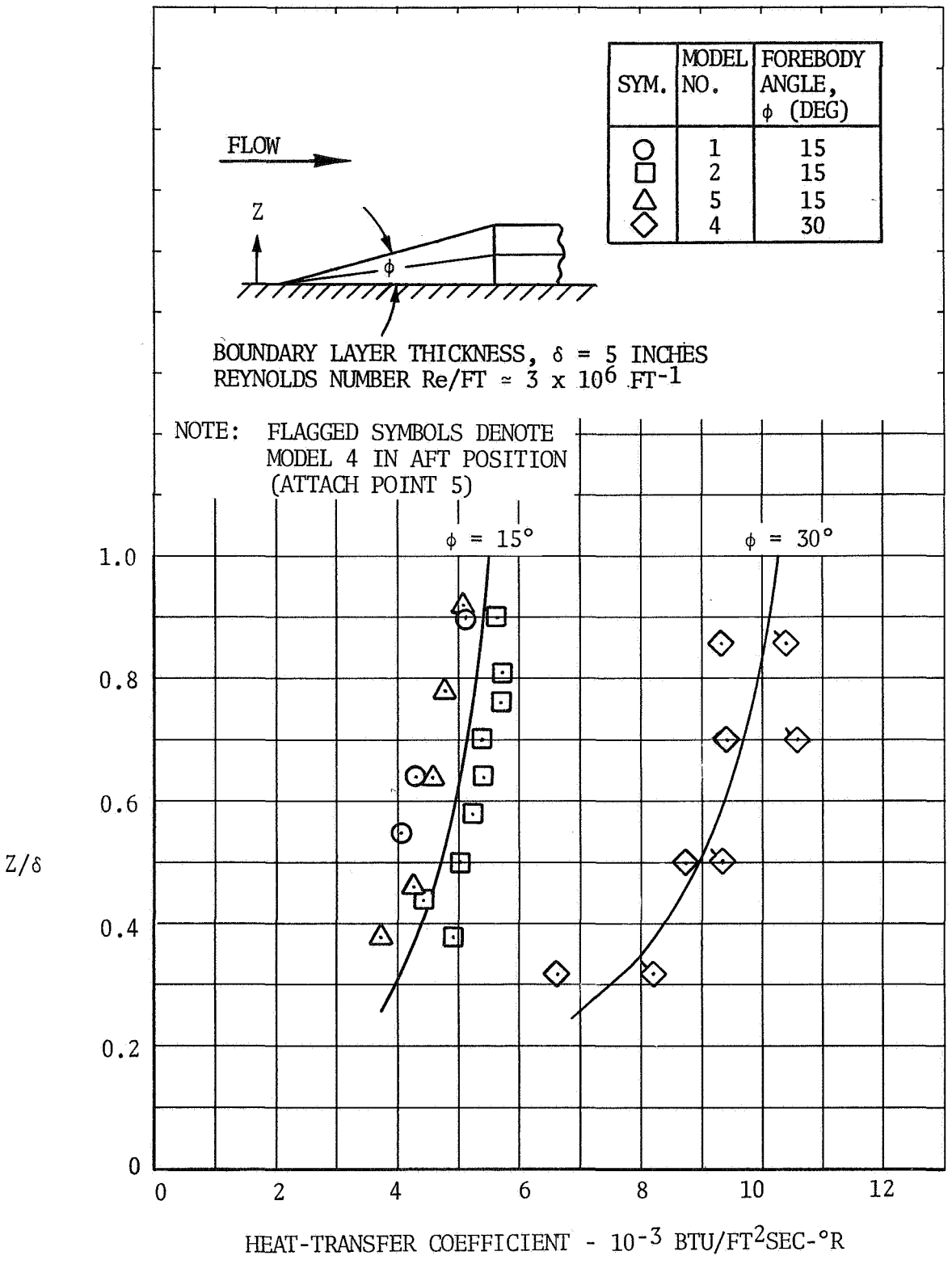

FIGURE 4-17. HEAT-TRANSFER COEFFICIENTS ON MODEL FOREBODIES - MODELS 1, 2, 4 AND 5 (M = 3.51)

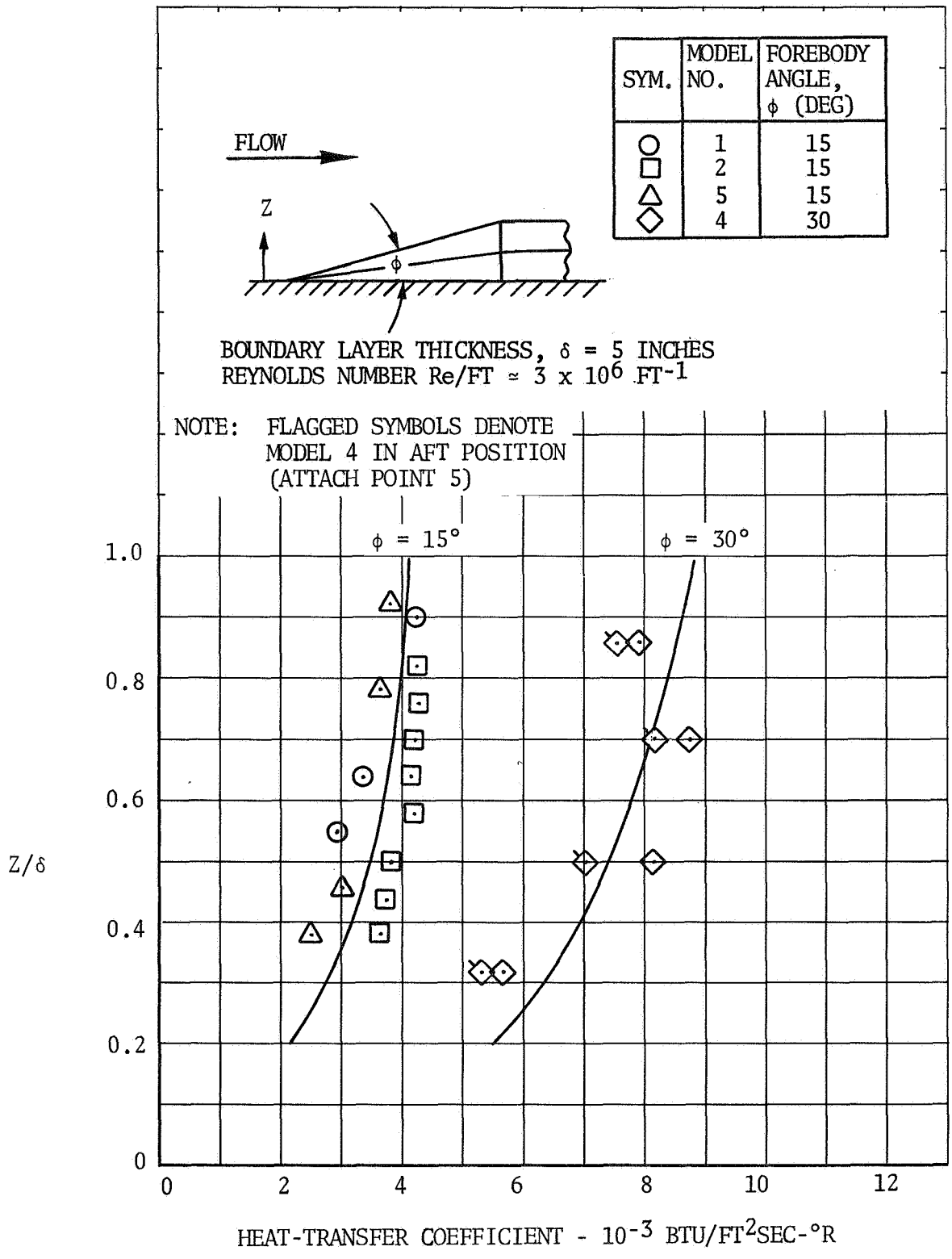

FIGURE 4-18. HEAT-TRANSFER COEFFICIENTS ON MODEL FOREBODIES - MODELS 1, 2, 4 AND 5 (M = 4.44)

5.0 HAT SECTION AND GAP ENVIRONMENT

Hat section models (Models 13 through 16) were added as a part of the protuberance test program after analysis indicated that hat sections which had been placed between stringers on the S-IVB forward skirt would significantly increase the local heating environment. The main heating problem was not the local increases caused by protuberance effects but high heating on the stringers caused by gaps which existed between the anti-flutter hat sections and the stringers. Because of the complexity of the flow field, this configuration was added to the protuberance test to verify the analysis.

Only one of the four hat section models (Model 13) tested, produced sufficient data for correlation purposes. The other hat section configurations provided only enough data to observe general trends (lack of instrumentation). These data are contained in Appendix A as heat-transfer coefficient ratios (Figures A-64 through A-69) and in Reference 1 as basic coefficients. The following paragraphs describe the heating and pressure data obtained on the plate around the hat section and in the gaps between stringers and hat sections.

The Model 13 hat sections were 0.5 inch in height and 0.5 inch wide (Figure 2-3) and are mounted between stringers as shown in Figure 2-1 (configurations 11 and 12). The hat sections are immersed in a 5-inch turbulent boundary layer. Figures 5-1, 5-2, and 5-3 show the pressure coefficient distributions on the plate caused by the hat sections (configuration 11) for Mach numbers of 2.49, 3.51 and 4.44. It is evident that there is a significant pressure increase ahead of the hat sections which diminishes with successive hat sections as would be expected with losses in total pressure with each hat section encountered. The pressure rise is well below that which would be caused by a normal shock (using Mach number at top of hat) and corresponds to that which would exist under flow separation conditions ahead of the hat sections. Figure 5-4 shows a comparison of the pressure data ahead of the first hat section compared with data from Reference 8. The pressure data of this test correlates with the other test data and shows a significant boundary layer effect. The pressure also seems to be more dependent on free-stream Mach number as the wall surface is approached. The equation (Reference 9) shown on Figure 5-4 along with the data is sufficient to provide a method of estimating pressures ahead of a forward facing step submerged in a boundary layer.

The flat plate heating distributions for the hat section, configuration 11, are shown in Figures 5-5, 5-6, and 5-7. There is a rapid rise in heating ahead of each hat section with the peak values ahead of each hat in the train being about the same. Behind each hat section the heating drops below flat plate values. The average value of heating over the entire plate with hat sections is approximately the same as if there were no hat sections (data oscillates around $h/h_o = 1$). Data from various Y-coordinate locations have been plotted on these figures to more fully describe the interference region.

5.0 (Continued)

Pressure measurements were made on both the stringer and plate immediately ahead of the hat section and in the gap between the stringer and hat section. These data are plotted in Figure 5-8 in pressure coefficient form for all Mach numbers and for the first hat section in the train. It is evident at all Mach numbers that the pressure on the leeward side of the hat section is significantly lower than the front side pressures and indicates a choked flow condition (M = 1) in the gap. Figure 5-9 shows the heating on the stringer caused by the hat sections and gaps. The four double data points (at each Mach number) indicate the heating data within the gaps. The first two double data points are in the first hat section gap and the last two are in the second hat section gap. There is a significant heating gradient within the gap and the stringer heating ahead of and in the hat section gap is significantly above the clean plate heating.

Attempts have been made to correlate analytical calculations with the measured test data in the hat section gap. Since the flow in the gap was choked, it was assumed the boundary layer was laminar. The familiar Colburn equation for laminar flow was used with measured gap pressure to evaluate the heat-transfer coefficient. Figure 5-10 shows a comparison of the measured gap heat-transfer coefficient to the analytical calculation of an average gap coefficient and also the coefficient at X = L where L is the gap length. It is evident that the analytical calculations compare with the data when evaluated at X = L. The flow properties for these calculations were determined by evaluating the total temperature in the boundary layer at the top of the hat section using the boundary layer data of Reference 2. The static temperature in the gap was then evaluated using the total temperature at the top of the hat and a Mach number of 1. The transport properties of the air in the gap were then evaluated using the static temperature in the gap.

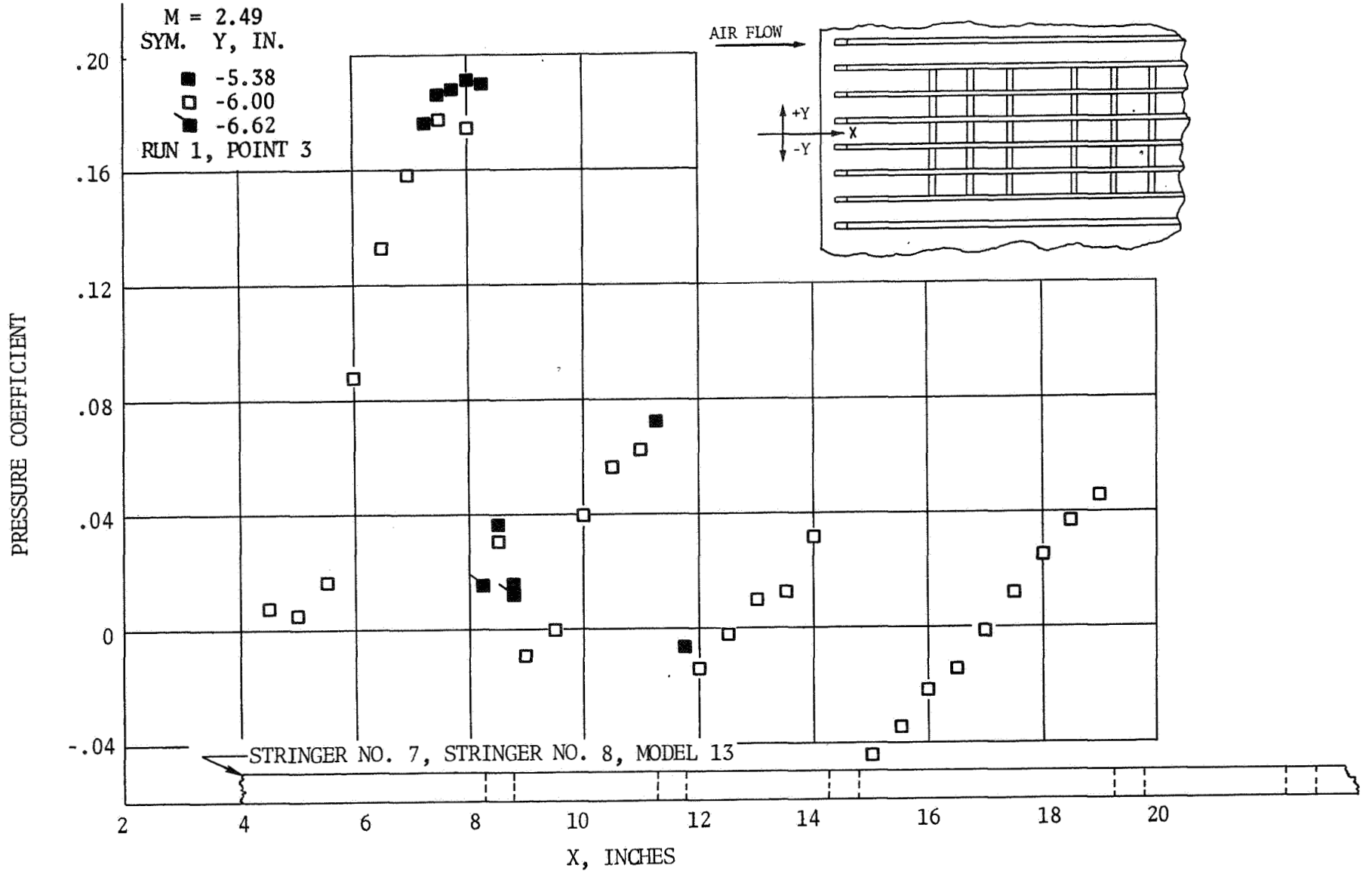

FIGURE 5-1. PLATE SURFACE PRESSURE COEFFICIENT DISTRIBUTION WITH STRINGERS AND HAT SECTIONS - CONFIGURATION 11 - M = 2.49

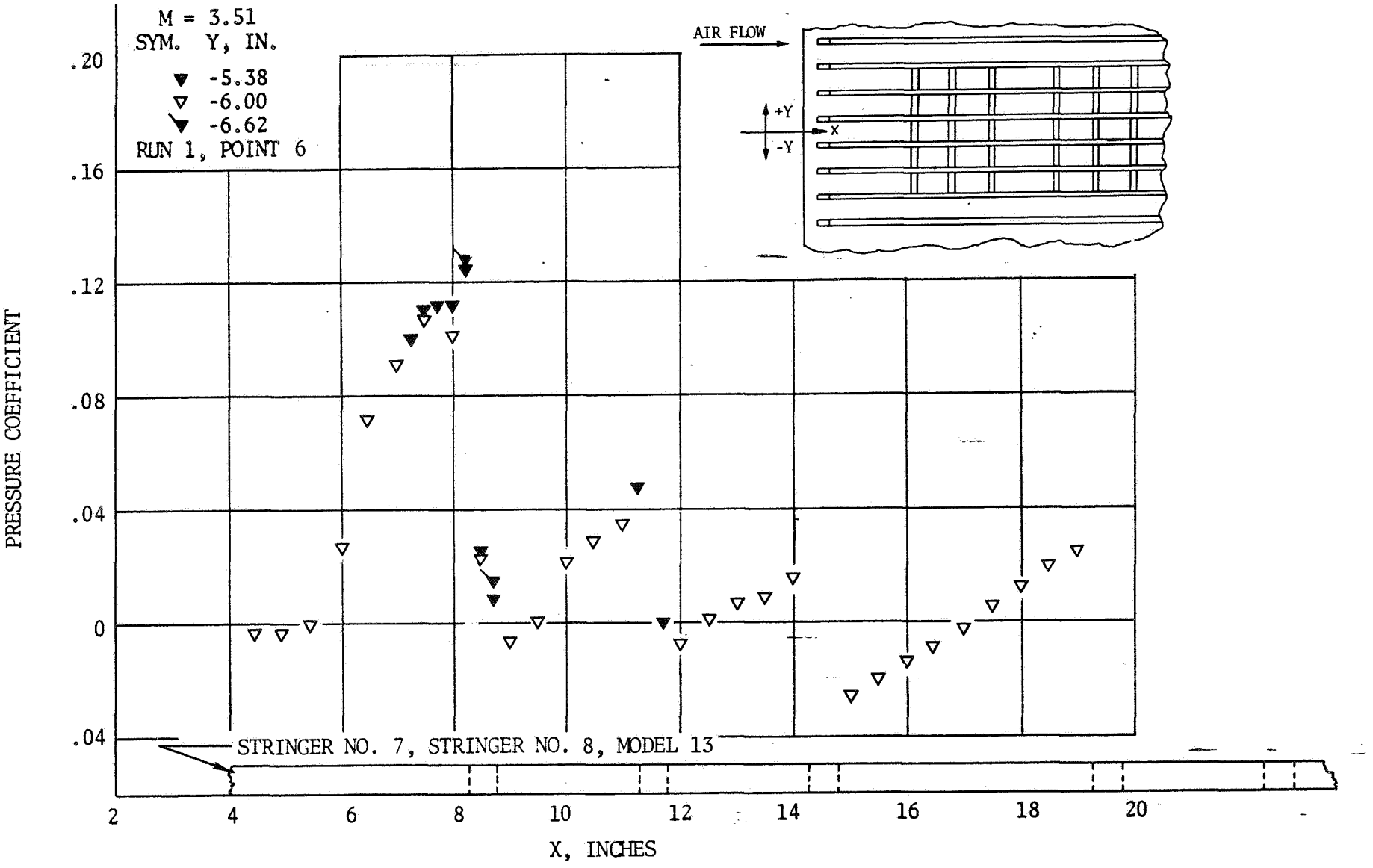

FIGURE 5-2. PLATE SURFACE PRESSURE COEFFICIENT DISTRIBUTION WITH STRINGERS AND HAT SECTIONS - CONFIGURATION 11 - M = 3.51

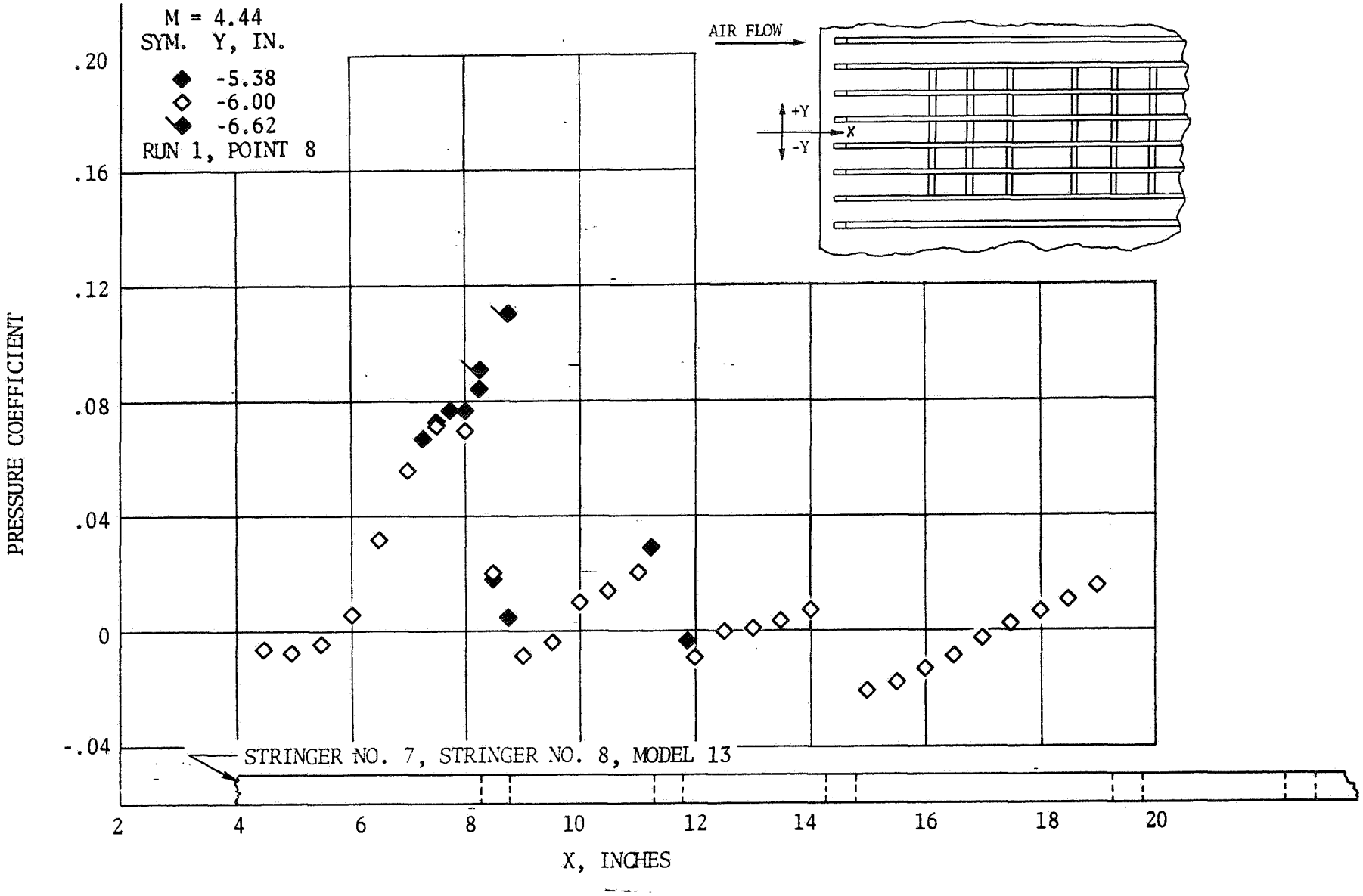

FIGURE 5-3. PLATE SURFACE PRESSURE COEFFICIENT DISTRIBUTION WITH STRINGERS AND HAT SECTIONS - CONFIGURATION 11 - M = 4.44

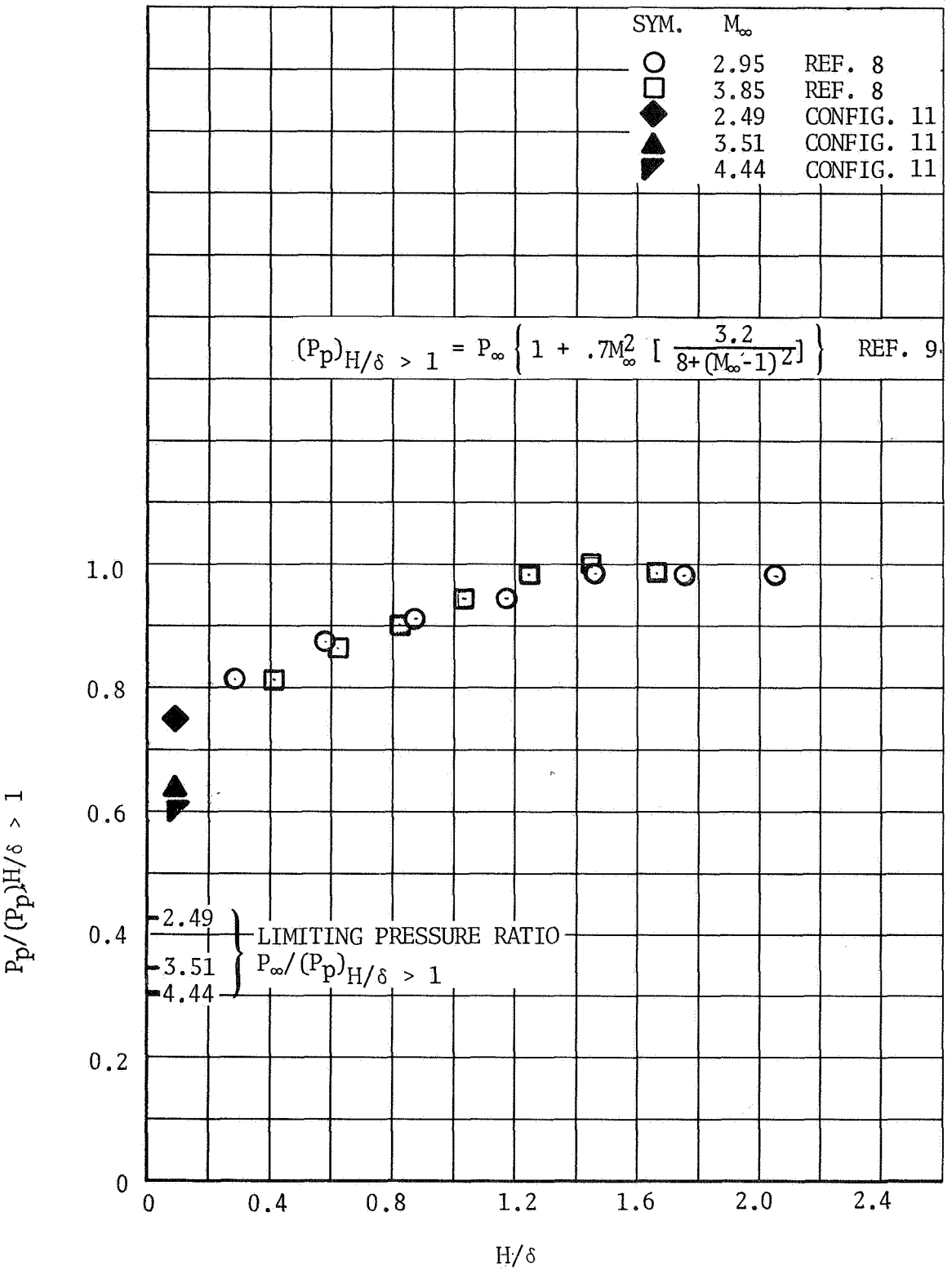

FIGURE 5-4. BOUNDARY LAYER EFFECTS ON PLATEAU PRESSURE AHEAD OF FIRST HAT SECTION (MODEL 13)

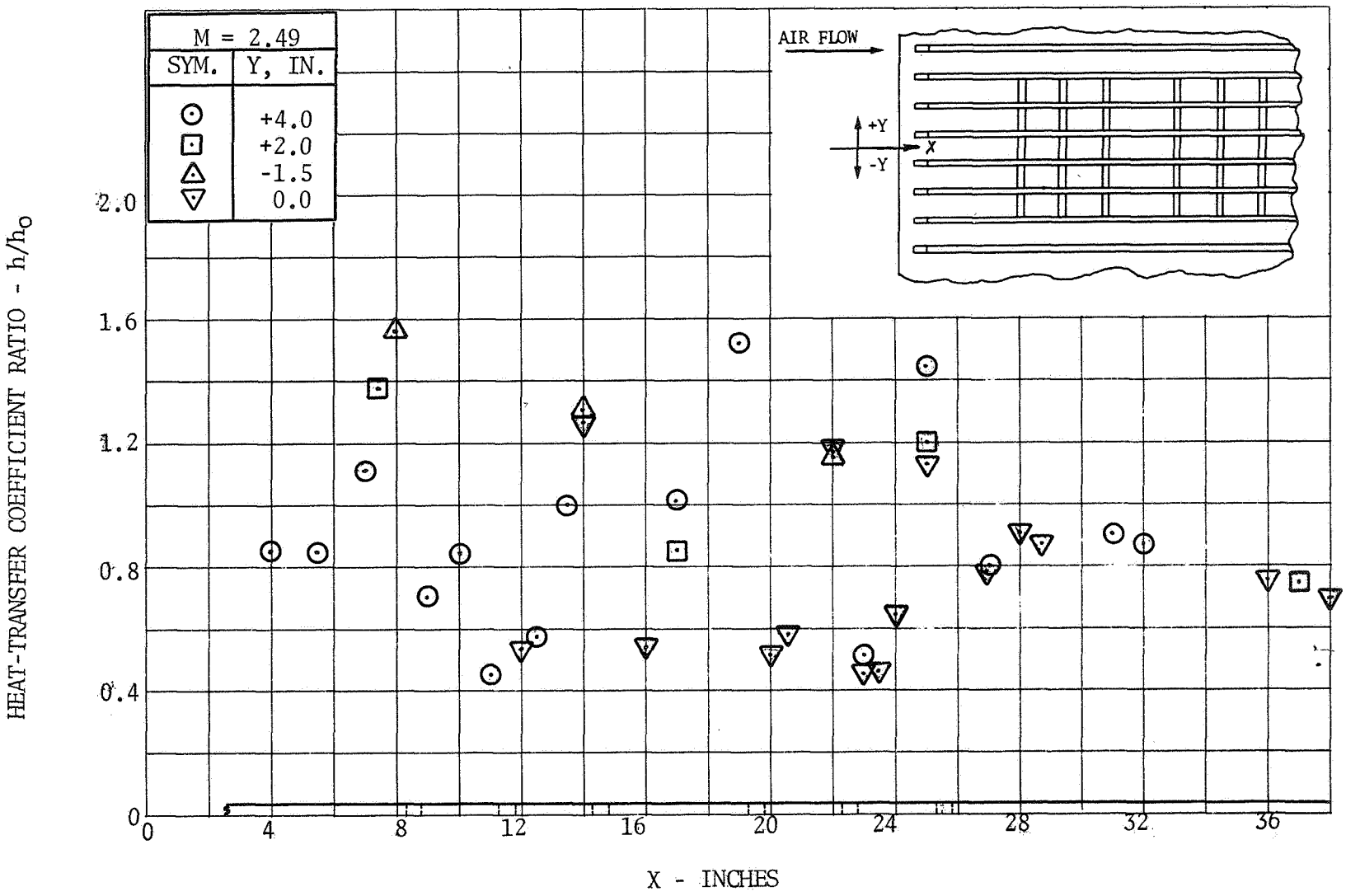

FIGURE 5-5. PLATE SURFACE HEAT-TRANSFER COEFFICIENT DISTRIBUTION WITH STRINGERS AND HAT SECTIONS - CONFIGURATION 11, M = 2.49

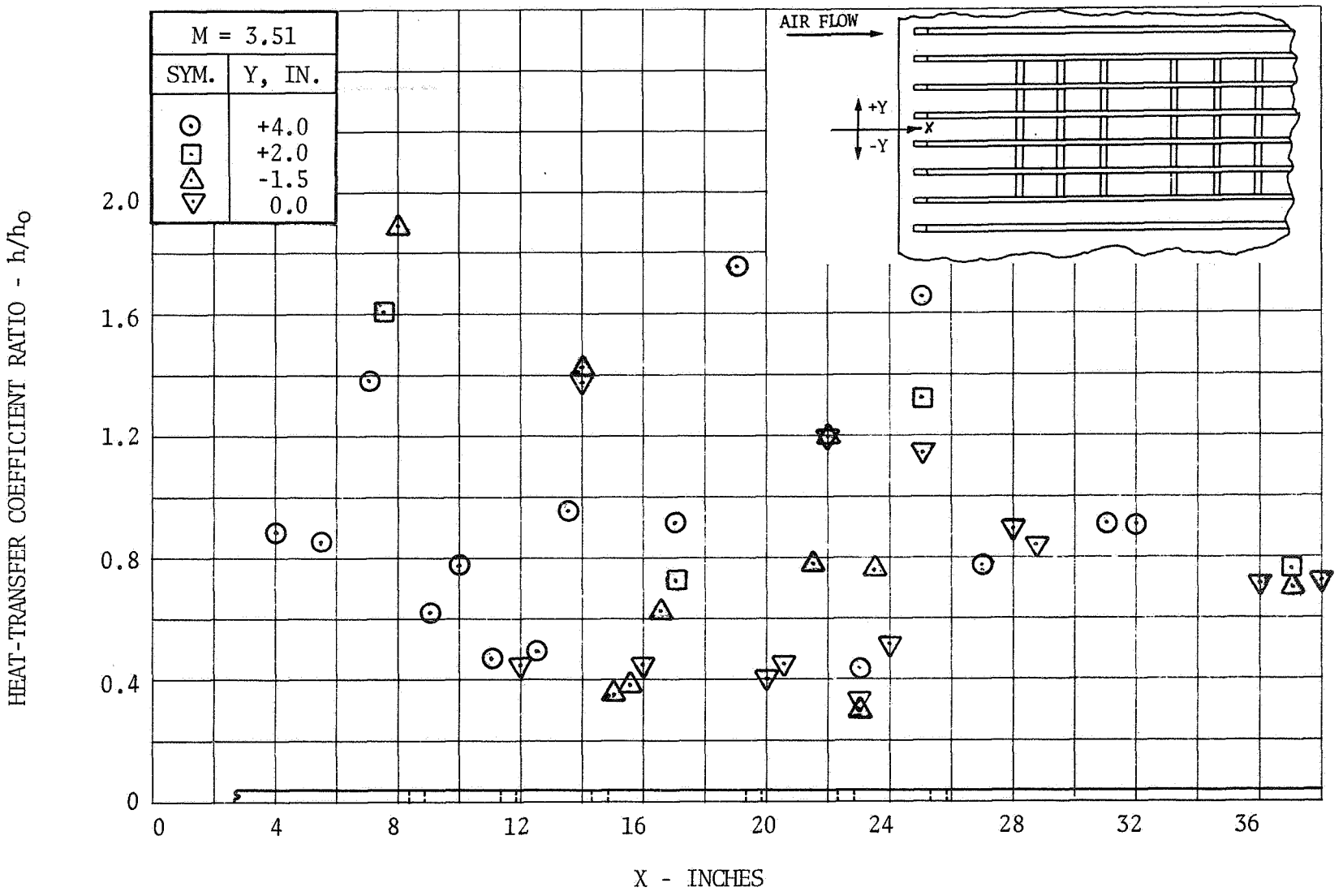

FIGURE 5-6. PLATE SURFACE HEAT-TRANSFER COEFFICIENT DISTRIBUTION WITH STRINGERS AND HAT SECTIONS - CONFIGURATION 11, M = 3.51

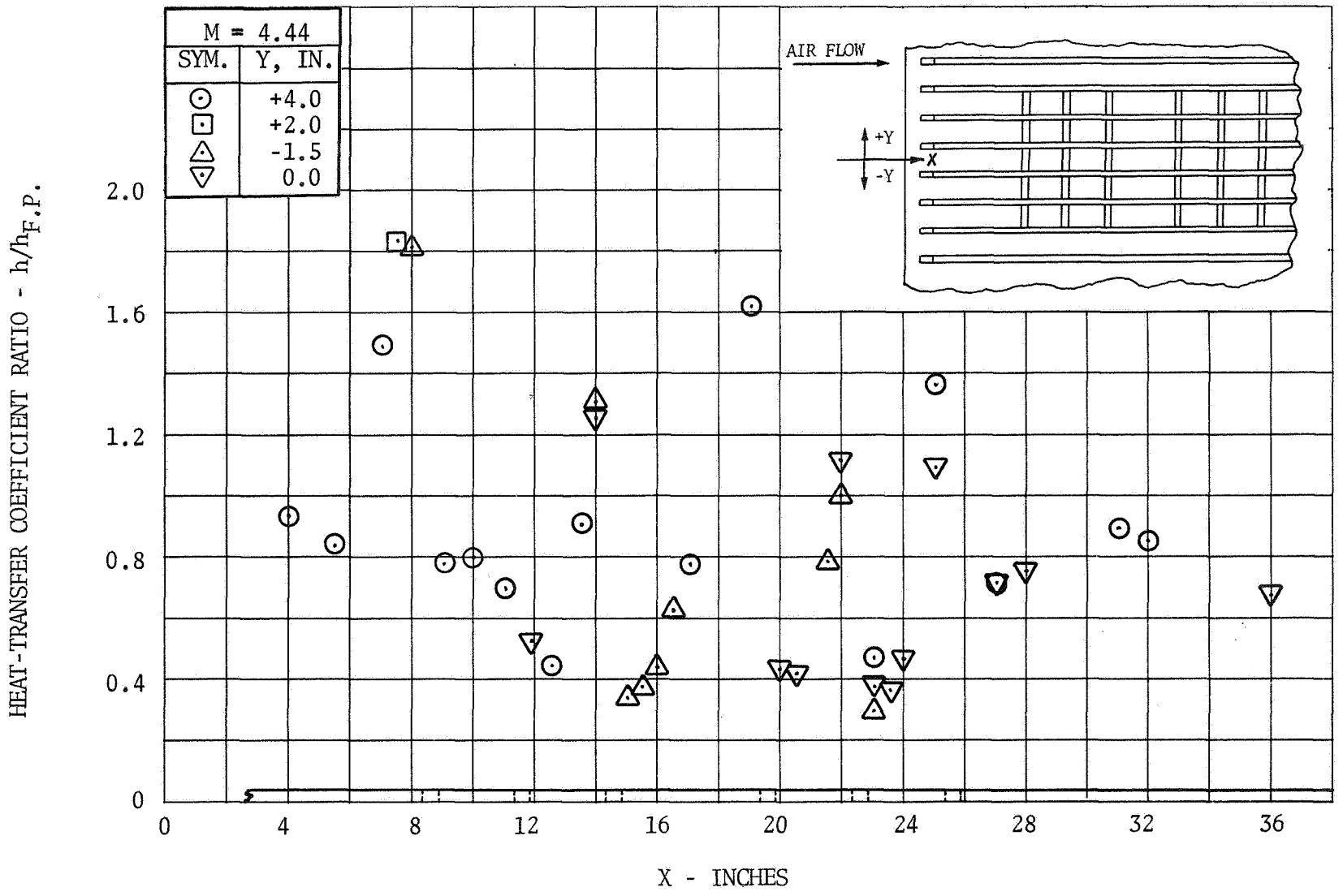

FIGURE 5-7. PLATE SURFACE HEAT-TRANSFER COEFFICIENT DISTRIBUTION WITH STRINGERS AND HAT SECTIONS - CONFIGURATION 11, M = 4.44

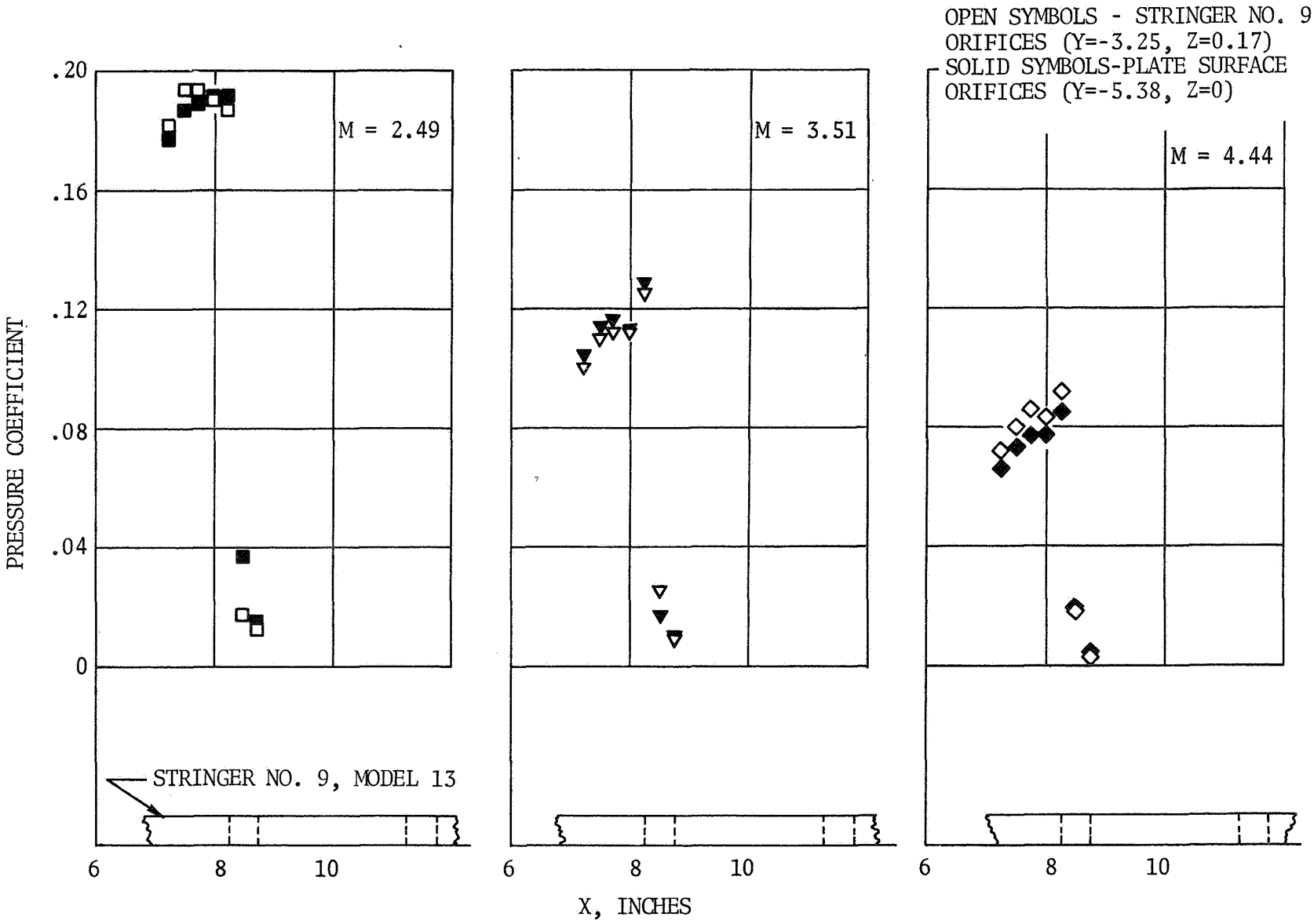

FIGURE 5-8. STRINGER NO. 9 AND GAP PRESSURE COEFFICIENT DISTRIBUTION - CONFIGURATION 11

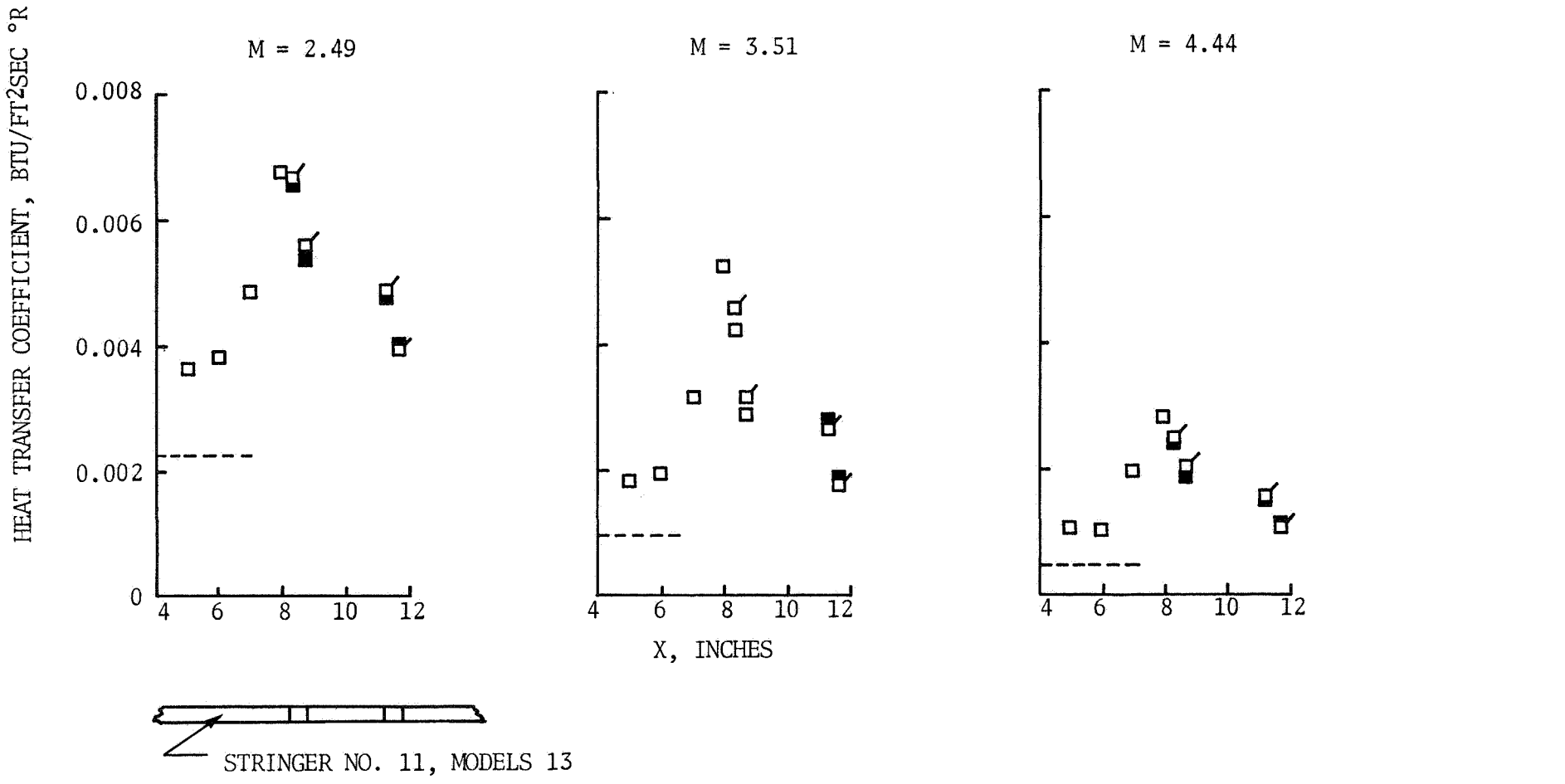

FIGURE 5-9. STRINGER NO. 11 AND GAP HEAT-TRANSFER COEFFICIENT DISTRIBUTION - CONFIGURATION 12

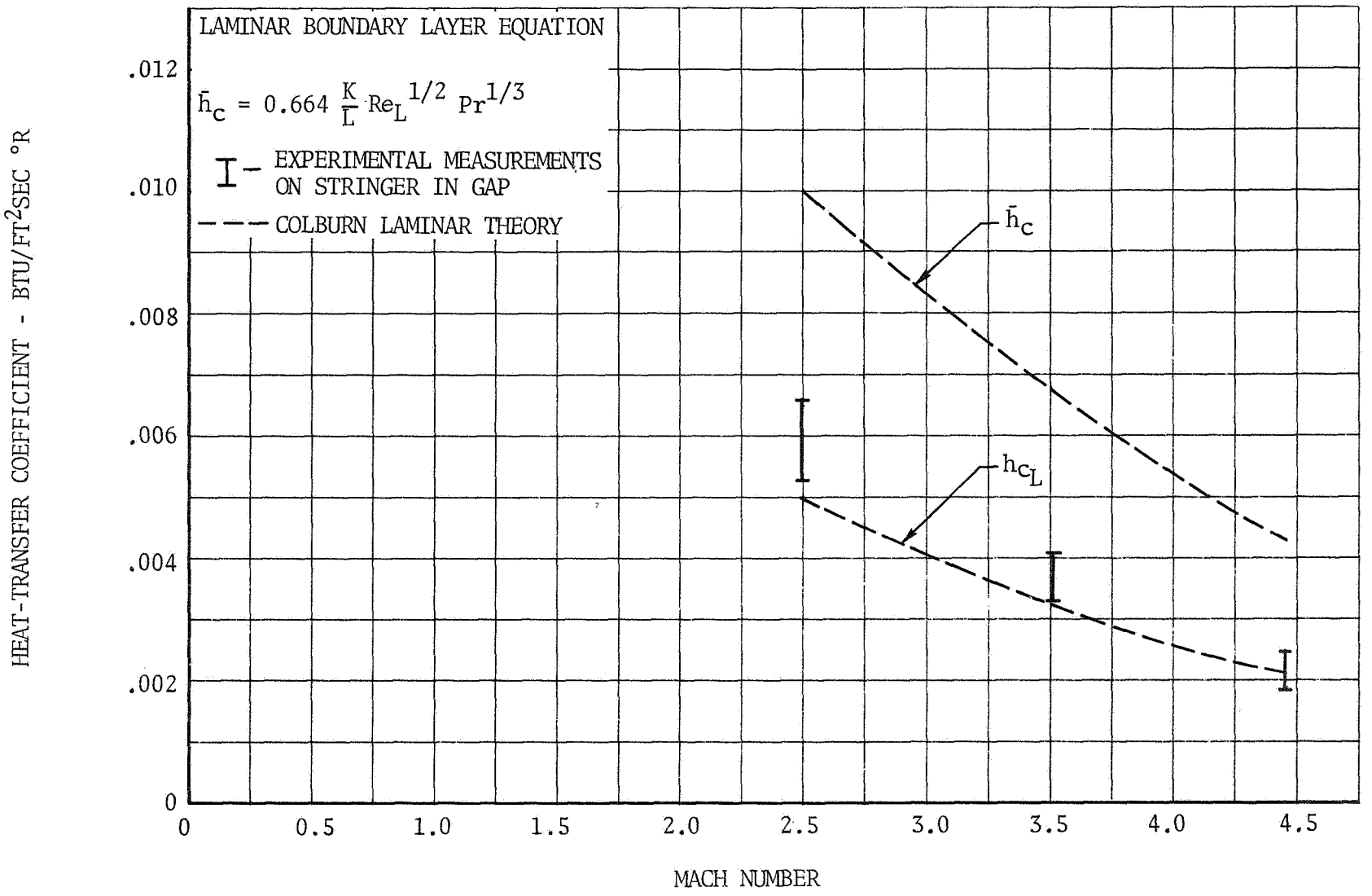

FIGURE 5-10. CORRELATION OF EXPERIMENTAL AND ANALYTICAL HEAT-TRANSFER COEFFICIENTS IN GAP

6.0 CONCLUSIONS

Flat Plate

1. The magnitude of heat-transfer coefficients measured on the clean plate surface were in reasonable agreement with those available from previous investigations, but were less than those predicted analytically.

2. The heat-transfer coefficient magnitude obtained on the plate with longitudinal stringers was reduced by 10 percent to 35 percent compared to the clean plate.

3. Multiple-protuberance interference heating effects in general were no more severe than for a single protuberance although a few single measurements on some multiple configurations were observed to have higher heating conditions. The distribution and surface areas affected by the increased heating have been modified. The maximum heat-transfer coefficient ratios (interference coefficient divided by clean plate coefficient) in the interference regions were approximately 2.0.

4. The plate heat-transfer coefficient magnitude obtained with multiple protuberance models with longitudinal stringers was generally less than that obtained for the equivalent model arrangement without stringers.

Protuberances

1. Protuberance forebody heating is significantly affected by the depth of immersion in the boundary layer. Heating in the lower portions of the boundary layer is considerably less.

2. Protuberance forebody heating decreases when the forebody is immersed in the aft wakes of other protuberances.

3. Analytically determined heat-transfer coefficients on a single protuberance forebody and centerbody compare favorably with measured values. No attempt was made to analytically determine flow properties or heating in protuberance wake regions.

4. Protuberance created shock waves which impinge on an adjacent protuberance will increase heating to that protuberance. The larger the forebody angle the stronger the shock and the greater the increase in heating.

Hat Section and Gap Heating

1. Significant increases in heating and pressure are realized on the surface ahead of hat sections ($H/\delta = 0.1$) placed perpendicular to the flow between stringers. The pressure rise has been correlated with empirical methods.

2. Pressures ahead of and behind the gap indicate a choked flow condition ($M = 1$) in the gap.

3. The heating in the gap between the stringers and hat sections can be significantly higher than clean plate heating. Laminar boundary layer theory with appropriate thermodynamic properties and length assumption and using measured pressure has been correlated with the heating in the gap. Peak heating in the gaps is reduced with successive downstream hat sections.

APPENDIX A

HEAT-TRANSFER COEFFICIENT RATIOS FOR TEST PLATE AND PROTUBERANCE MODELS

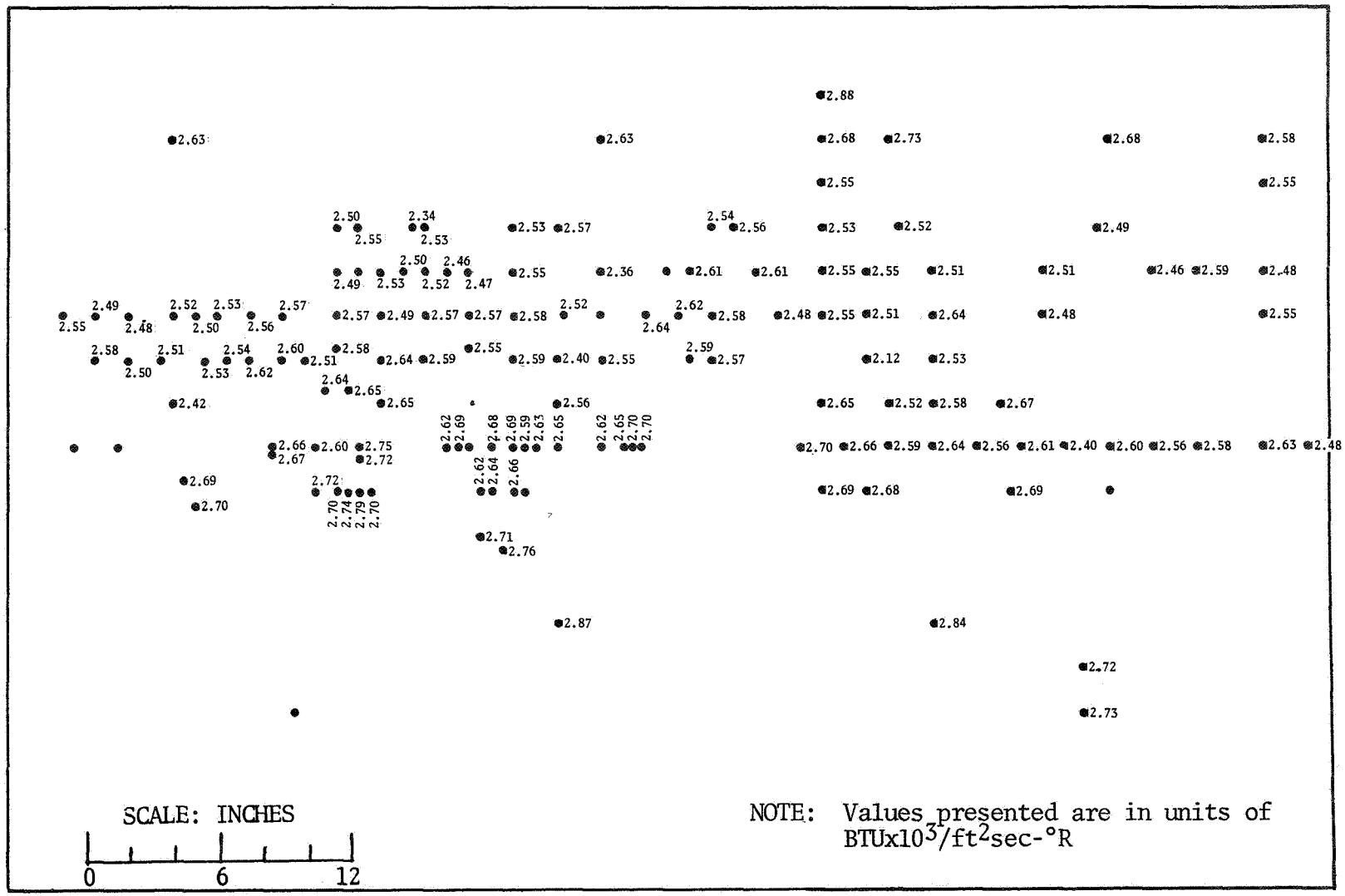

FIGURE A-1. CLEAN PLATE HEAT-TRANSFER COEFFICIENT DISTRIBUTION AT MACH NUMBER 2.49 - CONFIGURATION 1

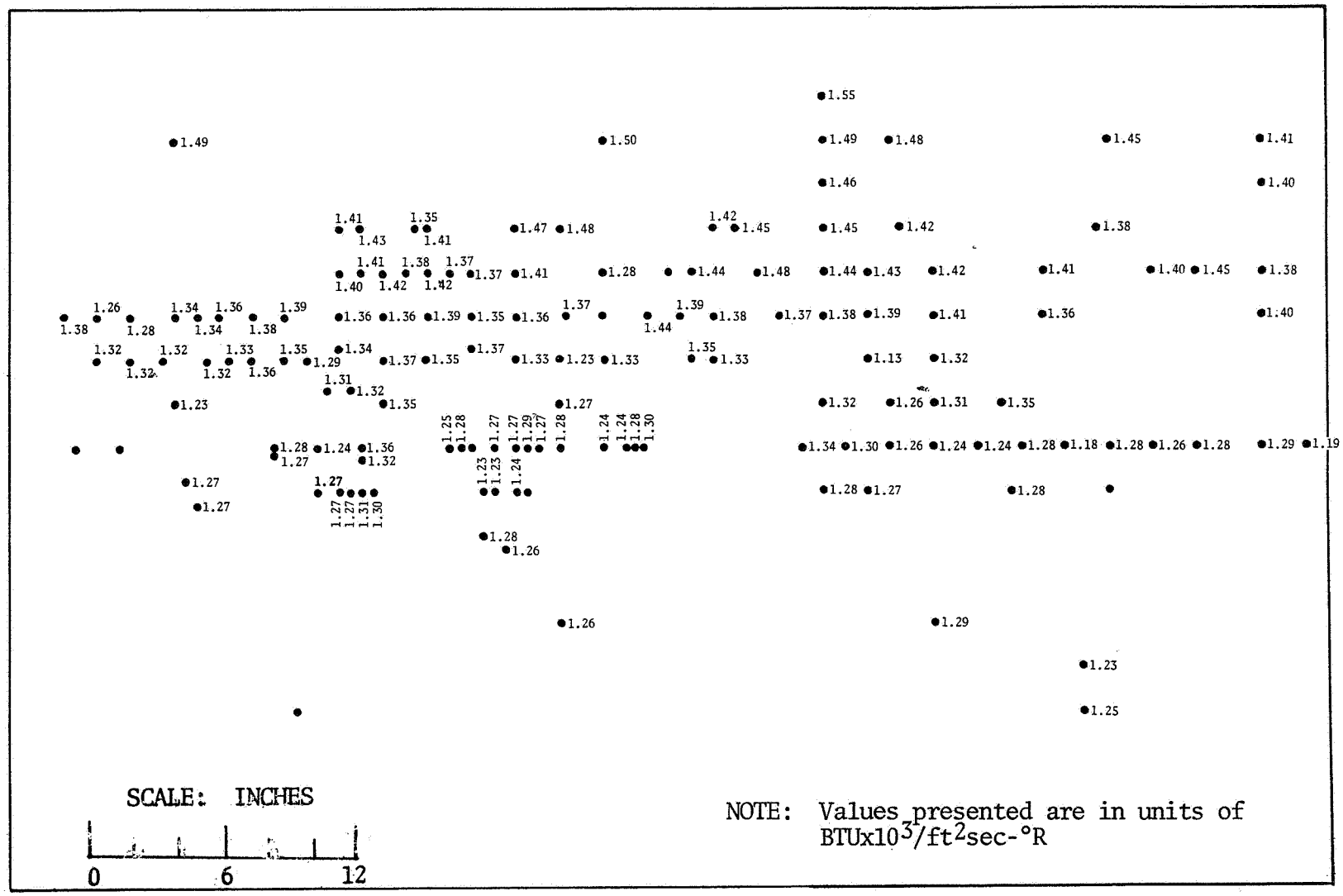

FIGURE A-2. CLEAN PLATE HEAT-TRANSFER COEFFICIENT DISTRIBUTION AT MACH NUMBER 3.51 - CONFIGURATION 1

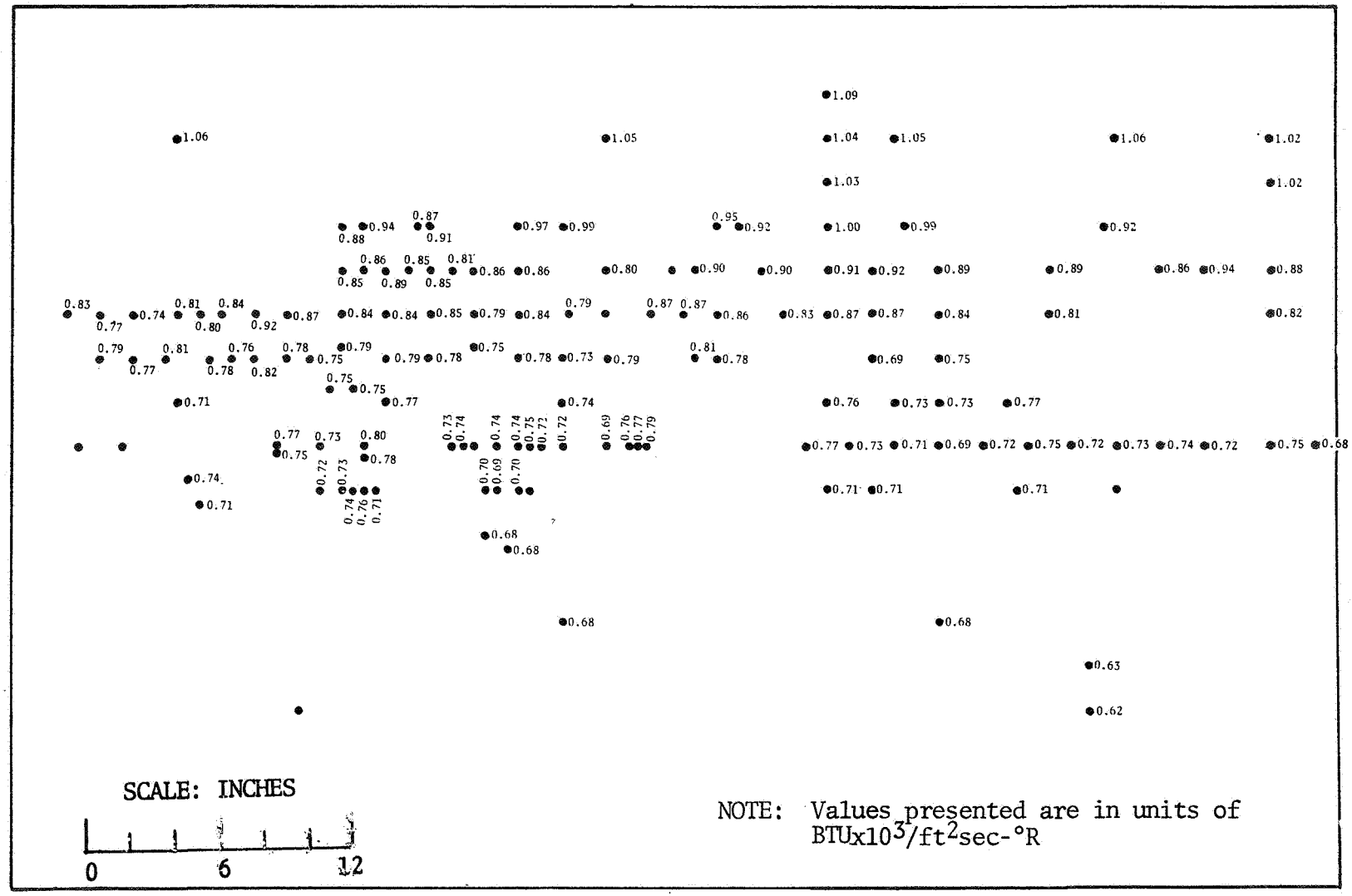

FIGURE A-3. CLEAN PLATE HEAT-TRANSFER COEFFICIENT DISTRIBUTION AT MACH NUMBER 4.44 - CONFIGURATION 1

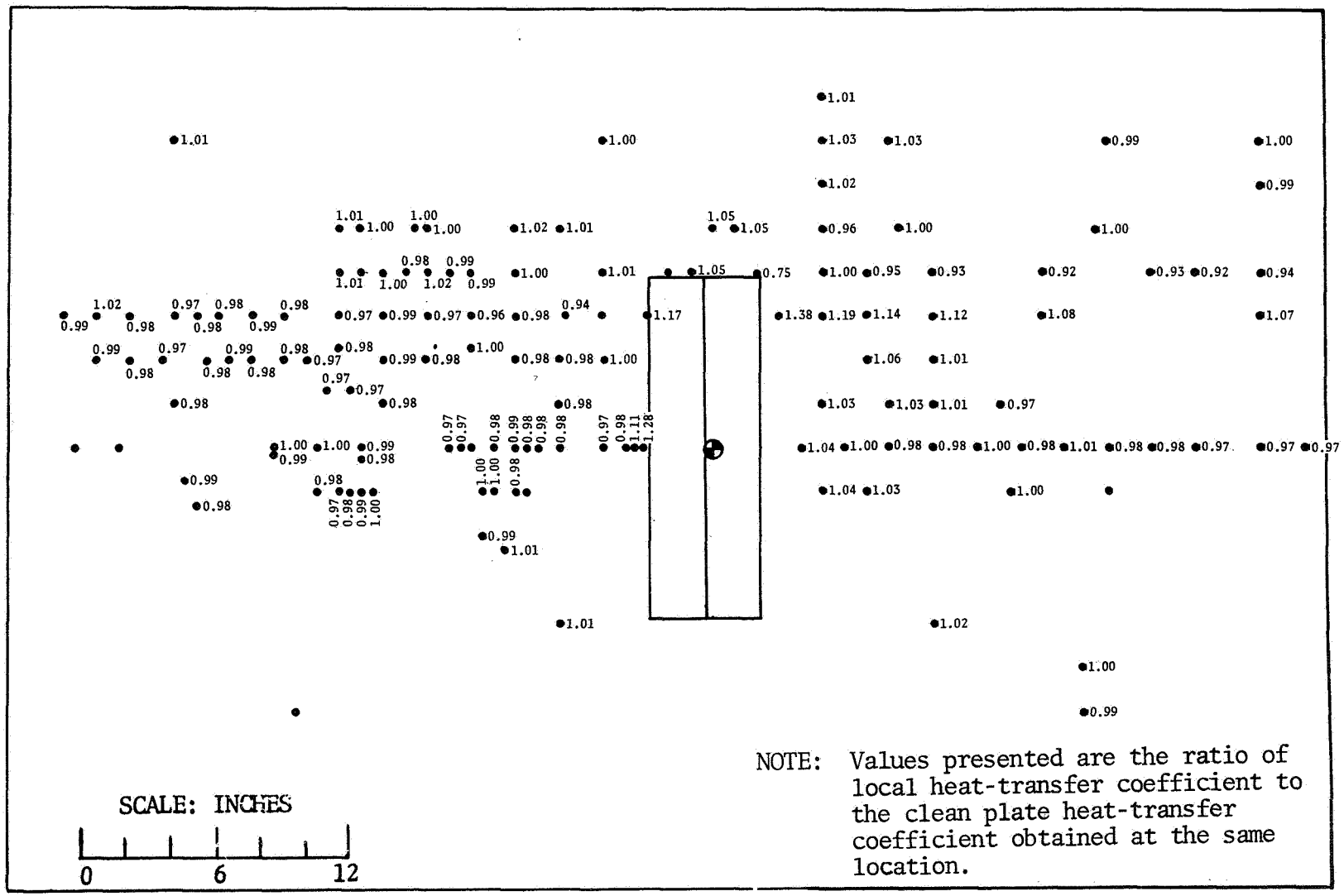

FIGURE A-4. EFFECT OF DOUBLE WEDGE (MODEL 12) ON PLATE HEATING DISTRIBUTION AT MACH NUMBER 2.49 - CONFIGURATION 2

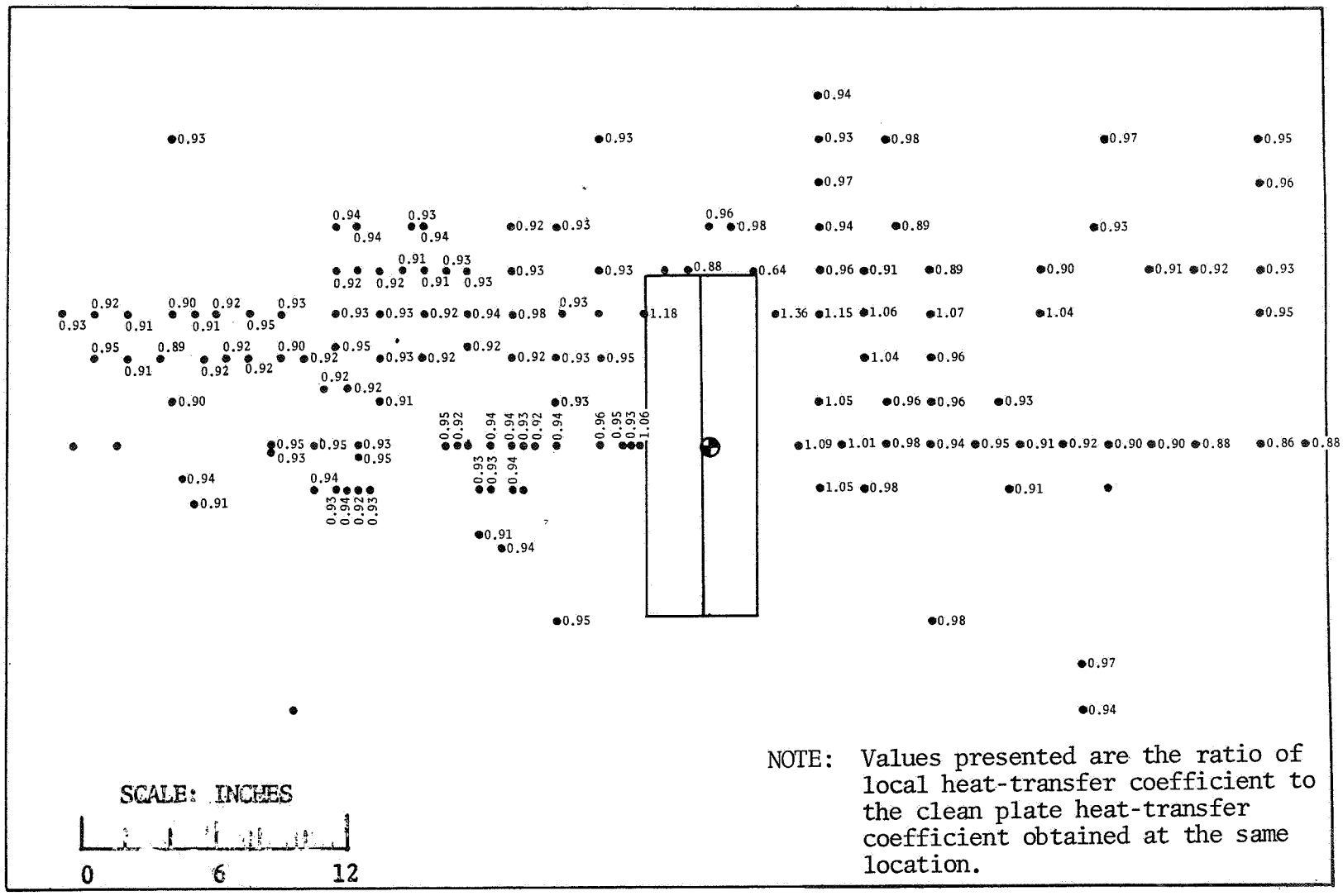

FIGURE A-5. EFFECT OF DOUBLE WEDGE (MODEL 12) ON PLATE HEATING DISTRIBUTION AT MACH NUMBER 3.51 - CONFIGURATION 2

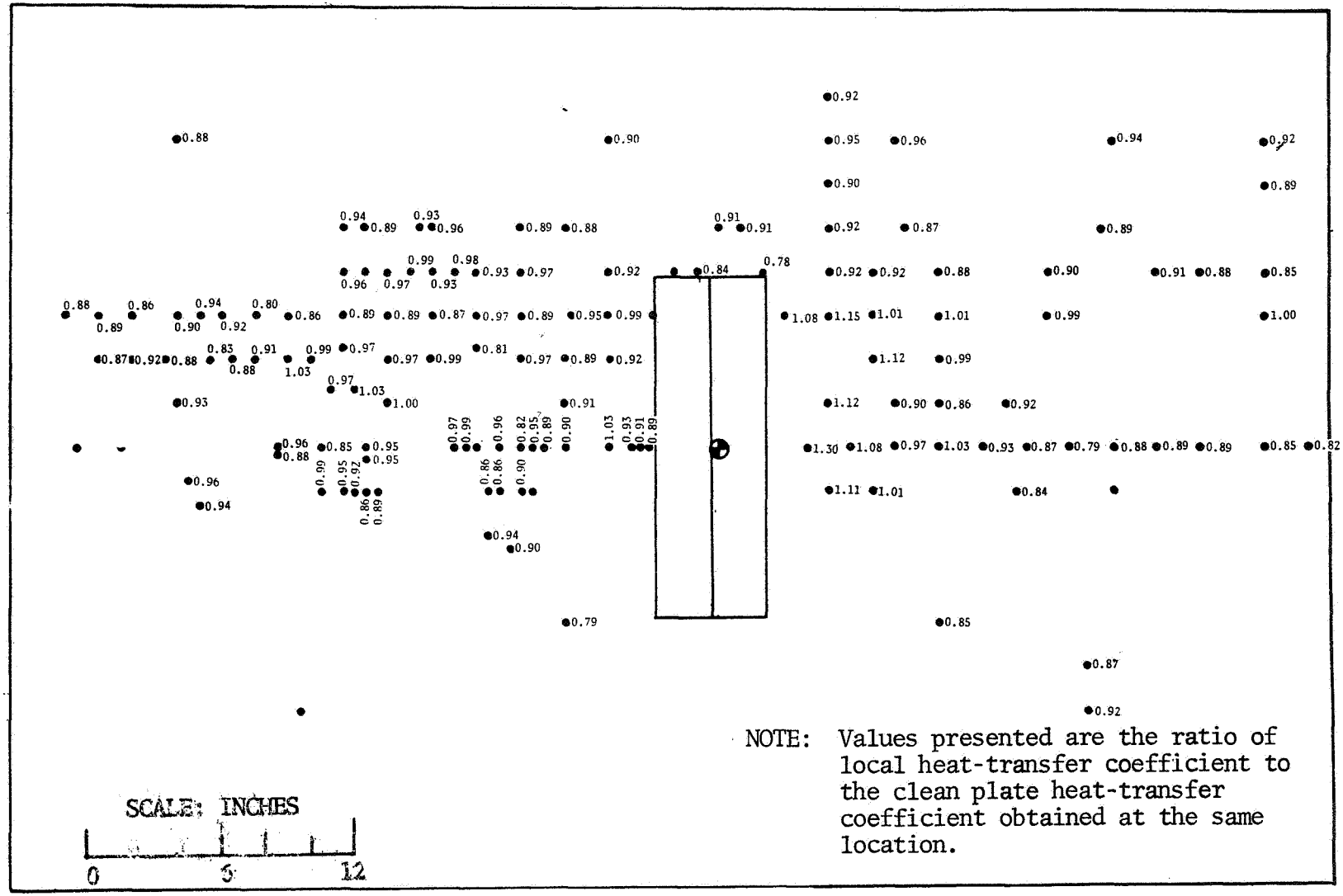

FIGURE A-6. EFFECT OF DOUBLE WEDGE (MODEL 12) ON PLATE HEATING DISTRIBUTION AT MACH NUMBER 4.44 - CONFIGURATION 2

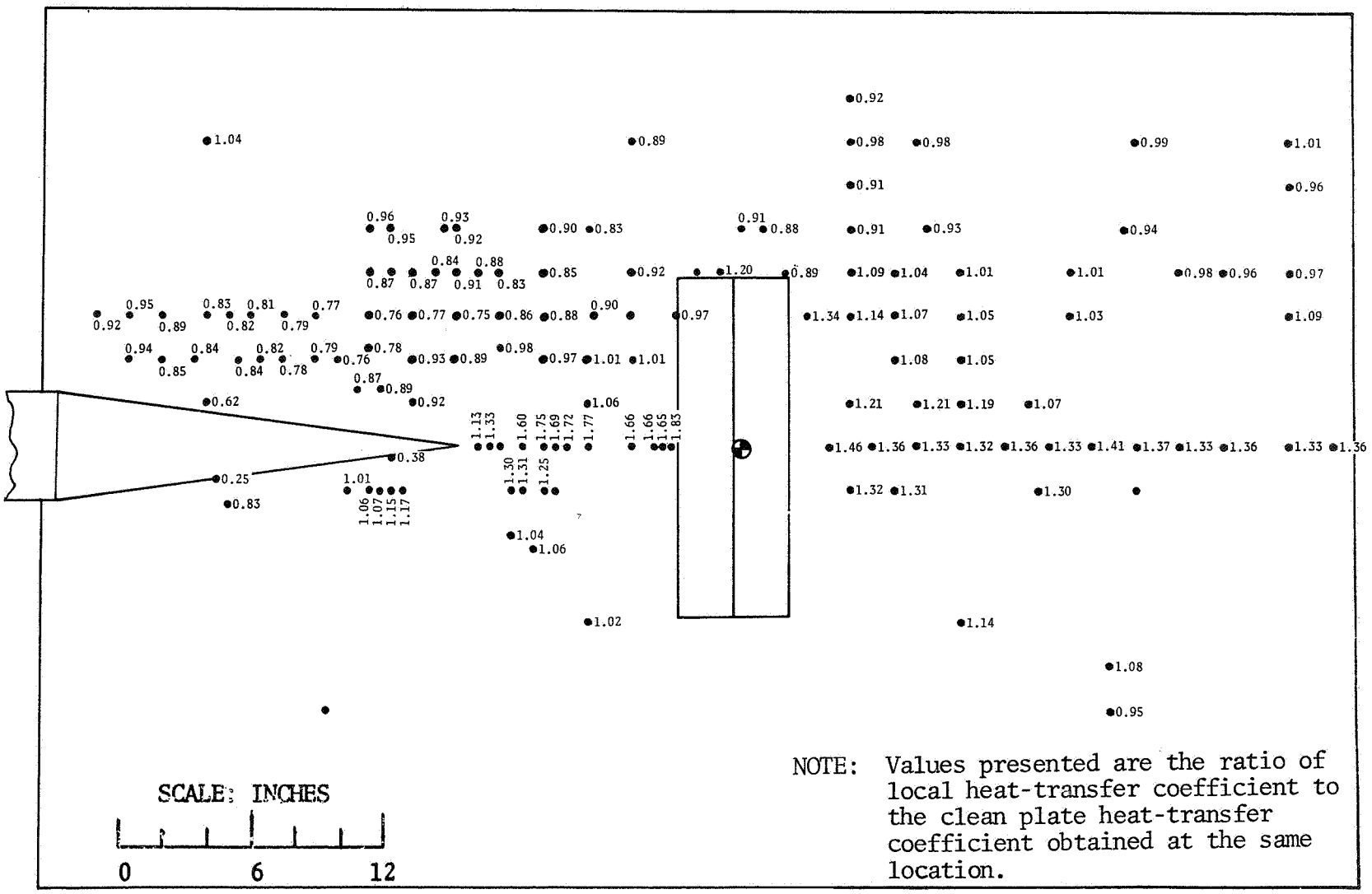

FIGURE A-7. EFFECT OF DOUBLE WEDGE (MODEL 12) IN MODEL 1 WAKE ON PLATE HEATING DISTRIBUTION AT MACH NUMBER 2.49 - CONFIGURATION 3

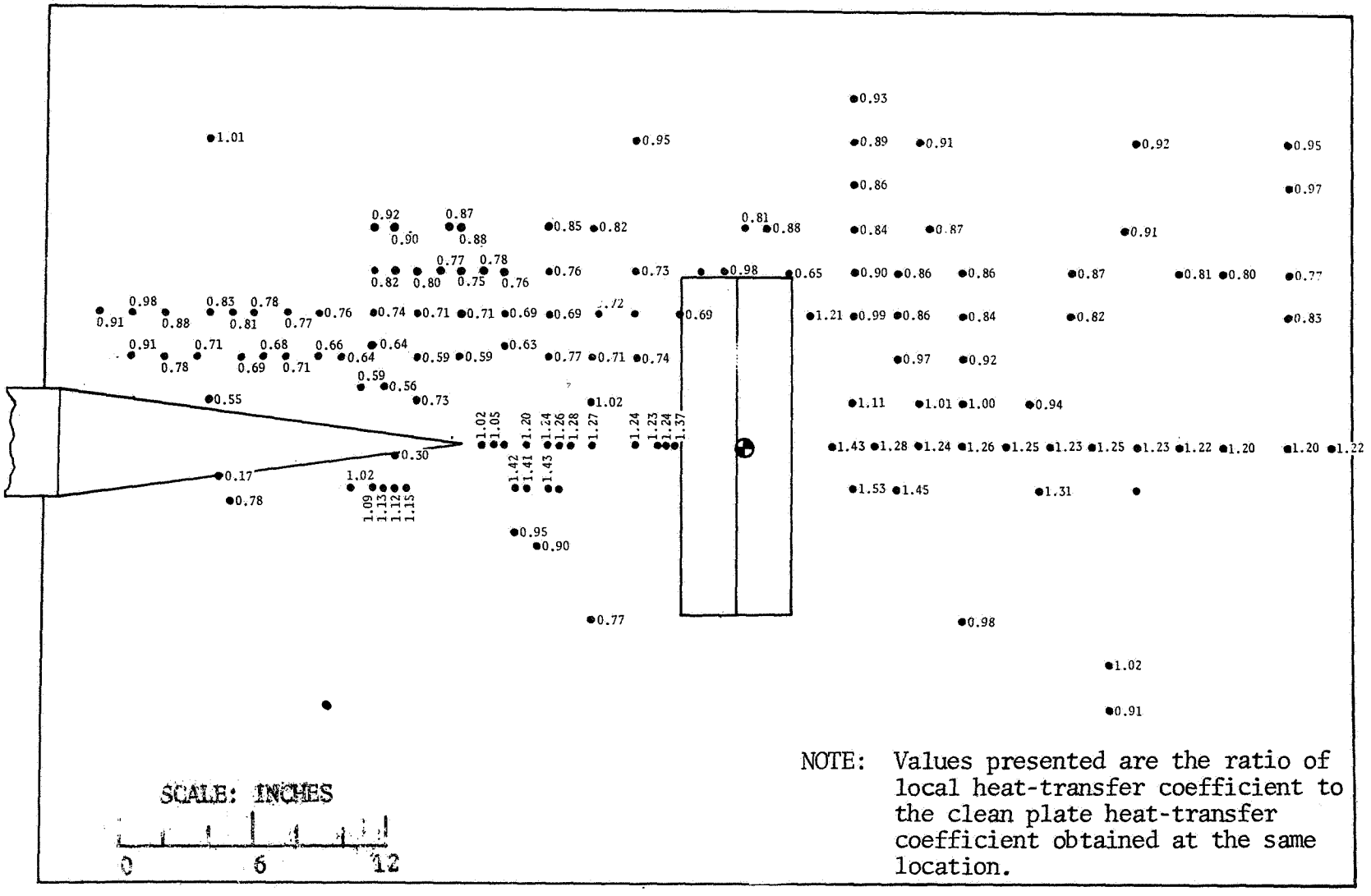

FIGURE A-8. EFFECT OF DOUBLE WEDGE (MODEL 12) IN MODEL 1 WAKE ON PLATE HEATING DISTRIBUTION AT MACH NUMBER 3.51 - CONFIGURATION 3

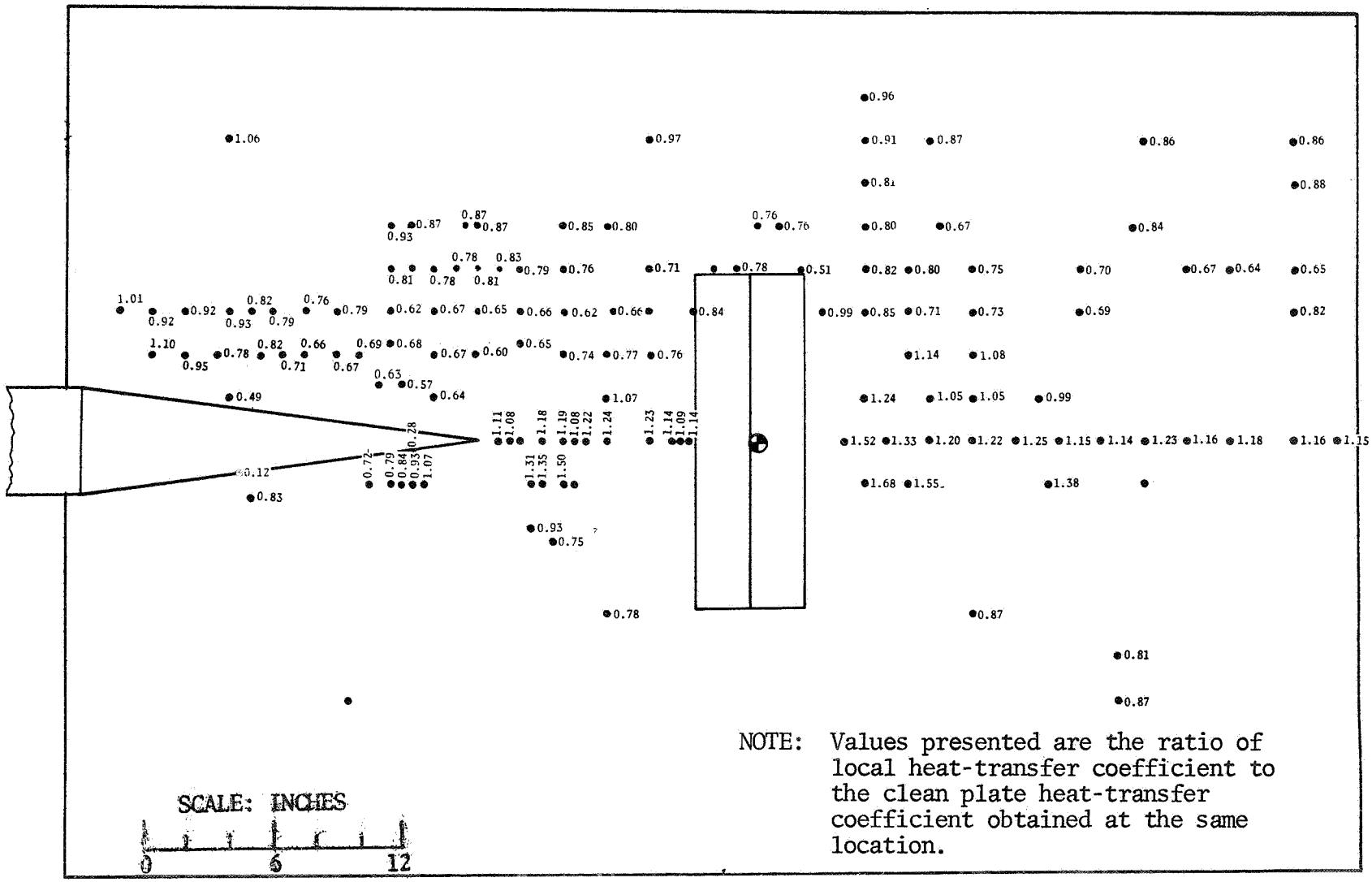

FIGURE A-9. EFFECT OF DOUBLE WEDGE (MODEL 12) IN MODEL 1 WAKE ON PLATE HEATING DISTRIBUTION AT MACH NUMBER 4.44 - CONFIGURATION 3

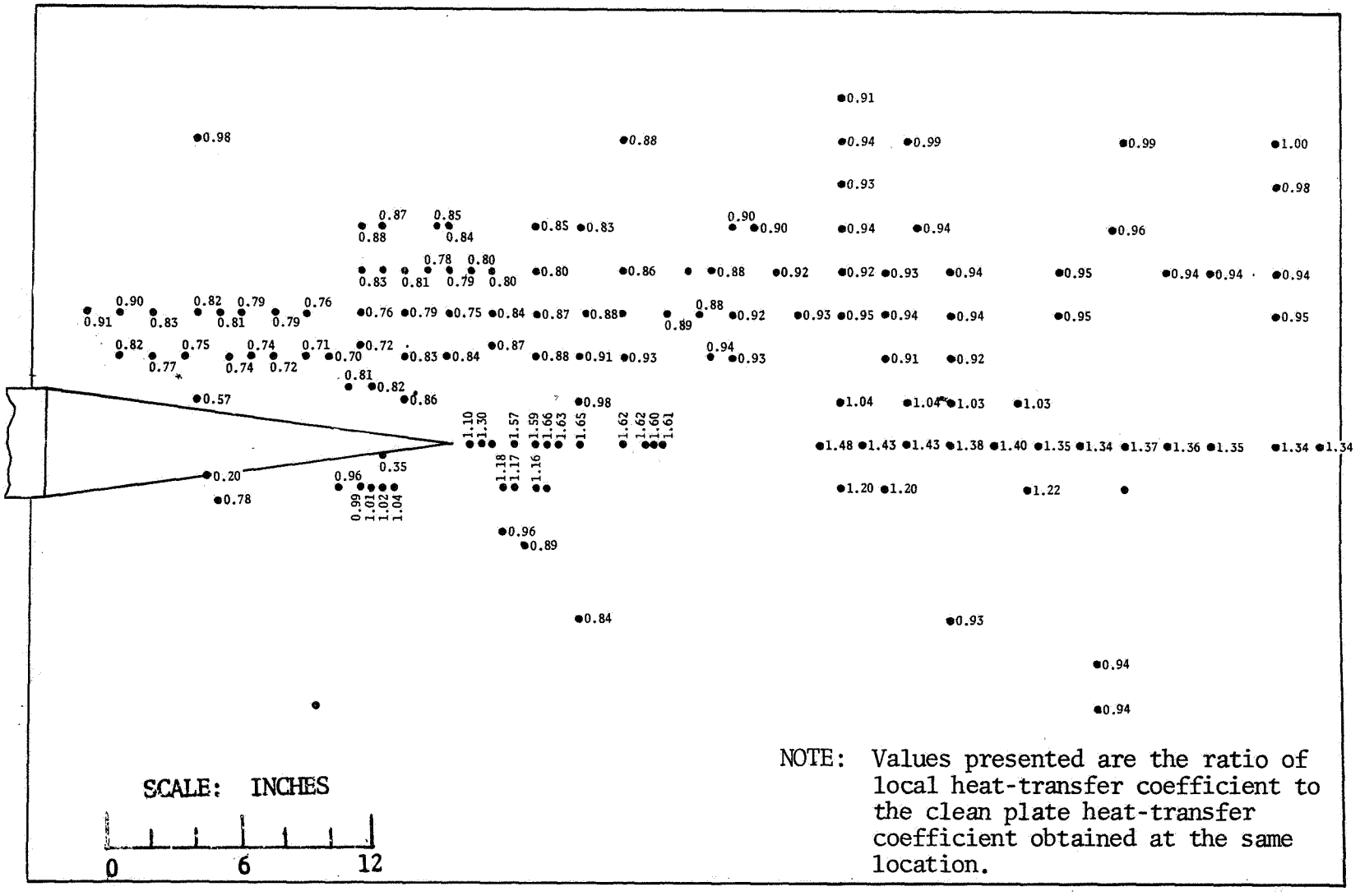

FIGURE A-10. EFFECT OF MODEL 1 WAKE ON PLATE HEATING DISTRIBUTION AT MACH NUMBER 2.49 - CONFIGURATION 4

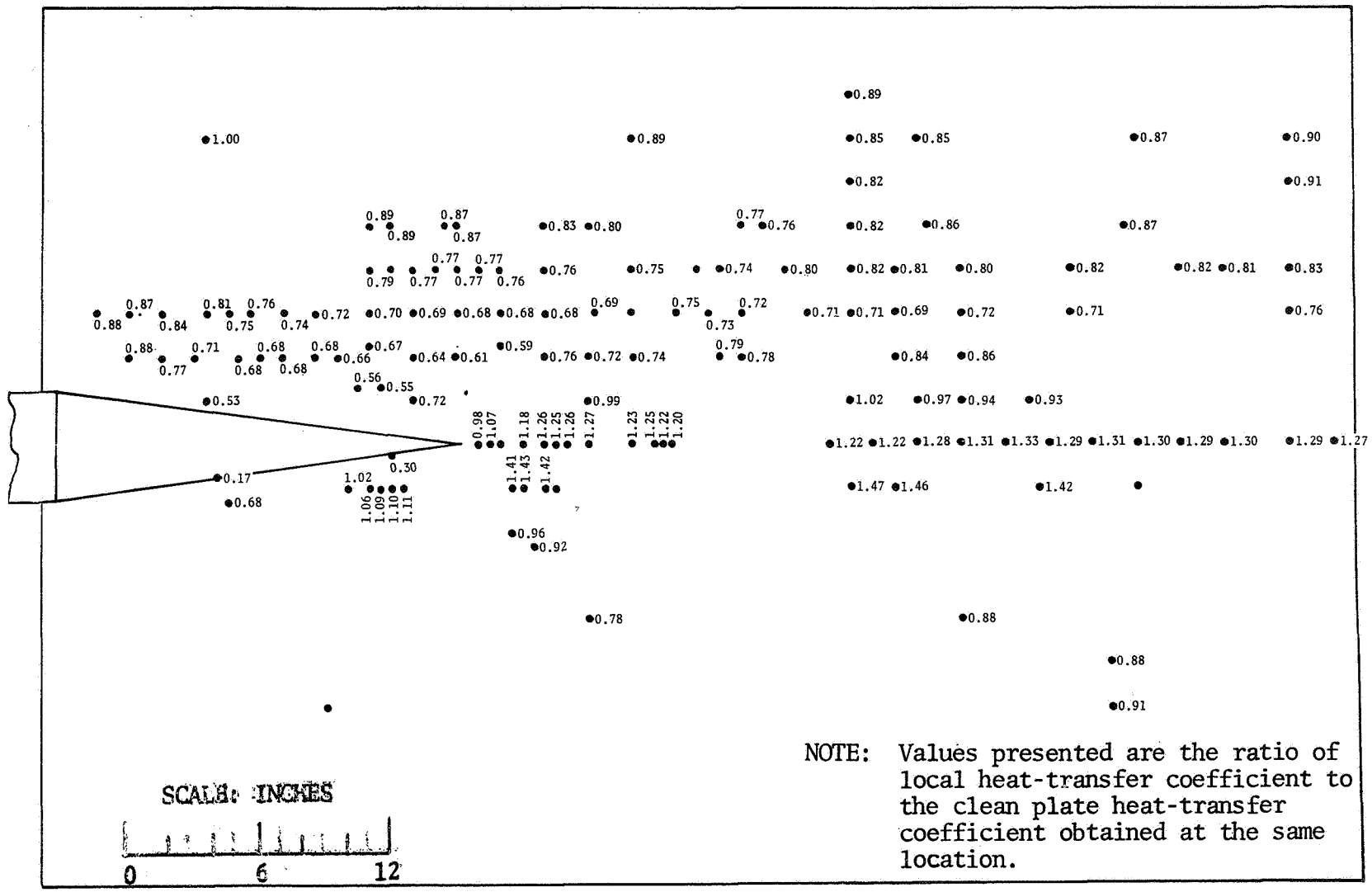

FIGURE A-11. EFFECT OF MODEL 1 WAKE ON PLATE HEATING DISTRIBUTION AT MACH NUMBER 3.51 - CONFIGURATION 4

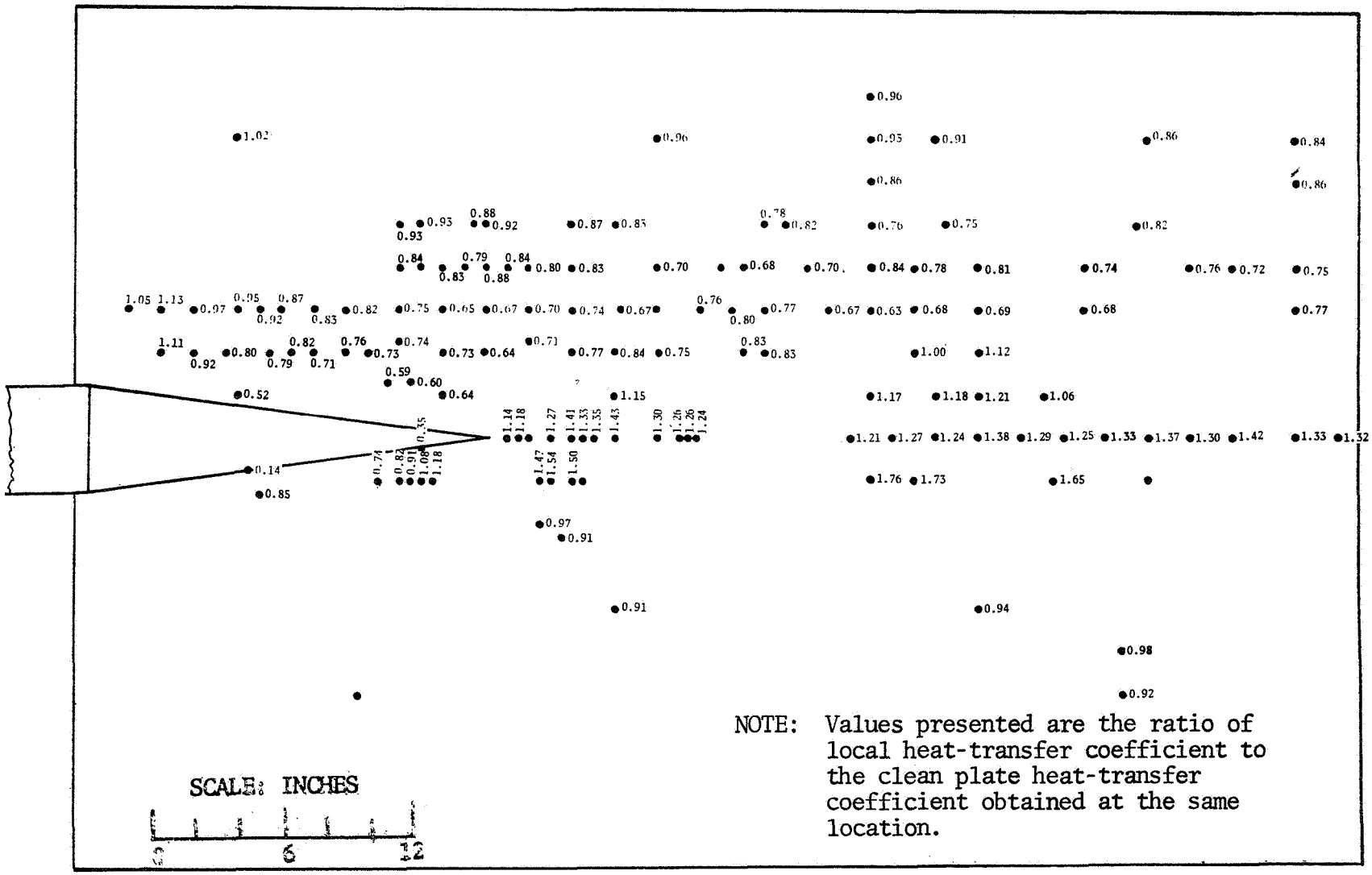

FIGURE A-12. EFFECT OF MODEL 1 WAKE ON PLATE HEATING DISTRIBUTION AT MACH NUMBER 4.44 - CONFIGURATION 4

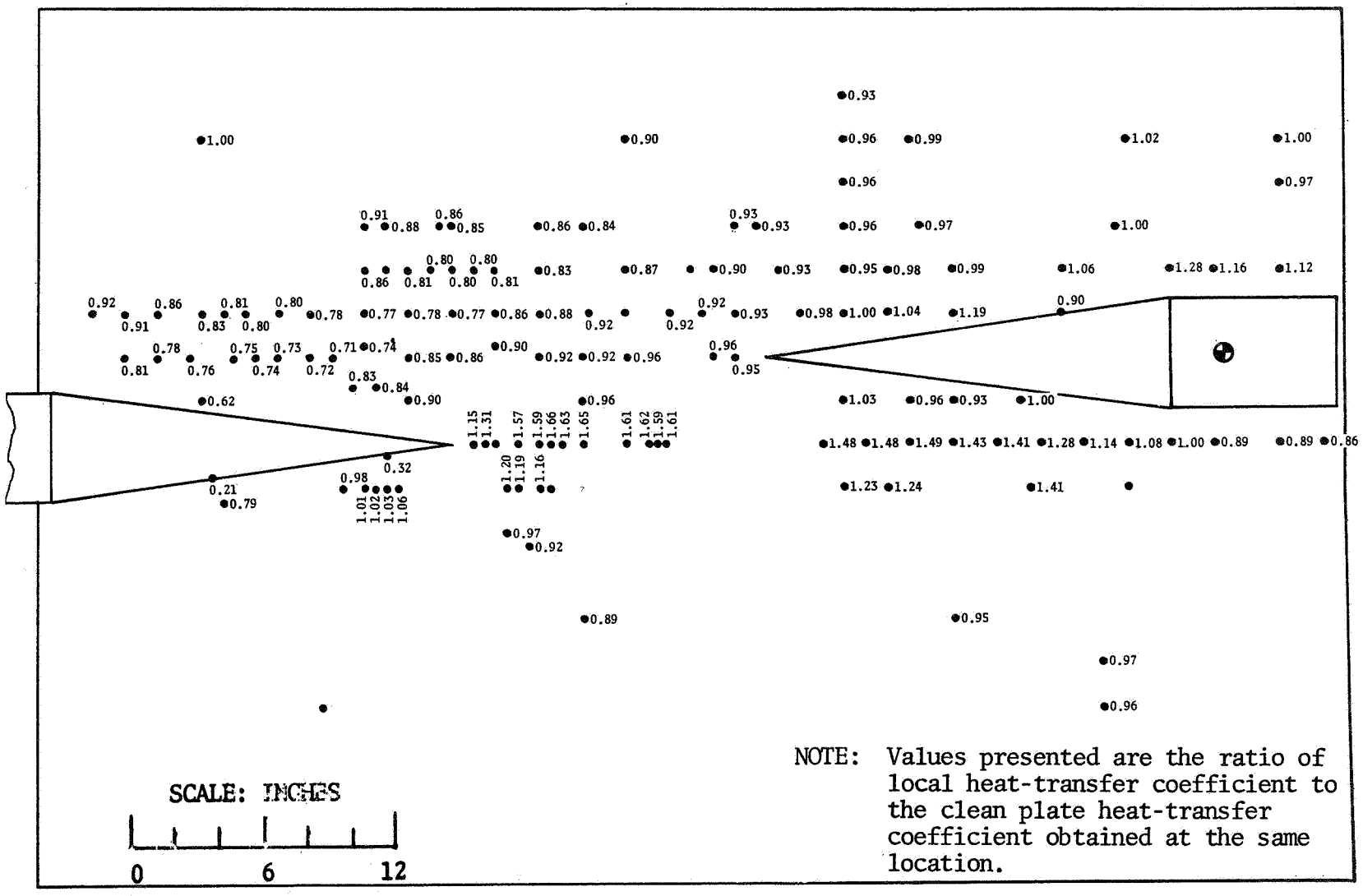

FIGURE A-13. EFFECT OF MODEL 5 IN MODEL 1 WAKE ON PLATE HEATING DISTRIBUTION AT MACH NUMBER 2.49 CONFIGURATION 5

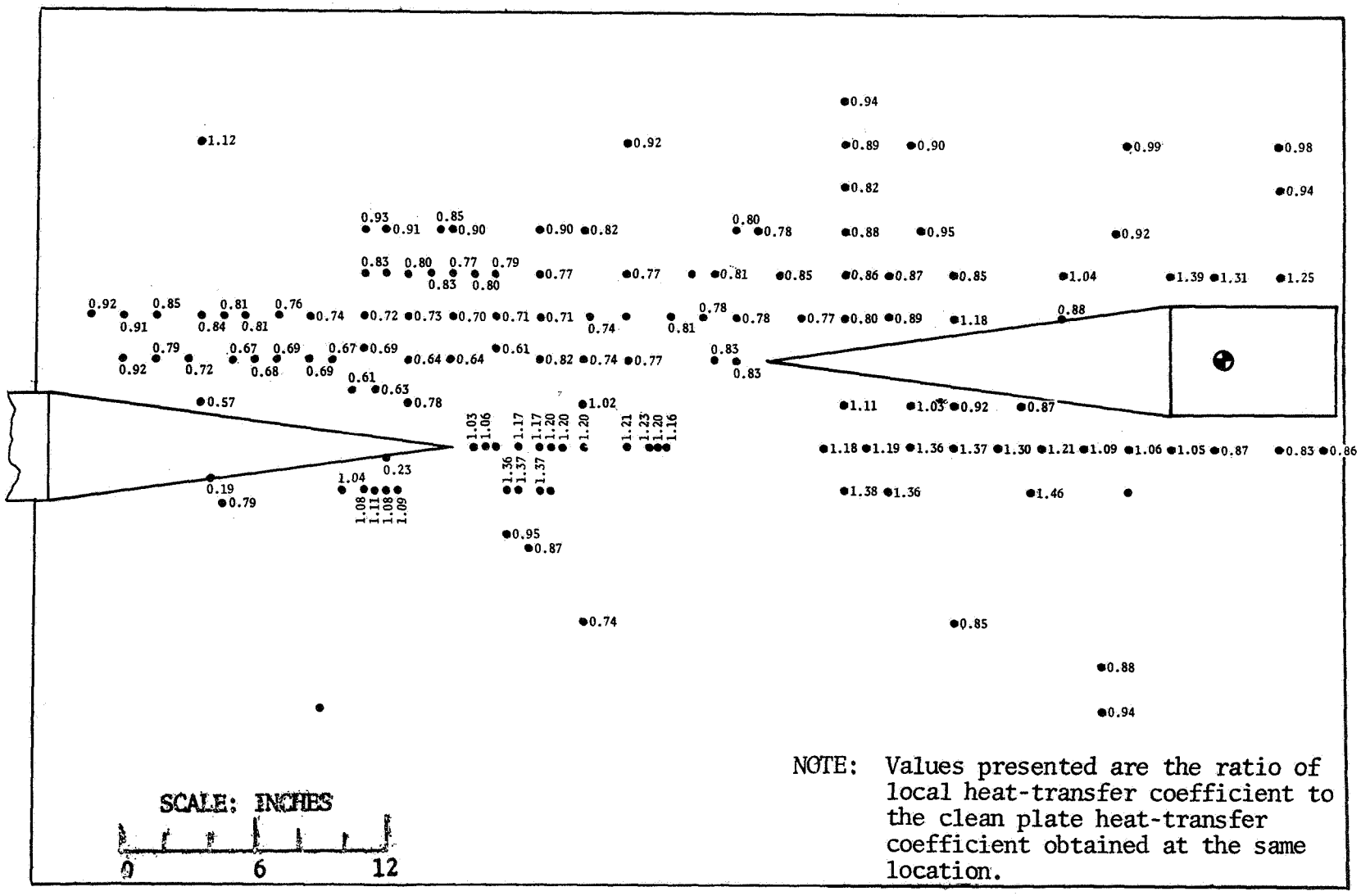

FIGURE A-14. EFFECT OF MODEL 5 IN MODEL 1 WAKE ON PLATE HEATING DISTRIBUTION AT MACH NUMBER 3.51 - CONFIGURATION 5

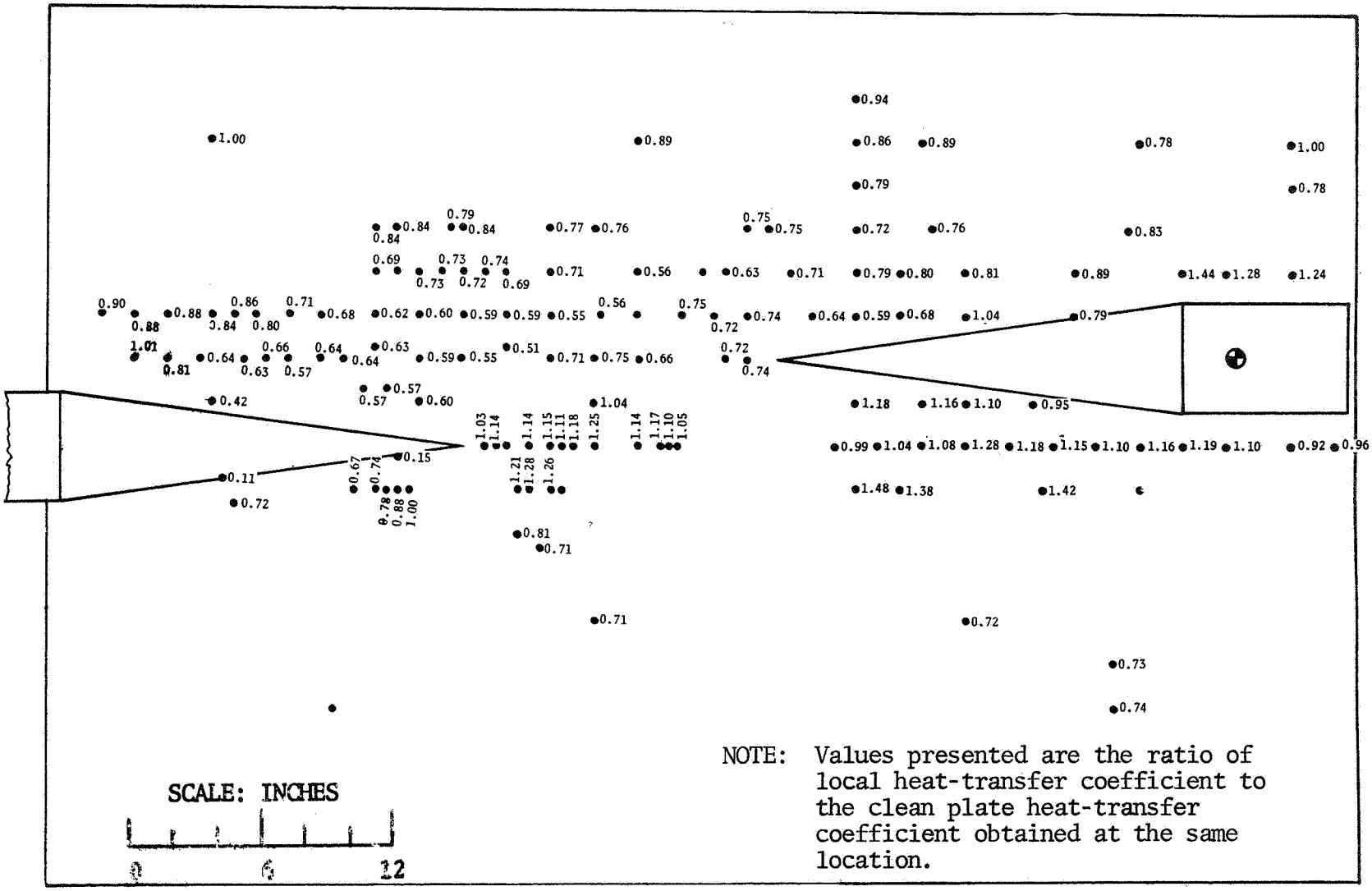

FIGURE A-15. EFFECT OF MODEL 5 IN MODEL 1 WAKE ON PLATE HEATING DISTRIBUTION AT MACH NUMBER 4.44 - CONFIGURATION 5

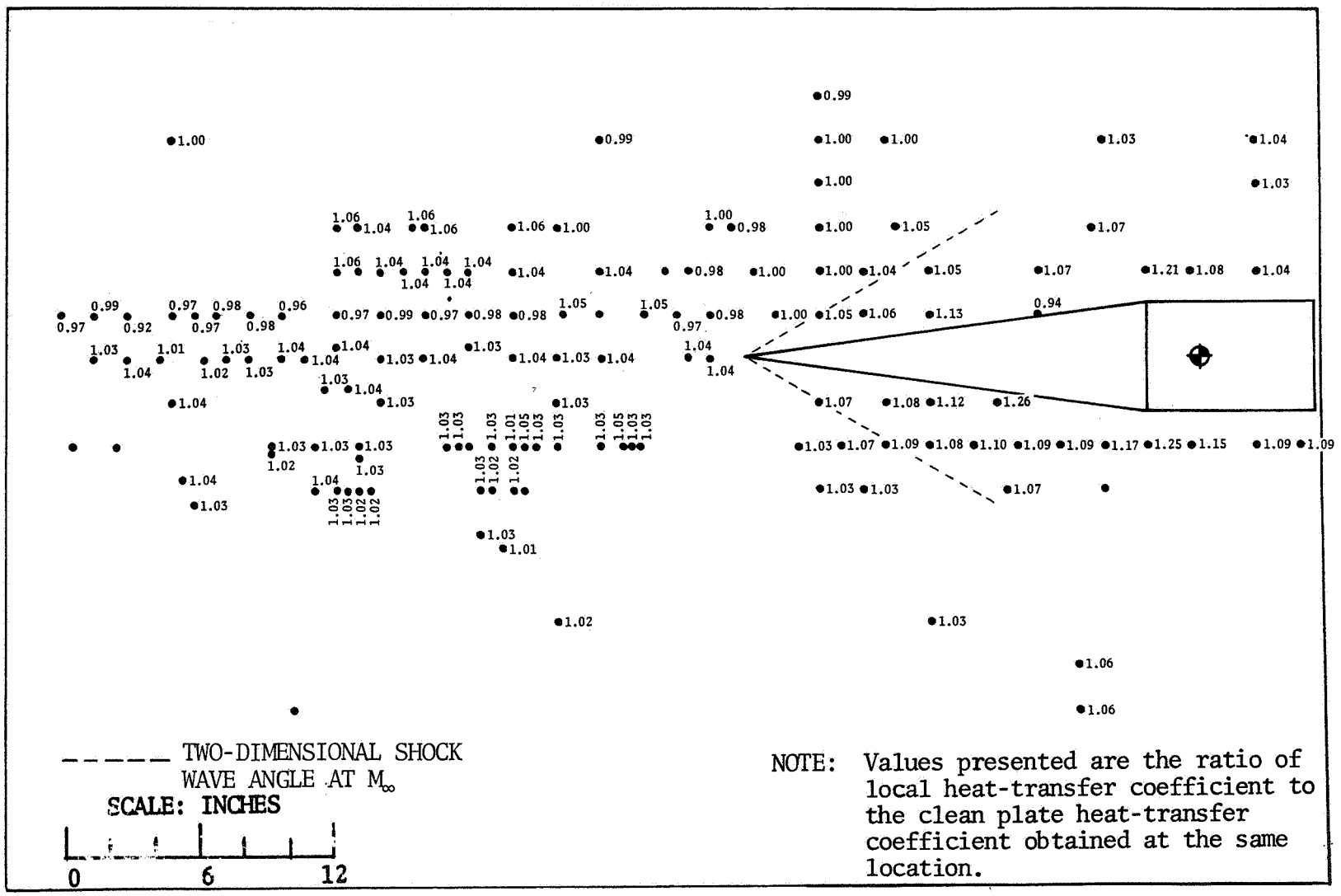

FIGURE A-16. EFFECT OF MODEL 5 ON PLATE HEATING DISTRIBUTION AT MACH NUMBER 2.49 - CONFIGURATION 6

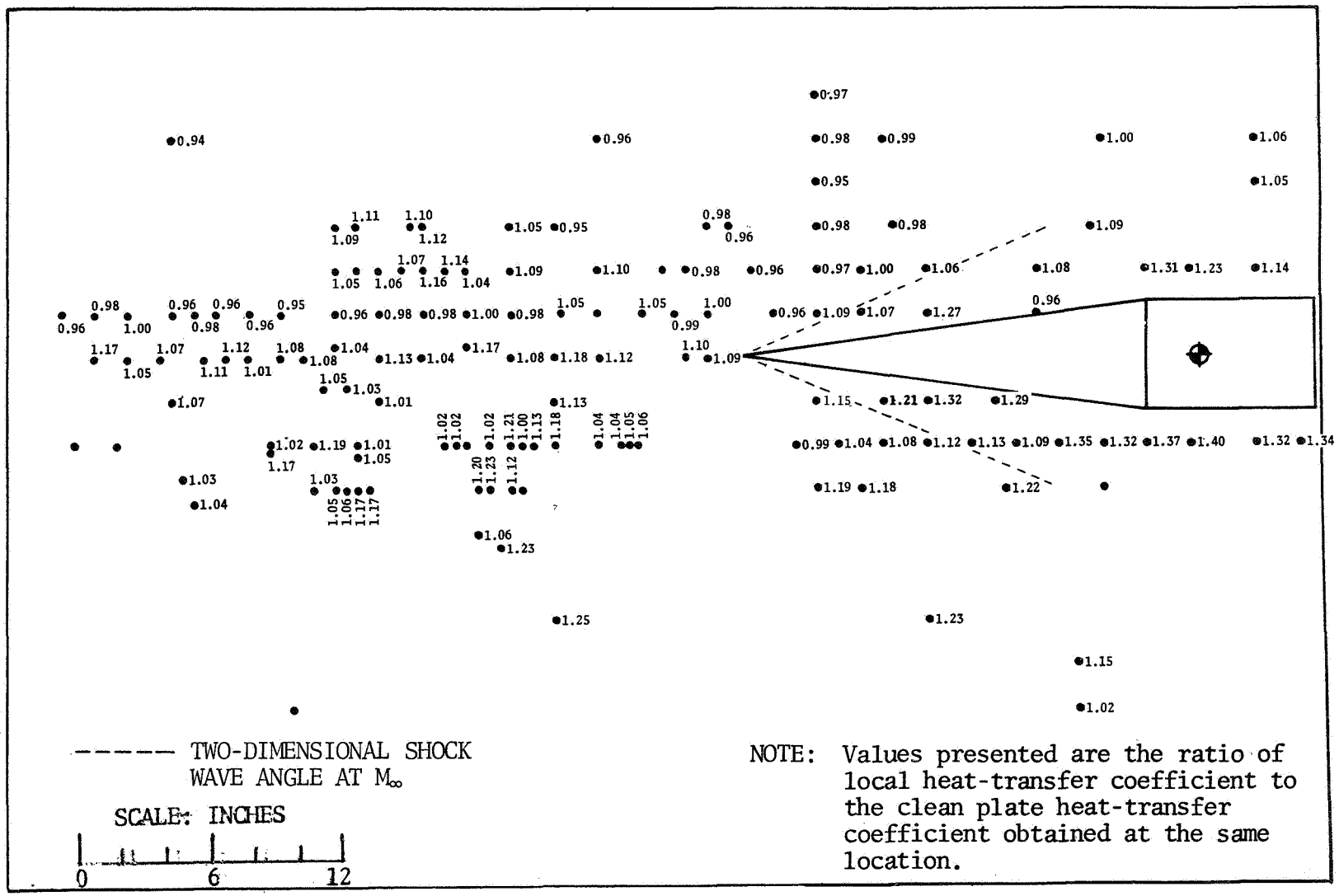

FIGURE A-17. EFFECT OF MODEL 5 ON PLATE HEATING DISTRIBUTION AT MACH NUMBER 3.51 - CONFIGURATION 6

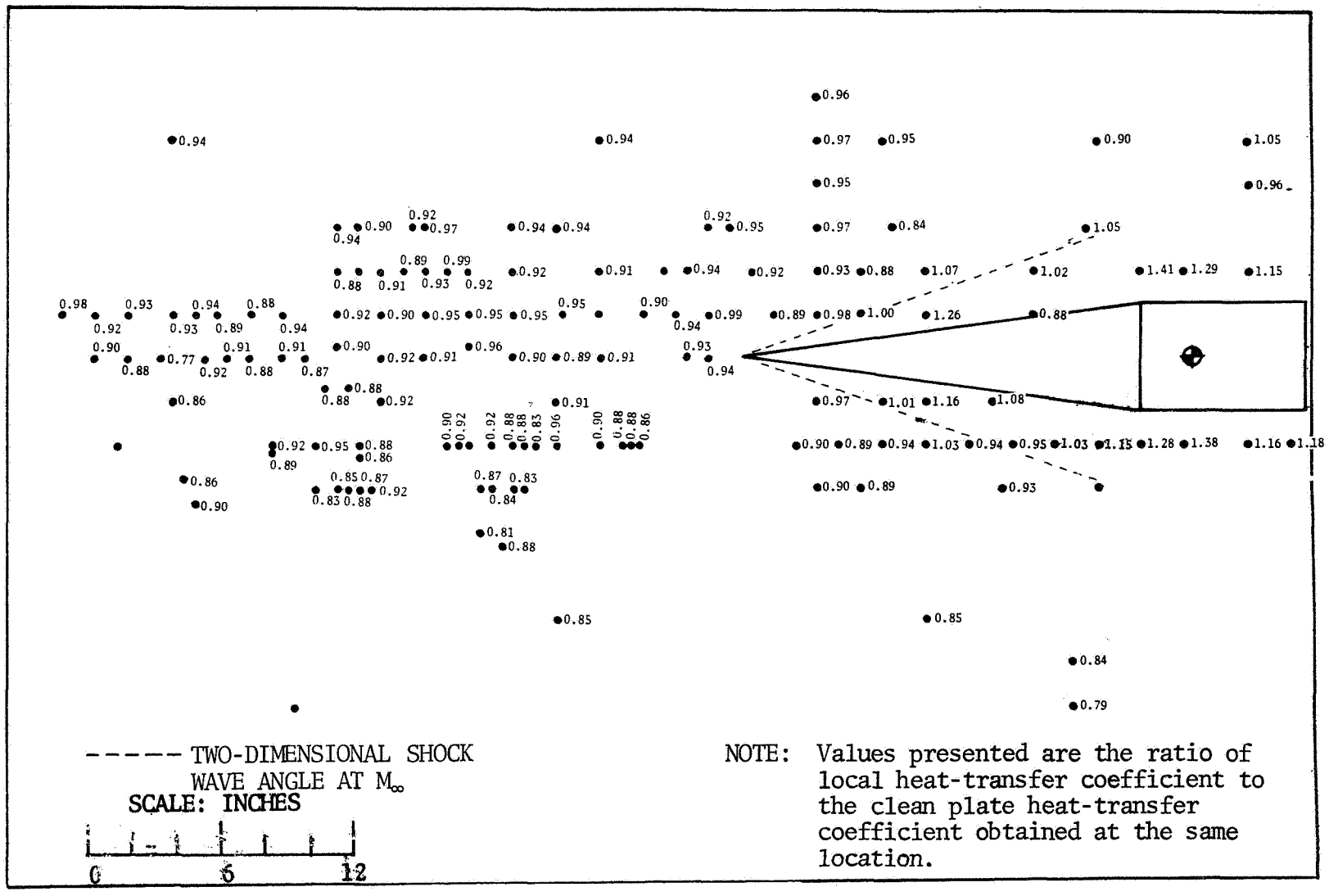

FIGURE A-18. EFFECT OF MODEL 5 ON PLATE HEATING DISTRIBUTION AT MACH NUMBER 4.44 - CONFIGURATION 6

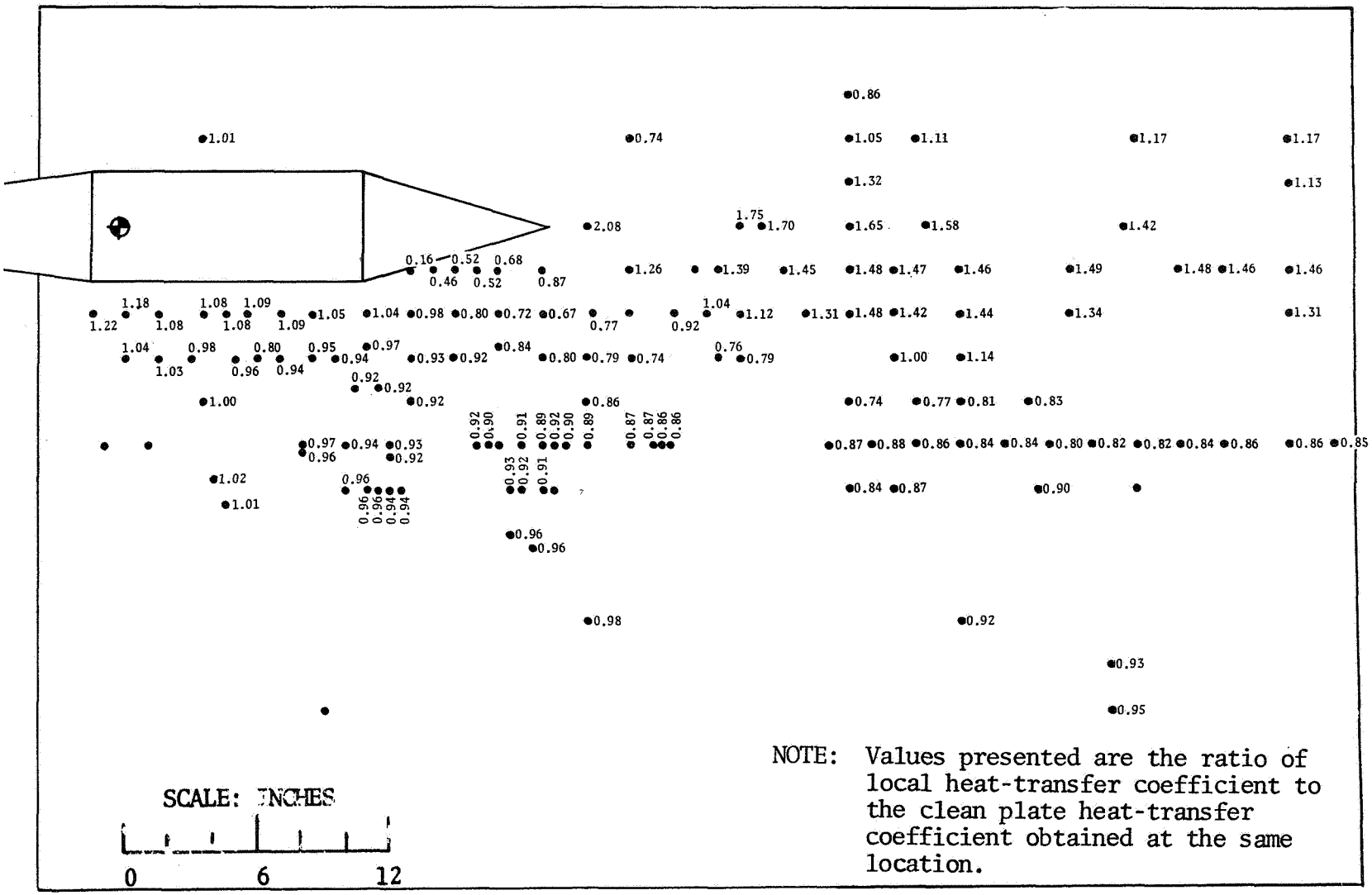

FIGURE A-19. EFFECT OF MODEL 2 ON PLATE HEATING DISTRIBUTION AT MACH NUMBER 2.49 - CONFIGURATION 7

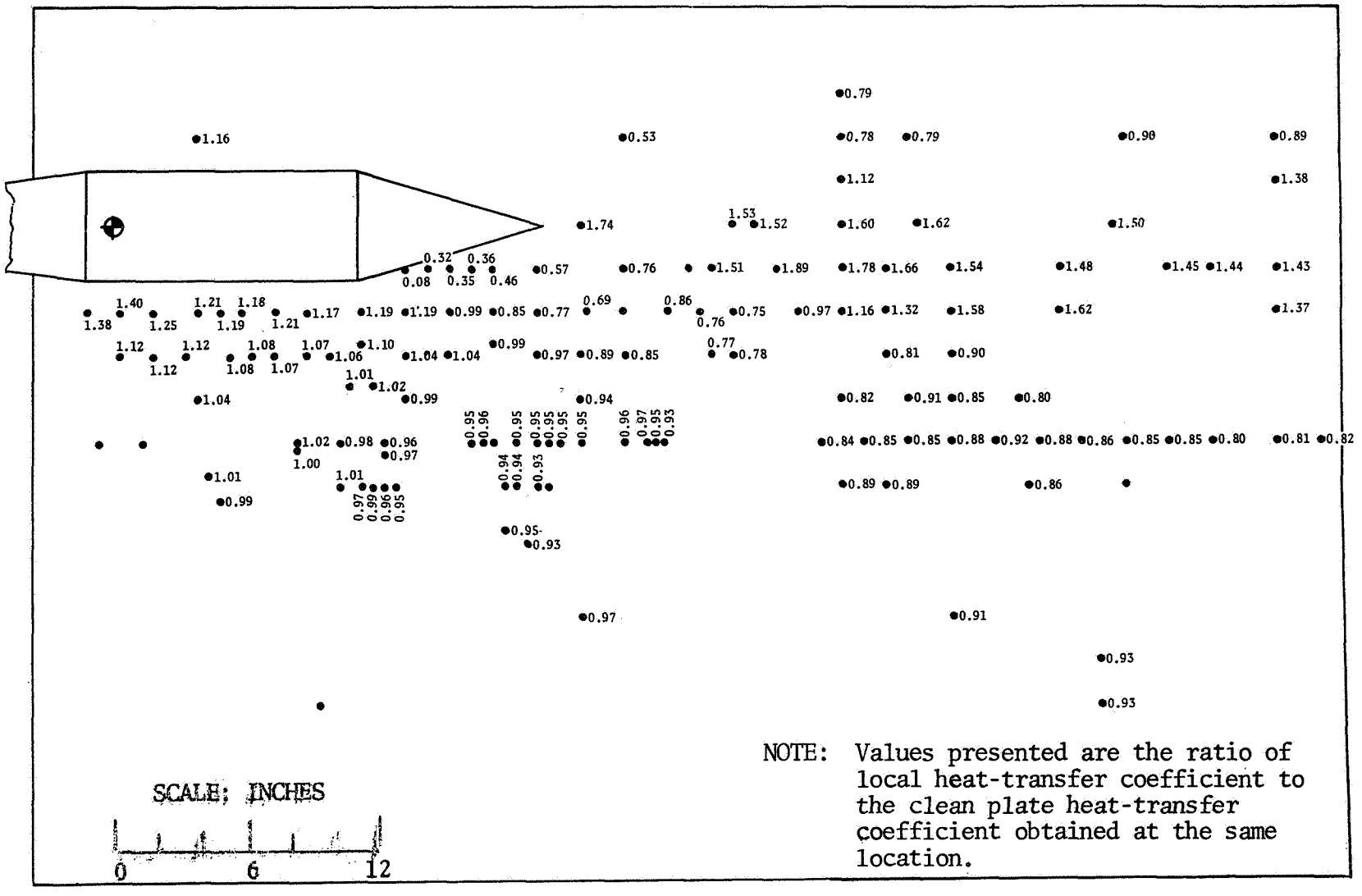

FIGURE A-20. EFFECT OF MODEL 2 ON PLATE HEATING DISTRIBUTION AT MACH NUMBER 3.51 - CONFIGURATION 7

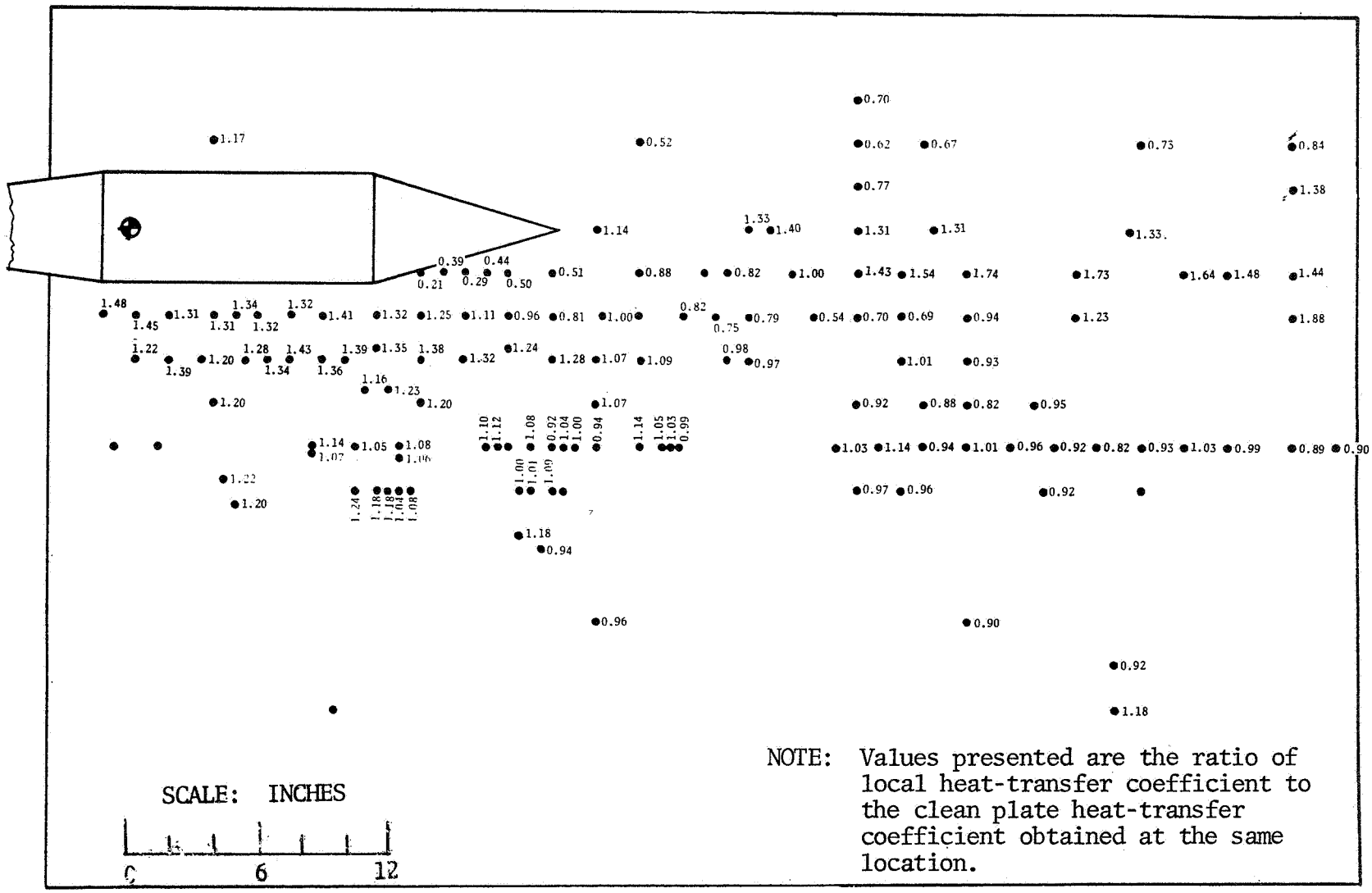

FIGURE A-21. EFFECT OF MODEL 2 ON PLATE HEATING DISTRIBUTION AT MACH NUMBER 4.44 - CONFIGURATION 7

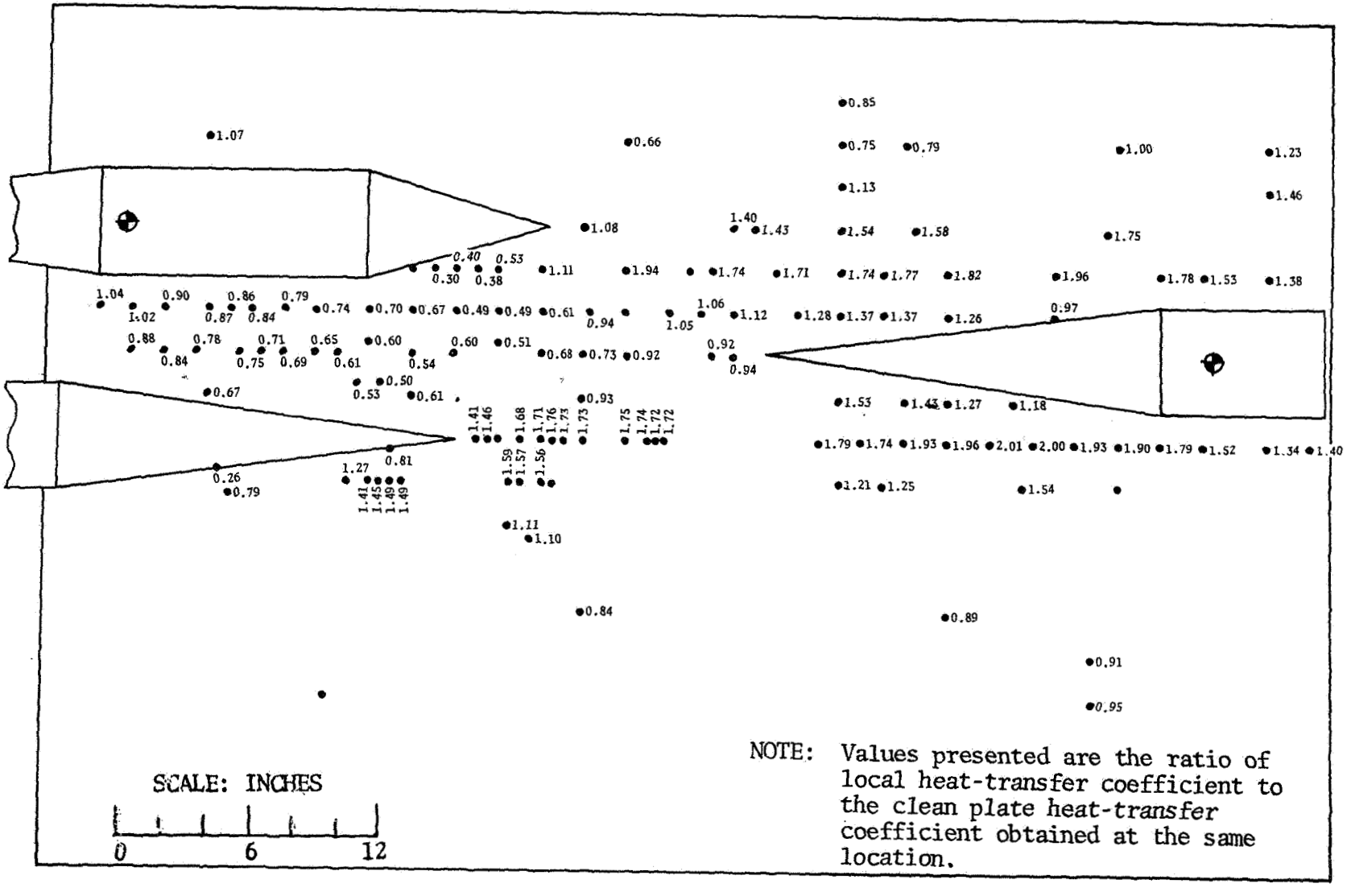

FIGURE A-22. EFFECT OF MODEL 5 IN MODELS 1 AND 2 AFT WAKES ON PLATE HEATING DISTRIBUTION AT MACH NUMBER 2.49 - CONFIGURATION 8

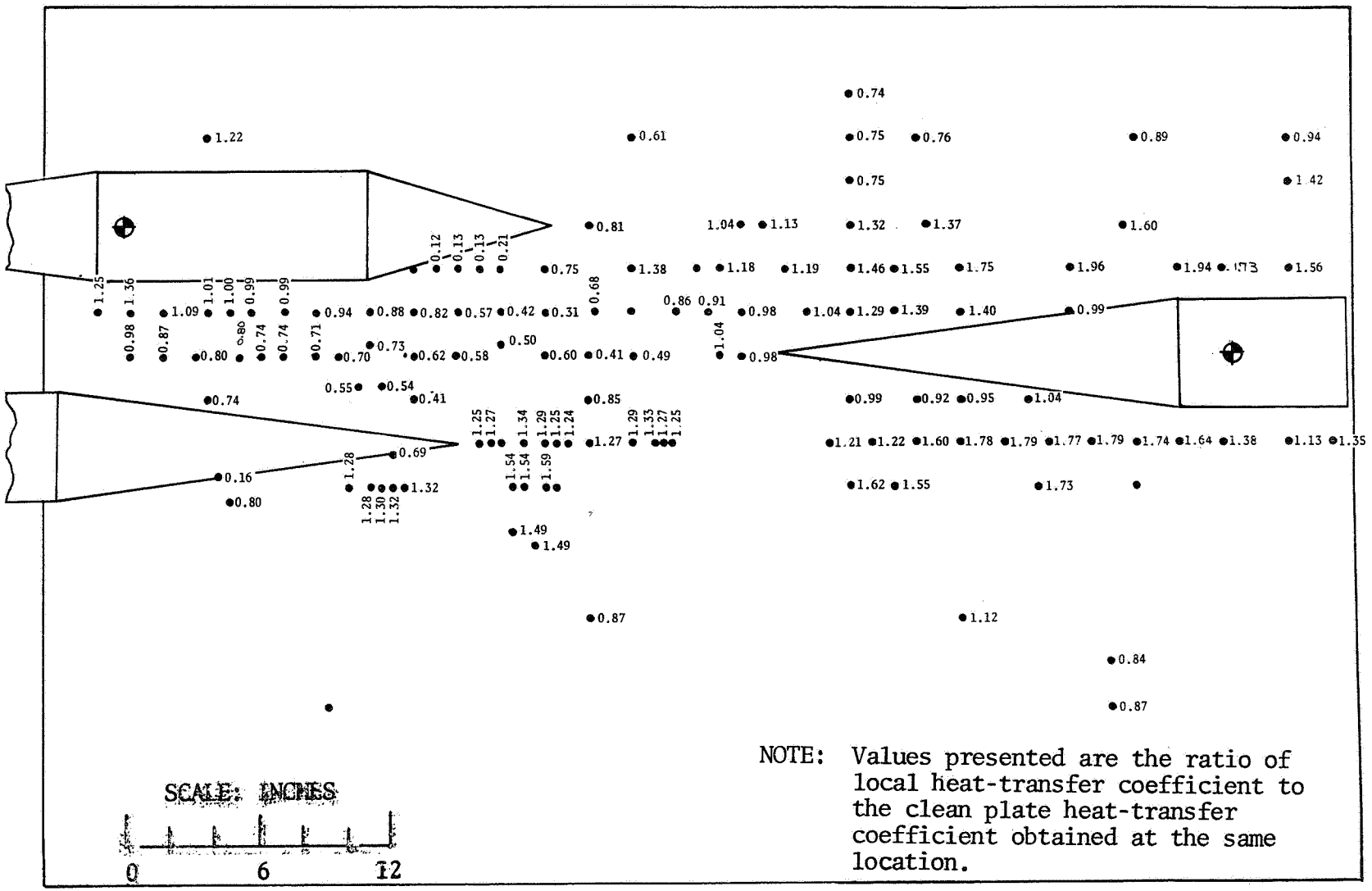

FIGURE A-23. EFFECT OF MODEL 5 IN MODELS 1 AND 2 AFT WAKES ON PLATE HEATING DISTRIBUTION AT MACH NUMBER 3.51 - CONFIGURATION 8

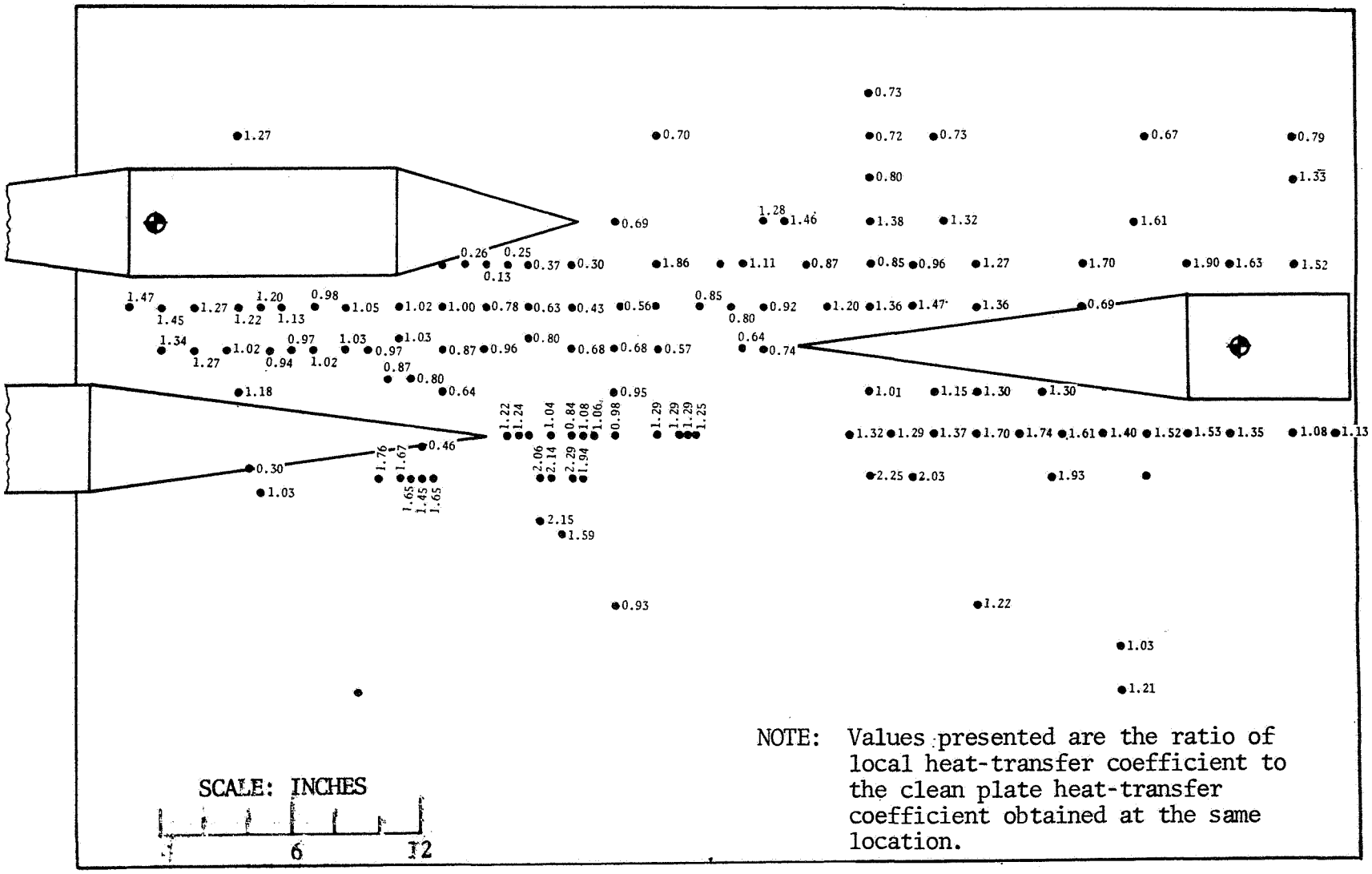

FIGURE A-24. EFFECT OF MODEL 5 IN MODELS 1 AND 2 AFT WAKES ON PLATE HEATING DISTRIBUTION AT MACH NUMBER 4.44 - CONFIGURATION 8

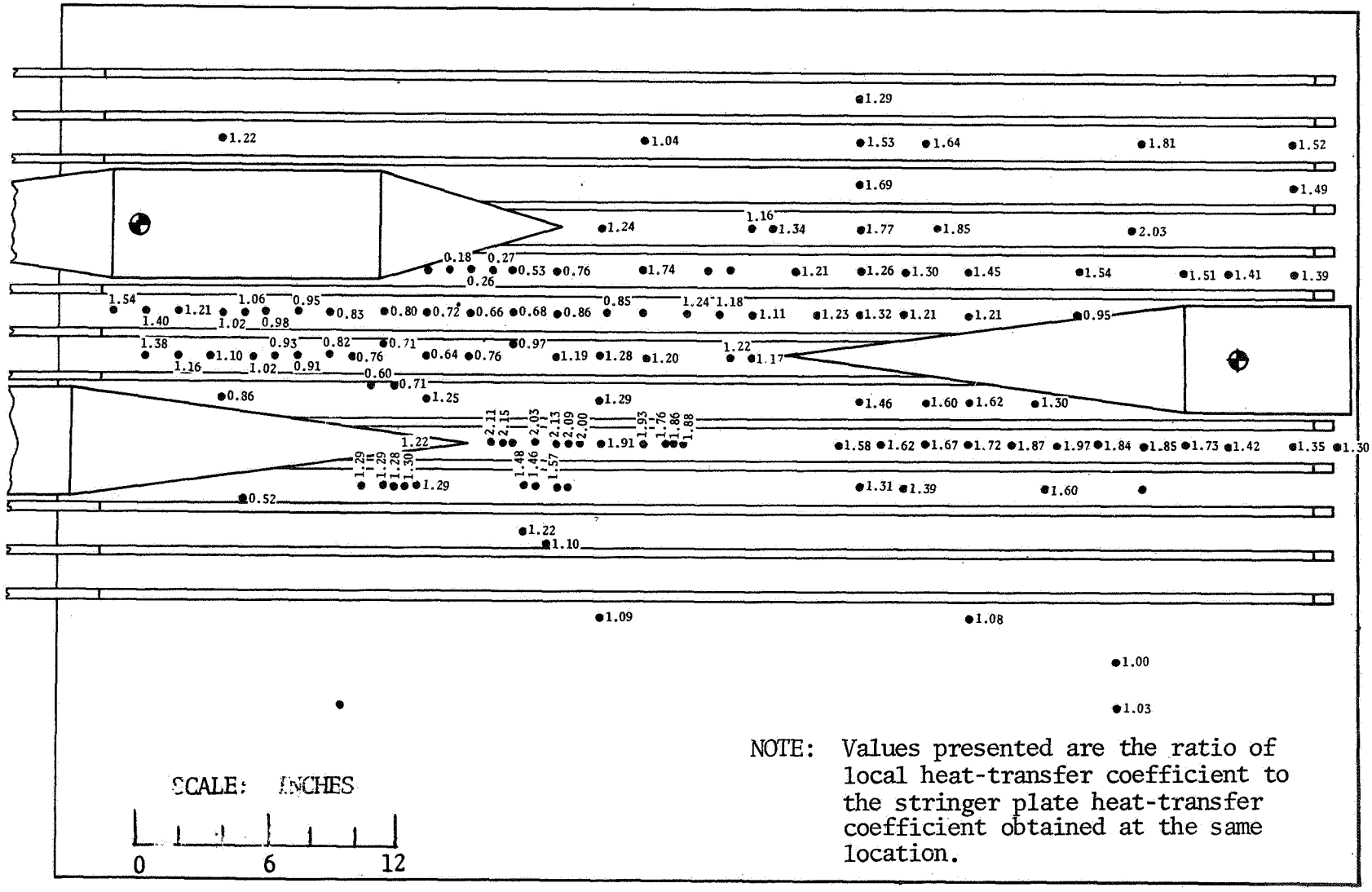

FIGURE A-25. EFFECT OF MODEL 5 IN MODELS 1 AND 2 AFT WAKES ON STRINGER PLATE HEATING DISTRIBUTION AT MACH NUMBER 2.49 - CONFIGURATION 9

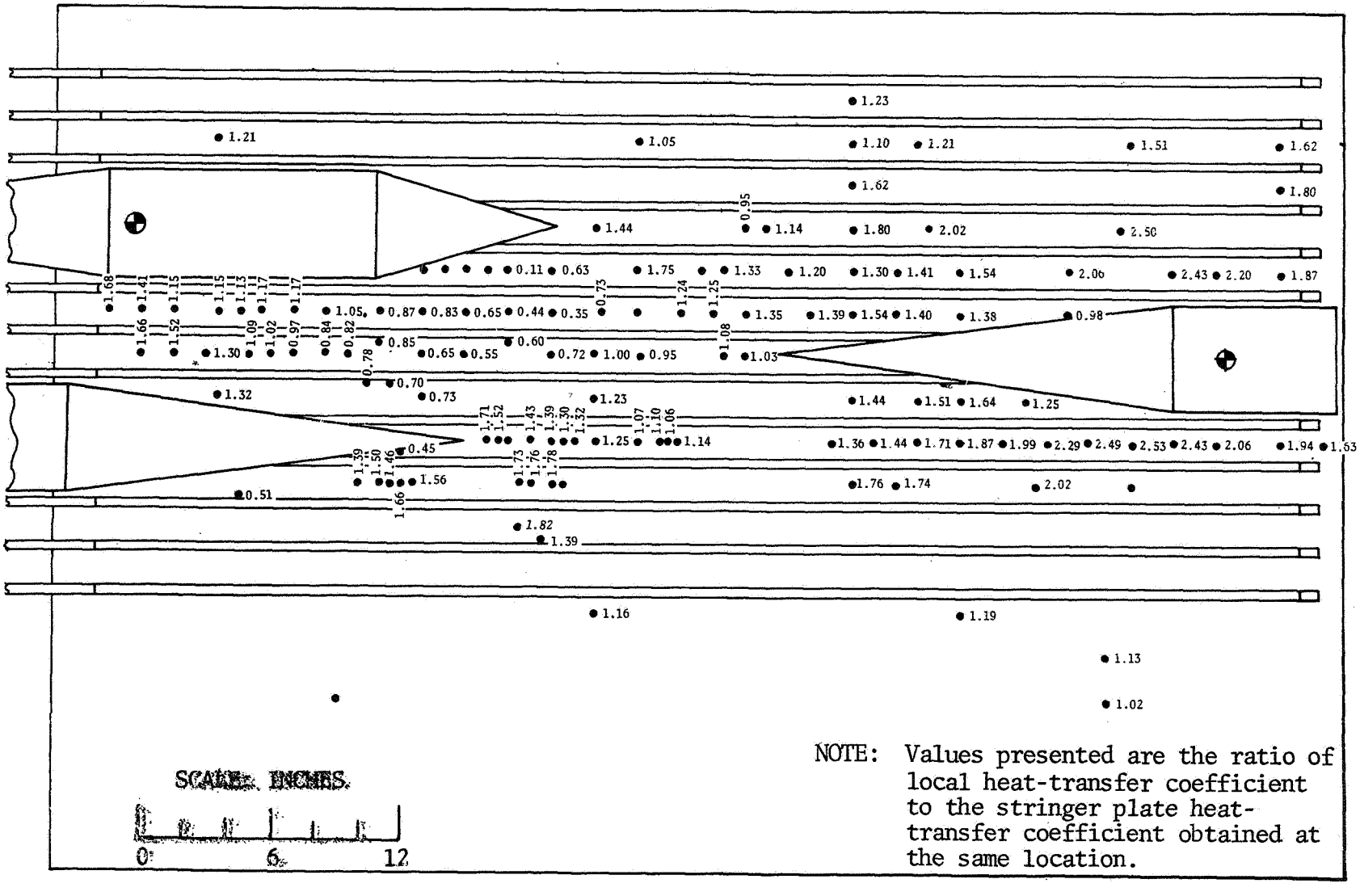

FIGURE A-26. EFFECT OF MODEL 5 IN MODELS 1 AND 2 AFT WAKES ON STRINGER PLATE HEATING DISTRIBUTION AT MACH NUMBER 3.51 - CONFIGURATION 9

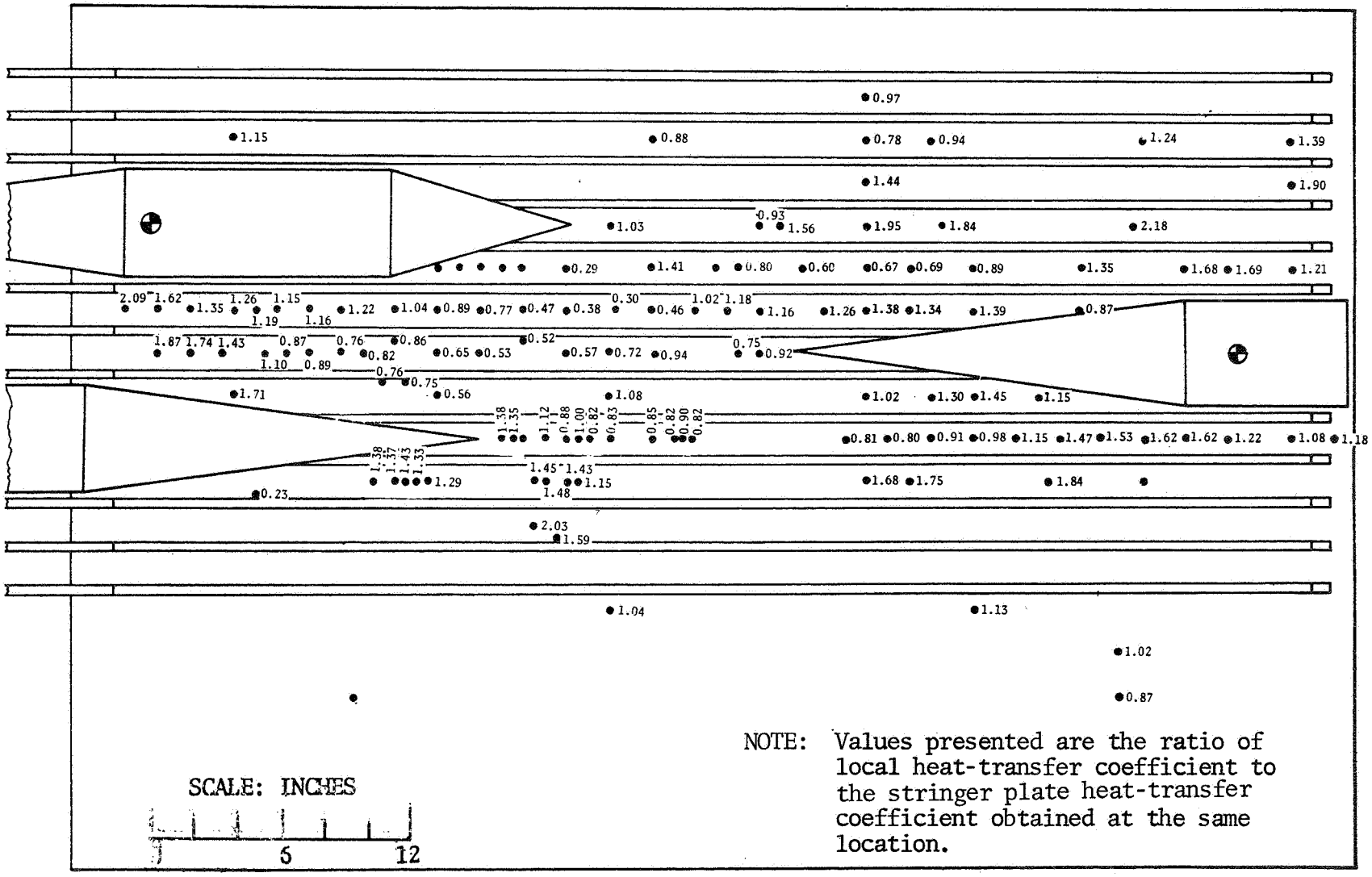

FIGURE A-27. EFFECT OF MODEL 5 IN MODELS 1 AND 2 AFT WAKES ON STRINGER PLATE HEATING DISTRIBUTION AT MACH NUMBER 4.44 - CONFIGURATION 9

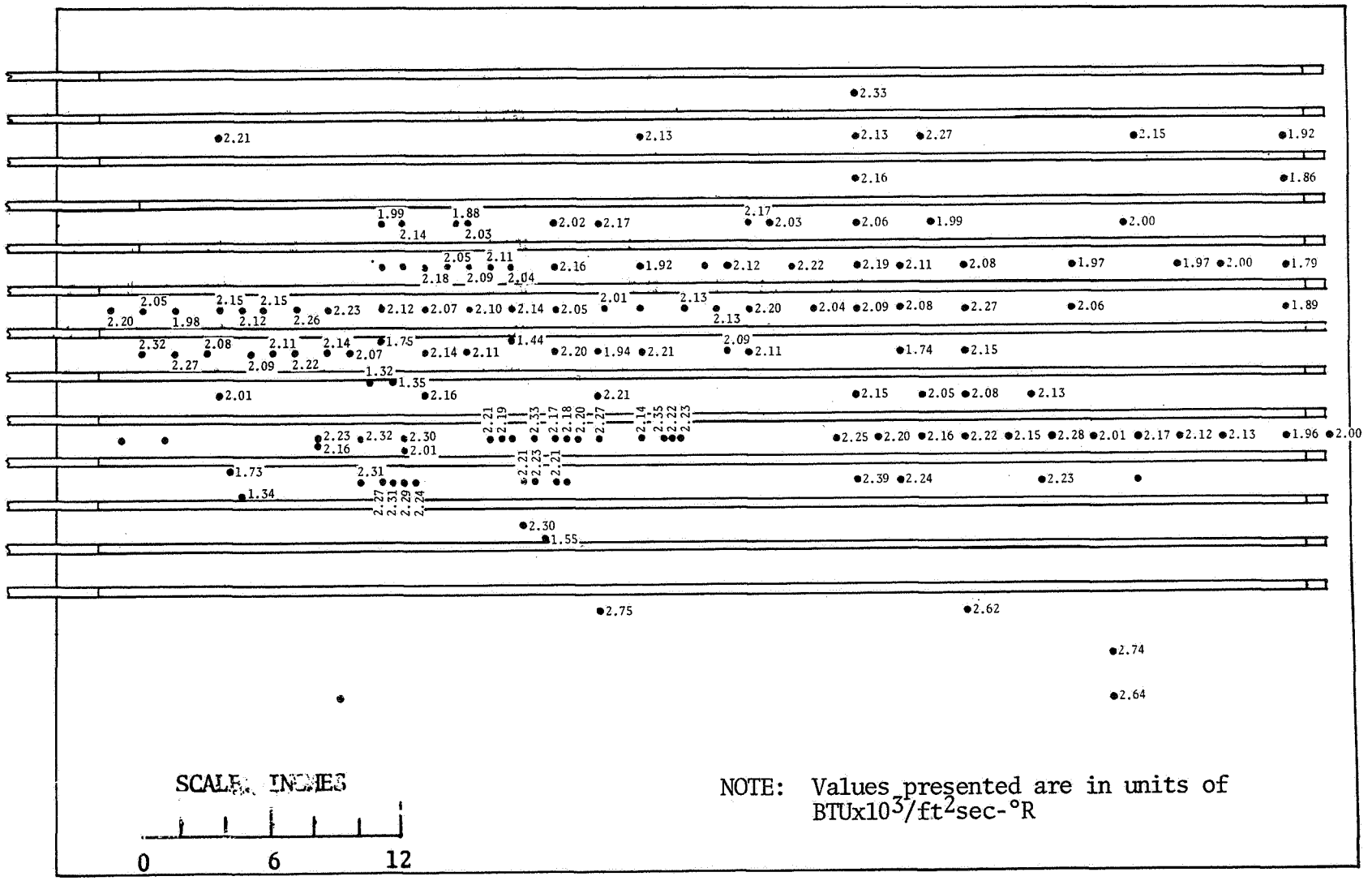

FIGURE A-28. STRINGER PLATE HEAT-TRANSFER COEFFICIENT DISTRIBUTION AT MACH NUMBER 2.49 - CONFIGURATION 10

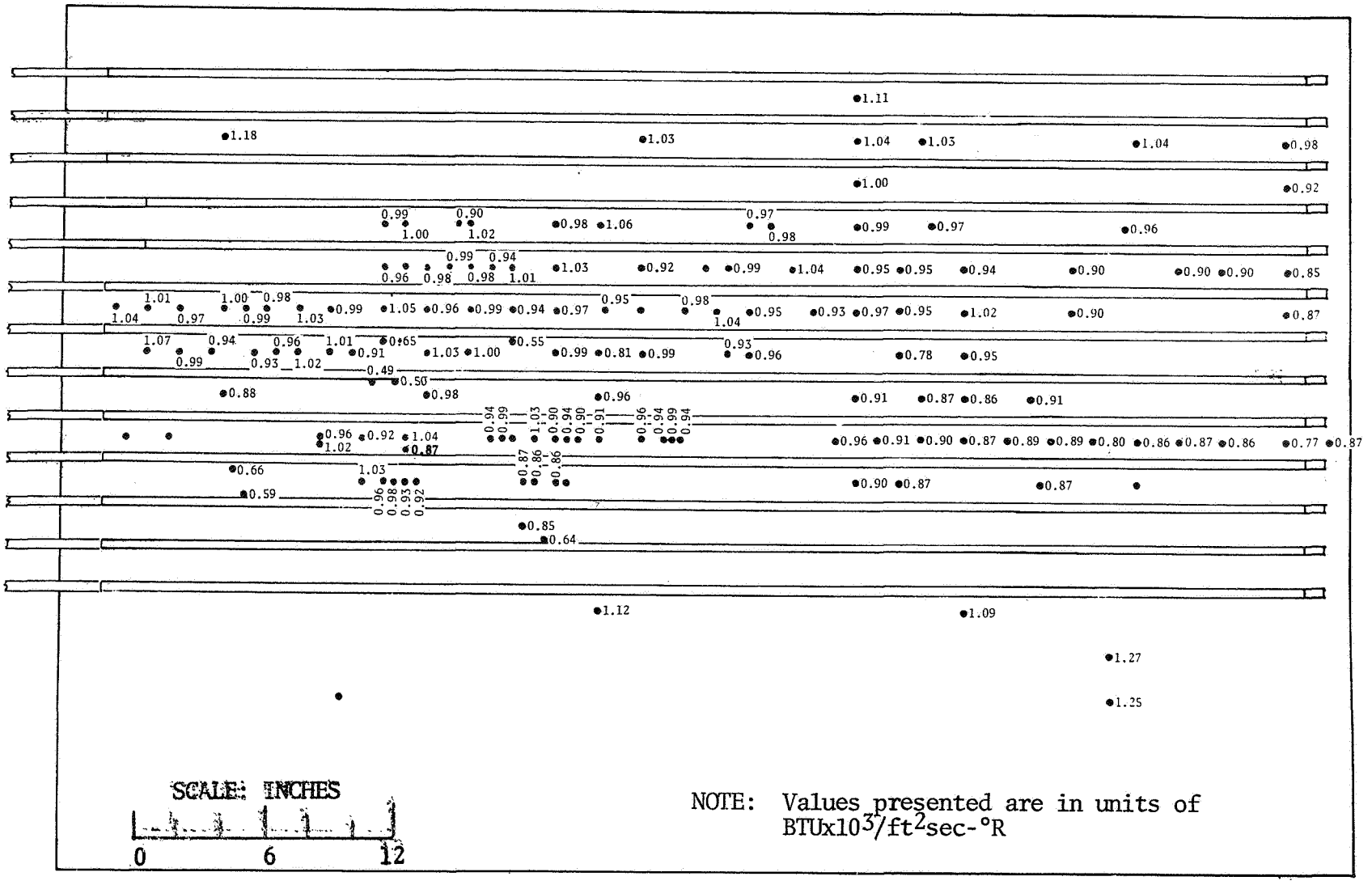

FIGURE A-29. STRINGER PLATE HEAT-TRANSFER COEFFICIENT DISTRIBUTION AT MACH NUMBER 3.51 - CONFIGURATION 10

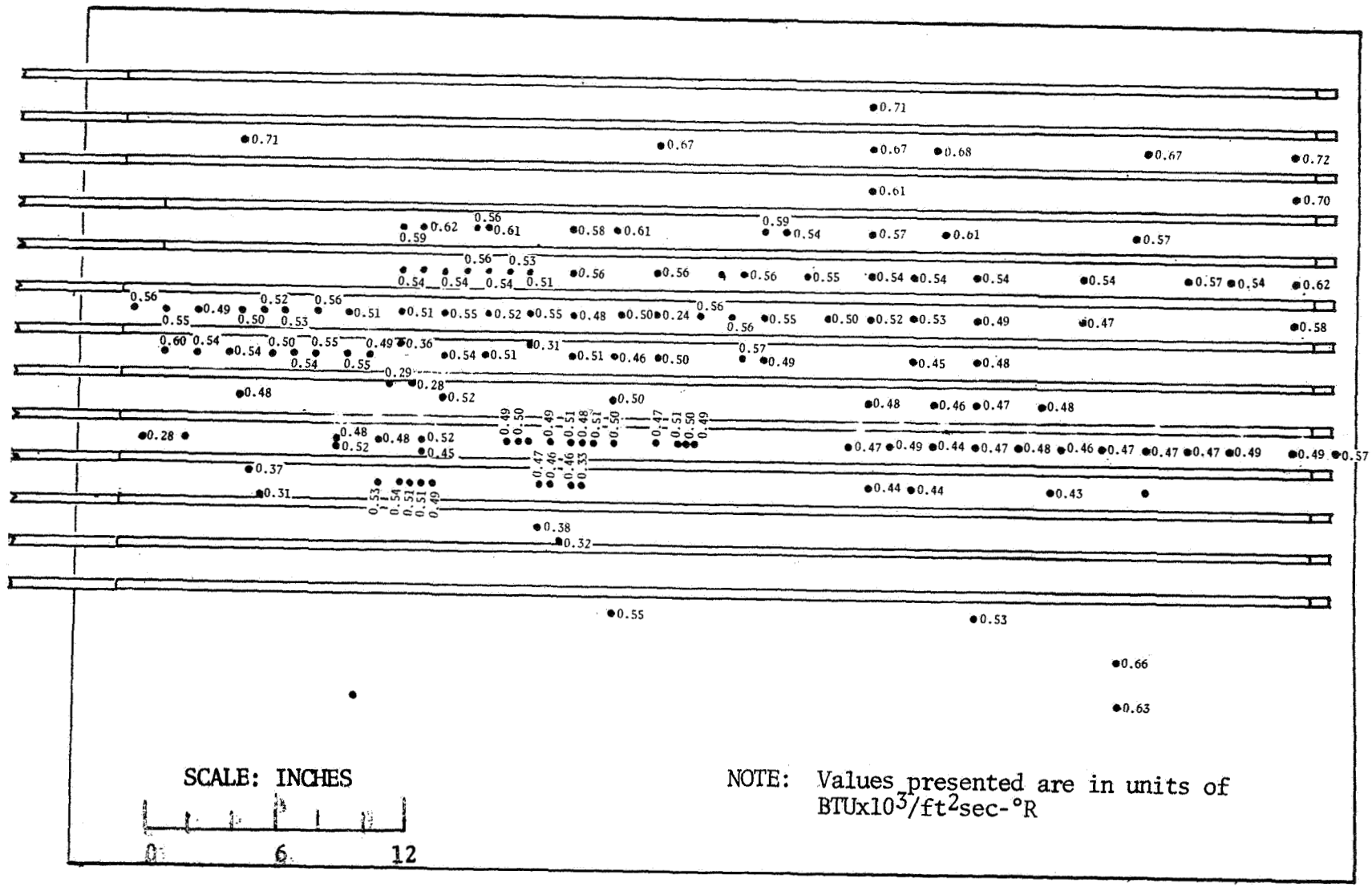

FIGURE A-30. STRINGER PLATE HEAT-TRANSFER COEFFICIENT DISTRIBUTION AT MACH NUMBER 4.44 - CONFIGURATION 10

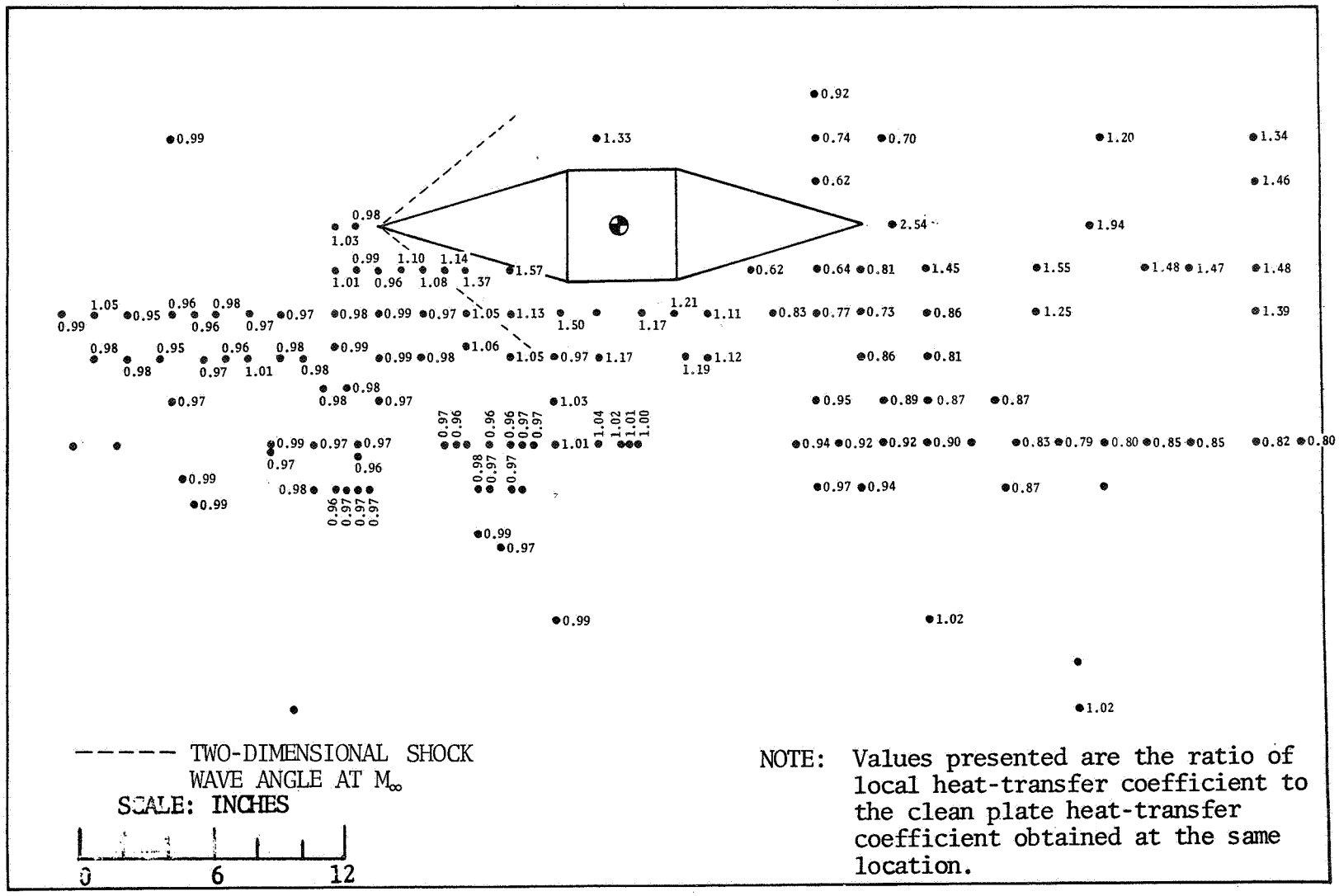

FIGURE A-31. EFFECT OF MODEL 4 ON PLATE HEATING DISTRIBUTION AT MACH NUMBER 2.49 - CONFIGURATION 14

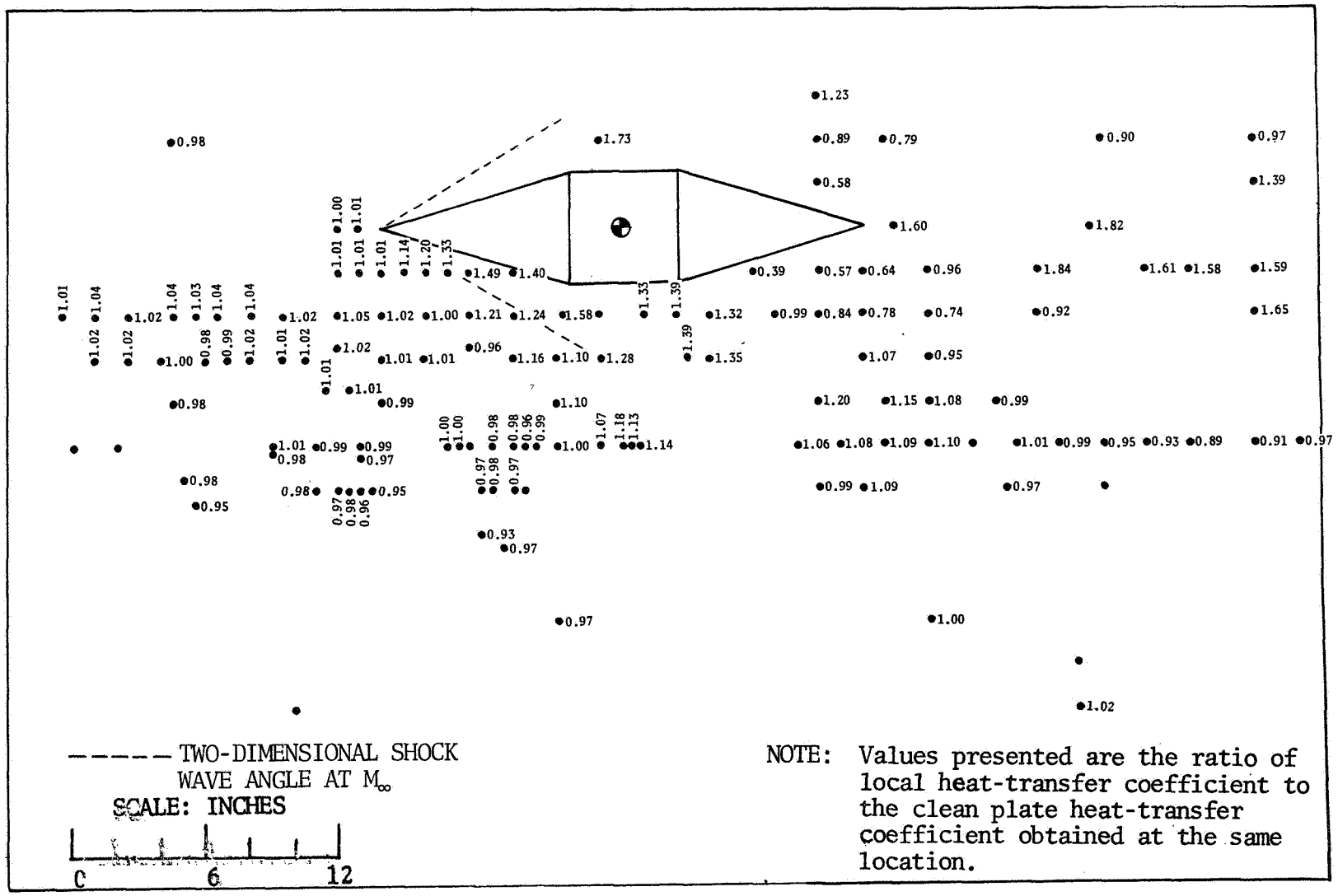

FIGURE A-32. EFFECT OF MODEL 4 ON PLATE HEATING DISTRIBUTION AT MACH NUMBER 3.51 - CONFIGURATION 14

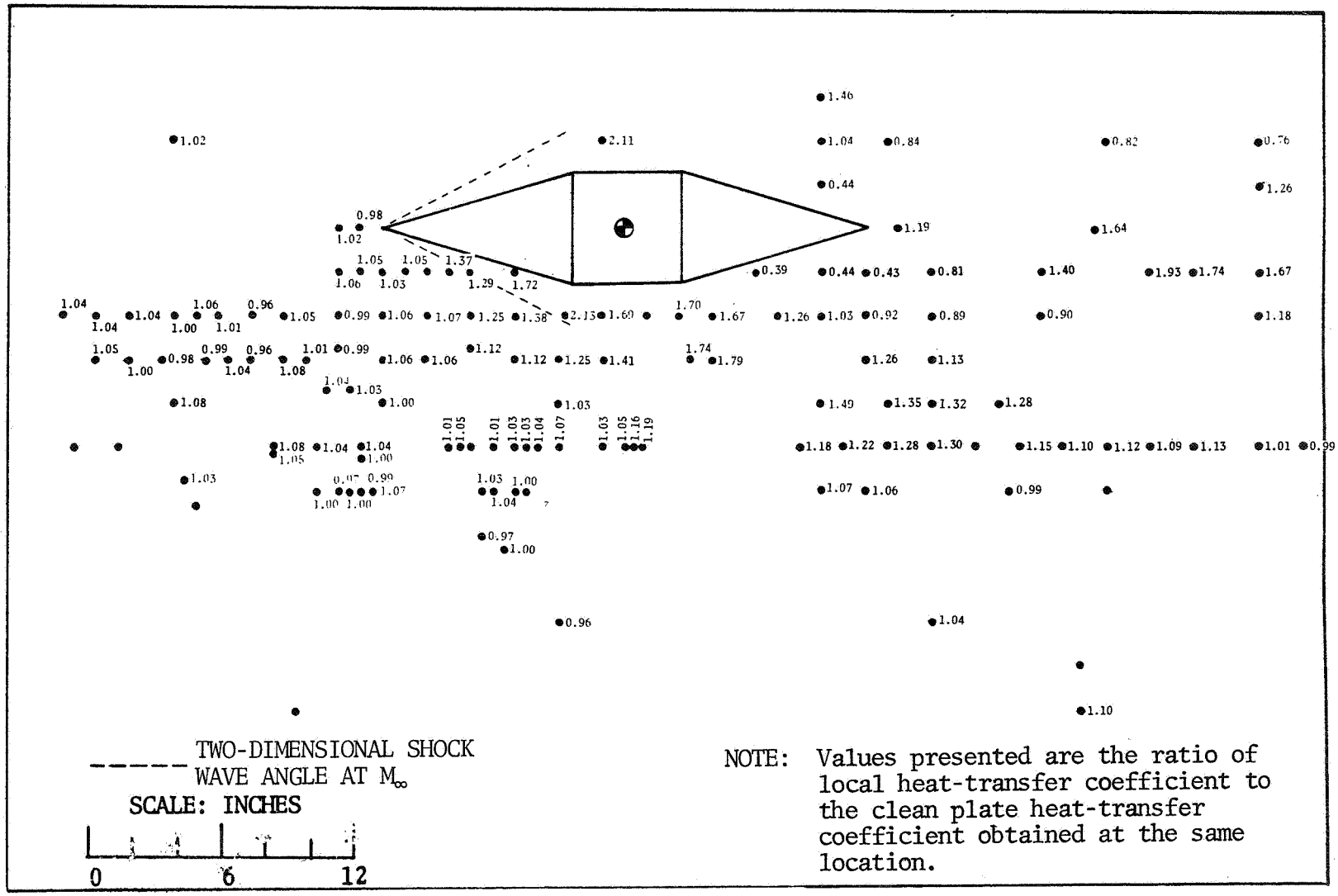

FIGURE A-33. EFFECT OF MODEL 4 ON PLATE HEATING DISTRIBUTION AT MACH NUMBER 4.44 - CONFIGURATION 14

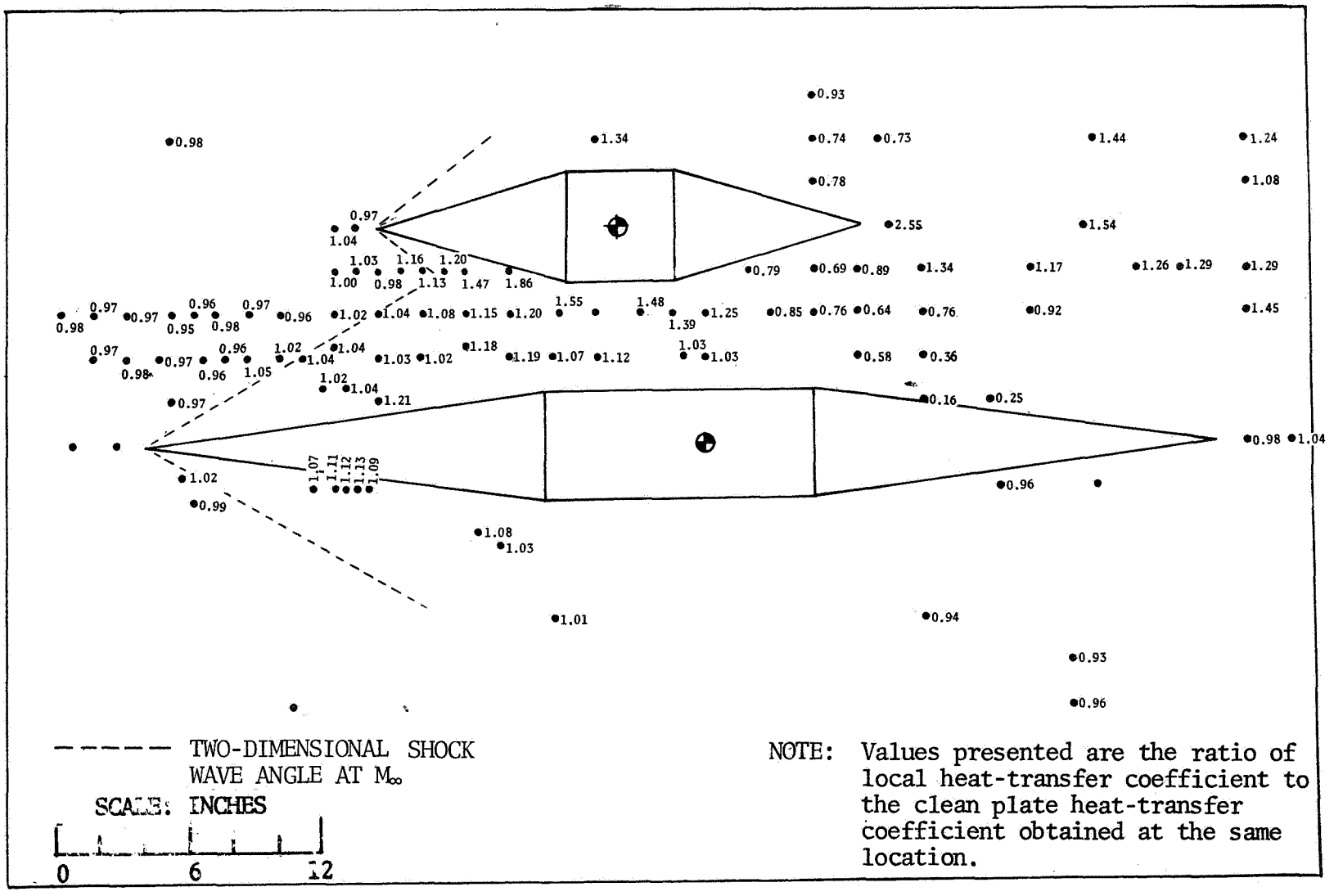

FIGURE A-34. EFFECT OF MODEL 4 SHOCK IMPINGEMENT ON MODEL 1 FOREBODY ON PLATE HEATING DISTRIBUTION AT MACH NUMBER 2.49 - CONFIGURATION 15

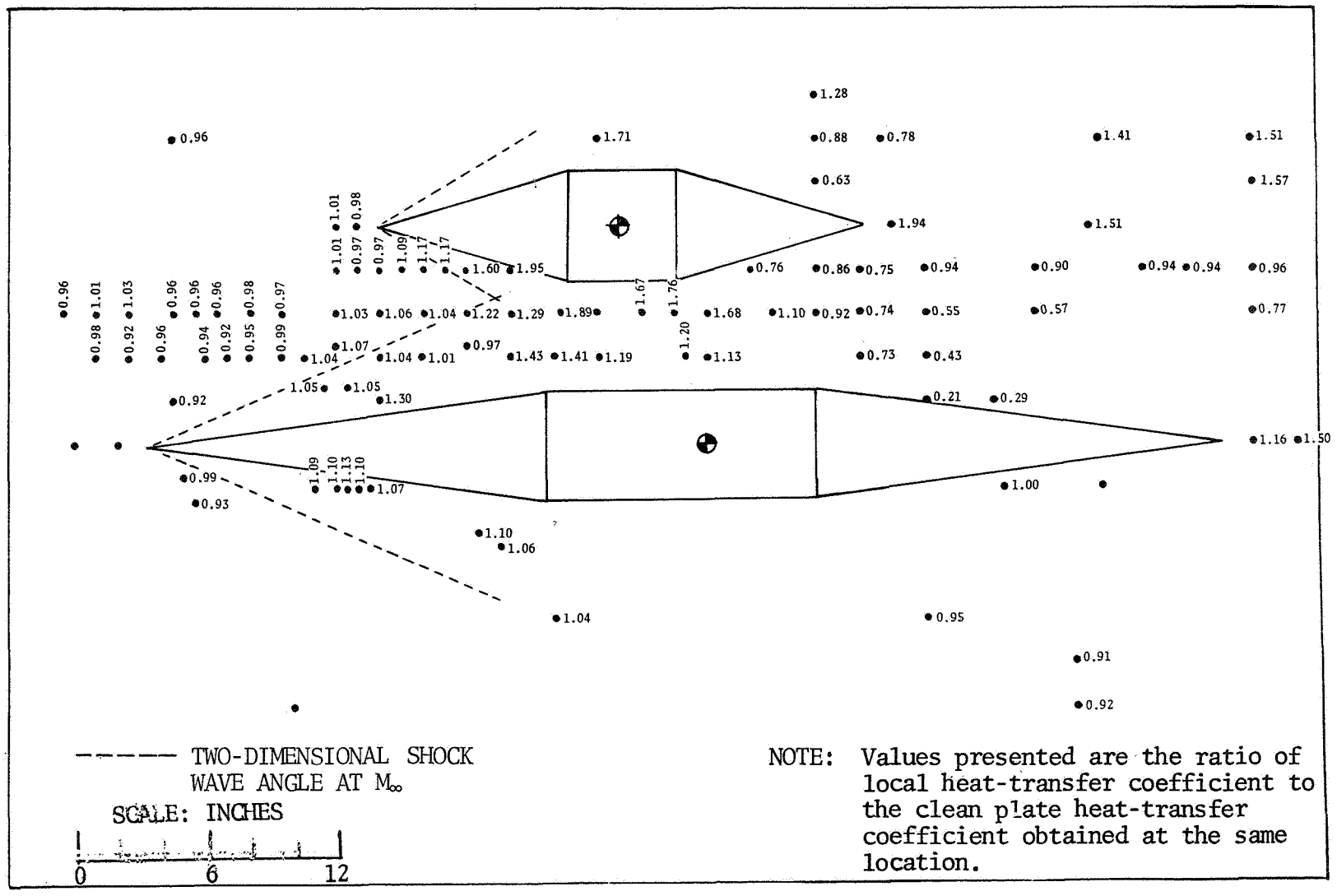

FIGURE A-35. EFFECT OF MODEL 4 SHOCK IMPINGEMENT ON MODEL 1 FOREBODY ON PLATE HEATING DISTRIBUTION AT MACH NUMBER 3.51 - CONFIGURATION 15

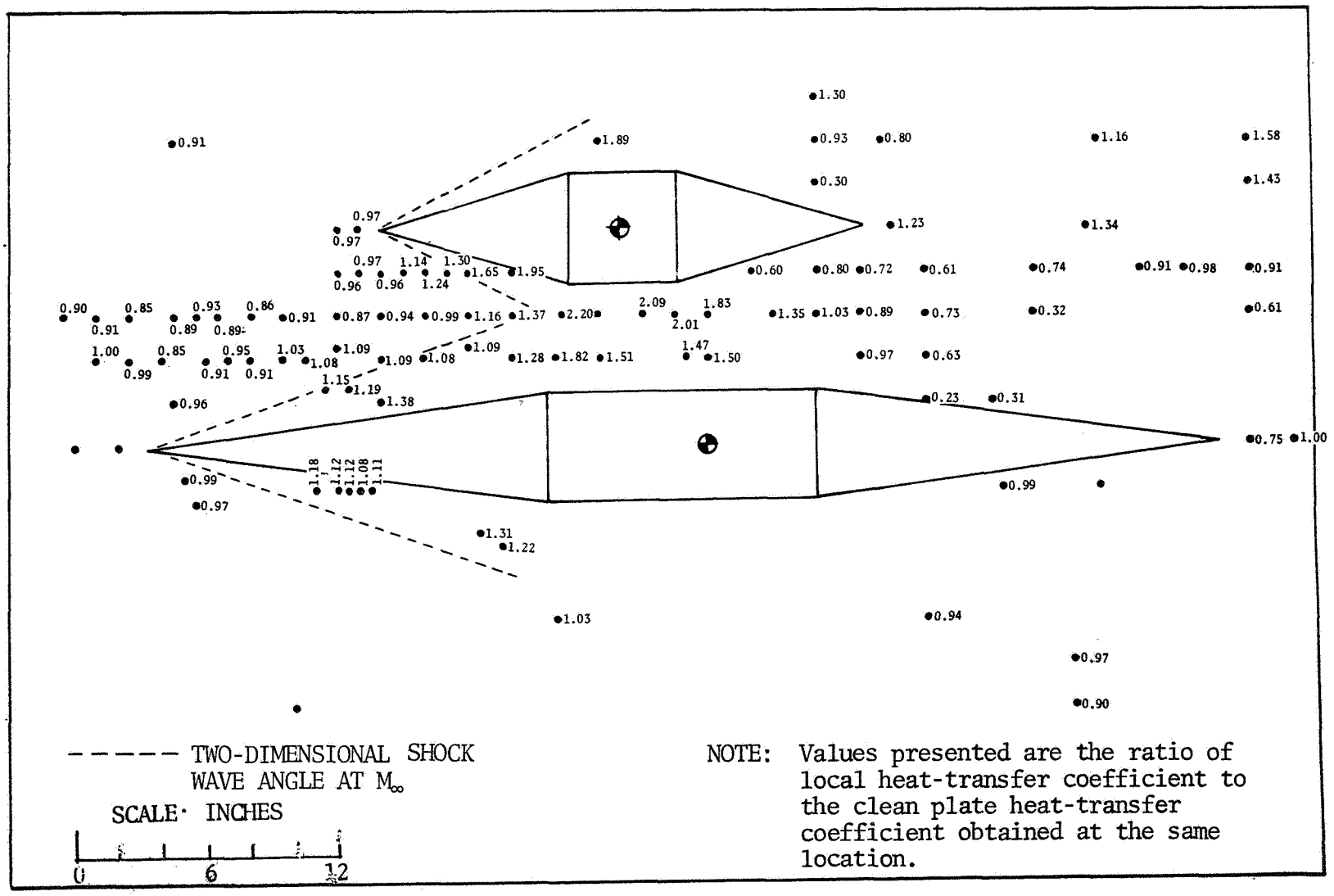

FIGURE A-36. EFFECT OF MODEL 4 SHOCK IMPINGEMENT ON MODEL 1 FOREBODY ON PLATE HEATING DISTRIBUTION AT MACH NUMBER 4.44 - CONFIGURATION 15

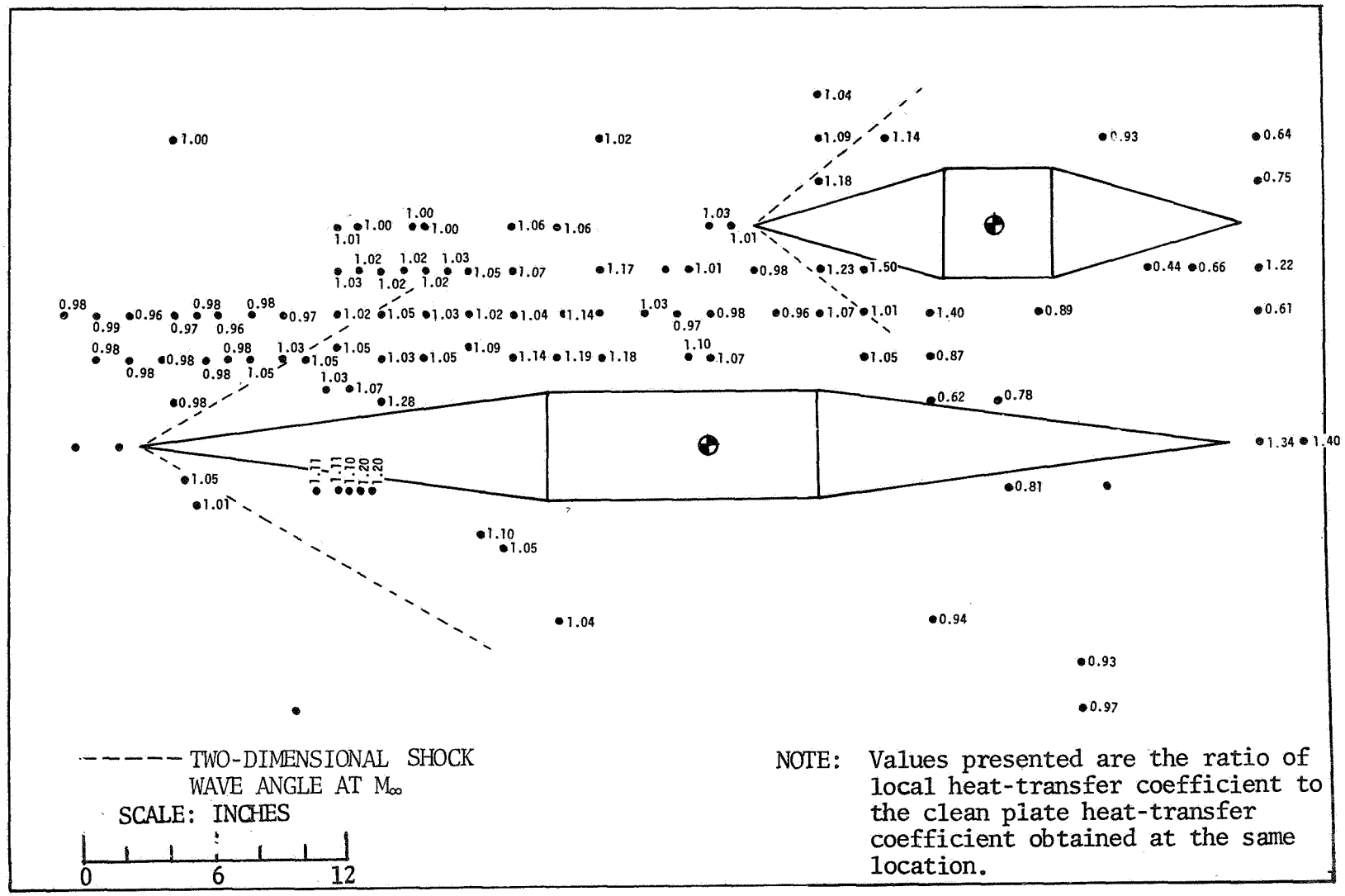

FIGURE A-37. EFFECT OF MODEL 4 SHOCK IMPINGEMENT ON MODEL 1 AFTERBODY ON PLATE HEATING DISTRIBUTION AT MACH NUMBER 2.49 - CONFIGURATION 16

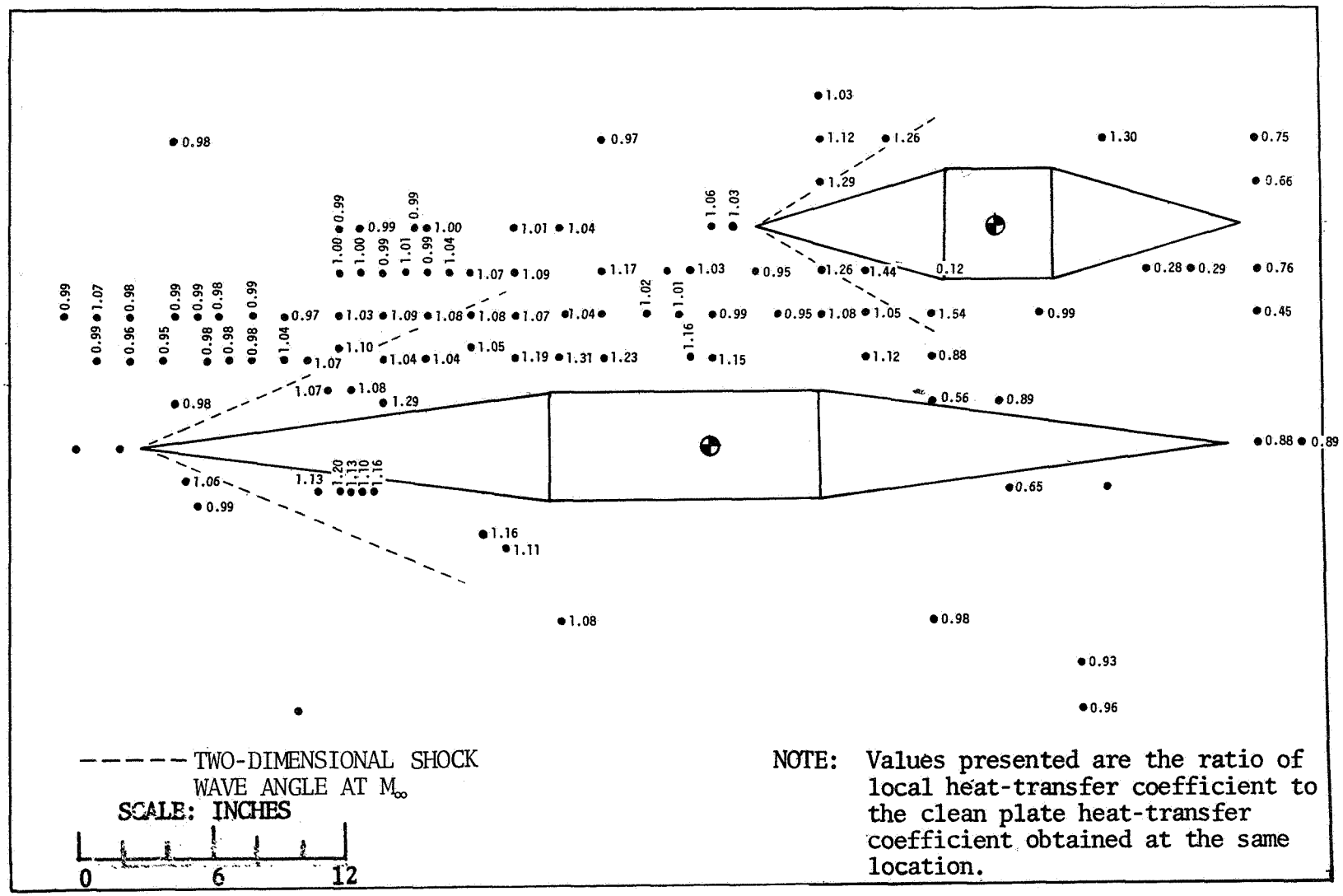

FIGURE A-38. EFFECT OF MODEL 4 SHOCK IMPINGEMENT ON MODEL 1 AFTERBODY ON PLATE HEATING DISTRIBUTION AT MACH NUMBER 3.51 - CONFIGURATION 16

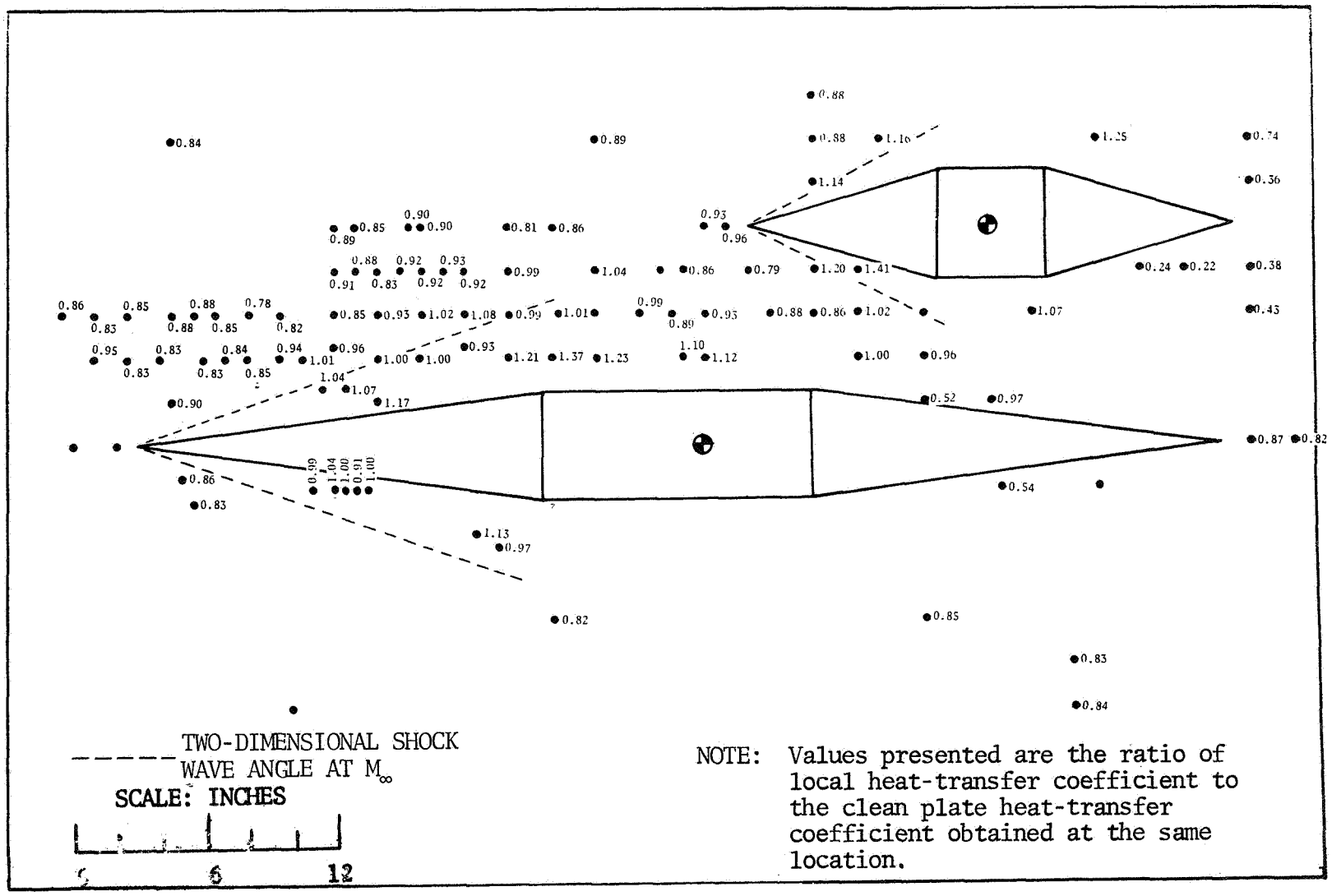

FIGURE A-39. EFFECT OF MODEL 4 SHOCK IMPINGEMENT ON MODEL 1 AFTERBODY ON PLATE HEATING DISTRIBUTION AT MACH NUMBER 4.44 - CONFIGURATION 16

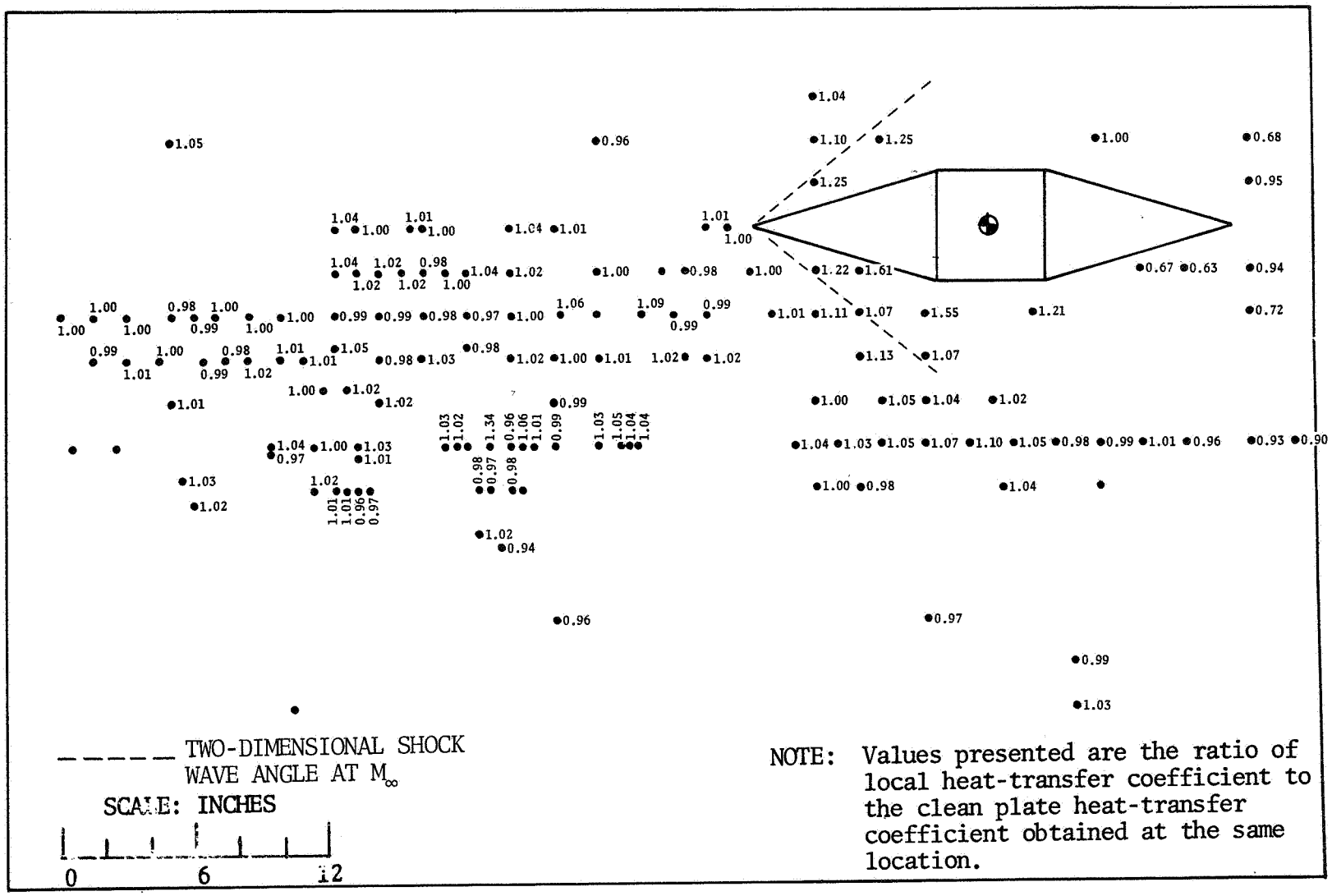

FIGURE A-40. EFFECT OF MODEL 4 ON PLATE HEATING DISTRIBUTION AT MACH NUMBER 2.49 - CONFIGURATION 17

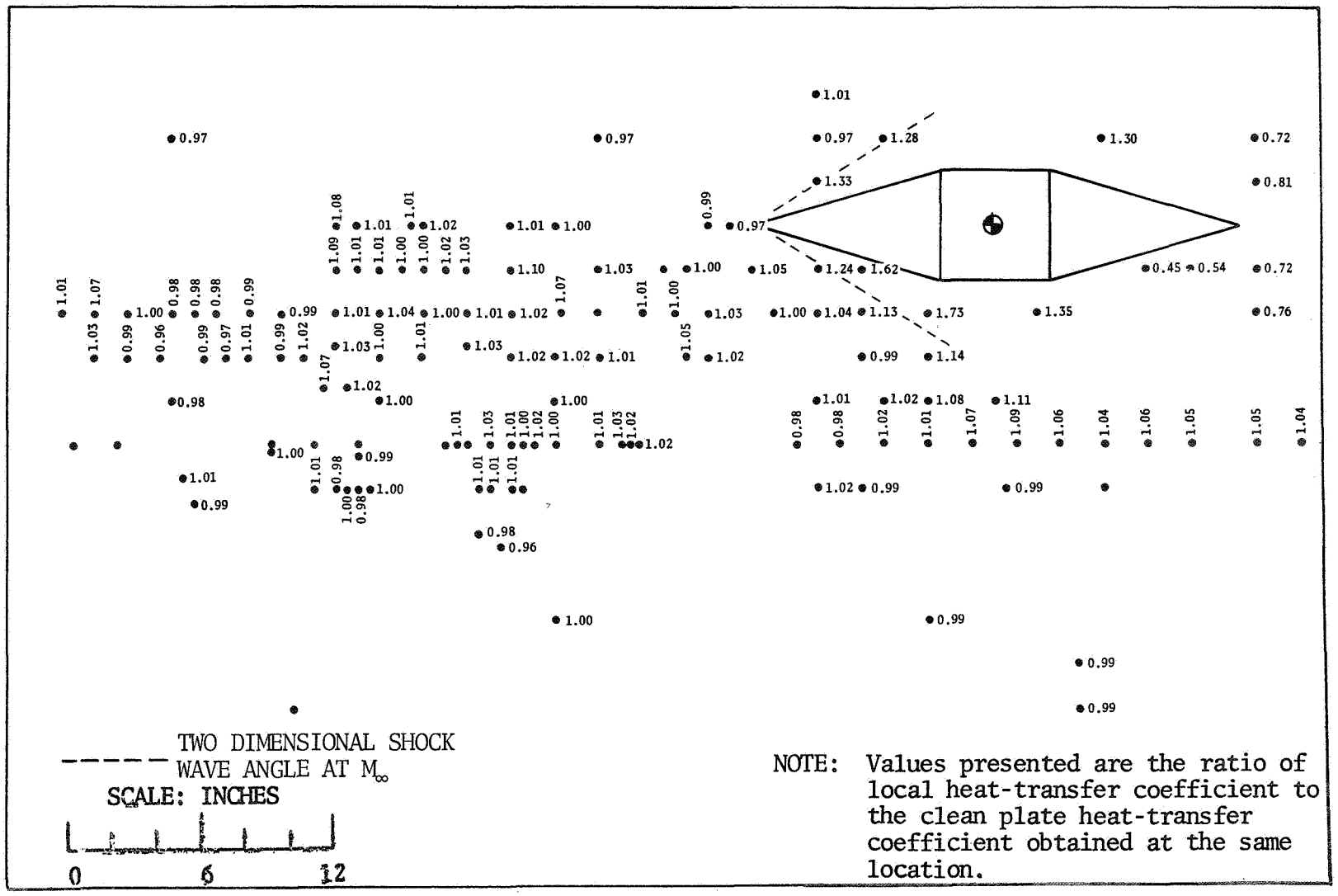

FIGURE A-41. EFFECT OF MODEL 4 ON PLATE HEATING DISTRIBUTION AT MACH NUMBER 3.51 - CONFIGURATION 17

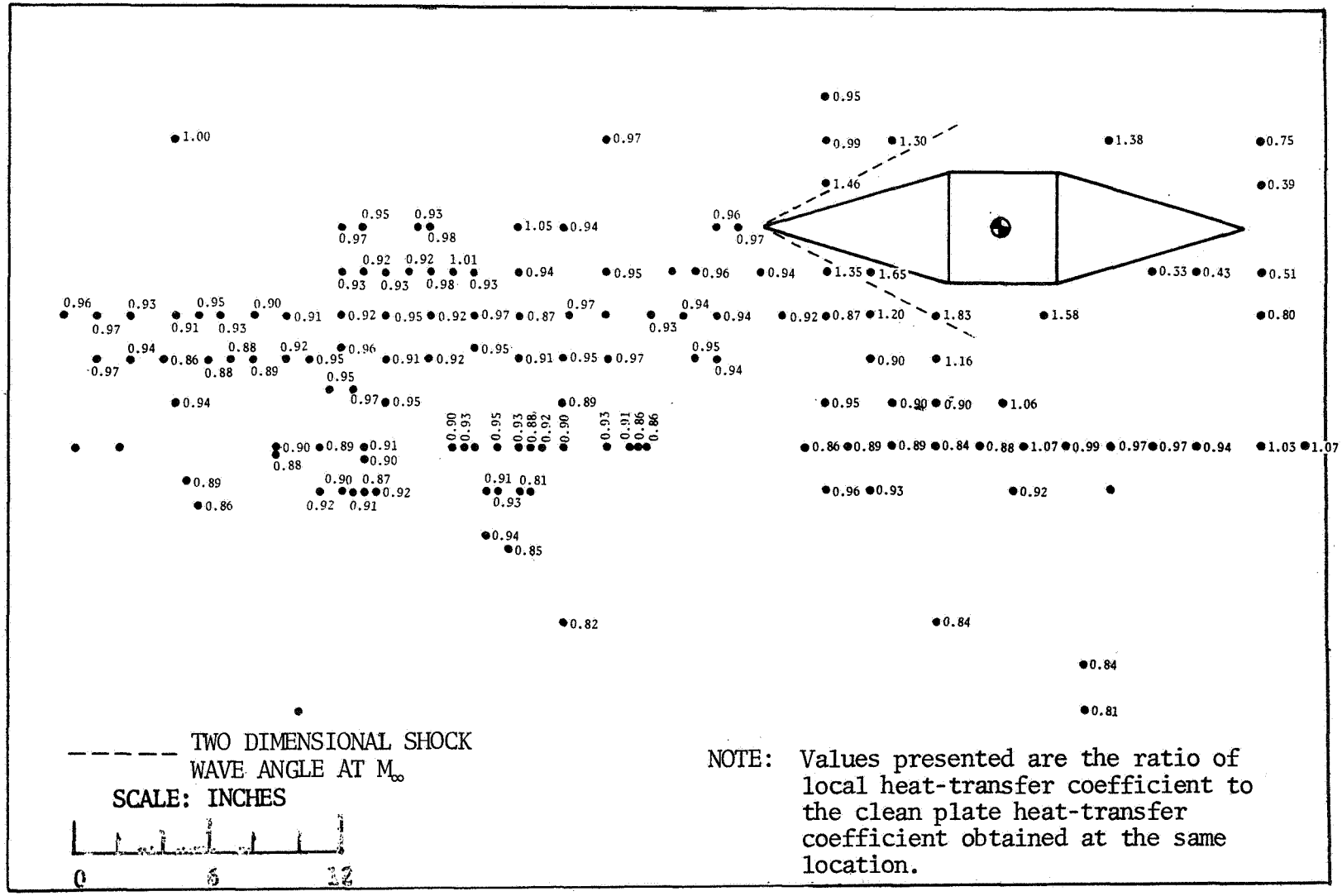

FIGURE A-42. EFFECT OF MODEL 4 ON PLATE HEATING DISTRIBUTION AT MACH NUMBER 4.44 - CONFIGURATION 17

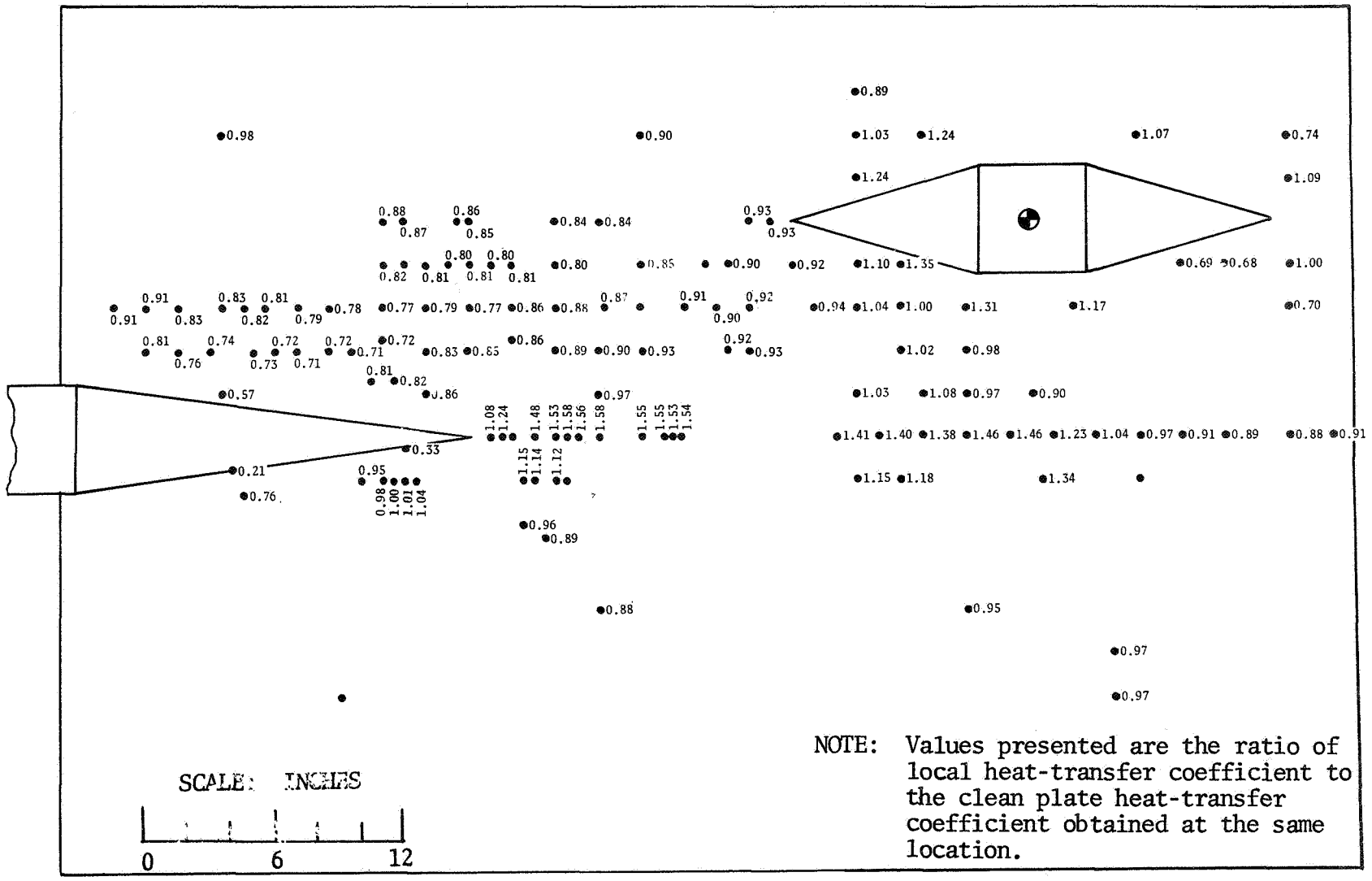

FIGURE A-43. EFFECT OF MODEL 4 IN MODEL 1 WAKE ON PLATE HEATING DISTRIBUTION AT MACH NUMBER 2.49 - CONFIGURATION 18

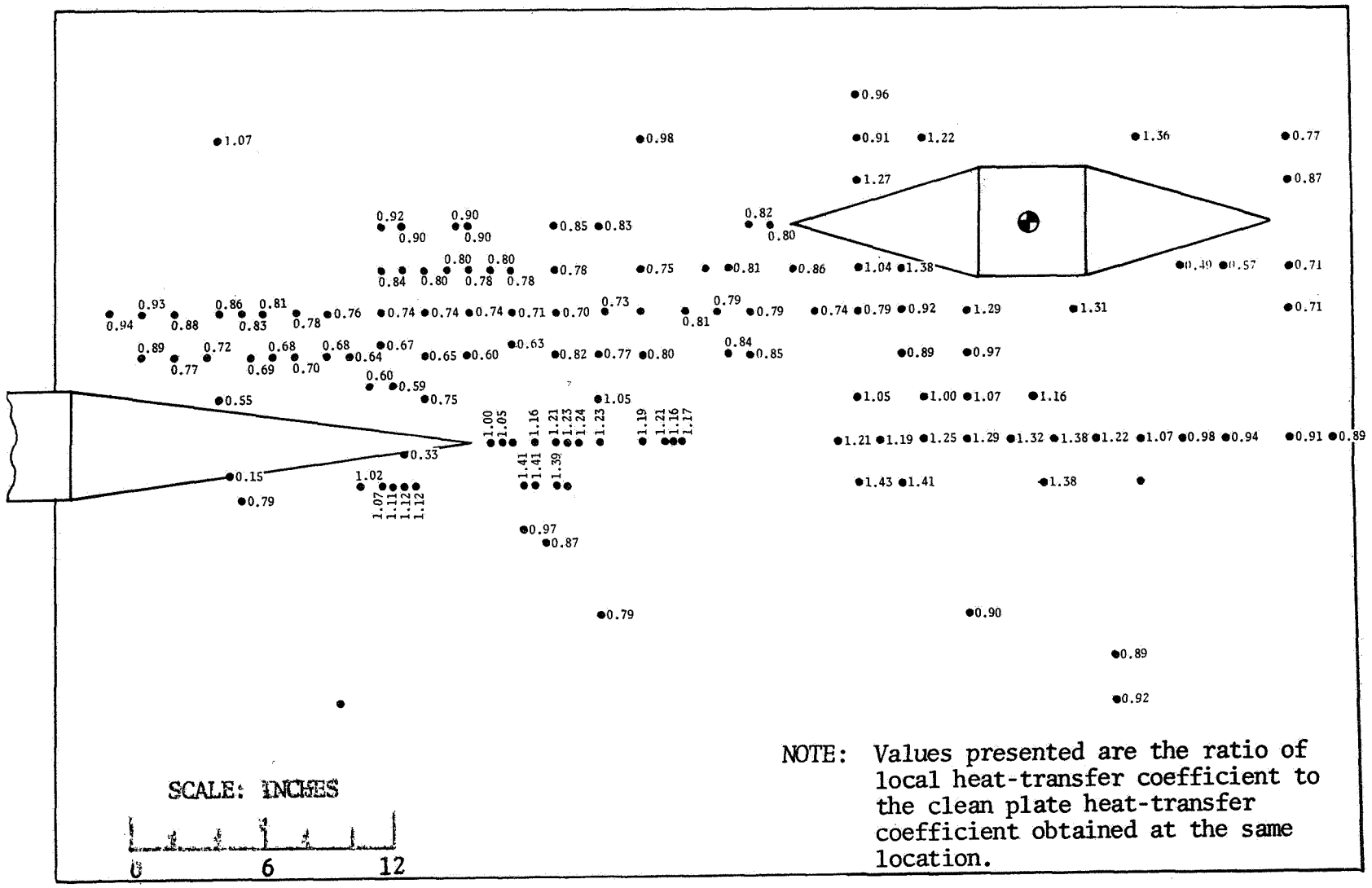

FIGURE A-44. EFFECT OF MODEL 4 IN MODEL 1 WAKE ON PLATE HEATING DISTRIBUTION AT MACH NUMBER 3.51 - CONFIGURATION 18

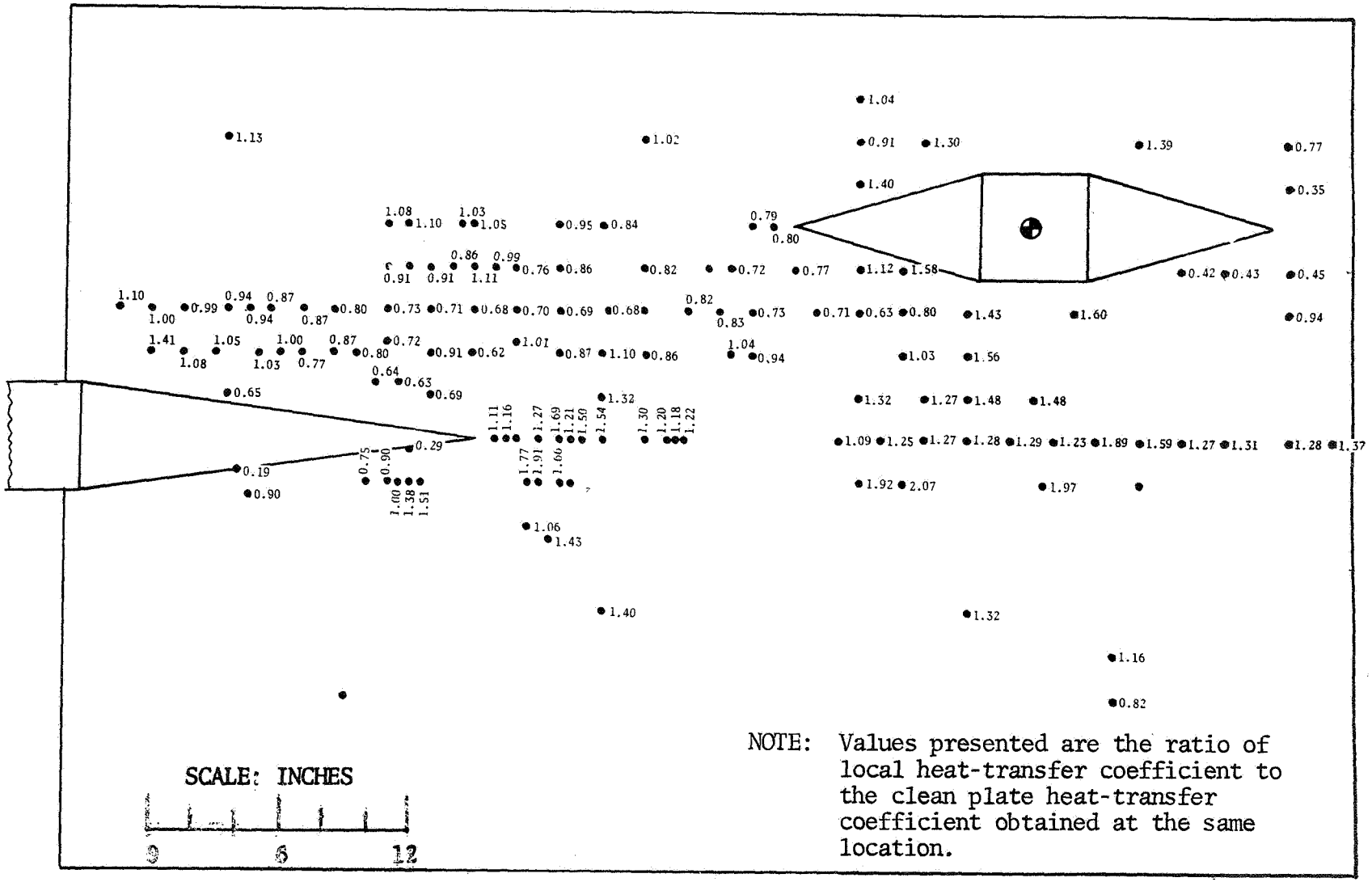

FIGURE A-45. EFFECT OF MODEL 4 IN MODEL 1 WAKE ON PLATE HEATING DISTRIBUTION AT MACH NUMBER 4.44 - CONFIGURATION 18

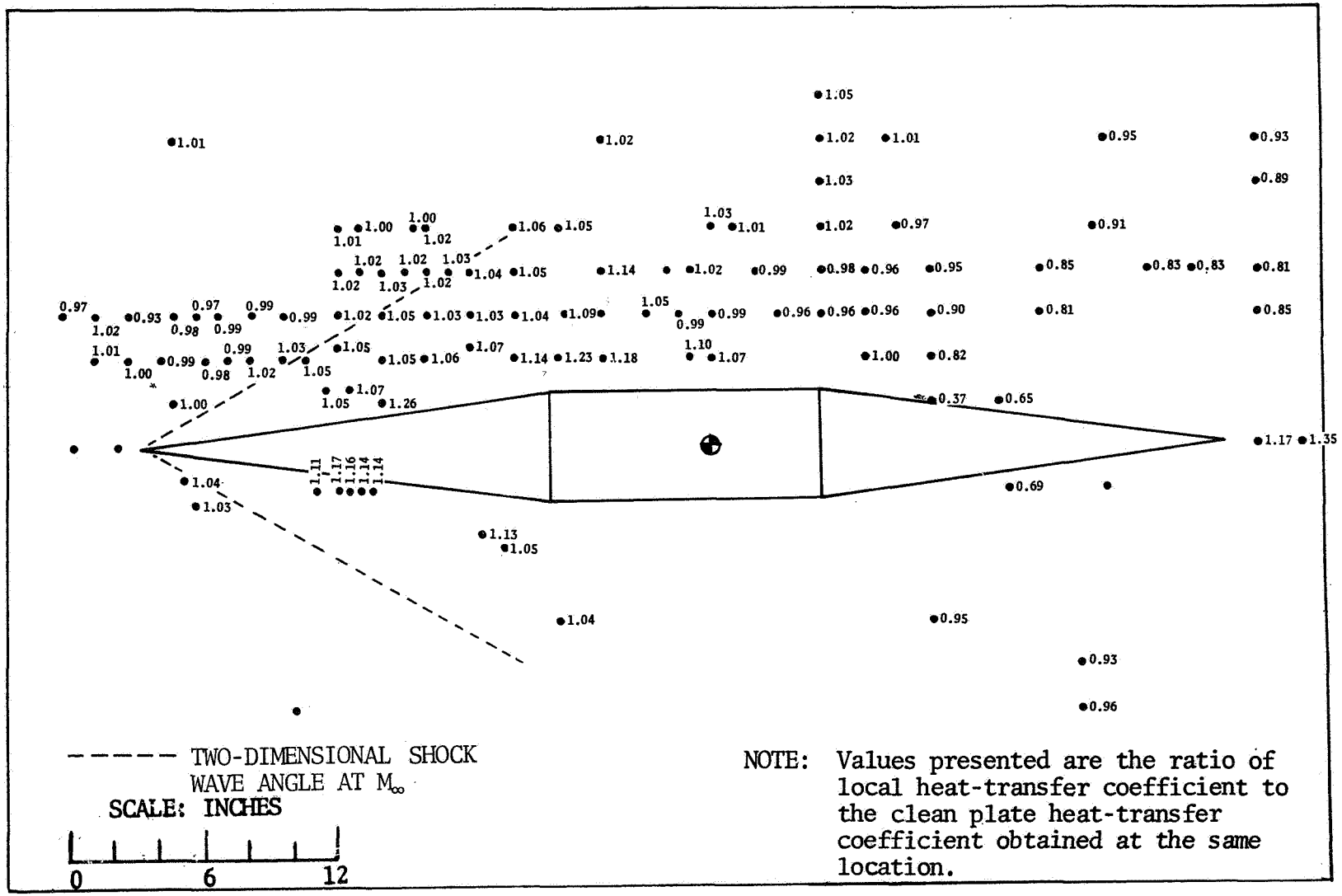

FIGURE A-46. EFFECT OF MODEL 1 ON PLATE HEATING DISTRIBUTION AT MACH NUMBER 2.49 - CONFIGURATION 19

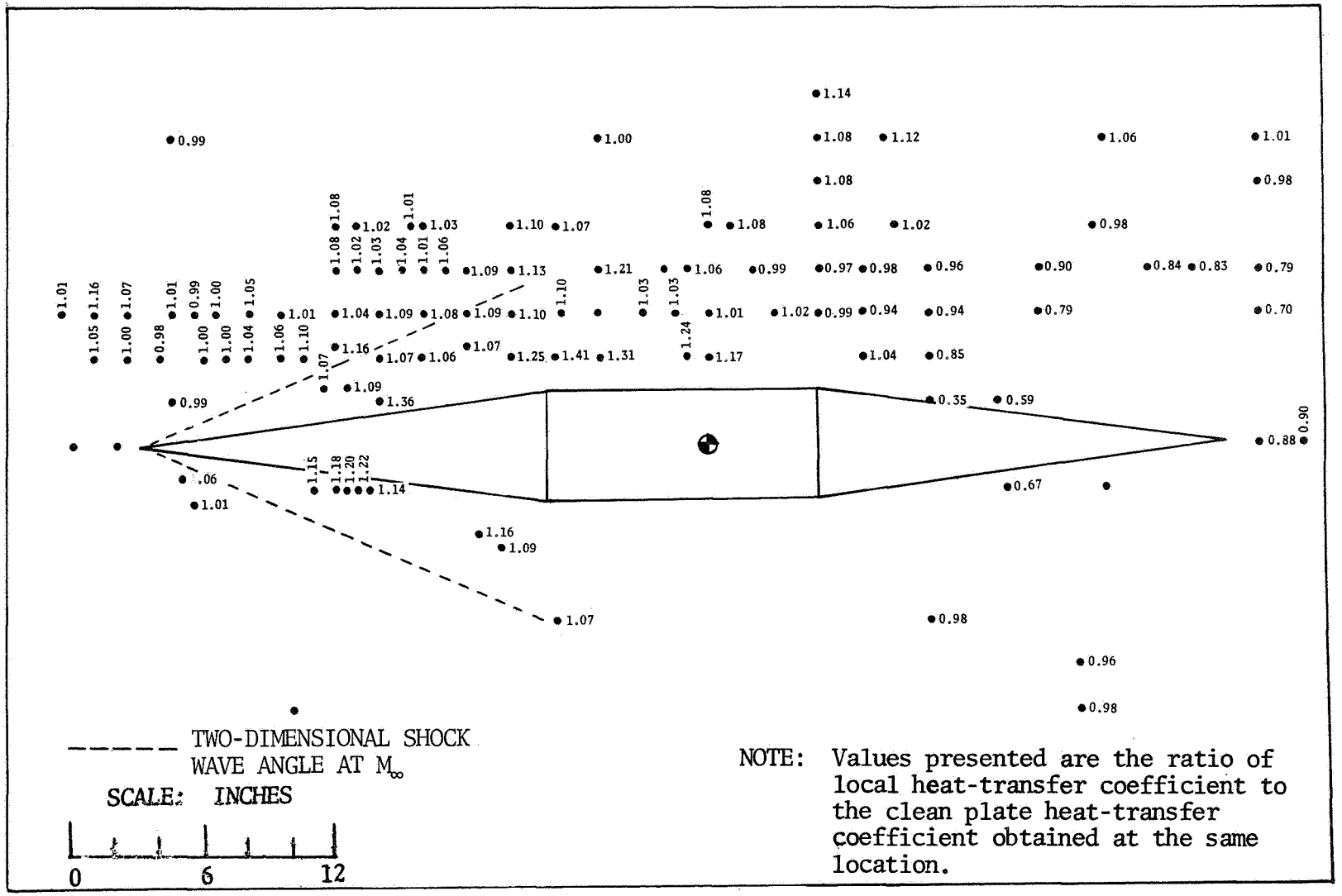

FIGURE A-47. EFFECT OF MODEL 1 ON PLATE HEATING DISTRIBUTION AT MACH NUMBER 3.51 - CONFIGURATION 19

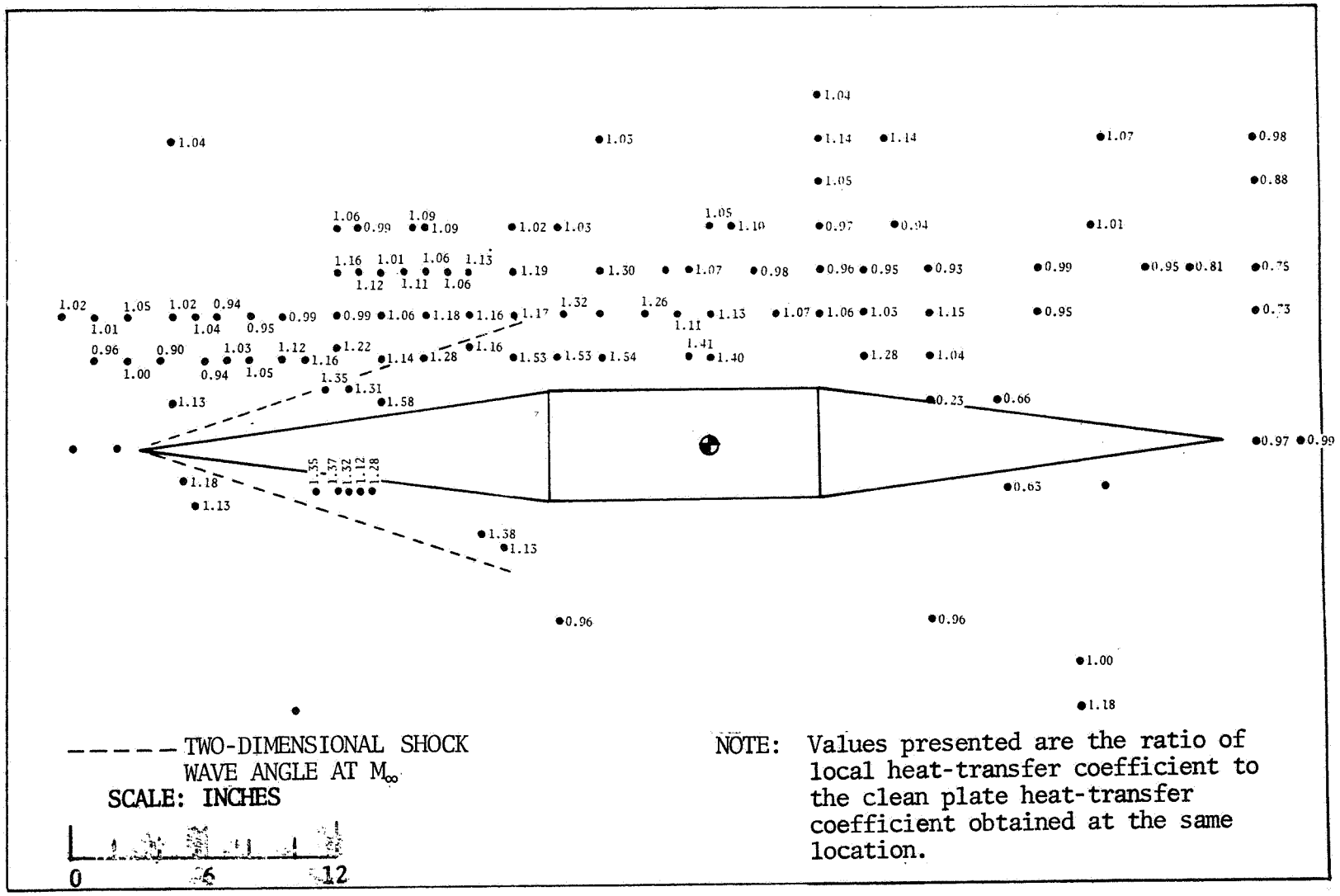

FIGURE A-48. EFFECT OF MODEL 1 ON PLATE HEATING DISTRIBUTION AT MACH NUMBER 4.44 - CONFIGURATION 19

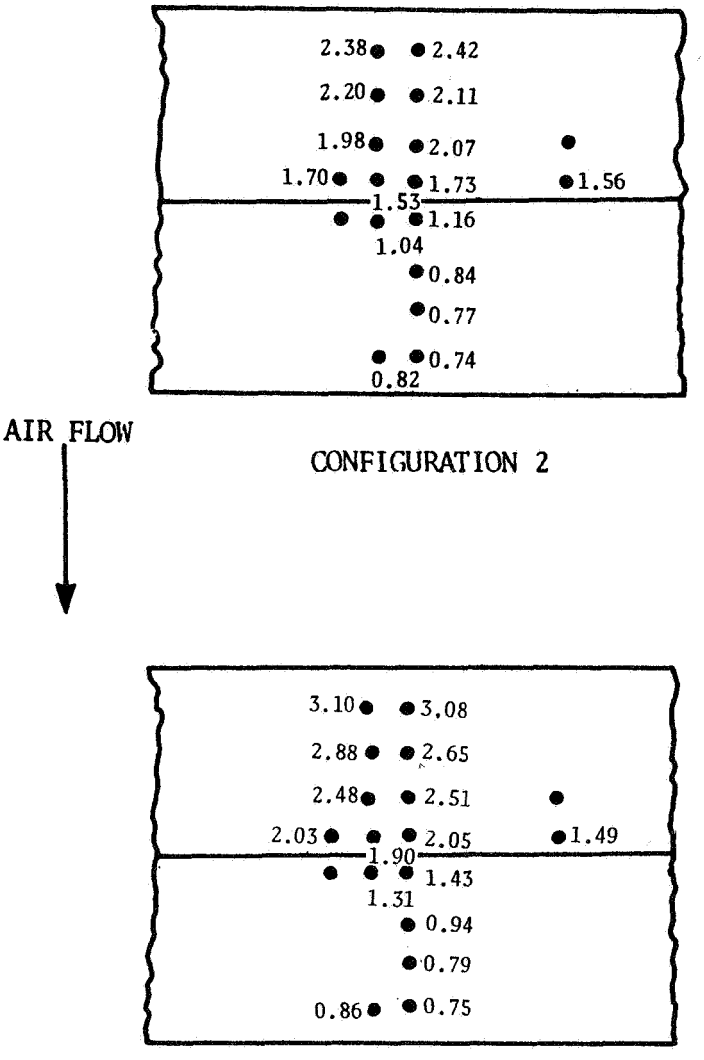

NOTE: Values presented are the ratio of local heat-transfer coefficient to an average of clean plate heat-transfer coefficients obtained in the area covered by Model 12 base (0.00264 Btu/ft^{2}sec-°R).

FIGURE A-49. EFFECT OF MODEL 1 WAKE ON DOUBLE WEDGE (MODEL 12) HEATING DISTRIBUTIONS AT MACH NUMBER 2.49

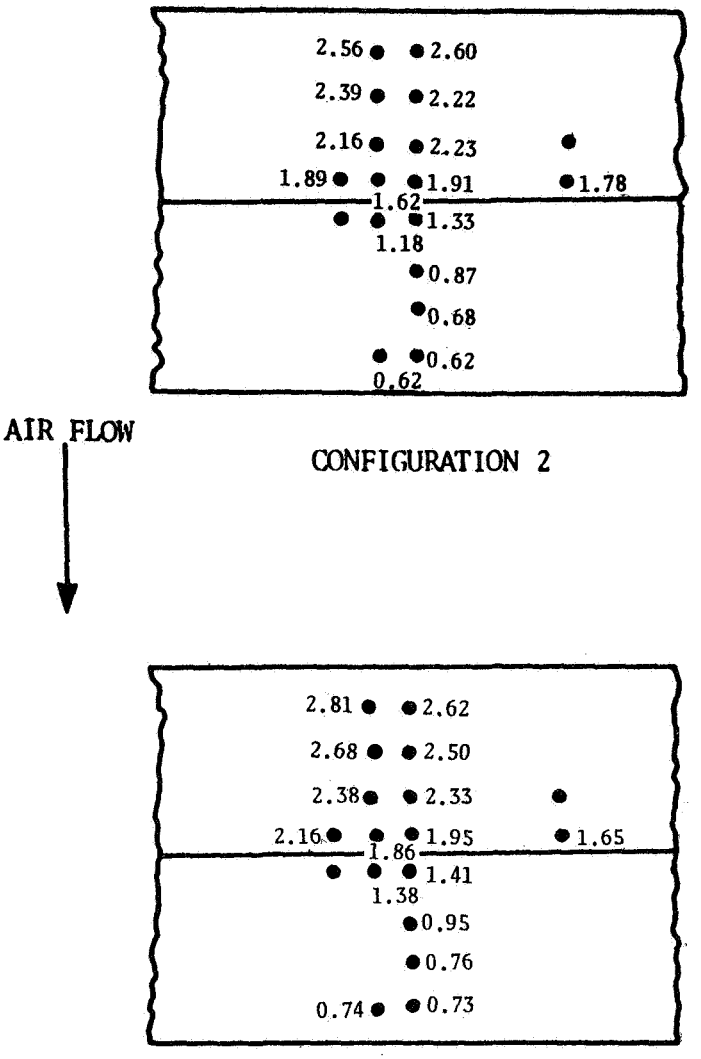

NOTE: Values presented are the ratio of local heat-transfer coefficient to an average of clean plate heat-transfer coefficients obtained in the area covered by Model 12 base (0.00133 Btu/ft^{2}sec-°R).

FIGURE A-50. EFFECT OF MODEL 1 WAKE ON DOUBLE WEDGE (MODEL 12) HEATING DISTRIBUTIONS AT MACH NUMBER 3.51

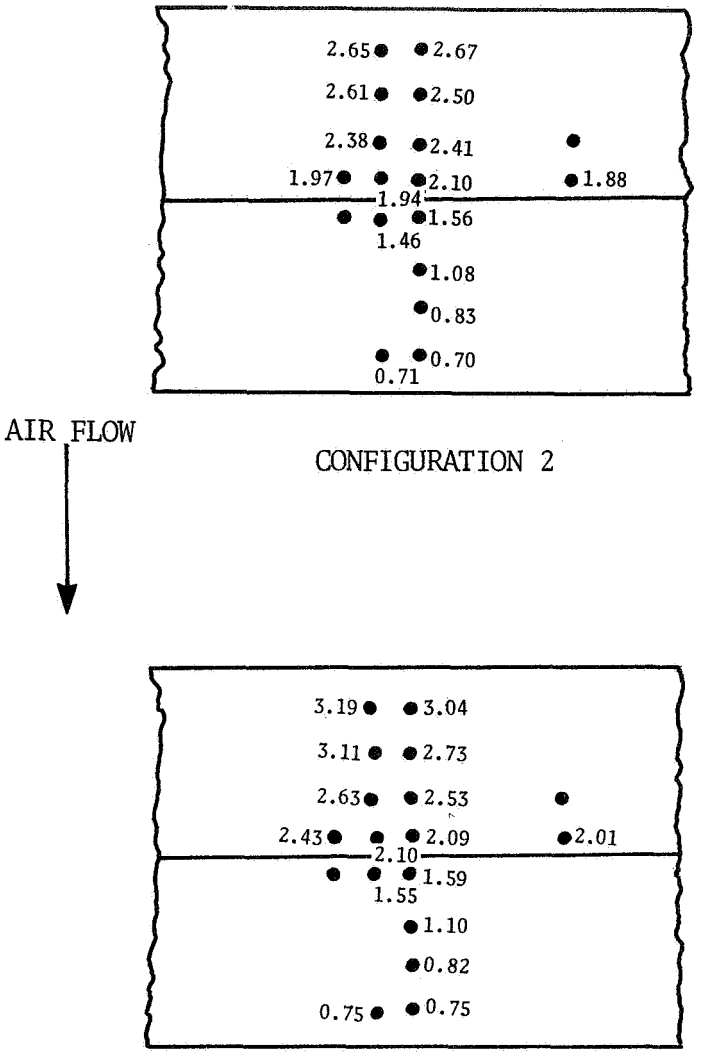

NOTE: Values presented are the ratio of local heat-transfer coefficient to an average of clean plate heat-transfer coefficients obtained in the area covered by Model 12 base (0.00076 Btu/ft^{2}sec-°R).

FIGURE A-51. EFFECT OF MODEL 1 WAKE ON DOUBLE WEDGE (MODEL 12) HEATING DISTRIBUTIONS AT MACH NUMBER 4.44

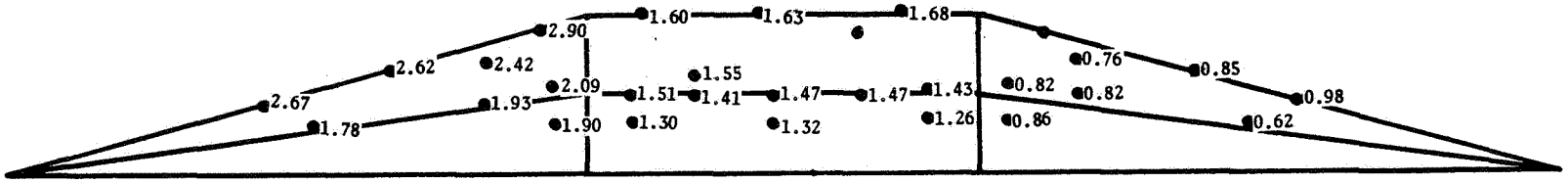

CONFIGURATION 19

AIR FLOW

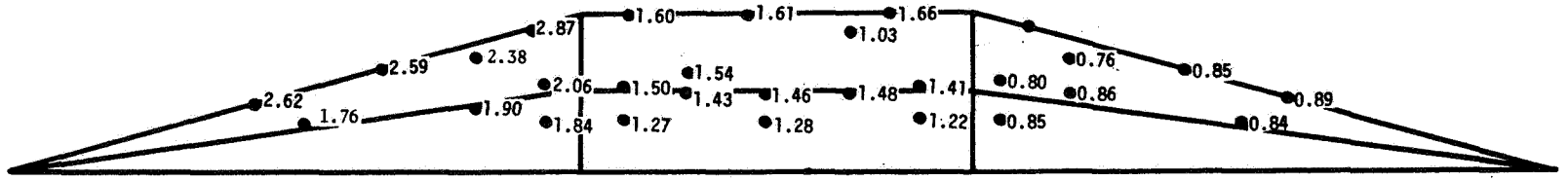

CONFIGURATION 16

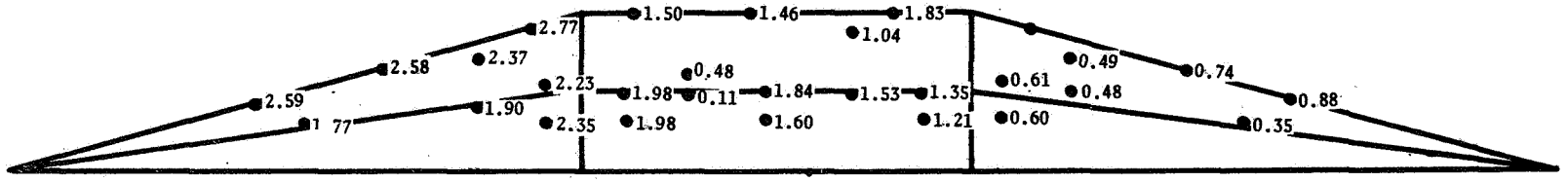

CONFIGURATION 15

NOTE: Values presented are the ratio of local heat-transfer coefficient to an average of clean plate heat-transfer coefficients obtained in the area covered by Model 1 base (0.00267 Btu/ft^{2}sec-°R).

FIGURE A-52. EFFECT OF MODEL 4 SHOCK IMPINGEMENT ON MODEL 1 HEATING DISTRIBUTIONS AT MACH NUMBER 2.49

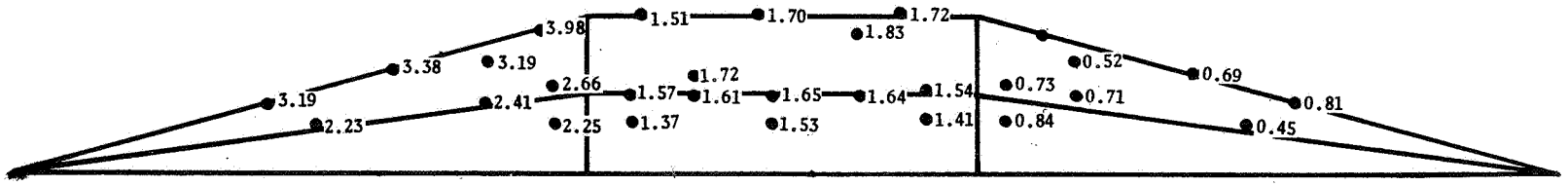

CONFIGURATION 19

AIR FLOW

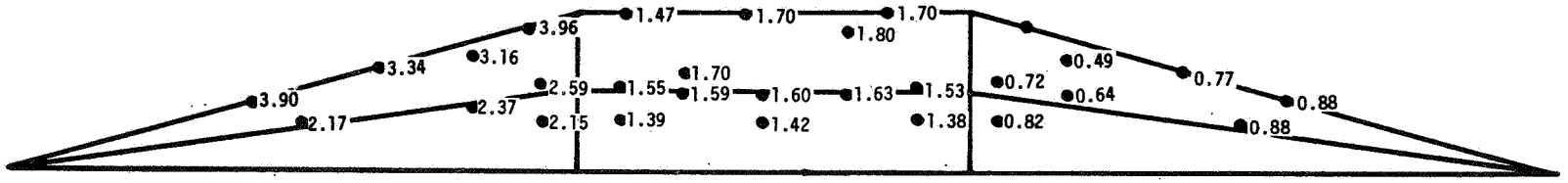

CONFIGURATION 16

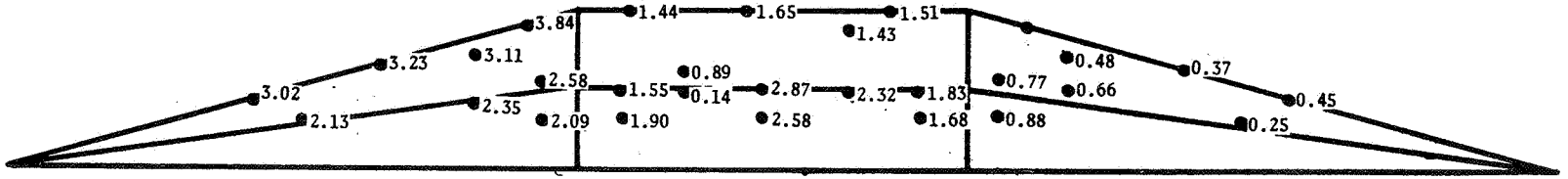

CONFIGURATION 15

NOTE: Values presented are the ratio of local heat-transfer coefficient to an average of clean plate heat-transfer coefficients obtained in the area covered by Model 1 base (0.00128 Btu/ft^{2}sec-°R).

FIGURE A-53. EFFECT OF MODEL 4 SHOCK IMPINGEMENT ON MODEL 1 HEATING DISTRIBUTIONS AT MACH NUMBER 3.51

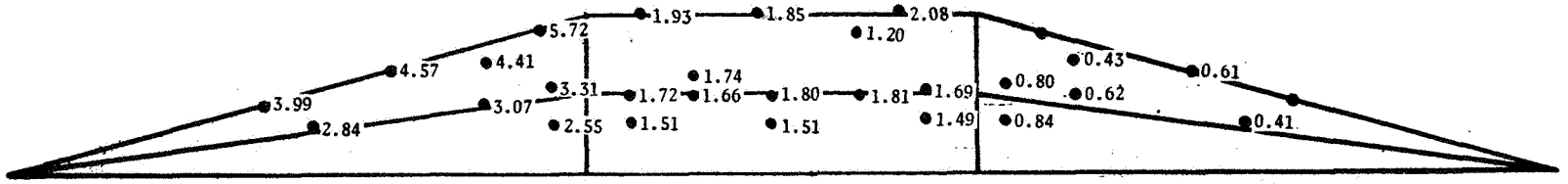

CONFIGURATION 19

AIR FLOW

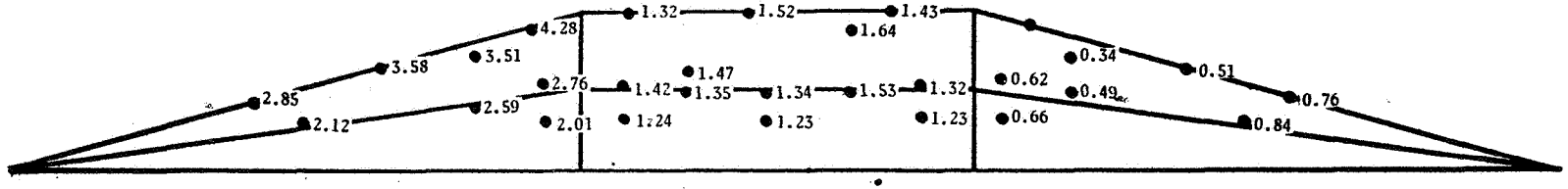

CONFIGURATION 16

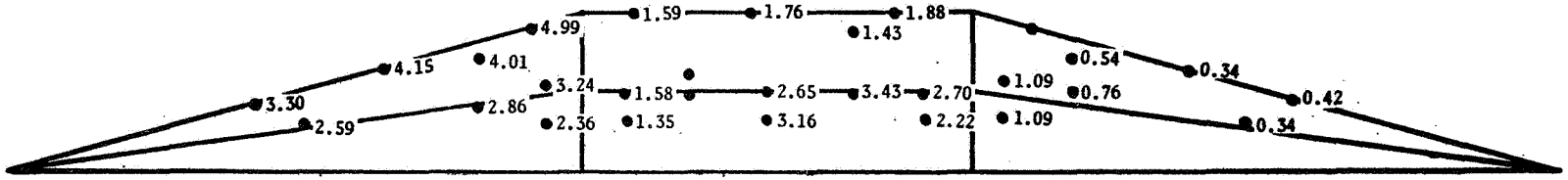

CONFIGURATION 15

NOTE: Values presented are the ratio of local heat-transfer coefficient to an average of clean plate heat-transfer coefficients obtained in the area covered by Model 1 base (0.00074 Btu/ft^{2}sec-°R).

FIGURE A-54. EFFECT OF MODEL 4 SHOCK IMPINGEMENT ON MODEL 1 HEATING DISTRIBUTIONS AT MACH NUMBER 4.44

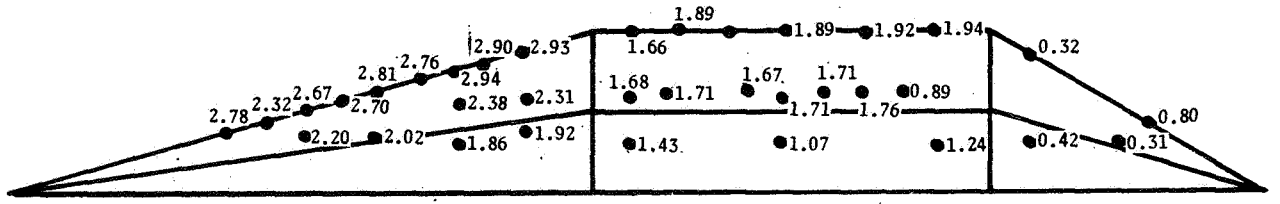

CONFIGURATION 7

AIR FLOW

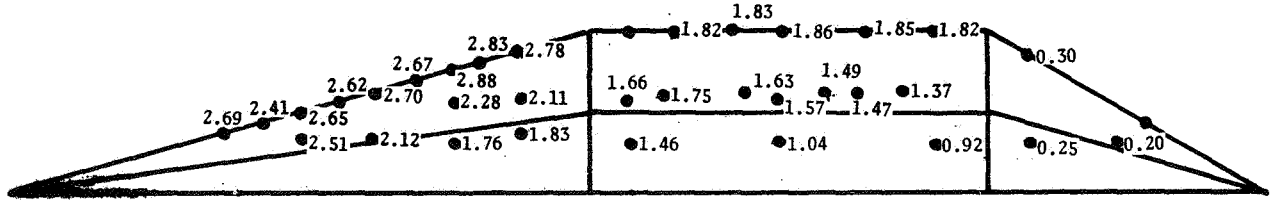

CONFIGURATION 8

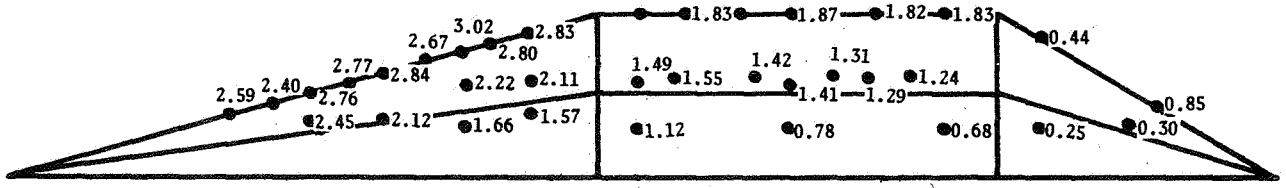

CONFIGURATION 9

NOTE: Values presented are the ratio of local heat-transfer coefficient to an average of clean plate heat-transfer coefficients obtained in the area covered by Model 2 base (0.00249 Btu/ft^{2}sec-°R).

FIGURE A-55. EFFECT OF MODEL 1 ON MODEL 2 HEATING DISTRIBUTIONS AT MACH NUMBER 2.49

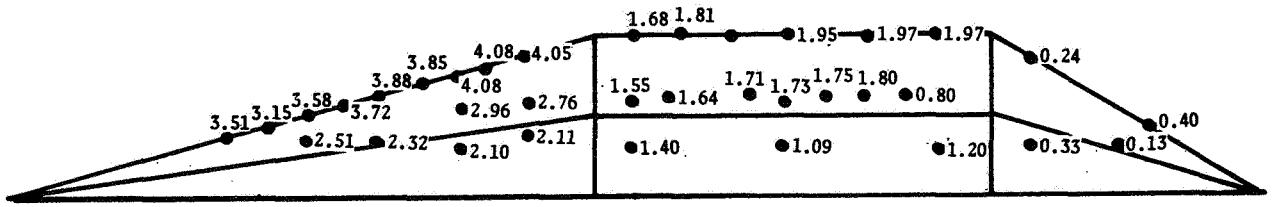

CONFIGURATION 7

AIR FLOW

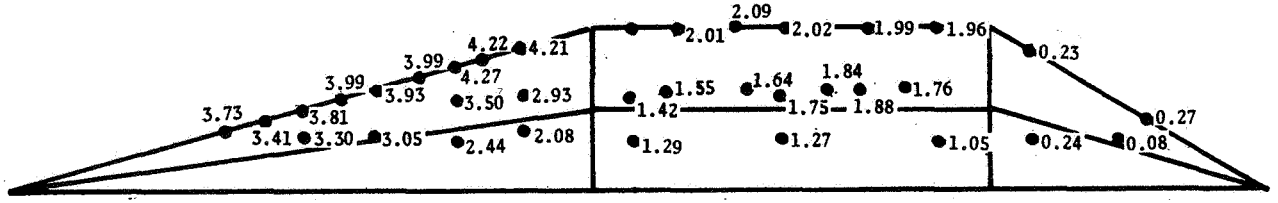

CONFIGURATION 8

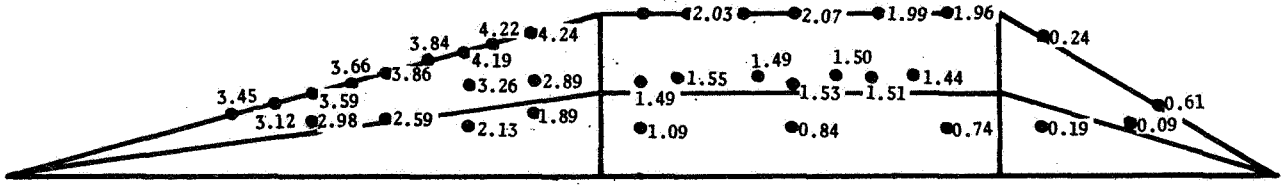

CONFIGURATION 9

NOTE: Values presented are the ratio of local heat-transfer coefficient to an average of clean plate heat-transfer coefficients obtained in the area covered by Model 2 base (0.00140 Btu/ft^{2}sec-°R)

FIGURE A-56. EFFECT OF MODEL 1 ON MODEL 2 HEATING DISTRIBUTIONS AT MACH NUMBER 3.51

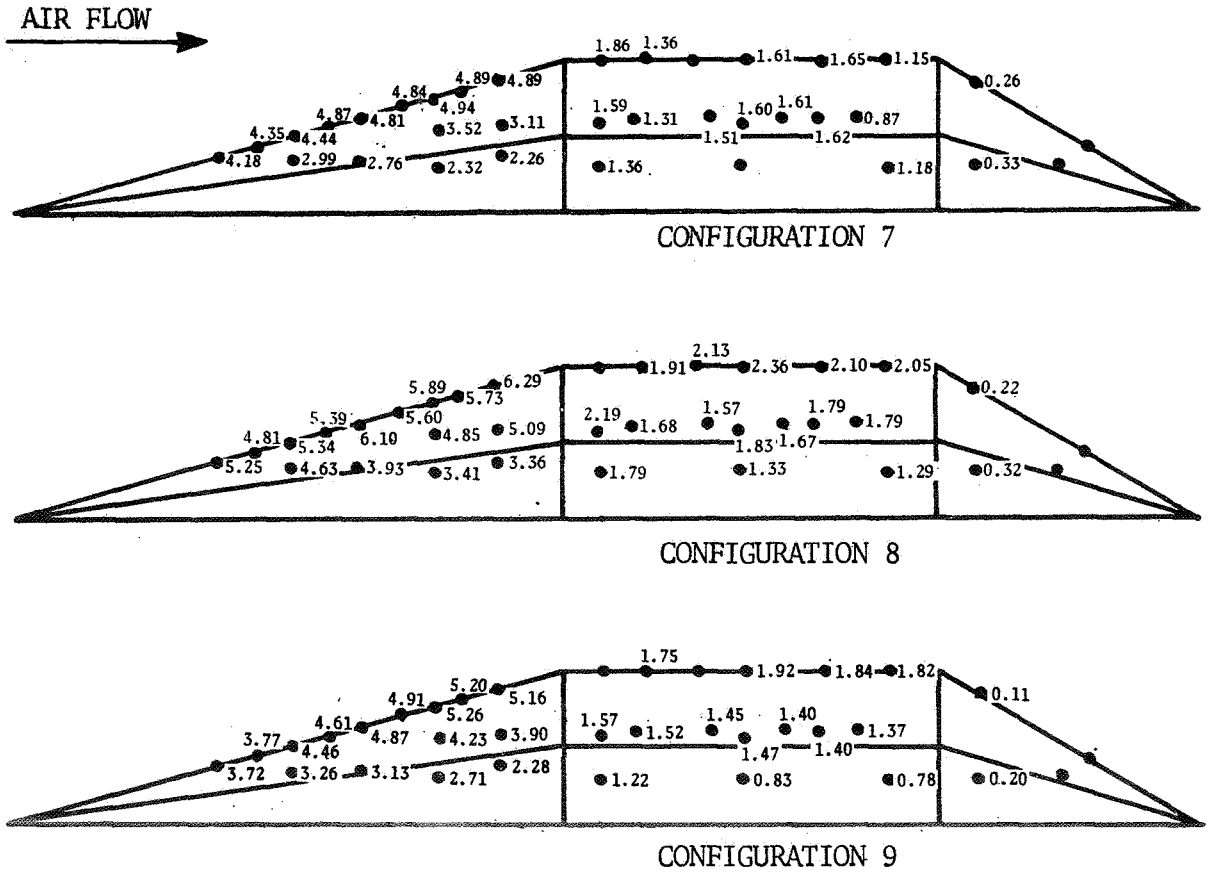

NOTE: Values presented are the ratio of local heat-transfer coefficient to an average of clean plate heat-transfer coefficients obtained in the area covered by Model 2 base (0.00087 Btu/ft^{2}sec-°R).

FIGURE A-57. EFFECT OF MODEL 1 ON MODEL 2 HEATING DISTRIBUTIONS AT MACH NUMBER 4.44

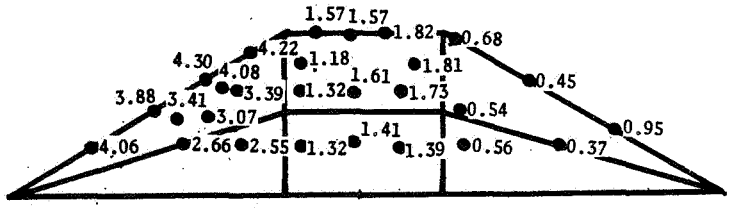

CONFIGURATION 17

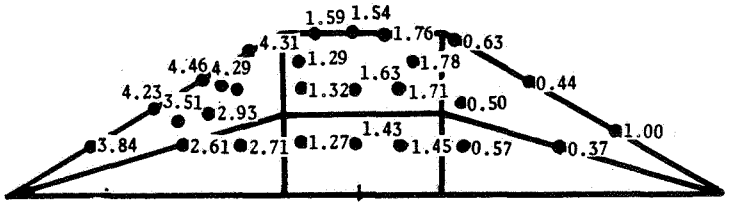

CONFIGURATION 14

AIR FLOW

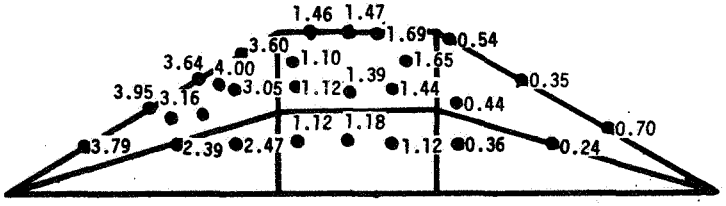

CONFIGURATION 16

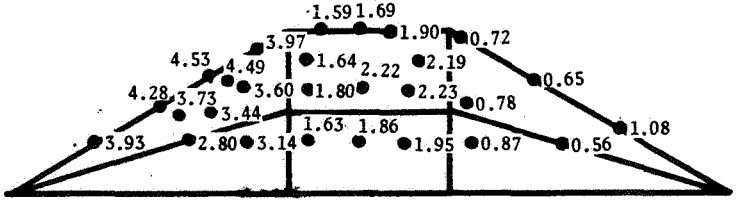

CONFIGURATION 15

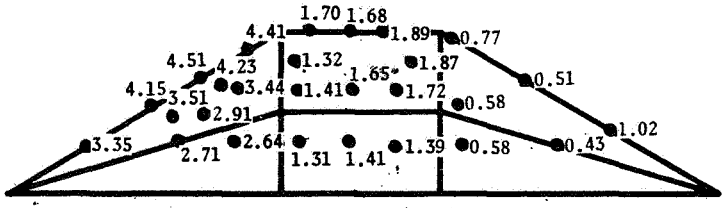

CONFIGURATION 18

NOTE: Values presented are the ratio of local heat-transfer coefficient to an average of clean plate heat-transfer coefficients obtained in the area covered by Model 4 base (0.00251 Btu/ft^{2}sec-°R).

FIGURE A-58. EFFECT OF MODEL 1 ON MODEL 4 HEATING DISTRIBUTIONS AT MACH NUMBER 2.49

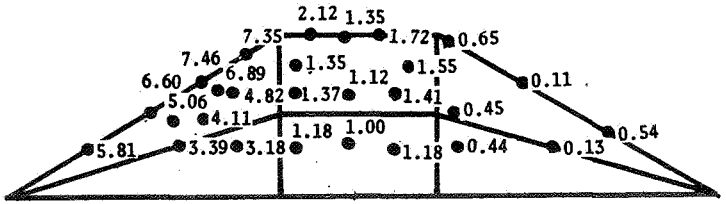

CONFIGURATION 17

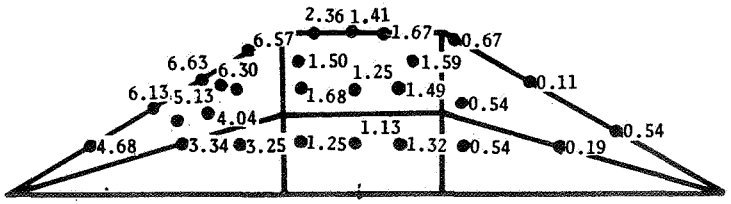

CONFIGURATION 14

AIR FLOW

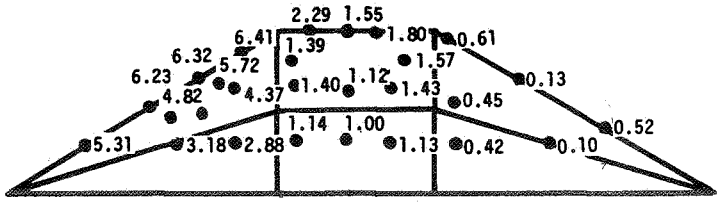

CONFIGURATION 16

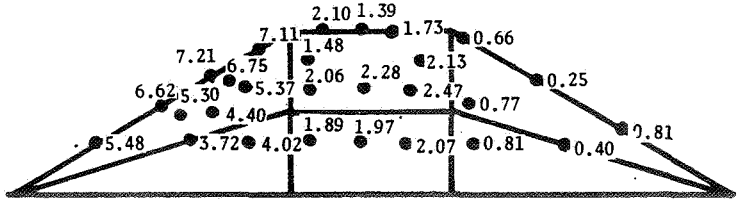

CONFIGURATION 15

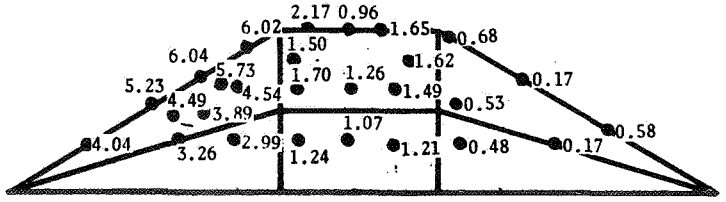

CONFIGURATION 18

NOTE: Values presented are the ratio of local heat-transfer coefficient to an average of clean plate heat-transfer coefficients obtained in the area covered by Model 4 base (0.00142 Btu/ft^{2}sec-°R).

FIGURE A-59. EFFECT OF MODEL 1 ON MODEL 4 HEATING DISTRIBUTIONS AT MACH NUMBER 3.51

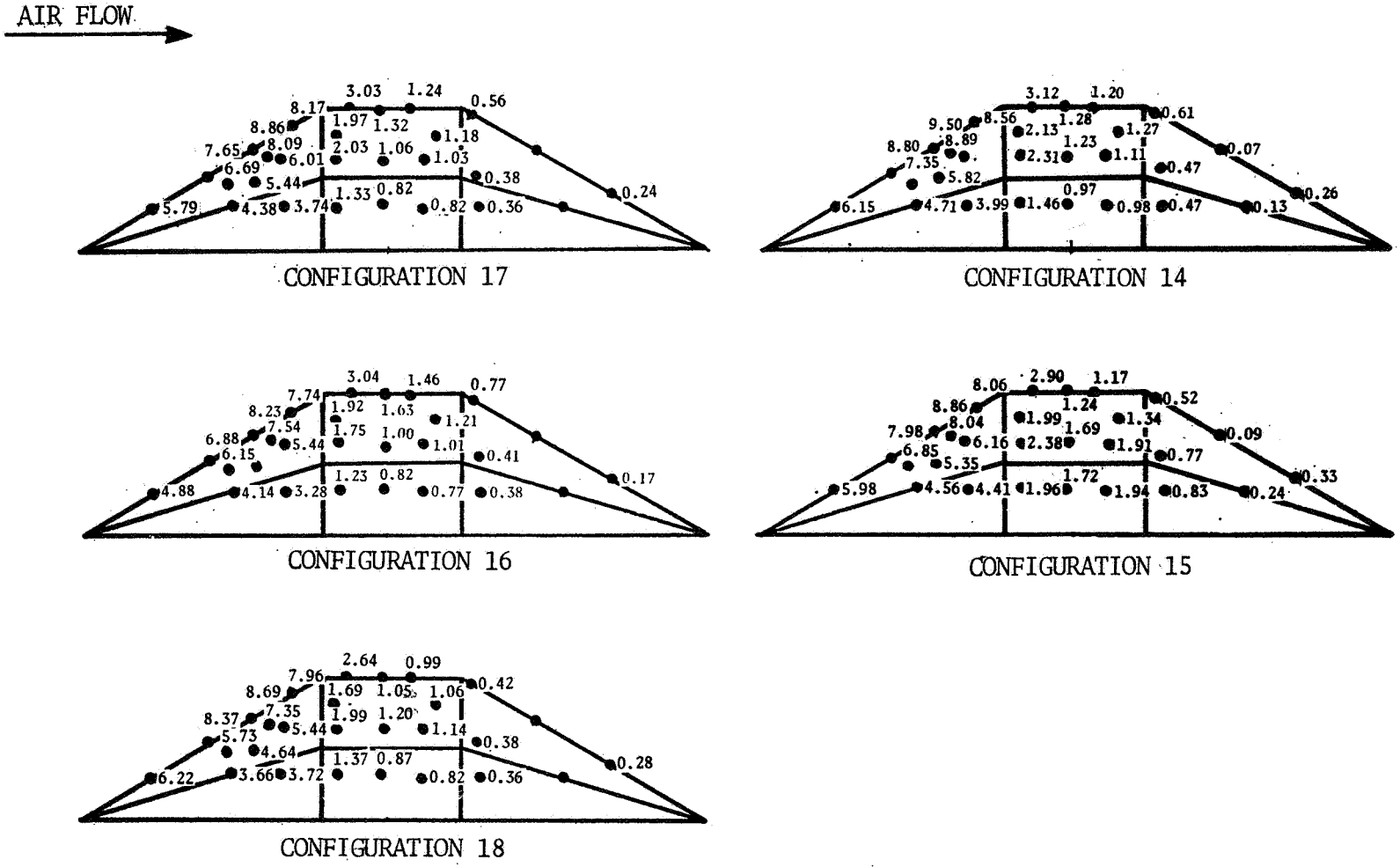

NOTE: Values presented are the ratio of local heat-transfer coefficient to an average of clean plate heat-transfer coefficients obtained in the area covered by Model 4 base (0.00092 Btu/ft^{2}sec-°R).

FIGURE A-60. EFFECT OF MODEL 1 ON MODEL 4 HEATING DISTRIBUTIONS AT MACH NUMBER 4.44

NOTE: * indicates measurement located on opposite side.

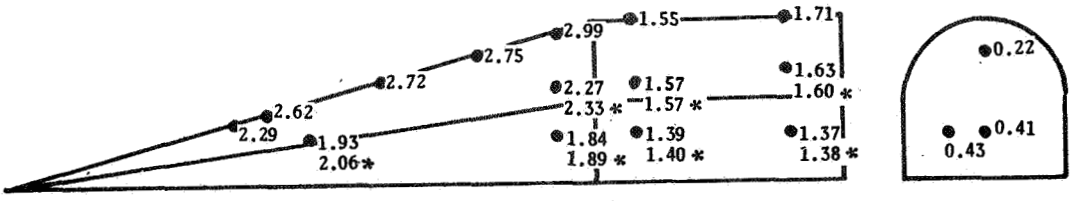

CONFIGURATION 6

AIR FLOW

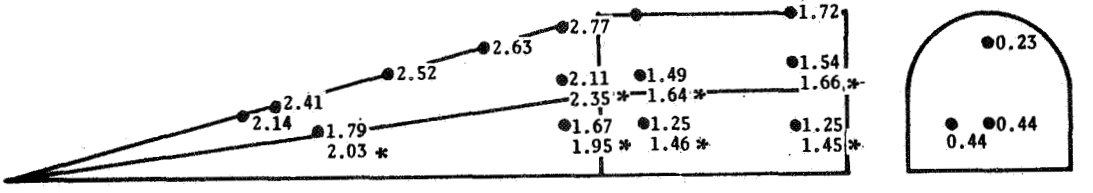

CONFIGURATION 5

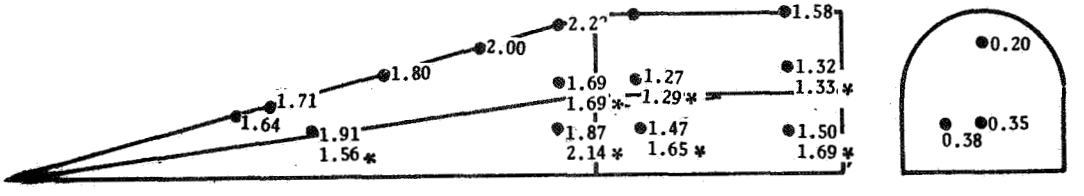

CONFIGURATION 8

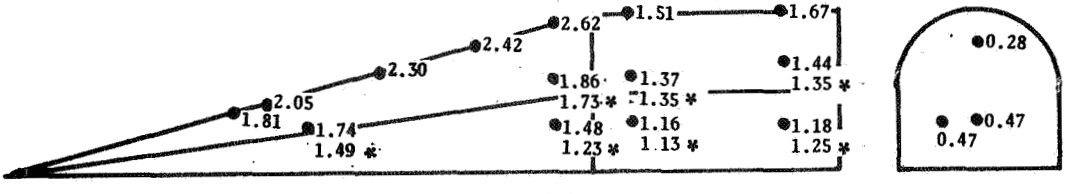

CONFIGURATION 9

NOTE: Values presented are the ratio of local heat-transfer coefficient to an average of clean plate heat-transfer coefficients obtained in the area covered by Model 5 base (0.00255 Btu/ft^{2}sec-°R).

FIGURE A-61. EFFECT OF MULTIPLE WAKES (MODELS 1 AND 2) ON MODEL 5 HEATING DISTRIBUTIONS AT MACH NUMBER 2.49

NOTE: * indicates measurement located on opposite side.

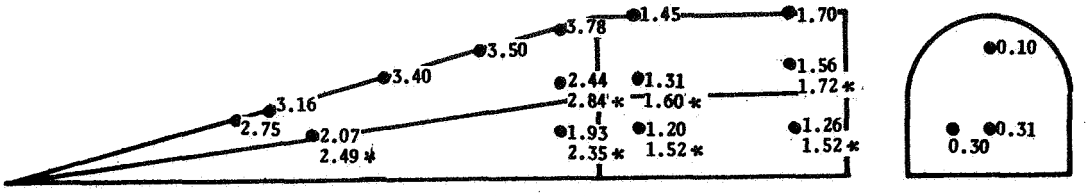

CONFIGURATION 6

AIR FLOW

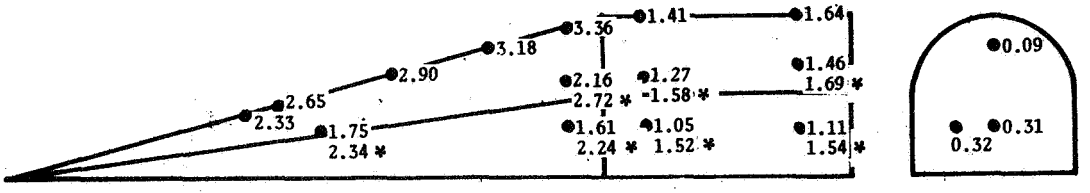

CONFIGURATION 5

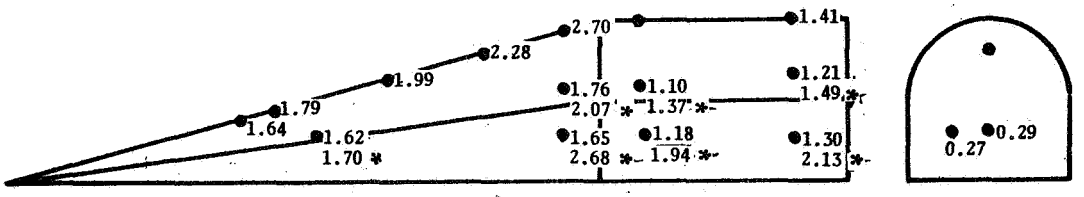

CONFIGURATION 8

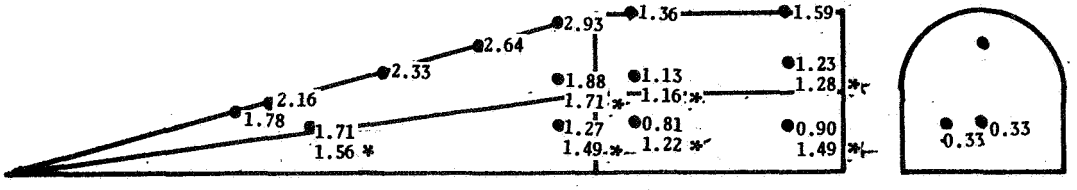

CONFIGURATION 9

NOTE: Values presented are the ratio of local heat-transfer coefficient to an average of clean plate heat-transfer coefficients obtained in the area covered by Model 5 base (0.00135 Btu/ft^{2}sec-°R).

FIGURE A-62. EFFECT OF MULTIPLE WAKES (MODELS 1 AND 2) ON MODEL 5 HEATING DISTRIBUTIONS AT MACH NUMBER 3.51

NOTE: * indicates measurement located on opposite side.

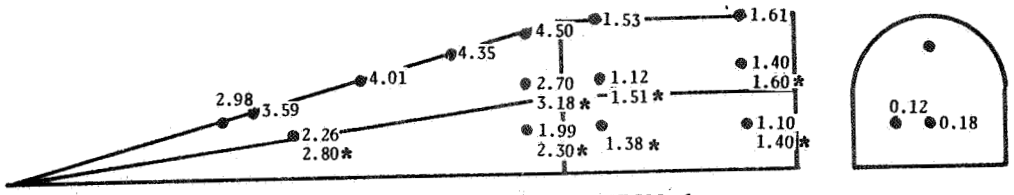

CONFIGURATION 6

AIR FLOW

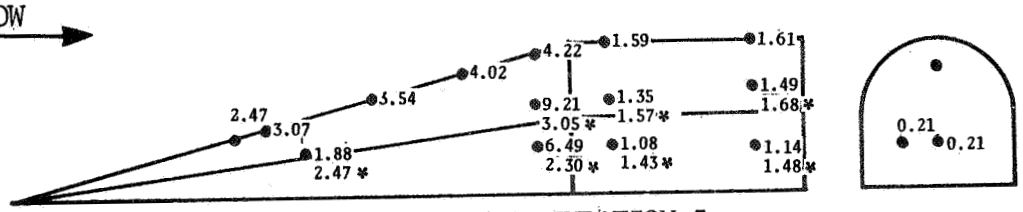

CONFIGURATION 5

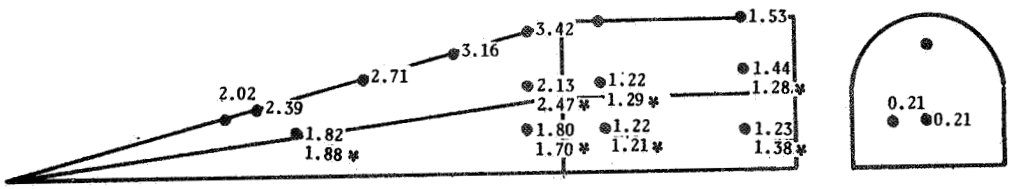

CONFIGURATION 8

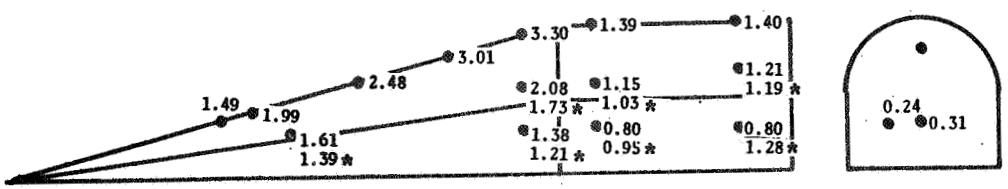

CONFIGURATION 9

NOTE: Values presented are the ratio of local heat-transfer coefficient to an average of clean plate heat-transfer coefficients obtained in the area covered by Model 5 base (0.00085 Btu/ft^{2}sec-°R).

FIGURE A-63. EFFECT OF MULTIPLE WAKES (MODELS 1 AND 2) ON MODEL 5 HEATING DISTRIBUTIONS AT MACH NUMBER 4.44

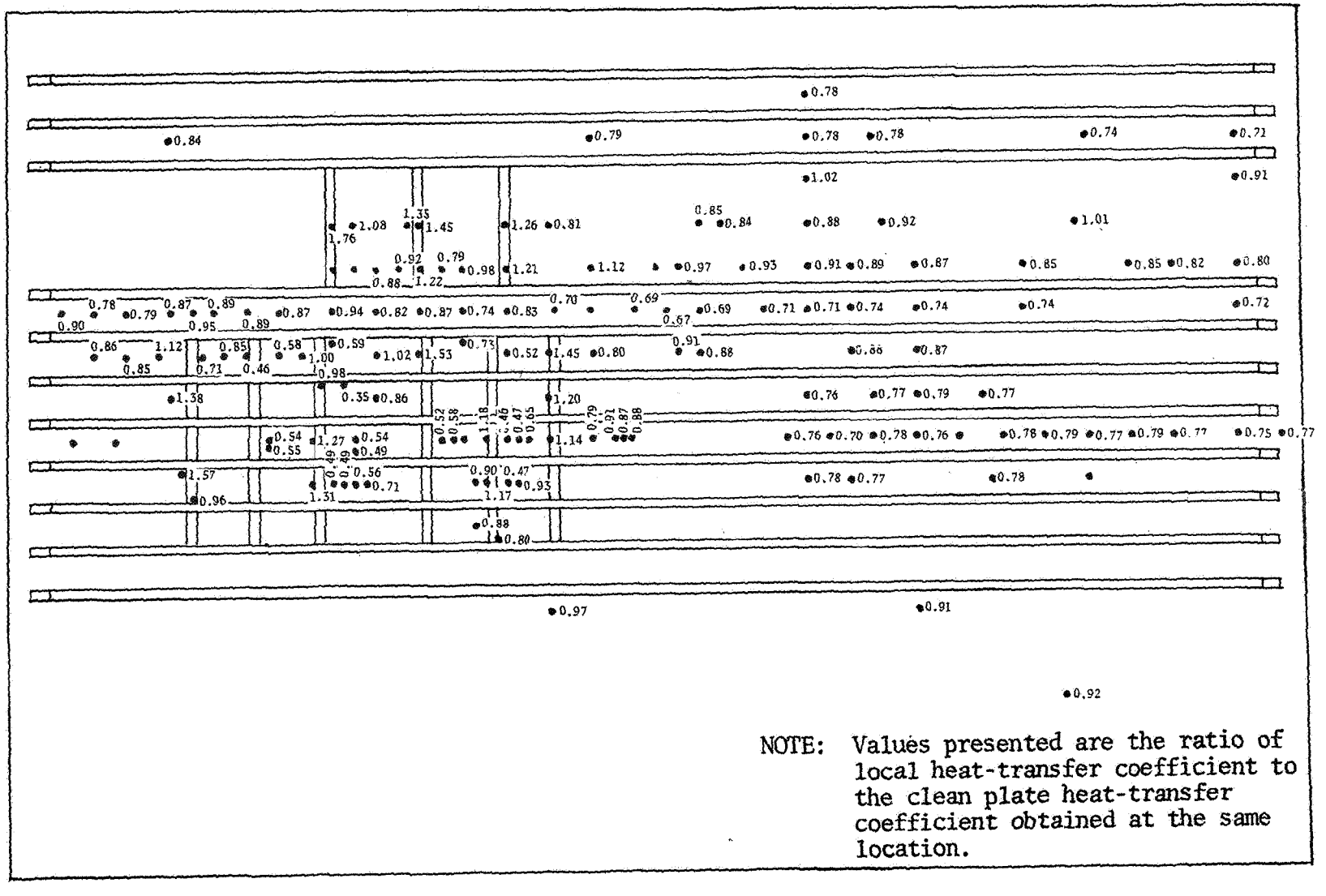

FIGURE A-64. EFFECT OF 0.5 INCH HIGH HAT SECTIONS (MODELS 13 AND 14) ON PLATE HEATING DISTRIBUTION AT MACH NUMBER 2.49 - CONFIGURATION 12

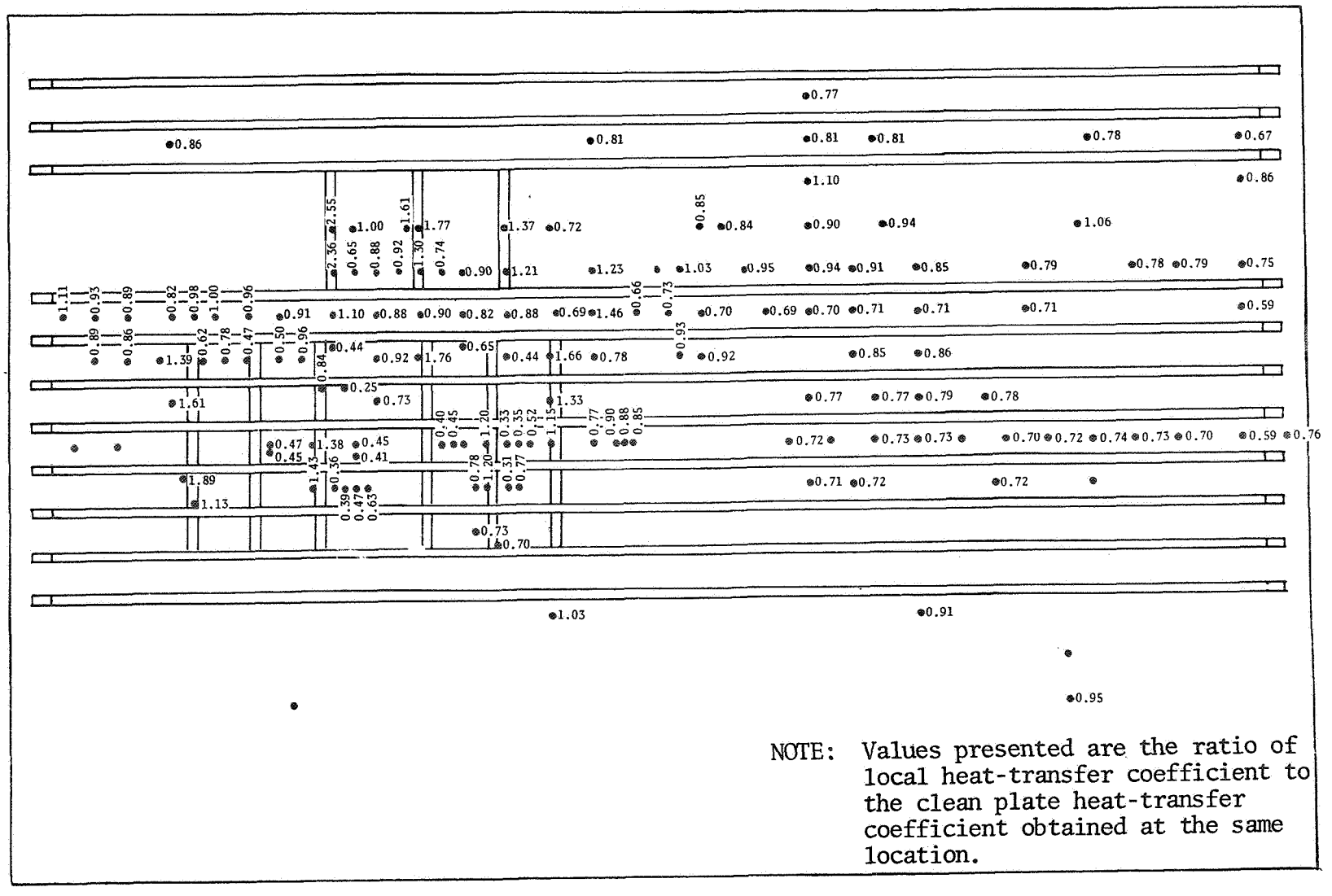

FIGURE A-65. EFFECT OF 0.5 INCH HIGH HAT SECTIONS (MODELS 13 AND 14) ON PLATE HEATING DISTRIBUTION AT MACH NUMBER 3.51 - CONFIGURATION 12

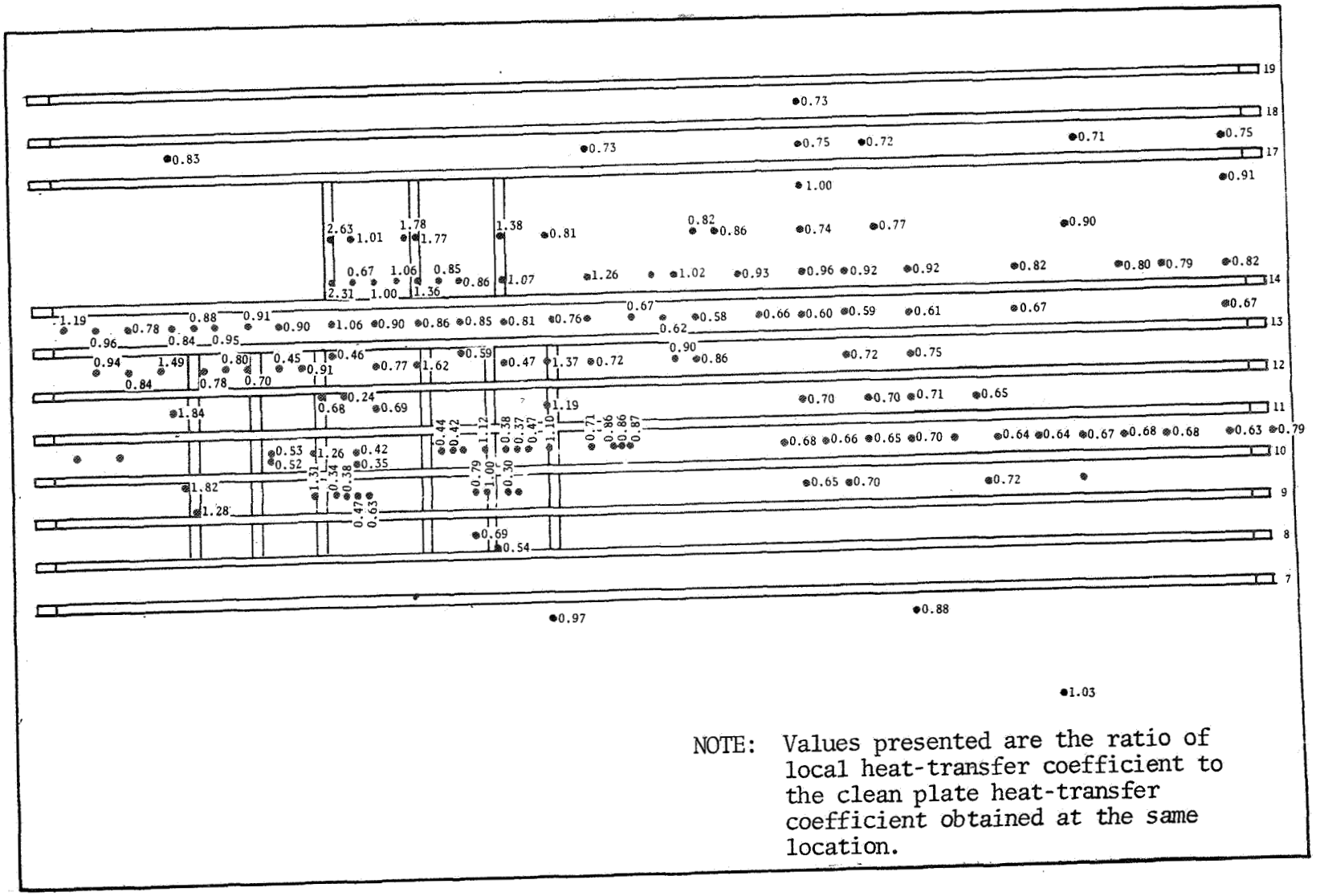

FIGURE A-66. EFFECT OF 0.5 INCH HIGH HAT SECTIONS (MODELS 13 AND 14) ON PLATE HEATING DISTRIBUTION AT MACH NUMBER 4.44 - CONFIGURATION 12

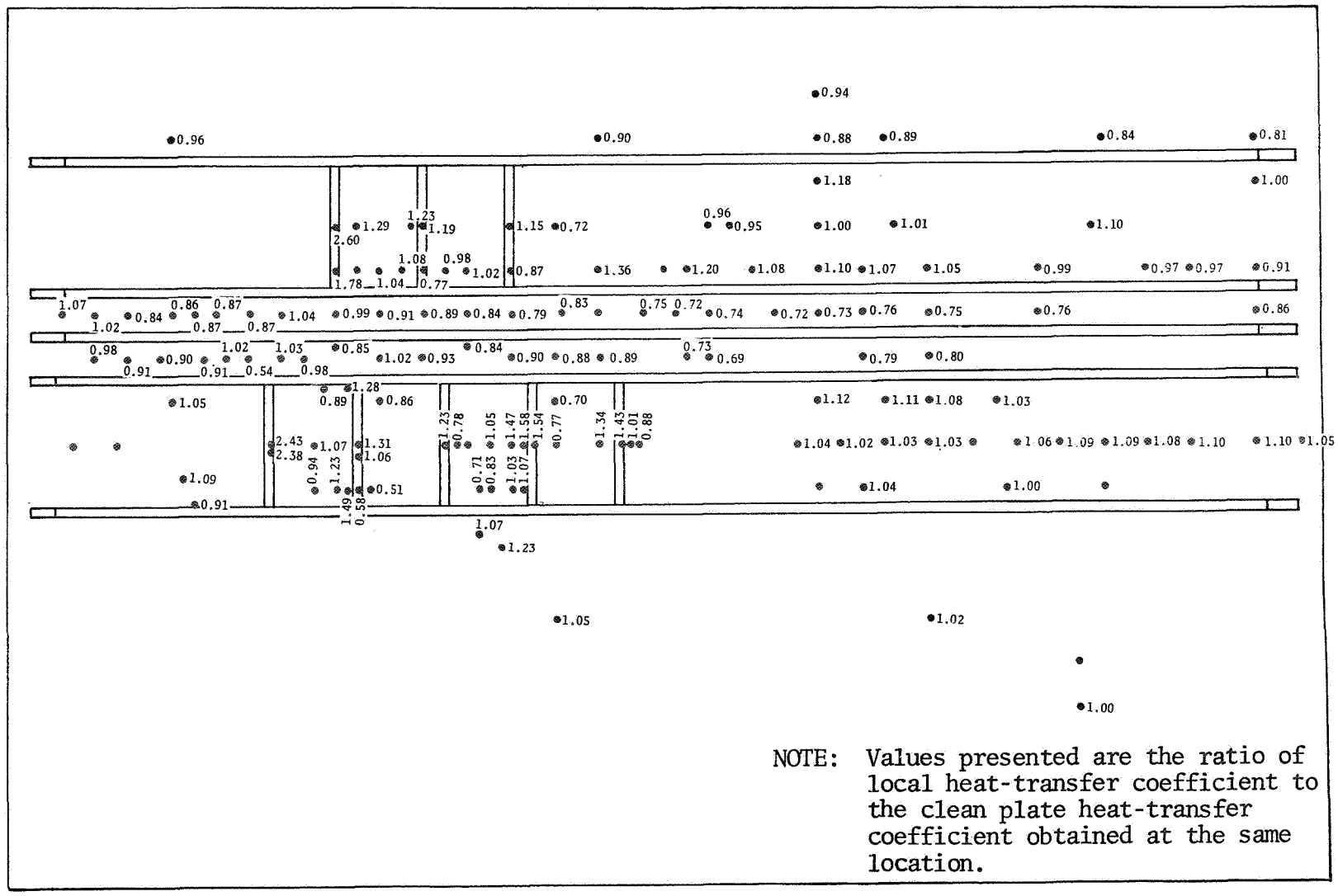

FIGURE A-67. EFFECT OF 0.75 AND 1.0 INCH HIGH HAT SECTIONS (MODELS 15 AND 16) ON PLATE HEATING DISTRIBUTION AT MACH NUMBER 2.49 - CONFIGURATION 13

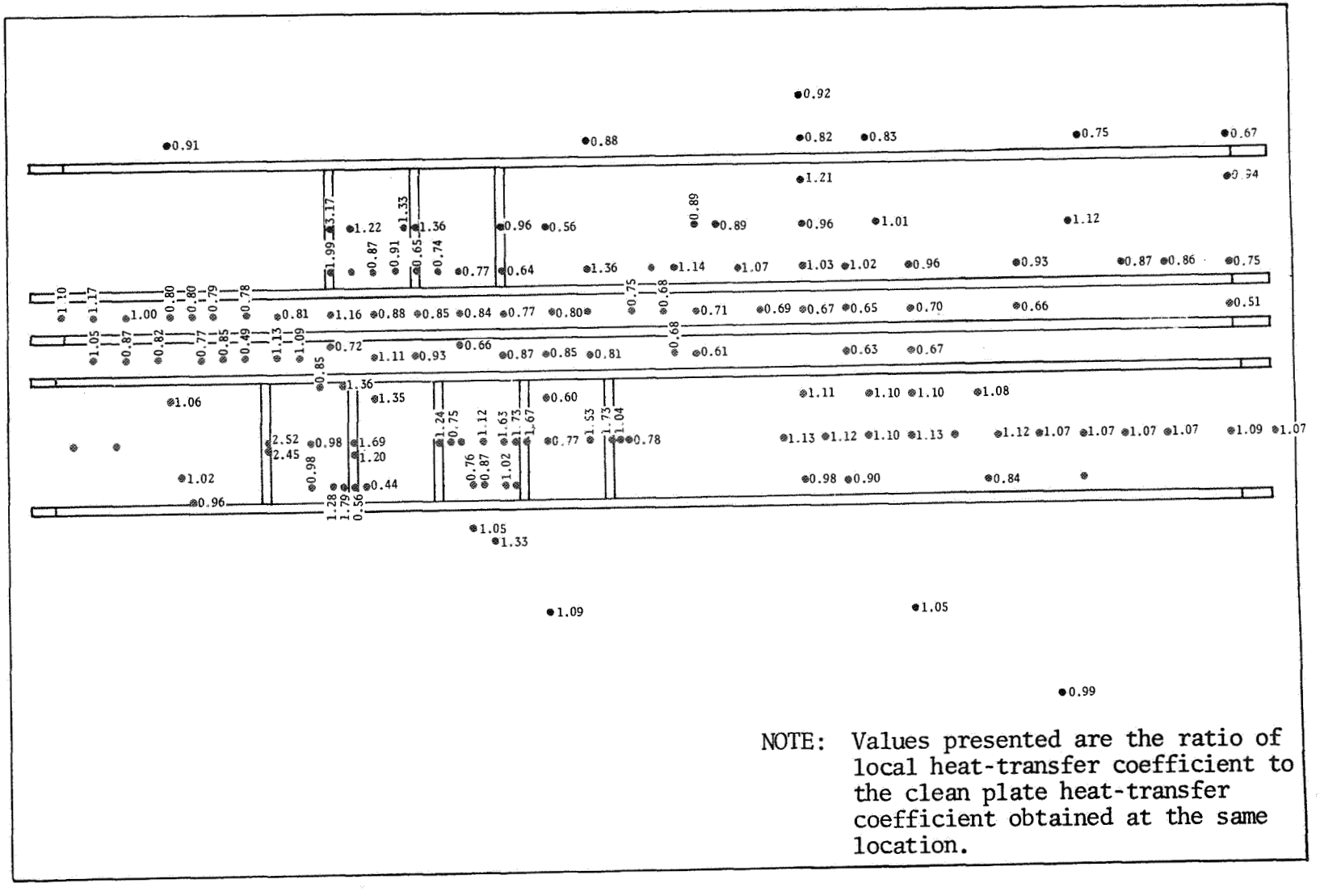

FIGURE A-68. EFFECT OF 0.75 AND 1.0 INCH HIGH HAT SECTIONS (MODELS 15 AND 16) ON PLATE HEATING DISTRIBUTION AT MACH NUMBER 3.51 - CONFIGURATION 13

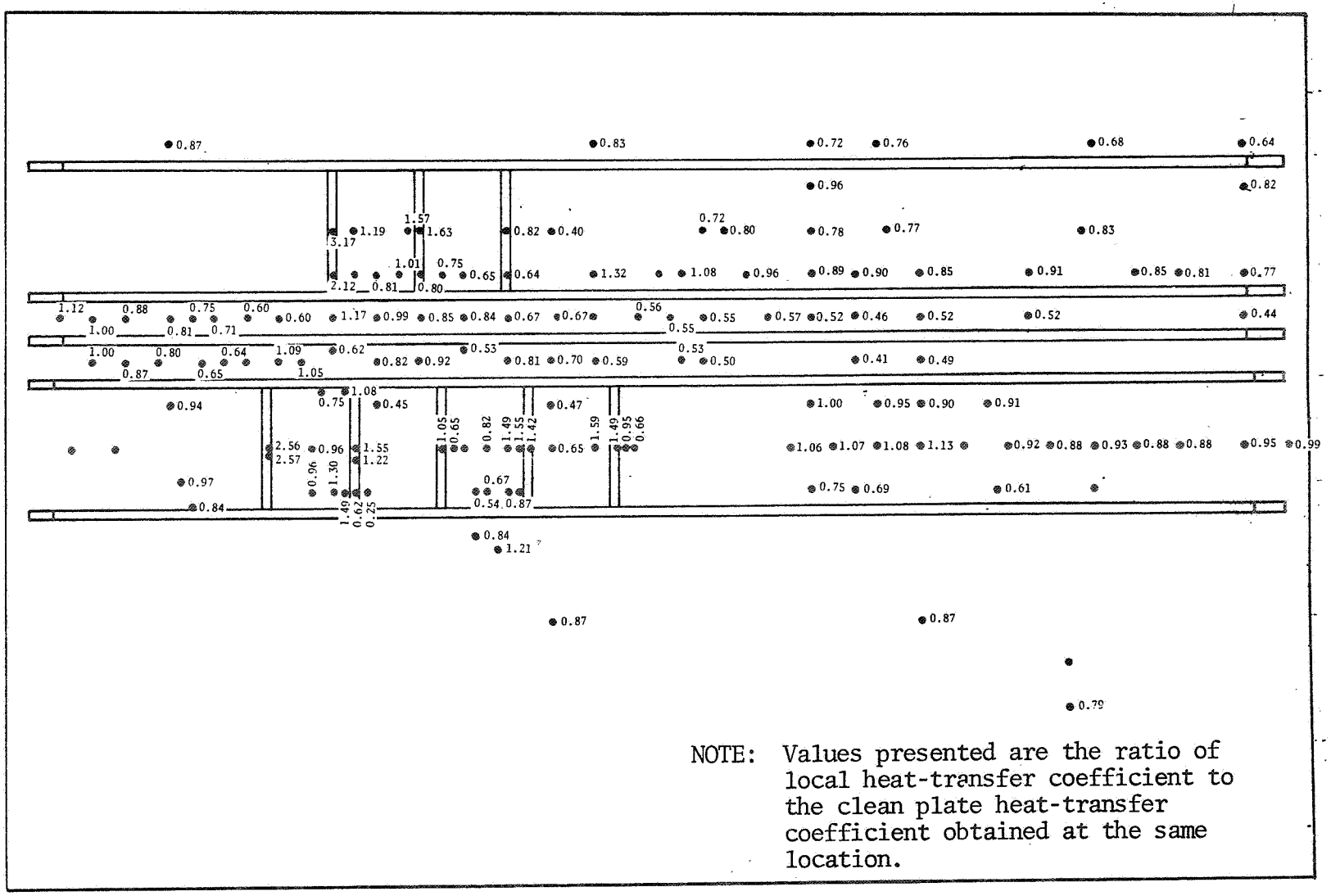

FIGURE A-69. EFFECT OF 0.75 AND 1.0 INCH HIGH HAT SECTIONS (MODELS 15 AND 16) ON PLATE HEATING DISTRIBUTION AT MACH NUMBER 4.44 - CONFIGURATION 13